# Present and past changes in continental weathering and ocean circulation from radiogenic Nd, Hf and Pb isotopes

Veit Dausmann

Dissertation - Kiel, 2018

# Present and past changes in continental weathering and ocean circulation from radiogenic Nd, Hf and Pb isotopes

Dissertation zur Erlangung des Doktorgrades
Dr. rer. nat.

der Mathematisch-Naturwissenschaftlichen Fakultät der
Christian-Albrechts-Universität zu Kiel

vorgelegt von

**Veit Dausmann**

Kiel, 2018

1. Gutachter und Betreuer: Prof. Dr. Martin Frank

2. Gutachter: Dr. Germain Bayon

Eingereicht am: 11. Januar 2018

Tag der Disputation: 16. Februar 2018

Zum Druck genehmigt: 16.Februar 2018

Gez. Prof. Dr. Natascha Oppelt, Dekanin

## ERKLÄRUNG

Hiermit erkläre ich an Eides statt, dass ich die vorliegende Abhandlung, abgesehen von der Beratung durch meinen Betreuer, nach Inhalt und Form selbstständig erarbeitet habe und keine anderen, als die von mir aufgeführten Quellen und Hilfsmittel, verwendet wurden.

Diese Arbeit ist unter Einhaltung der Regeln guter wissenschaftlicher Praxis der Deutschen Forschungsgemeinschaft entstanden und wurde weder in Auszügen noch in ganzer Form an einer anderen Stelle im Rahmen eines Prüfungsverfahrens eingereicht.

Teile dieser Arbeit sind bereits in einer Fachzeitschrift veröffentlicht, wurden zur Veröffentlichung eingereicht oder sind in Vorbereitung eingereicht zu werden.

Kiel, den 16. Februar 2018

Veit Dausmann

**CONTENTS**

## ABSTRACT

The ongoing global climate change in the recent years has created an urgent demand for knowledge about our planet's climatic system. Given that it redistributes heat and moisture on a global scale, ocean circulation is a key player in the Earth's climate system. In addition, continental weathering conditions and subsequent weathering inputs to the oceans also carry valuable information about the variability of the climate. Thus, reliable evaluations and predictions of present-day and future changes of the Earth's environment, respectively, ask for reliable reconstructions of past variations.

The past and present variability of ocean circulation and weathering inputs can be reconstructed from the geochemical composition of seawater and marine sediments. Among other proxies, the radiogenic isotope compositions of neodymium (Nd), hafnium (Hf) and lead (Pb) have been applied to reliably trace variations in the ocean that have been related to climate change. However, not all mechanisms and processes governing the geochemical cycling and redistribution of these isotopes are understood in sufficient detail. In order to improve the understanding of some of these mechanisms, the subject of the studies presented in this thesis are the evolution of the radiogenic isotopes of Nd, Hf and Pb in the hydrosphere from the first release into solution during continental weathering via the cycling in present day seawater to the marine sediments, where the information about variations in past ocean circulation and weathering inputs is stored.

The reconstruction of variations in past weathering intensities using Nd, Hf and Pb isotope compositions are primarily based on differences in incongruent weathering processes between these isotope systems during the weathering of rocks. Accordingly, the Nd, Hf and Pb isotope signatures released during weathering are the result of both the distinct isotope compositions of the rock-forming minerals and their relative abundances as well as differences in their resistance to dissolution. To date, however, there has not been a comprehensive experimental investigation of these processes. Chapter 3 of this thesis provides first combined, quantitative experimental evidence for the impact of the mineralogy of granitic rocks on incongruent weathering of Nd, Hf and Pb isotopes. The experimental data suggest that preferential dissolution of labile accessory minerals, in particular apatite and sphene, dominate the release of radiogenic Nd, Hf and Pb during weak chemical weathering. Nevertheless, under incipient weathering conditions Pb isotope signatures, contrary to expectations, show congruent release of Pb from freshly exposed mineral surfaces. During more intense chemical weathering, as well as enhanced physical weathering conditions, the dissolution of major minerals (e.g. feld-

spars) becomes dominant for Nd and Pb isotope signatures resulting in isotope compositions similar to those of the bulk rocks. Hafnium isotopes, on the other hand, are still overprinted by contributions from more radiogenic minerals under more intense weathering conditions. Leaching experiments of zircon separates were performed to test the specific role of zircons for Hf isotope compositions of weathering solutions. It is demonstrated that zircons are more efficiently dissolved when physical weathering is enhanced. The increased Hf release from partial zircon dissolution, however, is not large enough to explain less radiogenic Hf isotope signatures in seawater during climatic episodes of enhanced mechanical erosion. Moreover, observed additions of Hf from the more congruent dissolution of the zircon-free fractions due to increased physical weathering indicate that the latter minerals also play an important role in controlling Hf isotope signatures released during changing physical weathering conditions.

When the weathering solutions reach the oceans, the isotope compositions released from the weathered rocks are added to the mixture of local and advected water masses. In recent years the direct measurement of dissolved Nd and Hf concentrations and isotope compositions in seawater has become a standard chemical oceanographic tool for the estimation of water mass mixing ratios and the impact of local weathering inputs. In this thesis, surface- and deep-water masses from the Bay of Biscay were analyzed for combined Nd and Hf concentrations and isotope compositions together with Rare Earth Element (REE) concentrations (chapter 4). Subsurface Eastern North Atlantic Central Water (ENACW) shows a distinct Nd isotope composition of $\varepsilon_{Nd}$ = -12.0 at the southwestern most station and is significantly diluted on its way along the European margin by mixing with more radiogenic waters from above and below. Furthermore, the Nd isotope data clearly show the declining influence of radiogenic Mediterranean Outflow Water (MOW; $\varepsilon_{Nd}$ = -10.1) at intermediate depths on its way north as it is diluted with ENACW. It is demonstrated that only 40% to 60% of MOW still present at the Galician margin arrives at stations further north along its pathway. A potentially temporal feature of Nd isotope changes in MOW is identified when comparing the results of this study with those of earlier studies from the same area, which possibly reflects the meandering flow path of MOW. Higher proportions of MOW-like Nd signatures are also manifested in elevated Nd and Hf concentrations likely originating from increased terrestrial inputs to the Mediterranean Sea and are then transported as far as the Galician margin. The deep-water Nd isotope signatures in the Capbreton region strongly suggest exchange with local shelf sediments. In contrast, the Hf isotope compositions of all water masses of the Bay of Biscay are generally overprinted by local inputs and do not reflect the mixing of respective water masses.

In chapter 5 the reconstruction of past changes in ocean circulation and continental weathering inputs since the Mid-Miocene is presented using combined seawater radiogenic Hf and Nd isotope compositions extracted from bulk sediment leachates and foraminifera of Site 1088, ODP Leg 177, 2082 m water depth on the Agulhas Ridge. Due to its intermediate water depth the sediments of this core sensitively recorded changes in admixture of North Atlantic Deep Water (NADW) to the Antarctic Circumpolar Current (ACC) as a function of the strength of the Atlantic Meridional Overturning Circulation (AMOC). Nd isotope compositions range from $\varepsilon_{Nd}$ = -7 to -11 with glacial values generally 1 to 3 $\varepsilon_{Nd}$-units more radiogenic than during the interglacials of the Quaternary. The data reveal episodes of significantly increased AMOC strength during the late Miocene and Pliocene warm periods whereas peak radiogenic $\varepsilon_{Nd}$ values mark a strongly diminished AMOC during the major intensification of Northern Hemisphere Glaciation near 2.8 Ma and during the glacials of the Pleistocene after 1.5 Ma. In contrast, the Hf isotope compositions document a long-term transition in dominant weathering inputs, in that inputs from South America were replaced by sources from Southern Africa. Moreover, peak radiogenic values provide evidence for the supply of radiogenic Hf originating from Patagonian rocks to the Atlantic sector of the Southern Ocean via dust inputs.

## KURZZUSAMMENFASSUNG

Der rasante Klimawandel der vergangenen Jahre stellt hohe Anforderungen an die Erforschung der grundliegenden Prozesse des Klimas auf unserer Erde. Die Ozeanzirkulation spielt eine wesentliche Rolle bei der Verteilung von Wärmeenergie und Feuchtigkeit auf globalen Skalen und ist deshalb einer der Schlüsselfaktoren in unserem Klimasystem. Weiterhin spiegeln die Verwitterungsbedingungen und deren Einträge in die Meere die Veränderungen in den klimatischen Bedingungen auf den Kontinenten wider. Um verlässliche Aussagen über momentane wie auch zukünftige Veränderungen der Umwelt auf unserem Planeten treffen zu können, sind zuverlässige Rekonstruktionen vergangener Veränderungen unseres Klimas unerlässlich.

Die gegenwärtige sowie vergangene Veränderlichkeit von Ozeanzirkulation und Verwitterungseinträgen wird meist mit Hilfe der geochemischen Zusammensetzung von Meerwasser oder mariner Sedimente rekonstruiert. Neben anderen Proxies, hat sich die Anwendung der Isotopenverhältnisse von Neodym (Nd), Hafnium (Hf) und Blei (Pb) bei der Darstellung von mit dem Klimawandel zusammenhängenden Variationen im Meer bewährt. Jedoch sind bis dato nicht alle Mechanismen und Prozesse, welche die geochemischen Kreisläufe und Umverteilung dieser Isotope beeinflussen, vollständig erforscht. Die Forschungsergebnisse, die in den einzelnen Kapiteln dieser Arbeit präsentiert werden, sollen zum besseren Verständnis einiger dieser Mechanismen und Prozesse beitragen. Dabei wird die Entwicklung der radiogenen Isotope von Nd, Hf und Pb in der Hydrosphäre vom erstmaligen Lösen durch die kontinentale Verwitterung über die Zirkulation im heutigen Meerwasser bis hin zur Sedimentation am Meeresboden, wo die Information über vergangene Veränderungen der Ozeanzirkulation und Verwitterungseinträge gespeichert ist, beleuchtet.

Rekonstruktionen von Verwitterungsintensitäten in der Vergangenheit mit Hilfe von Nd, Hf und Pb Isotopenzusammensetzungen stützen sich hauptsächlich auf Unterschiede in den inkongruenten Verwitterungsprozessen dieser Isotopensysteme während der Zersetzung des Gesteins. Dementsprechend sind die Isotopenzusammensetzungen von Nd, Hf und Pb, die während der Verwitterung freigesetzt werden das Resultat von einerseits der spezifischen Isotopenzusammensetzung der gesteinsbildenden Minerale und deren relative Häufigkeit und andererseits ihrer Beständigkeit gegenüber Verwitterung. Bislang gibt es jedoch keine eingehenden Untersuchungen dieser Prozesse mit Hilfe von Experimenten. In Kapitel 3 werden erste experimentelle Beweise für den Einfluss der Mineralogie granitischer Gesteine auf die inkongruente Verwitterung von Nd, Hf und Pb Isotopen dargestellt. Die Er-

gebnisse deuten darauf hin, dass die bevorzugte Zersetzung von labilen Spurenmineralen, besonders Apatit und Titanit, die Freisetzung von radiogenem Nd, Hf und Pb bei schwacher chemischer Zersetzung überwiegt. Wider Erwarten zeigen Pb Isotopenzusammensetzungen bei beginnender Verwitterung jedoch eine kongruente Freisetzung von Pb aus frisch exponierten Mineralflächen. Unter intensiverer chemischer Zersetzung, sowie bei erhöhter physikalischer Verwitterung, dominiert die Auflösung der Hauptminerale (z.B. Feldspäte) die Nd und Pb Isotopensignaturen, was in einer Isotopenzusammensetzung ähnlich der des Gesamtgesteins resultiert. Hf Isotope werden hingegen selbst unter intensiven Verwitterungsbedingungen noch von den Einflüssen radiogenerer Minerale geprägt. Um die spezifische Rolle von Zirkonen für die Hf Isotopenzusammensetzung zu ermitteln, wurden Zersetzungsexperimente mit Zirkonseparaten durchgeführt. Dabei wurde festgestellt, dass bei intensiver physikalischer Zerkleinerung die Zirkone effizienter angelöst werden. Die erhöhte Hf Freisetzung aus der partiellen Auflösung von Zirkonen ist jedoch nicht groß genug um die weniger radiogene Hf Isotopenzusammensetzungen von Meerwasser zu erklären, die während klimatischen Phasen mit erhöhter mechanischer Verwitterung beobachtet wurde. Die erhöhte Beimengung von Hf aus der kongruenteren Verwitterung der Zirkon-freien Fraktionen unter erhöhter physikalischer Beanspruchung hingegen, weist darauf hin, dass diese Mineralfraktion ebenfalls eine wichtige Rolle für die Hf Isotopenzusammensetzungen der Verwitterungslösungen unter veränderlichen physikalischen Verwitterungsbedingungen spielt.

Erreichen diese Verwitterungslösungen den Ozean, vermengen sich deren Isotopenzusammensetzungen mit denen der dort vorhandenen Wassermassen. In den vergangenen Jahren hat sich die direkte Messung der gelösten Nd und Hf Konzentrationen und Isotopenzusammensetzung im Meerwasser als chemisches Standardwerkzeug der Ozeanographie durchgesetzt, um Wassermassenmischungsverhältnisse und lokale Verwitterungseinträge zu bestimmen. In dieser Arbeit wurden die Hf und Nd Konzentrationen und Isotopenzusammensetzungen zusammen mit den Seltenen Erden Element (REE) Konzentrationen von Oberflächen- und Tiefenwasser aus der Biskaya analysiert (Kapitel 4). Eastern North Atlantic Central Water (ENACW) weist dabei eine spezifische Nd Isotopenzusammensetzung von $\varepsilon_{Nd}$ = -12.0 in der südwestlichsten Station auf und wird auf seinem Weg entlang der Iberischen Halbinsel mit radiogenerem Wasser verdünnt. Außerdem demonstrieren die Nd Isotopen Daten den sich in Strömungsrichtung verringernden Einfluss von radiogenerem Mediterranean Outflow Water (MOW; $\varepsilon_{Nd}$ = -10.1) im Zwischenwasser, da es auf seinem Weg Richtung Norden mit ENACW verdünnt wird. Es wird aufgezeigt, dass lediglich 40% bis 60% des sich am Galizischen Schelf befindlichen MOW die weiteren Stationen seines Verlaufs erreichen. Des weiteren wurde ein vermutlich temporäres Merkmal der Nd Isotopenveränderung des MOW durch den Ver-

gleich der Ergebnisse dieser Studie mit denen einer früheren Studie desselben Gebiets identifiziert. Dieses Merkmal stellt wahrscheinlich den mäandrierenden Fluss des MOW dar. Höhere MOW Anteile werden ebenfalls durch erhöhte Nd und Hf Konzentrationen widergespiegelt und stammen vermutlich von erhöhten terrestrischen Einträgen in das Mittelmeer. Die Tiefenwasser Nd Isotopensignaturen in der Capbreton Region weisen stark auf einen Austausch mit den Schelfsedimenten hin. Die Hf Isotopenzusammensetzung aller Wassermassen in der Biskaya hingegen sind generell von lokalen Einträgen überprägt und reflektieren nicht die Mischungsverhältnisse verschiedener Wassermassen.

In Kapitel 5 wird die Rekonstruktion von Veränderungen der Ozeanzirkulation und kontinentaler Verwitterungseinträge seit dem mittleren Miozän beschrieben. Dies geschieht mit Hilfe von der Kombination von Nd und Hf Isotopenzusammensetzungen des ehemaligen Meerwassers, die aus marinen Sedimenten von der ODP Site 1088 vom Agulhas Rücken extrahiert wurden. Aufgrund ihrer Lage in einer mittleren Tiefe zeichneten die Sedimente dieses Bohrkerns die Veränderungen in der Beimischung von Nordatlantischem Tiefenwasser (NADW) zu den Wassermassen des Zirkumantarktischen Stroms (ACC) als eine Funktion der Stärke der Atlantischen Meridionalen Umwälzungsbewegung (AMOC) auf. Die Nd Isotopenzusammensetzungen der Sedimente des Agulhas Rückens variieren zwischen $\varepsilon_{Nd}$ = -7 und -11, wobei glaziale Werte generell 1 bis 3 $\varepsilon_{Nd}$-Einheiten radiogener sind als die Werte der Interglaziale im Quartär. Weiterhin lassen die Daten Episoden erhöhter AMOC Stärke während den Warmphasen des späten Miozäns und Pliozäns erkennen, wohingegen radiogene $\varepsilon_{Nd}$-Maxima stark verringerte AMOC Intensitäten während der Intensivierung der Vereisung der Nordhemisphäre (2.8 Ma) und während der Glaziale des Pleistozäns nach 1.5 Ma markieren. Die Hf Isotopenzusammensetzung hingegen dokumentiert eine langfristige Umstellung der dominanten Verwitterungseinträge  in sofern, dass Einträge von Südamerika durch Einträge aus dem südlichen Afrika ersetzt werden. Weiterhin belegen $\varepsilon_{Hf}$-Maxima die Zulieferung von radiogenem Hf, welches durch Staubeinträge aus Patagonien in den atlantischen Sektor des Südozeans gelangte.

# 1 Introduction

## 1.1 Ocean circulation, climate and weathering

The interior of the oceans is stratified resulting in distinctive water masses caused by differences in their heat and salinity contents. These differences are the main drivers of the thermohaline circulation also described as the "global conveyor belt" (Broecker 1991). Predominantly in the polar regions colder or more saline bodies of water sink to form deep-waters flowing towards the equator. Examples for deep-water masses are North Atlantic Deep Water (NADW), which forms in the high northern latitudes of the Atlantic, Antarctic Bottom Water (AABW) and Circumpolar Deep Water (CDW), which are formed around the Antarctic continent. The surface ocean, in contrast, is mainly affected by interactions with the atmosphere, such as heat, moisture, gas exchange, and wind stress. These surface exchange processes represent direct interactions between ocean circulation and global climate, whereas the deep ocean water masses, being the main reservoir of climate sensitive greenhouse gases, influence climate indirectly. These direct and indirect interactions suggest that for example variations in ocean circulations cause changes in global climate. In particular, the redistribution of heat and moisture from lower to higher latitudes via ocean currents (e.g. Gulf Stream) has been shown to have a significant impact on local and global climate (e.g. Haug and Tiedemann 1998).

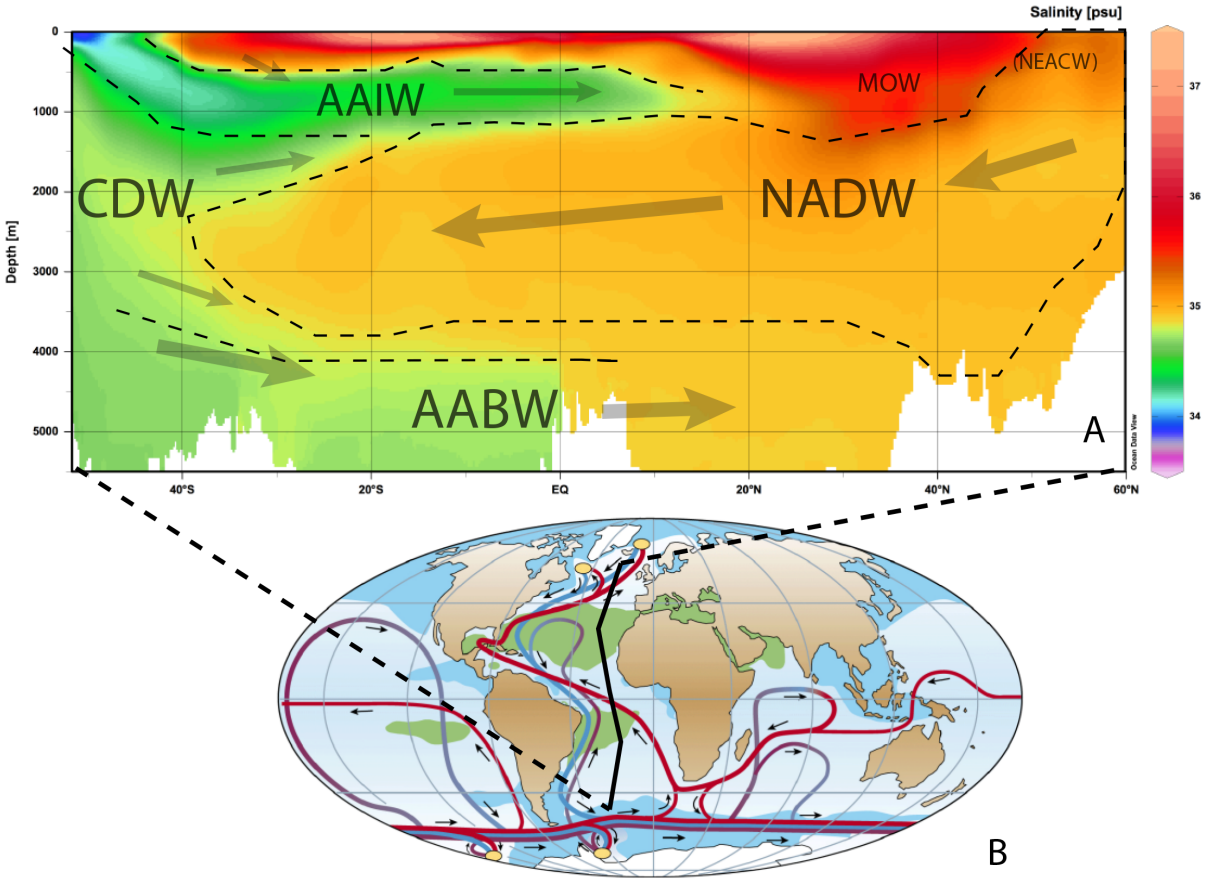


**Figure 1.1: Salinity profile (A) through the Atlantic Ocean including schematic water masses and their direction of flow as part of the Atlantic Meridional Overturning Circulation (NADW: North Atlantic Deep Water; MOW: Mediterranean Outflow Water; NEACW: Northeast Atlantic Central Water; AAIW: Antarctic Intermediate Water; CDW: Circumpolar Deep Water; AABW: Antarctic Bottom Water). (B) Simplified global thermohaline circulation pathways. Yellow areas represent regions of deep-water formation; red path segments: near-surface ocean circulation; blue path segments: deep-water circulation; and purple path segments: bottom currents. The surface salinity gradient is also represented by the color scheme decreasing from green to light blue to blue. Figure from Rahmstorf (2002).**

One of the main parts of the global conveyor belt is the so-called Atlantic Meridional Overturning Circulation (AMOC; Figure 1.1). Southward flowing NADW is counterbalanced by northward moving water masses from the Southern Ocean such as AABW, CDW and Antarctic Intermediate Water (AAIW) at different depth levels of the Atlantic Ocean. The Agulhas leakage originating from the Indian Ocean is the main source of warm and salty waters advected to the subpolar North Atlantic as the upper limb of the AMOC (Biastoch et al. 2008) and representing the only mode of a net energy transfer from the Southern to the Northern Hemisphere (Hall and Lutjeharms 2011). Consequently, in agreement with the above-mentioned impact of ocean circulation on global climate, past variations in water mass supply from the Southern and Indian Oceans to the Atlantic Ocean, as well as advection of water masses from the North Atlantic to the Southern Ocean reflect climate evolution on glacial-interglacial timescales (e.g. Rutberg et al. 2000; Piotrowski 2005; Yu et al. 2016).

Accordingly, the AMOC has been suggested to have operated at a shallower and possibly more sluggish mode during glacials and was likely shut off almost entirely during Heinrich-events (Figure 1.2; Rahmstorf 2002; Böhm et al. 2015).

On even longer timescales, before the intensification of Northern Hemisphere glaciation, a strong thermohaline circulation in the Atlantic, however, was most likely active during periods of early Pliocene warmth (e.g. Raymo et al. 1996; Billups 2002), which may have acted as a precondition for the onset of Northern Hemisphere glaciation 2.7 million years ago due to the persistent transport of moisture to the high northern latitudes (e.g Haug & Tiedemann 1998; Bartoli et al. 2005).

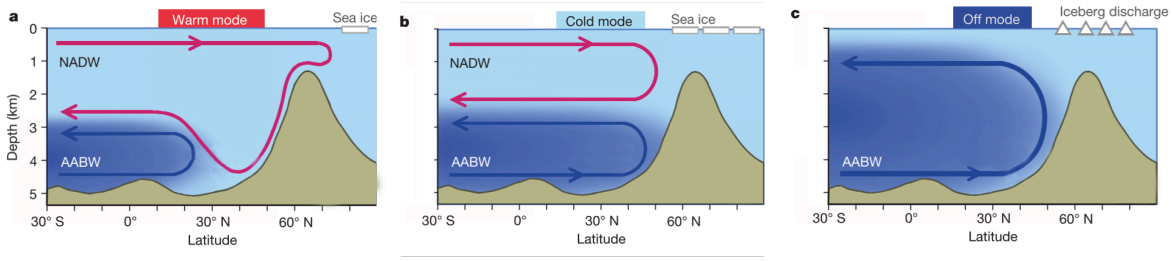


**Figure 1.2: Schematic representation of different operation modes of AMOC in relation to climatic stages (here in the North Atlantic). Mode (a) represents the modern or interglacial warm mode with a deep and vigorous overturning circulation. In contrast, during glacials the AMOC operated in a shallower more sluggish cold mode (b) or even halted during particular Heinrich Events (c). Modified from Rahmstorf (2002).**

The waxing and waning of continental ice shields, in turn, has had a pronounced influence on regional climate and weathering conditions (e.g. Vance and Burton 1999; Gutjahr et al. 2009, 2014; Kurzweil et al. 2010). Furthermore, global climate has also been strongly affected by weathering rates of silicate rocks on tectonic time scales as chemical weathering draws down $CO_2$ from the atmosphere influencing the oceanic carbon cycling (e.g. Berner et al. 1983; Raymo and Ruddiman 1992). Moreover, weathering intensities on the continents exert strong influence on the abundance of nutrients in the ocean and can in this way create climatic feedbacks when marine organic carbon sequestration was being increased (e.g. Broecker 1982; Sigman and Boyle 2000; Hain et al. 2010). Hence monitoring the variability of continental weathering regimes provides valuable information about past climatic conditions on the continents.

Considering the current need for the understanding of the earth's climate system it is essential to have an accurate knowledge of present and past variations of ocean circulation and weathering conditions on the continents. In most cases the reconstruction of these variations is based on proxies recorded in marine archives.

## 1.2 Radiogenic isotopes as tracers of present and past ocean circulation and terrestrial weathering

### 1.2.1 Neodymium isotopes as tracers of ocean circulation

Present ocean circulation is traced using conservative water mass properties such as salinity, potential temperature or oxygen and nutrient content. In addition to these classical water mass tracers, another group of geochemical proxies has gained significant attention as tracers of ocean circulation and weathering - radiogenic isotopes. One major advantage of these indirect proxies is that, in contrast to the classical water mass tracers, their variations are recorded in marine sediments and thus permit the reconstruction of changes in ocean circulation and weathering in the past.

Ideally tracers of ocean circulation should comply with the following requirements:

(1) The residence time of the tracers has to be on a similar scale as the global overturning circulation (1500 years; Broecker and Peng 1983) allowing long distance transport of deep water mass signatures but preventing complete homogenization.

(2) The dominant sources of the tracers are well known and deliver spatially distinct signatures to the ocean. Water masses thus should be clearly distinguishable by their isotope signature and their mixing can be traced quasi-conservatively.

(3) Non-conservative inputs and fractionation processes are negligible or can be evaluated on a site-by-site basis.

Radiogenic neodymium (Nd) isotopes have been shown to be potentially ideal tracers of past (and present) ocean circulation in numerous studies (for a review see Frank 2002). With the average residence time of Nd in the order of several hundreds to about 2,000 years (e.g. Frank 2002 and references therein), Nd isotope signatures that are transferred to seawater from continental inputs at a particular site can be traced along the entire global overturning circulation system. For example, the two major deep-water end-members in the Atlantic Ocean NADW and Pacific-influenced water masses (AABW, AAIW and CDW) have pronouncedly different radiogenic Nd isotope signatures. These differences are based on the distinct Nd isotope signatures of the rocks of the continents surrounding these water masses.

Furthermore, in contrast to traditional tracers such as stable carbon isotopes ($\delta^{13}C$) or Cd/Ca ratios biological processes do not affect radiogenic Nd isotope com-

positions significantly. Therefore, variations in seawater Nd isotope signatures are principally driven by conservative mixing of water masses and to a lesser extent by non-conservative (local) inputs, such as exchange with the sediments, the dissolution of sinking particles and adsorption-desorption processes (Lacan and Jeandel 2005a, 2005b; Carter et al. 2012; Rickli et al. 2014). These processes, however, can be assessed by evaluation of regional input systems, which is subject of this thesis.

### *1.2.2 Hafnium and lead isotopes as tracers of continental weathering inputs*

There are radiogenic isotope systems that are sensitive to changes in continental weathering rates and regimes. The temporal and spatial distribution and changes of radiogenic Hf and Pb isotopes for example are potential oceanic proxies to track changes of continental weathering regimes. This is based on the fact that different rock forming minerals with distinct Hf and Pb isotope compositions are differently susceptible to weathering (e.g. Erel et al. 1994; von Blanckenburg and Nägler 2001; van de Flierdt et al. 2002; Bayon et al. 2006; Crocket et al. 2013). In contrast to Nd and other proxies of continental weathering (such as Sr or Os isotopes), the residence times of Hf and Pb in the oceans are relatively short (Henderson and Maier-Reimer 2002; Rickli et al. 2009; Stichel et al. 2012), thus limiting the application as water mass tracers but enabling reconstructions of short-term and regional variations in weathering. Although, Hf and Pb have been applied as marine proxies of continental weathering intensities their exact behavior during weathering processes is not entirely understood and is one of the main topics of this thesis.

## *1.3 Geochemistry of Sm-Nd, Lu-Hf and U-Th-Pb in the solid Earth*

The term "radiogenic" implies the generation of an isotope by radioactive decay. The radiogenic isotope $^{143}Nd$ is produced via α-decay of the radioactive isotope $^{147}Sm$ with a half-life of $1.18\times10^{11}$ years (Kinoshita et al. 2002). Consequently, the abundance of $^{143}Nd$ in a rock is constantly growing (at a very small rate) depending on the abundance of the radioactive parent isotope $^{147}Sm$ that leads to measurable differences in the budget of $^{143}Nd$. Since these differences are very small they are commonly given in the dimension-free ε-notation:

$$(1)\ \varepsilon = \left( \frac{\left({}^{Abundance\ of\ radiogenic\ isotope}/_{Abundance\ of\ primordial\ isotope}\right)_{sample}}{\left({}^{Abundance\ of\ radiogenic\ isotope}/_{Abundance\ of\ primordial\ isotope}\right)_{CHUR}} - 1 \right) \times 10{,}000.$$

whereby in the case of radiogenic Nd isotopes the primordial isotope is naturally occurring $^{144}Nd$ and the ratio of the Chondritic Uniform Reservoir $(^{143}Nd/^{144}Nd)_{CHUR}$ has a modern value of 0.512638 (Jacobsen and Wasserburg 1980).

The radiogenic isotope $^{176}Hf$ is the product of the β-decay of the radioactive isotope $^{176}Lu$ with a half-life of $3.7 \times 10^{10}$ years (Hult et al. 2014). Analogous to Nd, the ingrowth and variation of radiogenic $^{176}Hf$ is also commonly presented in the ε-notation (1) with the primordial isotope being $^{177}Hf$ and the ratio of CHUR $(^{176}Hf/^{177}Hf)_{CHUR}$ having a modern value of 0.282785 (Bouvier et al. 2008).

In the case of Pb there are three radiogenic isotopes $^{206}Pb$, $^{207}Pb$ and $^{208}Pb$ that are the stable end products of the decay series of the respective parent isotopes $^{238}U$, $^{235}U$ and $^{232}Th$ with half-lives of $4.5 \times 10^9$, $0.7 \times 10^9$ and $14.01 \times 10^9$ years (Steiger and Jäger 1977), respectively. Abundances of radiogenic Pb isotopes are usually normalized to primordial $^{204}Pb$.

During the differentiation of the Earth's crust from the mantle and the formation of silicate rocks from magma or partial melts Nd, Hf and Pb as well as Sm, Lu, U and Th are fractionated according to their ability to substitute for a major element in the lattice of minerals. This so-called compatibility is based on the similarity of ionic radii and oxidation state of major element and substituent. Samarium, Nd and Lu all belong to the group of the Rare Earth Elements (REEs) showing very similar chemical behavior, valence states and ionic radii. Nevertheless, in the case of the Sm-Nd system Nd is somewhat less compatible than Sm leading to high Sm/Nd ratios in minerals with early crystallization behavior (retained in the mantle) and low Sm/Nd ratios in minerals that crystallize from depleted melts (migrating to the crust). Similarly, Hf is less compatible than Lu, leading to an analogous behavior of Lu/Hf ratios and Sm/Nd ratios. Since the compatibilities of Lu and Hf differ more than those of Sm and Nd, the former are fractionated to a comparatively greater extent.

Uranium and Th behave geochemically relatively similarly and are concentrated in the liquid phase during differentiation. Therefore, they are preferentially migrating into the Earth's crust. The fact that the radioactive parent isotopes are enriched in the crust and depleted in the mantle explains higher abundances of radiogenic Pb in the rocks of the continental crust and unradiogenic compositions in the rocks derived from the mantle (Figure 1.3A). The opposite is true for Sm-Nd and Lu-Hf, for which the parent isotopes are depleted in the crust and enriched in the mantle (Figure 1.3B). Therefore, the rocks of the continental crust (especially old cratons that have already lost a significant amount of the parent isotopes due to decay) are characterized by unradiogenic Nd and Hf compositions (low $\varepsilon_{Nd}$ and $\varepsilon_{Hf}$). In contrast, young volcanic rocks of mantle origin (Ocean island basalts or similar) have higher abundances of radiogenic Nd and Hf (high $\varepsilon_{Nd}$ and $\varepsilon_{Hf}$).

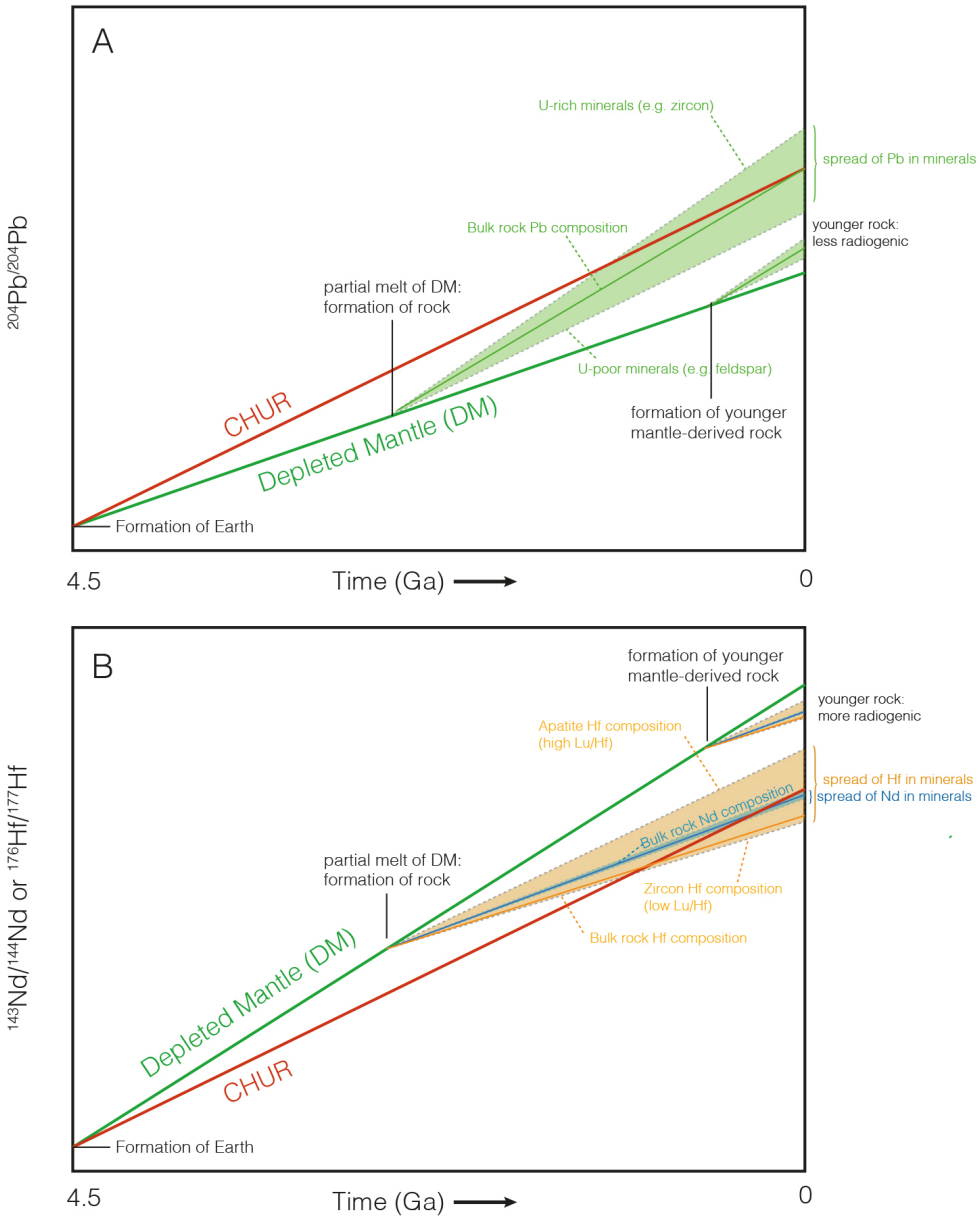


**Figure 1.3: Schematic evolution of A: Pb isotopes and B: Nd and Hf isotopes over time.**

Average concentrations of U and Th in the common rock-forming minerals are uniformly low while they are enriched in accessory minerals such as zircon, monazite, apatite, sphene etc. (Faure and Mensing 2005). The REEs, on the other hand, are present as constituents of accessory minerals as well as in trace amounts in the major rock-forming minerals. Different minerals, however, tend to show distinct selectivity for different groups of REE. Apatite or feldspar for example tend to concentrate the light REEs (including Nd and Sm) while zircon, pyroxene and garnets tend to incorporate heavy REEs.

In particular, zircons are of fundamental importance for the Lu-Hf isotope system. Due to the fact that Hf is a chemical twin element of Zr (the main constitu-

ent of zircon), Hf is highly enriched in zircon minerals (up to 2 wt%). Compared to Hf, the REE Lu is relatively rare in zircon leading to low Lu/Hf ratios and thus unradiogenic Hf isotope compositions of these minerals.

### *1.4 Geochemistry of Sm-Nd, Lu-Hf and U-Th-Pb during weathering*

As described above, geochemical processes in the Earth's interior have produced rocks with distinct isotope compositions depending mainly on the time of extraction from the Depleted Mantle (DM) or remelting of already differentiated material. When those rocks are exposed to weathering processes their minerals are dissipated according to their chemical resistance, which can lead to differences between isotope compositions of the host rocks and weathering fluids.

In the Sm-Nd system, parent and daughter isotopes are chemically similar and therefore variations of Sm/Nd between different minerals are rather small. This leads to relatively congruent weathering outputs. The Lu-Hf and U-Th-Pb systematics, on the other hand, produce parent to daughter isotope ratios that vary largely between different minerals. Since the weathering resistance of the different minerals differs, the result is a largely incongruent behavior of Hf and Pb isotope compositions when these minerals are exposed to weathering. Thus these isotope systems are sensitive to changes in weathering conditions.

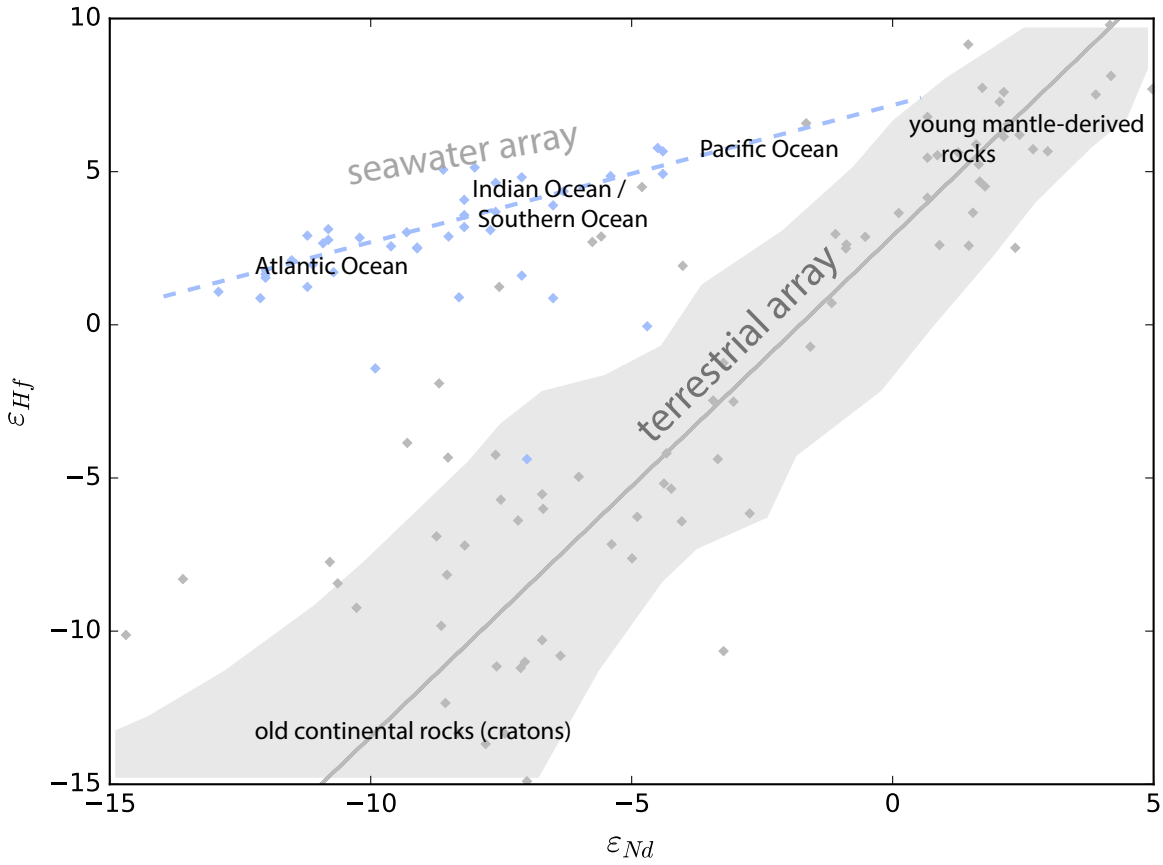


**Figure 1.4: Cross-plot of Hf and Nd isotope compositions displaying the distinct systematics of terrestrial rocks (terrestrial array; Vervoort et al. 1999) and seawater (seawater array; Albarède et al. 1998).**

When comparing the Sm-Nd and Lu-Hf isotope systems in seawater and rocks (Figure 1.4) the two isotope systems behave relatively similar in igneous rocks due to their similar fractionation behavior during the formation of the rocks. The "seawater array" (Albarède et al. 1998), on the other hand, is shifted towards more radiogenic Hf isotope compositions in comparison with that of the igneous rocks (Vervoort et al. 1999) and clearly displays the incongruent behavior of Hf isotopes during continental weathering (van de Flierdt et al. 2007). The important role of zircon minerals for this relationship was described as the "zircon-effect" (White et al. 1986), which is based on the fact that zircons are highly resistant to chemical weathering and therefore retain a significant fraction of the host rock's (unradiogenic) Hf during release to solution. Based on these assumptions excursions of marine Hf isotope signatures to more radiogenic values for a given Nd isotope composition coinciding with enhanced glacial activity on the continents has been associated with changing weathering regimes due to the more efficient Hf release from physically ground zircon minerals (Piotrowski et al. 2000; van de Flierdt et al. 2002; Dausmann et al. 2015). More recent studies, however, point out that for the oceanic budget an easily accessible source of more radiogenic Hf (for example apatites) may

also play an important role for the formation of the systematic variations in $\varepsilon_{Hf}$-$\varepsilon_{Nd}$ space (Bayon et al. 2006, 2009; van de Flierdt et al. 2007; Chen et al. 2011, 2013).

In the case of radiogenic Pb the decay of the parent isotopes via the intermediate daughter isotopes causes radiation damage to the crystal structure of a mineral. This leaves the radiogenic daughter isotopes more mobile at mineral boundaries than non-radiogenic $^{204}$Pb. This fact raised the hypothesis that during weathering radiogenic isotopes of Pb are released more easily and that this is the reason for Pb isotope compositions of weathering solutions and finally seawater differing largely from those of the source rocks (e.g. Erel et al. 1994; von Blanckenburg and Nägler 2001).

## *1.5 Geochemistry of Sm-Nd, Lu-Hf and U-Th-Pb in the ocean*

The principal source of Nd, Hf and Pb in the ocean is the input originating from the weathering of continental material (e.g. Frank 2002). Riverine inputs may transport Nd, Hf and Pb in particulate or dissolved form, adsorbed to particles or as colloids. Atmospheric transport of dust particles from the continents to the oceans also delivers significant amounts of Nd, Hf and Pb as these particles dissolve directly in seawater. Thereby, again, Hf isotopes are fractionated due to the different weathering resistance of the dust minerals, which may also have experienced some sorting during weathering and transport prior to their arrival in the surface waters, as has been demonstrated by analyses of dust inputs to the Eastern Atlantic (Rickli et al. 2010) and in the frame of leaching experiments (Chen et al. 2013).

Another important source of Nd and Hf (and presumably Pb) is the direct input from the sea floor via dissolution and exchange processes at the ocean-rock/sediment interface (termed boundary-exchange; Lacan and Jeandel 2005b). These non-conservative inputs (boundary exchange) have been shown to be important close to the sea-floor or continental margins (e.g. Rickli et al. 2009, 2014; Carter et al. 2012) and modeling experiments have indicated that this source may be at least as important as riverine inputs (Arsouze et al. 2009; Rempfer et al. 2011).

Furthermore, the direct input of radiogenic isotopes at hydrothermal vent sites has been under debate for a long time. For Nd this source, however, has been shown to be of only minor importance as it is removed from the water-column close to the vent sites (German et al. 1990; Halliday et al. 1992). Hafnium and Pb isotope budgets have been suggested to be at least locally affected by hydrothermal inputs (White et al. 1986; Barrett et al. 1987; Bau and Koschinsky 2006) but these sources are probably not significant for the global oceanic Hf budget (Chen et al. 1986; van de Flierdt et al. 2007).

When introduced into seawater the concentrations of Nd, Hf and Pb are affected by reversible scavenging and advection with water masses to variable extents. Caused by the tendency of these elements to adsorb to sinking particles reversible scavenging is not only responsible for the residence time of these elements in seawater (and thus their maximum travel ranges) but also their vertical distribution. Consequently, concentrations of Nd, Hf and Pb in seawater are typically high in regions of low scavenging rates (e.g. deep open oceans) and low at the ocean surface where scavenging rates are high.

Seawater is labeled with the Nd isotope compositions of the source rocks at the ocean margins and these are then advected with the water masses along the global conveyor belt. The predominantly old and thus unradiogenic continental rocks present in the North Atlantic region, for instance, are responsible for the relatively unradiogenic Nd isotope composition of NADW, while the young mantle-derived Ocean Island Basalts surrounding the Pacific lead to relatively radiogenic Nd isotope compositions in this ocean basin. Hafnium and Pb, on the other hand, are scavenged even more efficiently than Nd (e.g. Rickli et al. 2009) and therefore lose their distinct isotope signatures much faster when advected over larger distances.

In the open ocean, as outlined above, the particle reactive elements show a nutrient-like vertical distribution due to reversible scavenging, i.e. the adsorption to and incorporation into particles at the surface, sinking and partial redissolution in greater depth (e.g. Siddall et al. 2008). Neodymium, Hf and Pb are removed from the water column with the particles, they are adsorbed to or are coprecipitated with Fe-Mn oxihydroxides forming encrustations of sediment grains, test fragments or rock surfaces (e.g. Koschinsky and Halbach 1995).

## *1.6 Major research goals*

### *1.6.1 Origin of incongruent behavior of radiogenic isotopes during continental weathering processes*

The decoupling of isotope signatures of Nd and Hf in seawater has previously been shown to be mainly caused by processes occurring during the weathering of continental rocks (e.g. van de Flierdt et al. 2007; Chen et al. 2013). Similarly, it has been demonstrated that radiogenic Pb isotope compositions of weathering solutions vary significantly over time when weathering conditions are changing (e.g. Erel et al. 1994, 2004; von Blanckenburg and Nägler 2001). However, the exact mechanisms releasing distinct isotope signatures to weathering solutions is not characterized sufficiently. Understanding how these dissolution processes work,

nevertheless, is essential when relating combined Nd-Hf isotope data of modern and paleoceanographic studies to present and past continental weathering conditions. The particularly important role of differential weathering of both very resistant minerals (such as zircon) as well as very reactive minerals (such as apatite) has already been suggested in earlier studies (Bayon et al. 2006; Rickli et al. 2013, 2017). This thesis aims to test these hypotheses under different experimental settings, simulating different weathering conditions with a particular focus on the effect of glacial activity on the continents.

### *1.6.2 Conservative and non-conservative processes governing the distribution of Nd and Hf in seawater*

The application of Nd and Hf isotopes as tracers of past ocean circulation is based on understanding the cycling and input mechanisms of Nd and Hf in the modern ocean. Ideally the two elements are delivered to the oceans solely from continental weathering and would then be conservatively mixed with the water masses. Earlier studies, however, have suggested that other non-conservative processes can significantly alter local Nd and Hf isotope distributions in seawater and therefore obscure the advected information. To this end it is necessary to evaluate, on a site-by-site basis, to which degree Nd and Hf isotope variability can be ascribed to changes in ocean circulation or to non-conservative/local inputs. In this thesis, the distribution of Nd and Hf concentrations and their isotopic compositions of surface and deep-water samples from 5 sites in the Bay of Biscay are presented. These data contribute to better understand quantitative water mass mixing and the relative impact of non-conservative behavior of Nd and Hf in this region.

### *1.6.3 Paleoceanographic application: long-term reconstructions of Atlantic Meridional Overturning Circulation and weathering inputs from combined Nd and Hf isotopes*

Since advanced analytical techniques to extract Hf isotope compositions from marine sediments have emerged only recently, there are only few studies combining the evolution of Nd and Hf isotopes as paleoceanographic tracers of ocean circulation and weathering inputs.

In this thesis, combined seawater radiogenic Hf and Nd isotope compositions were extracted from bulk sediment leachates and foraminifera of Site 1088, Ocean Drilling Program Leg 177, 2082 m water depth on the Agulhas Ridge in the Cape Basin of the Southern Ocean.

The new data provide a continuous reconstruction of long- and short-term changes in ocean circulation and continental weathering inputs since the mid-Miocene. Due to its intermediate water depth, Nd isotope signatures in the sediments of this core sensitively recorded changes in admixture of North Atlantic Deep Water to the Antarctic Circumpolar Current as a function of the strength of the Atlantic Meridional Overturning Circulation (AMOC). Hf isotopes, on the other hand, are not likely to be affected by changes in ocean circulation and thus document the long-term transition in dominant weathering inputs on the nearby continents.

## *1.7 Outline of the thesis and declaration of my own contribution to the following chapters*

Chapter 1 introduces geochemical background and principles of radiogenic isotopes of Nd, Hf and Pb in crustal rocks, marine sediments and seawater. Previous applications in paleoenvironmental and paleoceanographic studies are also presented. The major research questions including the origin of incongruent behavior of radiogenic isotopes during weathering and their impact on the application in long-term paleoceanographic studies are discussed.

Chapter 2 presents the principal chemical procedures applied to extract and purify the Nd-Hf fractions of leachates and detrital fractions from marine sediments, and seawater. The mass spectrometric measurements of Nd and Hf isotopes are also described in detail.

The following chapters 3, 4 and 5 address the research goals listed in section 1.6 following different approaches.

Chapter 3 (submitted to **Chemical Geology**) discusses the importance of the partial dissolution of accessory mineral phases during continental weathering for the distribution of Nd, Hf and Pb isotopes in the aqueous system based on a series of dissolution and leaching experiments of granitic rocks.

**Chapter 3 declaration:** Marcus Gutjahr proposed the study and him, Urs Schaltegger (University of Geneva) and myself collected the sample material. Kalin Kouzmanov performed the automated mineralogical analyses. I designed and carried out the experiment and the elemental and isotopic analyses, interpreted the data and wrote the manuscript. All co-authors helped improving the manuscript.

Chapter 4 describes conservative and non-conservative processes governing the distribution of Nd and Hf in water masses in the Bay of Biscay.

**Chapter 4 declaration:** Martin Frank proposed the study. Moritz Zieringer and Martin Frank collected the samples during RV Meteor cruise M84-5. I carried out the analyses, interpreted the data and wrote the chapter. Martin Frank revised and improved this chapter.

Chapter 5 (published in **Paleoceanography**, 32, 265-283, 2017) presents the extraction of seawater Nd and Hf isotope compositions from authigenic Fe-Mn fractions of marine sediments from the Atlantic Sector of the Southern Ocean for a long-term reconstruction of AMOC strength and weathering inputs from near-by continents since the mid-Miocene. The results include evidence for reduced overturning circulation during glacial episodes throughout the analyzed period of time.

**Chapter 5 declaration:** Martin Frank proposed the study. I have selected intervals to be analyzed and retrieved the sample material from the IODP core repository in Bremen. I carried out the analyses and interpretation and wrote the manuscript. All co-authors and three anonymous reviewers helped to improve the manuscript.

The last chapter (Chapter 6) presents a brief summary of this thesis and an outlook to future studies.

***References***

Albarède, F., Simonetti, A., Vervoort, J.D., Blichert-Toft, J. and Abouchami, W., 1998. A Hf-Nd isotopic correlation in ferromanganese nodules. *Geophysical Research Letters*, 25(20), p.3895.DOI:10.1029/1998GL900008

Arsouze, T., Dutay, J.-C., Lacan, F. and Jeandel, C., 2009. Reconstructing the Nd oceanic cycle using a coupled dynamical – biogeochemical model. *Biogeosciences Discussions*, 6(3), pp.5549–5588.DOI:10.5194/bgd-6-5549-2009

Barrett, T.J., Taylor, P.N. and Lugowski, J., 1987. Metalliferous Sediments from Dsdp-Leg-92 - the East Pacific Rise Transect. *Geochimica Et Cosmochimica Acta*, 51(9), pp.2241–2253.DOI:Doi 10.1016/0016-7037(87)90278-X

Bartoli, G., Sarnthein, M., Weinelt, M., Erlenkeuser, H., Garbe-Sch??nberg, D. and Lea, D.W., 2005. Final closure of Panama and the onset of northern hemisphere glaciation. *Earth and Planetary Science Letters*, 237(1–2), pp.33–44.DOI:10.1016/j.epsl.2005.06.020

Bau, M. and Koschinsky, A., 2006. Hafnium and neodymium isotopes in seawater and in ferromanganese crusts: The "element perspective." *Earth and Planetary Science Letters*, 241(3–4), pp.952–961.DOI:10.1016/j.epsl.2005.09.067

Bayon, G., Burton, K.W., Soulet, G., Vigier, N., Dennielou, B., Etoubleau, J., Ponzevera, E., German, C.R. and Nesbitt, R.W., 2009. Hf and Nd isotopes in marine sediments: Constraints on global silicate weathering. *Earth and Planetary Science Letters*, 277(3–4), pp.318–326.DOI:10.1016/j.epsl.2008.10.028

Bayon, G., Vigier, N., Burton, K.W., Brenot, A., Carignan, J., Etoubleau, J. and Chu, N.C., 2006. The control of weathering processes on riverine and seawater hafnium isotope ratios. *Geology*, 34(6), pp.433–436.DOI:10.1130/G22130.1

Berner, R.A., Lasaga, A.C. and Garrels, R.M., 1983. The carbonate-silicate geochemical cycle and its effect on atmospheric carbon dioxide over the past 100 million years. *American Journal of Science*, 283(7), pp.641–683.DOI:10.2475/ajs.283.7.641

Biastoch, A., Böning, C.W. and Lutjeharms, J.R.E., 2008. Agulhas leakage dynamics affects decadal variability in Atlantic overturning circulation. *Nature*, 456(7221), pp.489–492.DOI:10.1038/nature07426

Billups, K., 2002. Late Miocene through early Pliocene deep water circulation and climate change viewed from the sub-Antarctic South Atlantic. *Palaeogeography, Palaeoclimatology, Palaeoecology*, 185(3–4), pp.287–307.DOI:10.1016/S0031-0182(02)00340-1

von Blanckenburg, F. and Nägler, T.F., 2001. Weathering versus circulation controlled changes in radiogenic isotope tracer composition of the Labrador Sea and North Atlantic Deep Water. *Paleoceanography*, 16(4), pp.424–434.

Böhm, E., Lippold, J., Gutjahr, M., Frank, M., Blaser, P., Antz, B., Fohlmeister, J., Frank, N., Andersen, M.B. and Deininger, M., 2015. Strong and deep Atlantic meridional overturning circulation during the last glacial cycle. *Nature*, 517(7534), pp.73–76.DOI:10.1038/nature14059

Bouvier, A., Vervoort, J.D. and Patchett, P.J., 2008. The Lu-Hf and Sm-Nd isotopic composition of CHUR: Constraints from unequilibrated chondrites and implications for the bulk composition of terrestrial planets. *Earth and Planetary Science Letters*, 273(1–2), pp.48–57.DOI:10.1016/j.epsl.2008.06.010

Broecker, W.S., 1982. Ocean chemistry during glacial time. *Geochimica et Cosmochimica Acta*, 46(10), pp.1689–1705.DOI:10.1016/0016-7037(82)90110-7

Broecker, W.S., 1991. The Great Ocean Conveyor. *Oceanography*, 4(2), pp.79–89.

Broecker, W.S. and Peng, T.H., 1983. Tracers in the sea. *Geochimica et Cosmochimica Acta*, 47(7), p.1336.DOI:10.1016/0016-7037(83)90075-3

Carter, P., Vance, D., Hillenbrand, C.D., Smith, J.A. and Shoosmith, D.R., 2012. The neodymium isotopic composition of waters masses in the eastern Pacific sector of the Southern Ocean. *Geochimica et Cosmochimica Acta*, 79, pp.41–59.DOI:10.1016/j.gca.2011.11.034

Chen, J.H., Wasserburg, G.J., von Damm, K.L. and Edmond, J.M., 1986. The U-Th-Pb systematics in hot springs on the East Pacific Rise at 21°N and Guaymas Basin. *Geochimica et Cosmochimica Acta*, 50(11), pp.2467–2479.DOI:10.1016/0016-7037(86)90030-X

Chen, T.Y., Li, G., Frank, M. and Ling, H.F., 2013. Hafnium isotope fractionation during continental weathering: Implications for the generation of the seawater Nd-Hf isotope relationships. *Geophysical Research Letters*, 40(5), pp.916–920.DOI:10.1002/grl.50217

Chen, T.Y., Ling, H.F., Frank, M., Zhao, K.D. and Jiang, S.Y., 2011. Zircon effect alone insufficient to generate seawater Nd-Hf isotope relationships. *Geochemistry, Geophysics, Geosystems*, 12(5).DOI:10.1029/2010GC003363

Crocket, K.C., Foster, G.L., Vance, D., Richards, D.A. and Tranter, M., 2013. A Pb isotope tracer of ocean-ice sheet interaction: The record from the NE Atlantic during the Last Glacial/Interglacial cycle. *Quaternary Science Reviews*, 82, pp.133–144.DOI:10.1016/j.quascirev.2013.10.020

Dausmann, V., Frank, M., Siebert, C., Christl, M. and Hein, J.R., 2015. The evolution of weathering inputs and deep ocean circulation in the Arctic Ocean since the Late Miocene : Radiogenic isotope evidence. *Earth and Planetary Science Letters*, 419, pp.111–124.DOI:10.1016/j.epsl.2015.03.007

Erel, Y., Blum, J.D., Roueff, E. and Ganor, J., 2004. Lead and strontium isotopes as monitors of experimental granitoid mineral dissolution. *Geochimica et Cosmochimica Acta*, 68(22), pp.4649–4663.DOI:10.1016/j.gca.2004.04.022

Erel, Y., Harlavan, Y. and Blum, J.D., 1994. Lead isotope systematics of granitoid weathering. *Geochimica et Cosmochimica Acta*, 58(23), pp.5299–5306.DOI:10.1016/0016-7037(94)90313-1

Faure, G. and Mensing, T.M., 2005. *Isotopes : principles and applications*. 3rd Editio., Wiley.

van de Flierdt, T., Frank, M., Lee, D.C. and Halliday, A.N., 2002. Glacial weathering and the hafnium isotope composition of seawater. *Earth and Planetary Science Letters*, 201(3–4), pp.639–647.DOI:10.1016/S0012-821X(02)00731-8

van de Flierdt, T., Goldstein, S.L., Hemming, S.R., Roy, M., Frank, M. and Halliday, A.N., 2007. Global neodymium-hafnium isotope systematics - revisited. *Earth and Planetary Science Letters*, 259(3–4), pp.432–441.DOI:10.1016/j.epsl.2007.05.003

Frank, M., 2002. Radiogenic isotopes: Tracers of past ocean circulation and erosional input. *Reviews of Geophysics*, 40(1).DOI:10.1029/2000RG000094

German, C.R., Klinkhammer, G.P., Edmond, J.M., Mura, A. and Elderfield, H., 1990. Hydrothermal scavenging of rare-earth elements in the ocean. *Nature*, 345(6275), pp.516–518.DOI:10.1038/345516a0

Gutjahr, M., Frank, M., Halliday, A.N. and Keigwin, L.D., 2009. Retreat of the Laurentide ice sheet tracked by the isotopic composition of Pb in western North Atlantic seawater during termination 1. *Earth and Planetary Science Letters*, 286(3–4), pp.546–555.DOI:10.1016/j.epsl.2009.07.020

Gutjahr, M., Frank, M., Lippold, J. and Halliday, A.N., 2014. Peak Last Glacial weathering intensity on the North American continent recorded by the authigenic Hf isotope composition of North Atlantic deep-sea sediments. *Quaternary Science Reviews*, 99, pp.97–117.DOI:10.1016/j.quascirev.2014.06.022

Hain, M.P., Sigman, D.M. and Haug, G.H., 2010. Carbon dioxide effects of Antarctic stratification, North Atlantic Intermediate Water formation, and subantarctic nutrient drawdown during the last ice age: Diagnosis and synthesis in a geochemical box model. *Global Biogeochemical Cycles*, 24(4), pp.1–19.DOI:10.1029/2010GB003790

Hall, C. and Lutjeharms, J.R.E., 2011. Cyclonic eddies identified in the Cape Basin of the South Atlantic Ocean. *Journal of Marine Systems*, 85(1–2), pp.1–10.DOI:10.1016/j.jmarsys.2010.10.003

Halliday, A.N., Davidson, J.P., Holden, P., Owen, R.M. and Olivarez, A.M., 1992. Metalliferous sediments and the scavenging residence time of Nd near hydrothermal vents. *Geophysical Research Letters*, 19(8), pp.761–764.DOI:10.1029/92GL00393

Haug, G.H. and Tiedemann, R., 1998. Effect of the formation of the Isthmus of Panama on Atlantic Ocean thermohaline circulation. *Nature*, 393(6686), pp.673–676.DOI:10.1038/31447

Henderson, G.M. and Maier-Reimer, E., 2002. Advection and removal of 210Pb and stable Pb isotopes in the oceans: A general circulation model study. *Geochimica et Cosmochimica Acta*, 66(2), pp.257–272.DOI:10.1016/S0016-7037(01)00779-7

Hult, M., Vidmar, T., Rosengård, U., Marissens, G., Lutter, G. and Sahin, N., 2014. Half-life measurements of lutetium-176 using underground HPGe-detectors. *Applied Radiation and Isotopes*, 87, pp.112–117.DOI:10.1016/j.apradiso.2013.11.071

Jacobsen, S.B. and Wasserburg, G.J., 1980. Sm-Nd isoopic evolution of chondrites. *Earth and Planetary Science Letters*, 50(1), pp.139–155.

Kinoshita, N., Nakanishi, T. and Yokoyama, A., 2002. The half-life of Sm-147.

Koschinsky, A. and Halbach, P., 1995. Sequential leaching of marine ferromanganese precipitates: Genetic implications. *Geochimica et Cosmochimica Acta*, 59(24), pp.5113–5132.DOI:10.1016/0016-7037(95)00358-4

Kurzweil, F., Gutjahr, M., Vance, D. and Keigwin, L., 2010. Authigenic Pb isotopes from the Laurentian Fan: Changes in chemical weathering and patterns of North American freshwater runoff during the last deglaciation. *Earth and Planetary Science Letters*, 299(3–4), pp.458–465.DOI:10.1016/j.epsl.2010.09.031

Lacan, F. and Jeandel, C., 2005a. Acquisition of the neodymium isotopic composition of the North Atlantic Deep Water. *Geochemistry, Geophysics, Geosystems*, 6(12).DOI:10.1029/2005GC000956

Lacan, F. and Jeandel, C., 2005b. Neodymium isotopes as a new tool for quantifying exchange fluxes at the continent-ocean interface. *Earth and Planetary Science Letters*, 232(3–4), pp.245–257.DOI:10.1016/j.epsl.2005.01.004

Piotrowski, A.M., 2005. Temporal Relationships of Carbon Cycling and Ocean Circulation at Glacial Boundaries. *Science*, 307(5717), pp.1933–1938.DOI:10.1126/science.1104883

Piotrowski, A.M., Lee, D.-C., Christensen, J.N., Burton, K.W., Halliday, A.N., Hein, J.R. and Günther, D., 2000. Changes in erosion and ocean circulation recorded in the Hf isotopic compositions of North Atlantic and Indian Ocean ferromanganese crusts. *Earth and Planetary Science Letters*, 181(3), pp.315–325.DOI:10.1016/S0012-821X(00)00205-3

Rahmstorf, S., 2002. Ocean circulation and climate during the past 120,000 years. *Nature*, 419(6903), pp.207–214.DOI:10.1038/nature01090

Raymo, M.E., Grant, B., Horowitz, M. and Rau, G.H., 1996. Mid-Pliocene warmth: stronger greenhouse and stronger conveyor. *Marine Micropaleontology*, 27(1–4), pp.313–326.DOI:10.1016/0377-8398(95)00048-8

Raymo, M.E. and Ruddiman, W.F., 1992. Tectonic forcing of late Cenozoic climate. *Nature*, 359(6391), pp.117–122.DOI:10.1038/359117a0

Rempfer, J., Stocker, T.F., Joos, F., Dutay, J.C. and Siddall, M., 2011. Modelling Nd-isotopes with a coarse resolution ocean circulation model: Sensitivities to model parameters and source/sink distributions. *Geochimica et Cosmochimica Acta*, 75(20), pp.5927–5950.DOI:10.1016/j.gca.2011.07.044

Rickli, J., Frank, M., Baker, A.R., Aciego, S., de Souza, G., Georg, R.B. and Halliday, A.N., 2010. Hafnium and neodymium isotopes in surface waters of the eastern Atlantic Ocean: Implications for sources and inputs of trace metals to the ocean. *Geochimica et Cosmochimica Acta*, 74(2), pp.540–557.DOI:10.1016/j.gca.2009.10.006

Rickli, J., Frank, M. and Halliday, A.N., 2009. The hafnium–neodymium isotopic composition of Atlantic seawater. *Earth and Planetary Science Letters*, 280(1–4), pp.118–127.DOI:10.1016/j.epsl.2009.01.026

Rickli, J., Frank, M., Stichel, T., Georg, R.B., Vance, D. and Halliday, A.N., 2013. Controls on the incongruent release of hafnium during weathering of metamorphic and sedimentary catchments. *Geochimica et Cosmochimica Acta*, 101, pp.263–284.DOI:10.1016/j.gca.2012.10.019

Rickli, J., Gutjahr, M., Vance, D., Fischer-Gödde, M., Hillenbrand, C.-D. and Kuhn, G., 2014. Neodymium and hafnium boundary contributions to seawater along the West Antarctic continental margin. *Earth and Planetary Science Letters*, 394, pp.99–110.DOI:10.1016/j.epsl.2014.03.008

Rickli, J., Hindshaw, R.S., Leuthold, J., Wadham, J.L., Burton, K.W. and Vance, D., 2017. Impact of glacial activity on the weathering of Hf isotopes - observations from Southwest Greenland. *Geochimica et Cosmochimica Acta*, 215, pp.295–316.DOI:10.1016/j.gca.2017.08.005

Rutberg, R., Hemming, S. and Goldstein, S., 2000. Reduced North Atlantic Deep Water flux to the glacial Southern Ocean inferred from neodymium isotope ratios. *Nature*, 405(6789), pp.935–8.DOI:10.1038/35016049

Siddall, M., Khatiwala, S., van de Flierdt, T., Jones, K., Goldstein, S.L., Hemming, S. and Anderson, R.F., 2008. Towards explaining the Nd paradox using reversible scavenging in an ocean general circulation model. *Earth and Planetary Science Letters*, 274(3–4), pp.448–461.DOI:10.1016/j.epsl.2008.07.044

Sigman, D.M. and Boyle, E.A., 2000. Glacial/interglacial variations in atmospheric carbon dioxide. , 407(October), pp.859–869.

Steiger, R.H. and Jäger, E., 1977. Subcommission on geochronology: Convention on the use of decay constants in geo- and cosmochronology. *Earth and Planetary Science Letters*, 36(3), pp.359–362.DOI:10.1016/0012-821X(77)90060-7

Stichel, T., Frank, M., Rickli, J. and Haley, B. a., 2012. The hafnium and neodymium isotope composition of seawater in the Atlantic sector of the Southern Ocean. *Earth and Planetary Science Letters*, 317–318, pp.282–294.DOI:10.1016/j.epsl.2011.11.025

Vance, D. and Burton, K., 1999. Neodymium isotopes in planktonic foraminifera: A record of the response of continental weathering and ocean circulation rates to climate change. *Earth and Planetary Science Letters*, 173(4), pp.365–379.DOI:10.1016/S0012-821X(99)00244-7

Vervoort, J.D., Patchett, P.J., Blichert-Toft, J. and Albarède, F., 1999. Relationships between Lu-Hf and Sm-Nd isotopic systems in the global sedimentary system. *Earth and Planetary Science Letters*, 168(1–2), pp.79–99.DOI:10.1016/S0012-821X(99)00047-3

White, W.M., Patchett, J. and BenOthman, D., 1986. Hf isotope ratios of marine sediments and Mn nodules: evidence for a mantle source of Hf in seawater. *Earth and Planetary Science Letters*, 79(1–2), pp.46–54.DOI:10.1016/0012-821X(86)90039-7

Yu, J., Menviel, L., Jin, Z.D., Thornalley, D.J.R., Barker, S., Marino, G., Rohling, E.J., Cai, Y., Zhang, F., Wang, X., Dai, Y., Chen, P. and Broecker, W.S., 2016. Sequestration of carbon in the deep Atlantic during the last glaciation. *Nature Geoscience*, 9(4), pp.319–324.DOI:10.1038/ngeo2657

# 2 Methods

In this chapter a complete description of the applied analytical procedures for the extraction, purification and measurement of the seawater and sediment samples for Hf and Nd concentrations and isotope compositions is given. Further details concerning material and methodology, especially the experimental setup in chapter 3, are described in the material and methods subsections of the respective chapters.

## *2.1 Nd and Hf from seawater samples*

The procedures applied to extract and analyze Nd and Hf differ only little from those described in previous studies (e.g. Godfrey et al. 2009; Rickli et al. 2009; Zimmermann et al. 2009; Stichel et al. 2012) and the protocols follow the ones approved by the GEOTRACES program for the measurement of radiogenic Nd and Hf isotope compositions of seawater.

### *2.1.1 Sample collection and chemical procedures prior to ion chromatographic purification of the samples*

Sample volumes of 20 to 80 l were recovered from the entire water column using Niskin bottles mounted to a stainless steel CTD rosette and were subsequently collected in acid-cleaned 20 l LDPE-collapsible cubitainers and filtered through 0.45 µm Millipore® filters within 12 h after collection. The same happened for the surface water samples (between 20 and 140 l), which were collected using a stainless steel towed fish while the ship was underway. The filtered seawater samples were then acidified to pH ~2 using distilled concentrated nitric acid. From each sample an aliquot of 2 liters was kept: 1 liter for isotope dilution concentration analysis of Nd and Hf and another liter aliquot for the determination of REE concentrations by Online-Preconcentration ICP-MS and for potential other future measurements. About 5 mg iron (Fe) per liter, in the form of dissolved Fe-chloride ($FeCl_3$, ~ 200 mg Fe per ml) was added to the main sample volumes and equilibration was allowed for 24 hours. The Fe chloride had previously been cleaned by dissolution in 6 M HCl, liquid-liquid extraction with ether (whereby the trace metals stay in the acid) and subsequent back-extraction with de-ionized water. In a second step, ammonia solution (25%, suprapure) was added to bring the pH to 8 in order to co-precipitate the dissolved trace metals with FeOOH (i.e. Hf and Nd). The supernatant was discarded and the residual FeOOH precipitate was transferred into 2 L wide mouth LDPE-bottles for transport to the home laboratory.

The FeOOH precipitates were centrifuged for 10 minutes at 3500 rpm in the home laboratory at GEOMAR in Kiel (Germany) and rinsed at least three times with de-ionized water (18.2 MΩ) followed by centrifugation to wash out major ions (Ca, Mg, K etc.). The samples were then dissolved in the centrifuge tubes with distilled 6M HCl, transferred into 60ml Teflon vials and then evaporated to dryness on a hotplate over night. Subsequently 4 ml aqua regia were added and left for at least 24 hours at 110°C in the closed vials to destroy organic components. Thereafter the samples were evaporated to dryness again and transferred to Cl-form by adding 4 ml of 6M HCl followed by another evaporation step. Afterwards, 4 ml of 6M HCl was added to redissolve the samples. The previously added amount of Fe was subsequently reduced in order not to exceed resin capacity during the following ion chromatographic separation step. For this purpose the iron was extracted by adding a suitable amount (5-15 ml) of previously cleaned di-ethyl ether to the dissolved samples. The ether and the samples separate into two phases due to the density contrast and the iron was transferred into the ether phase by homogenization with a pipette tip, while the trace metals stayed in the acidic phase. The ether complex containing about 90% of the iron was siphoned off with a pipette and discarded for each sample. This procedure, which is from hereon referred to as Fe-extraction, was repeated twice or more often until the sample solutions became pale yellow. Most of the samples formed a jelly-like precipitate, which scavenged about 90% of the Hf from the sample. This precipitate was separated from the sample by centrifugation and dissolved by adding 2M HF. After evaporation, the remainder of the sample was added to this precipitate followed by another evaporation step.

### 2.1.2 *Preparation for isotope dilution measurements*

The chemical procedure followed the ones of Rickli et al. (2009) and Stichel et al. (2012). Previously weighed $^{180}$Hf-single spike and $^{150}$Nd/$^{149}$Sm double-spike solutions were added to an acidified 1 L aliquot of each sample. The samples were left for 4 to 5 days for complete isotopic equilibration, and 12 µl to 15 µl of $FeCl_3$ solution (~ 200 mg Fe per ml) were added to each sample. After 12 to 24 hours the Fe was co- precipitated at pH 7 to 8 by adding 300 µl to 600 µl of ammonia solution (25%, Merck® suprapure). The precipitates were transferred into centrifuge tubes, centrifuged for 10 minutes at 3500 rpm and washed three times with Milli-Q water during subsequent centrifugation steps. The washed samples were then transferred into Teflon vials using 300 µl of concentrated HCl. After evaporation 0.5 ml of 1M HCl / 0.05M HF was added to redissolve the samples for column chemistry (see below).

## 2.2 Extraction of trace metals from marine sediment samples

### 2.2.1 Bulk sediment leaching procedures

Seawater Nd and Hf isotope signatures were extracted from authigenic ferromanganese oxyhydroxide coatings of bulk sediment samples (approximately 3 g; freeze-dried) following the leaching protocol of Gutjahr et al. (2007). The carbonate fraction was partly removed by adding 20 ml 2.8M acetic acid, 1M Na-acetate (pH ~4) on a shaking table for 2.5 h in order to reduce the amount of the disturbing carbonate matrix (which can result in a less efficient removal of Yb during chromatographic separation). The authigenic Fe-Mn oxyhydroxide fraction was subsequently dissolved in 25 ml 0.005M hydroxylamine hydrochloride, 1.5% acetic acid, and 0.03M Na-EDTA solution (HH) buffered to pH4 with suprapure NaOH for 90 min at room temperature (i.e., 10 times diluted relative to concentrations used by Gutjahr et al. 2007). Subsequently, the samples were centrifuged and the supernatants were dried and redissolved for ion exchange chromatography (see below).

### 2.2.2 Total dissolution

Bulk sample residues processed to extract seawater signatures (section 2.2.1) were further treated with a stronger reductive leaching solution (0.025 M HH) for 1 day to ensure complete removal of remaining Fe-Mn oxyhydroxides. Afterward, the samples were dried, ground, and 5% $H_2O_2$ was added for 72 h to oxidize organics that might otherwise disturb chemical purification. The samples were then further treated in aqua regia on a hotplate at 140°C preceding digestion in a mixture of concentrated $HNO_3$ and HF in steel jacketed high-pressure bombs at ~180–200°C for 4 days. After subsequent evaporation, fluorides that formed during cooking in concentrated HF were removed by the reaction with 1 ml perchloric acid, evaporating at ~180-190°C. Remaining perchloric acid was removed by evaporation together with concentrated $HNO_3$ multiple times at ~180-190°C. Finally, the samples were transferred into chloride form and redissolved for ion exchange chromatography (see below).

### 2.2.3 Extraction from foraminifera tests

Seawater Nd isotope signatures were also extracted from "uncleaned" mixed planktonic foraminifera samples following the procedure first described by Roberts et al. (2010). On average, 125mg of foraminifera tests were handpicked from the size fraction >315µm under a light microscope from freeze-dried and clay-free (wet-sieved at 63µm) sediment samples. The microfossil shells were subsequently cracked between glass plates to ensure that all chambers were opened and were ul-

trasonicated several times in deionized water and then in ethanol to ensure the removal of most of the clays and other silicate particles. The carbonates and associated ferromanganese coatings of the samples were then progressively dissolved by stepwise addition of dilute nitric acid. The solution was then centrifuged to ensure removal of smallest detrital particles, and subsequently transferred into chloride form before redissolving for ion exchange chromatography (see below).

## *2.3 Ion exchange chromatography*

For the analysis of Nd, Hf and Pb isotope ratios on a MC-ICP-MS, it is essential to previously isolate and pre-concentrate the elements to be measured. Therefore, dissolution and pre-concentration procedures described above are all followed by ion exchange chromatography separating Nd, Hf and Pb from other elements and chemical compounds that can cause isobaric interferences and matrix effects, respectively, during measurement.

### *2.3.1 Ion exchange chromatographic purification of Nd and Hf for isotope dilution measurements*

Neodymium and Hf separation was achieved by a cation chromatographic column separation step (1.4ml BIORAD® AG50W-X8, 200–400 µm mesh-size; Table 2.1). Hafnium was collected directly after loading onto the resin bed and washed down completely by adding another 2 ml of 1M HCl / 0.05M HF. Neodymium was eluted having washed out the Fe in 5 ml of 3M HCl and subsequently the barium (Ba) in 12 ml 2M $HNO_3$. The application of a $^{180}Hf$ spike required an additional step of column separation removing interfering $^{180}W$ from the first Hf cut (1.6ml BIO-RAD® AG1X-8 resin $Cl^-$ form, 200-400 µm mesh-size; Table 2.2) following the protocol of Sahoo et al. (2006). The respective Hf and Nd cuts were evaporated to dryness. Organic components were chemically removed prior to measurement on the MC-ICPMS by 0.5ml 0.5MHNO3/0.1MHF + 100µl H2O2 and 0.5MHNO3 + 100µl H2O2 for Hf and Nd, respectively.

**Table 2.1: AG50W-X8 (200-400 µm mesh-size, 1.4 ml resin bed) column chemistry.**

| Step | Volume | Reagent |
|---|---|---|
| Pre-clean | 10 ml | 6MHNO$_3$/0.5 M HF |
| Change the acid | 2 x 1 ml | MQ |
| Pre-clean | 0.5 ml | 1MHCl/0.05 HF |
| Pre-condition | 1 ml | 1MHCl/0.05 HF |
| Load and directly collect Hf | 1 ml | 1MHCl/0.05 HF (sample) |
| Collect Hf | 1.5 ml | 1MHCl/0.05 HF |
| Elute Fe | 5 ml | 3M HCl |
| Change the acid | 2 x 1 ml | MQ |
| Elute Ba | 10 ml | 2M HNO$_3$ |
| Collect Nd/REE | 6.5 ml | 6M HNO$_3$ |
| clean | 10 ml | 6M HNO$_3$/ 0.5M HF |
| Pass/store | 2 + 3 ml | MQ |

**Table 2.2: BIORAD® AG1X-8 ($Cl^-$ form, 200-400 µm mesh-size, 1.6ml resin bed) column chemistry.**

| Step | Volume | Reagent |
|---|---|---|
| Cleaning | 8 ml | 9M HCl/1M HF |
| Cleaning | 2 x 8 ml | MQ |
| Pre-condition | 8 ml | 0.1 M HF |
| Load the sample | 2 ml | 0.1 M HF (sample) |
| Elute Fe, Ti | 4 ml | 0.1 M HF + 2% $H_2O_2$ |
| Elute Zr, Ti (Hf) | 3 ml | 1 M HF + 0.2% $H_2O_2$ |
| Wash resin | 3 ml | MQ |
| Collect Hf | 6 + 2 ml | 6M HCl |
| Cleaning, elute W | 8 ml | 9M HCl/1M HF |
| Pass/Store | 2 + 3 ml | MQ |

### 2.3.2 *Ion exchange chromatography for isotope compositions measurements of Nd, Hf and Pb*

After extraction from their original phase the pre-concentrated sample solutions were dissolved and loaded onto columns containing ion exchange resins designed for the separation of ions as a function pH and presence of certain chemicals.

For the analysis of Pb, 10% of the total amount of the dissolved samples was passed through anion exchange columns, filled with 100 µl of AG1-X8 resin, mesh size 100-200 µm following a slightly modified version of the procedure of Galer and O'Nions (1989) shown in Table 2.3. For the isolation of Nd and Hf, the rest of the sample (in the case of the seawater samples the entire sample) was loaded onto cation exchange columns filled with 0.8 ml AG 50WX8 resin, mesh size 200-400 µm, to separate High Field Strength Elements (HFSE; including Hf) from REE (including Nd) following the elution scheme in Table 2.1. Then the HFSE and REE cuts were

each further purified using 1ml Eichrom®Ln-Spec (100-150µm; Table 2.4) following Münker et al. (2001) and 2 ml Eichrom® Ln-Spec (50-100 µm mesh size; Table 2.5) resin following Pin and Zalduegui (1997), respectively.

**Table 2.3: AG1-X8 resin ($NO_3^-$ form, 100-200 µm mesh size, ~100 µl resin bed) column chemistry for Pb purification.**

| Step | Volume | Reagent |
|---|---|---|
| Clean resin | 2 x 1 ml | 0.25M $HNO_3$ |
| Condition | 2 x 100 µl | 0.5M $HNO_3$ – 0.2M HBr |
| Load sample | 300 µl | 0.5M $HNO_3$ – 0.2M HBr |
| Elute matrix | 100 µl | 0.5M $HNO_3$ – 0.2M HBr |
| Elute matrix | 100 µl | 0.5M $HNO_3$ – 0.2M HBr |
| Elute matrix | 150 µl | 0.5M $HNO_3$ – 0.2M HBr |
| Elute matrix | 150 µl | 0.5M $HNO_3$ – 0.2M HBr |
| Collect Pb | 150 µl | 0.5M $HNO_3$ – 0.03M HBr |
| Collect Pb | 300 µl | 0.5M $HNO_3$ – 0.03M HBr |
| Collect Pb | 300 µl | 0.5M $HNO_3$ – 0.03M HBr |

**Table 2.4: Eichrom® Ln-Spec (100-150 µm mesh size; 1 ml resin bed) column chemistry for Hf purification.**

| Step | Volume | Reagent |
|---|---|---|
| Pre-cleaning | 15 ml | 6MHCl |
| Pre-cleaning | 15 ml | 2M HF |
| Wash HF | 2 ml | 3M HCl |
| Conditioning | 2 x 3 ml | 3MHCl |
| Add ascorbic acid to each sample/Load the sample | 4 ml+0.8 ml | 3MHCl+ 0.4M ascorbic acid |
| Elute matrix, REE | 2 x 25 ml | 6M HCl |
| Change the acid | 2 x 3 ml | MQ |
| Elute Ti | 30 ml | 0.45M$HNO_3$+ 0.09M citric acid + 1%wt $H_2O_2$ |
| Change the acid | 2 x 3 ml | MQ |
| Elute Zr | 5 ml | 2MHCl+0.1M HF |
| Collect Hf | 6 ml | 3MHCl+0.2M HF |
| Clean | 25 ml | 6M HCl |
| Clean | 25 ml | 2MHF |
| Pass/store | 3 ml | 1M HCl |

**Table 2.5: Eichrom® Ln-Spec resin (50-100 µm mesh size, 2 ml resin bed) column chemistry for Nd purification.**

| Step | Volume | Reagent |
|---|---|---|
| Pre-clean | 8 ml | 6M HCl |
| Pre-conditioning | 0.5 ml | 0.1M HCl |
| Pre-conditioning | 1 ml | 0.1M HCl |
| Load sample | 0.5 ml | 0.1M HCl |
| Wash in/elute Ba | 0.5 ml | 0.1M HCl |
| Elute LREE | 7.5 ml | 0.25M HCl |
| Collect Nd | 5 ml | 0.25M HCl |
| Clean | 8 ml | 6M HCl |
| Pass and store | 1+1 ml | 0.3M HCl |

## *2.4 Mass spectrometry*

### *2.4.1 Precise Nd and Hf concentration measurements using isotope dilution*

The measurement of Nd and Hf concentrations is based on the addition of a known amount of spike-solutions that are artificially enriched in the isotopes $^{150}$Nd ($^{150}$Nd/$^{144}$Nd = 199.6356) and $^{180}$Hf ($^{180}$Hf/$^{178}$Hf = 42.6962) in comparison to the natural ratios ($^{150}$Nd/$^{144}$Nd = 0.235873 and $^{180}$Hf/$^{178}$Hf =1.285879) to 1 liter aliquots of the samples. After the chemical treatment described above the isotope ratios were measured on a Nu Plasma (Nu Instruments Limited). These ratios are a combination of the relative abundances present in the spike and those of the samples and depend on the amount of spike added and the amount of Nd and Hf in the samples. To minimize the uncertainty of an ID measurement it is ideal to reach the optimum abundance ratios of $^{150}$Nd/$^{144}$Nd = 6.86 and $^{180}$Hf/$^{178}$Hf = 7.41 (see Stichel, 2010 and Chen, 2013). Thus, it is important to estimate the amount of Nd and Hf expected for a particular sample (e.g. from literature data of nearby locations or previous rough measurement). The detailed calculations of the ID method are described in Stichel (2010) and in Chen (2013).

## *2.5 Acquisition of Nd, Hf and Pb isotope ratios*

Most Nd, Hf and Pb isotope data were measured on a Neptune Plus (Thermo Scientific) MC-ICP-MS at GEOMAR, Kiel. Gain calibration for the Faraday cup was performed on the same day before the samples were measured and samples were introduced into the mass spectrometer dissolved in the carrier acid 0.5 M $HNO_3$ (for Nd and Pb) or 0.5 M $HNO_3$ 0.1 M HF (for Hf).

Before the actual isotope measurements were conducted, sample concentrations were estimated by diluting a small fraction of the sample in the carrier acid. Measuring sample intensities together with a series of standards with different con-

centrations allowed the approximation of sample concentrations, which were then adjusted to match those of the standards measured together with the samples. Instrumental mass bias was corrected applying an exponential mass fractionation law with a natural $^{176}Hf/^{177}Hf$ ratio of 0.7325 and $^{143}Nd/^{144}Nd$ of 0.7219, respectively. Additionally, mass bias correction during Nd isotope measurements on the Neptune Plus for samples with $^{140}Ce/^{144}Nd < 1$ were carried out following the approach of Vance and Thirlwall (2002). Mass bias correction during Pb isotope analyses was done externally using the Tl-doping technique (Belshaw et al. 1998) via addition of a NIST997 Tl standard solution (Pb:Tl = ~4:1). Given that Tl and Pb fractionate slightly differently during ionisation (cf. Vance and Thirlwall 2002) $^{205}Tl/^{203}Tl$ were determined on a session by session basis so that NBS981 Pb isotope compositions matched published compositions of Baker et al. (2004). Standard concentrations for all analyzed elements were adjusted to sample concentrations of each measurement batch based on the above-mentioned concentration approximation and the desolvating unit (Aridus II) was rinsed with a solution of 0.5M HNO3-0-05M HF between samples to ensure proper washout of both Pb and Tl. $^{176}Hf/^{177}Hf$ ratios of all samples were normalized to JMC475 = 0.282160 (Nowell et al. 1998). $^{143}Nd/^{144}Nd$ ratios were normalized to JNdi-1 = 0.512115 (Tanaka et al. 2000). Pb isotope ratios were normalized to NIST NBS981 ($^{206}Pb/^{204}Pb$ = 16.9416, $^{207}Pb/^{204}Pb$ = 15.4998 and $^{208}Pb/^{204}Pb$ = 36.7249; Baker et al. 2004).

## References

Baker, J., Peate, D., Waight, T. and Meyzen, C., 2004. Pb isotopic analysis of standards and samples using a 207Pb–204Pb double spike and thallium to correct for mass bias with a double-focusing MC-ICP-MS. *Chemical Geology*, 211(3), pp.275–303.DOI:10.1016/j.chemgeo.2004.06.030

Belshaw, N.., Freedman, P.., O'Nions, R.., Frank, M. and Guo, Y., 1998. A new variable dispersion double-focusing plasma mass spectrometer with performance illustrated for Pb isotopes. *International Journal of Mass Spectrometry*, 181(1–3), pp.51–58.DOI:10.1016/S1387-3806(98)14150-7

Chen, T., 2013. *The geochemical cycling and paleoceanographic application of combined oceanic Nd - Hf isotopes*. Dissertation. Christian-Albrechts-Universität zu Kiel.

Galer, S. and O'Nions, R., 1989. Chemical and isotopic studies of ultramafic inclusions from the San Carlos volcanic field, Arizona: A bearing on their petrogenesis. *Journal of Petrology*, 30(4), pp.1033–1064.DOI:10.1093/petrology/30.4.1033

Godfrey, L. V., Zimmermann, B., Lee, D.-C., King, R.L., Vervoort, J.D., Sherrell, R.M. and Halliday, A.N., 2009. Hafnium and neodymium isotope variations in NE Atlantic seawater. *Geochemistry, Geophysics, Geosystems*, 10(8), p.n/a-n/a.DOI:10.1029/2009GC002508

Gutjahr, M., Frank, M., Stirling, C.H., Klemm, V., van de Flierdt, T. and Halliday, A.N., 2007. Reliable extraction of a deepwater trace metal isotope signal from Fe-Mn oxyhydroxide coatings of marine sediments. *Chemical Geology*, 242(3–4), pp.351–370.DOI:10.1016/j.chemgeo.2007.03.021

Münker, C., Weyer, S., Scherer, E. and Mezger, K., 2001. Separation of high field strength elements (Nb, Ta, Zr, Hf) and Lu from rock samples for MC-ICPMS measurements. *Geochemistry, Geophysics, Geosystems*, 2(12).DOI:10.1029/2001GC000183

Nowell, G.M., Kempton, P.D., Noble, S.R., Saunders, A.D., Mahoney, J.J. and Taylor, R.N., 1998. High-precision Hf isotopic measurements of MORB and OIB by thermal ionization mass-spectrometry: insights into the depleted mantle. *Chemical Geology*, 149(3), pp.211–233.

Pin, C. and Zalduegui, J.F.S., 1997. Sequential separation of light rare-earth elements, thorium and uranium by miniaturized extraction chromatography: Application to isotopic analyses of silicate rocks. *Analytica Chimica Acta*, 339(1–2), pp.79–89.DOI:10.1016/S0003-2670(96)00499-0

Rickli, J., Frank, M. and Halliday, A.N., 2009. The hafnium–neodymium isotopic composition of Atlantic seawater. *Earth and Planetary Science Letters*, 280(1–4), pp.118–127.DOI:10.1016/j.epsl.2009.01.026

Roberts, N.L., Piotrowski, A.M., McManus, J.F. and Keigwin, L.D., 2010. Synchronous deglacial overturning and water mass source changes. *Science (New York, N.Y.)*, 327(5961), pp.75–78.DOI:10.1126/science.1178068

Sahoo, Y. V, Nakai, S. and Ali, A., 2006. Modified ion exchange separation for tungsten isotopic measurements from kimberlite samples using multi-collector inductively coupled plasma mass spectrometry. *Analyst*, 131(3), pp.434–439.DOI:10.1039/b511557d

Stichel, T., 2010. *Tracing water masses and continental weathering by neodymium and hafnium isotopes in the Atlantic sector of the Southern Ocean*. Dissertation. Christian-Albrechts-Universität zu Kiel.

Stichel, T., Frank, M., Rickli, J. and Haley, B. a., 2012. The hafnium and neodymium isotope composition of seawater in the Atlantic sector of the Southern Ocean. *Earth and Planetary Science Letters*, 317–318, pp.282–294.DOI:10.1016/j.epsl.2011.11.025

Tanaka, T., Togashi, S., Kamioka, H., Amakawa, H., Kagami, H., Hamamoto, T., Yuhara, M., Orihashi, Y., Yoneda, S., Shimizu, H., Kunimaru, T., Takahashi, K., Yanagi, T., Nakano, T., Fujimaki, H., Shinjo, R., Asahara, Y., Tanimizu, M. and Dragusanu, C., 2000. JNdi-1: A neodymium isotopic reference in consistency with LaJolla neodymium. *Chemical Geology*, 168(3–4), pp.279–281.DOI:10.1016/S0009-2541(00)00198-4

Vance, D. and Thirlwall, M., 2002. An assessment of mass discrimination in MC-ICPMS using Nd isotopes. *Chemical Geology*, 185(3), pp.227–240.DOI:10.1016/S0009-2541(01)00402-8

Zimmermann, B., Porcelli, D., Frank, M., Andersson, P.S., Baskaran, M., Lee, D.C. and Halliday, A.N., 2009. Hafnium isotopes in Arctic Ocean water. *Geochimica et Cosmochimica Acta*, 73(11), pp.3218–3233.DOI:10.1016/j.gca.2009.02.028

# 3 Experimental evidence for a mineral-controlled release of radiogenic Nd, Hf and Pb isotopes from granitic rocks during changing weathering conditions

**Submitted to ChemGeol as:** Dausmann, V., Gutjahr, M., Frank, M., Kouzmanov, K. and Schaltegger, U.: Experimental evidence for a mineral-controlled release of radiogenic Nd, Hf and Pb isotopes from granitic rocks during changing weathering conditions.

## Abstract

The role of accessory minerals in the incongruent release of Hf and Pb during continental weathering and its implications for the generation of distinct seawater isotope compositions has been invoked in a number of studies. Accordingly, the Hf and Pb isotope signatures released by dissolution of rocks are the result of the relative abundances of minerals with distinct radiogenic and unradiogenic compositions and differences in their resistance to dissolution. To date, however, there has not been a comprehensive experimental investigation of these processes. The present study provides first combined quantitative experimental evidence for the impact of the mineralogy of granitic rocks on incongruent weathering of Nd, Hf and Pb isotopes. Combined with major and rare earth element concentrations our new isotope data reveal systematic preferential release of radiogenic Nd, Hf and Pb isotopes primarily controlled by dissolution characteristics of the host rock's accessory and major minerals. The data demonstrate a high degree of coherence between all isotope systems, which suggests preferential dissolution of labile accessory minerals, in particular apatite and sphene, dominating the release of radiogenic Nd, Hf and Pb during weak chemical weathering. Moreover, Pb isotope signatures of incipient weathering conditions, contrary to expectations, indicate congruent release of Pb from freshly exposed mineral surfaces. During more intense chemical weathering, as well as increased physical weathering conditions, the dissolution of major minerals (i.e. feldspars) becomes dominant for Nd and Pb isotope signatures, whereas Hf isotopes are still dominated by contributions from radiogenic accessories. Leaching experiments of zircon separates were performed to test the specific role of zircons for Hf isotope compositions. It is demonstrated that zircon is more efficiently dissolved when physical weathering is enhanced. This increased Hf release from partial zircon dissolution, however, is not large enough to explain less radiogenic Hf isotope signatures in seawater during episodes of enhanced mechanical erosion. Moreover, observed additions of Hf from the more congruent dissolution of the zircon-free fractions due to increased physical weathering indicate that these minerals also play an important role in controlling Hf isotope signatures released under deglacial conditions. Our results document the important role of contributions from accessory minerals as a major source of variations in the isotope

compositions of Nd, Hf and Pb released during changing weathering conditions on the continents.

## *3.1 Introduction*

The distribution patterns of the radiogenic isotope compositions of Nd, Hf and Pb dissolved in oceans and rivers have been shown to respond sensitively to changes in water mass provenance and mixing as well as to variable weathering conditions on the continents (Silver et al. 1980; Patchett et al. 1984; White et al. 1986; Erel et al. 1994; Vance and Burton 1999; Öhlander et al. 2000; Harlavan and Erel 2002; van de Flierdt et al. 2002, 2004, 2007). In particular, the combined analysis of the Sm-Nd, Lu-Hf and U-Th-Pb systems provides powerful tools to investigate present-day continental weathering regimes and linked environmental conditions as well as their evolution over time (Albarède et al. 1998; Vervoort et al. 2011; Chen et al. 2012; Gutjahr et al. 2014; Dausmann et al. 2015, 2017; Bayon et al. 2016).

Principally, dissolved radiogenic Nd, Hf and Pb isotope compositions in weathering solutions are controlled by changes of the intensity of chemical and physical weathering, which depend on a variety of environmental factors including precipitation, temperature, timescales of water-rock interaction, the presence of continental ice (shields), oxygenation, the activity of organisms and many more. In addition to that, the age and lithological properties of weathered rocks exert an important influence on the transfer of radiogenic isotope signatures to weathering solutions. The physical and chemical properties of major and accessory rock-forming minerals determine its susceptibility to chemical or physical weathering. Furthermore, these rock-forming minerals vary significantly in their elemental Sm-Nd, Lu-Hf and U-Th-Pb compositions. The preferential dissolution or retention of particular mineral phases commonly leads to incongruent behavior of the respective isotope systems during weathering and may result in isotope compositions of the weathered runoff signals vastly different from those of the bulk rocks.

It has been demonstrated that Sm and Nd are fractionated during weathering processes, with Sm/Nd in weathering residues increasing with progressing alteration (e.g. Öhlander et al. 1996, 2000; Andersson et al. 2001) and resulting in Nd isotopic compositions of the weathered rocks and soils more radiogenic than those of unweathered host rocks. At the same time Nd isotopic compositions of the rivers draining these soils showed less radiogenic values in a field study from northern Sweden (Andersson et al. 2001). This has been attributed to enhanced release of relatively unradiogenic Nd lost with Rare Earth Element (REE) rich minerals such as monazite and allanite, which are preferentially dissolved during weathering.

Fractionation of Hf isotopes during weathering processes is even more pronounced, leading to the generation of typical Hf-Nd isotope relationships in global seawater (Albarede et al., 1998) most likely caused by two mineral-controlled effects. The so-called “zircon effect” describes the preferential retention of unradiogenic Hf in zircon which has been suggested as the principal mechanism controlling incongruent weathering of Hf isotopes (e.g. White et al. 1986; Albarède et al. 1998; David et al. 2001). This is based on the fact that zircons, which host most of a whole rock’s Hf (e.g. Garçon et al. 2013b), are highly resistant to chemical weathering (e.g. Balan et al. 2001) and thus efficiently retain unradiogenic Hf thereby preventing its transfer to weathering solutions, which has been shown to dominate the Hf isotope budget of the ocean (e.g. Bayon et al. 2006, 2009; van de Flierdt et al. 2007).

A second process suggested to contribute to the incongruent weathering of Hf is the preferential dissolution and release of a labile and highly radiogenic Hf fraction from Lu-rich accessory minerals (e.g. apatite, sphene) in the zircon-free portions of a rock termed the "phosphate effect" (Bayon et al. 2006; Godfrey et al. 2008, 2009), which has been proposed to explain highly radiogenic dissolved Hf isotope signatures in rivers of the Moselle Basin and the Hudson River. The relative importance of this readily accessible radiogenic Hf fraction increases with the incompleteness of chemical dissolution processes and therefore also depends on residence times and reactivity of weathering solutions at the site of weathering (Bayon et al. 2009, 2016; Rickli et al. 2017). Accordingly, the incongruence produced during weathering of Hf isotopes has been shown to be dependent on run-off and climatic conditions in the drainage basins in a broad variety of different settings (Rickli et al. 2010, 2013; Bayon et al. 2016). This was further complemented by observations of Gutjahr et al. (2014) who concluded that less congruent release of Hf was caused by the transition from a dominantly cold-based to a warm-based Laurentide Ice Sheet linked to increased leaching of Lu-rich minerals in sub-glacial deposits. Another logical implication of the preferential dissolution of easily alterable minerals is that Hf isotopes released during weathering should gradually become more congruent with increasing soil maturation (age), which has, however, not been assessed to date (Ma et al. 2010; Bayon et al. 2016).

The interplay and variable relative importance of these effects are most likely also reflected in past seawater Hf isotope records. Long-term records obtained from Fe-Mn crusts indicate that Hf isotopes have been weathered more congruently since the intensification of the Northern Hemisphere glaciation at 2.8 Ma (Piotrowski et al. 2000; van de Flierdt et al. 2002; Dausmann et al. 2015). This was further demonstrated for stadial and high glacial periods of the last glacial cycle based on Fe-Mn oxyhydroxide leachates of sediment cores from the Blake Ridge (Gutjahr et al. 2014) and central Artic sediments (Chen et al. 2012). Based on these interpretations it has

been hypothesized that enhanced mechanical erosion and physical weathering caused by the continental ice sheets made parts of the unradiogenic Hf bound in the zircon fraction available to chemical weathering (decreased zircon effect). This is based on the increase of the reactive surface of these minerals during glacial grinding (cf. Anderson 2007).

Different stages and intensities of silicate weathering have been simulated experimentally (e.g. Erel et al. 1994, 2004; Harlavan et al. 1998; Harlavan and Erel 2002). The results showed that the incongruent release of radiogenic Pb follows the preferential sequential dissolution of particular mineral phases during the dissolution of granitic rocks. Based on Pb isotopes and REE patterns, Harlavan and Erel (2002) demonstrated that weathering solutions are dominated by the dissolution of accessory minerals such as allanite, apatite and sphene during the early stages of granitoid weathering, represented by increased $^{206}Pb/^{207}Pb$ and $^{208}Pb/^{207}Pb$ ratios and REE patterns in solution compared to those of the bulk rock itself. The release of radiogenic Pb is further favored by the damage of mineral lattices at the site of radioactive decay of the parent U or Th isotopes known as α-recoil effect (e.g. Silver et al. 1980; Fleischer 1982). Once these accessory minerals are mostly lost the dissolution of feldspars (evident by increased release of unradiogenic Pb) and refractory minerals starts to govern Pb isotope signatures and REE patterns in weathering solutions. Furthermore, Erel et al. (2004) have been able to relate these stages of granitoid weathering to the duration of exposure to weathering conditions in temperate climates by comparison with field measurements in soil chrono-sequences from the Wind River and the Sierra Nevada Mountains (USA).

The presence of large ice-sheets on nearby continents has been shown to modify weathering inputs into the nearby ocean basins as evident from Fe-Mn crusts and authigenic phases in marine sediments (von Blanckenburg and Nägler 2001; Foster and Vance 2006; Gutjahr et al. 2009; Kurzweil et al. 2010; Crocket et al. 2012, 2013). Vance et al. (2009) suggested that reactive soil substrate is produced during glacial periods and weathered effectively during the following interglacials and may thus contribute to high time-integrated silicate weathering rates.

In summary, the Nd, Hf and Pb isotope compositions of weathering inputs into seawater (and finally the oceanic budget) is ultimately controlled by the interplay of environmental parameters such as host rock and soil age, morphology, climatic boundary conditions including glacial activity, temperature and precipitation. The impact of these key variables further depend on the mineralogical composition of weathered rocks, in particular the presence of specific accessory minerals. However, to date the significance of these parameters for each isotope system is not well constrained.

It is the main goal of this study to simulate incipient chemical weathering following mechanical grinding (glacial weathering) of essentially unweathered zircon-bearing rocks, in order to better understand the processes controlling the release of Hf, Nd and Pb isotopes from zircons and the zircon-free fraction to weathering solutions and into the dissolved (riverine/marine) reservoir. These results are compared to equivalent leaching experiments of sediments derived from the same parent rock, which had already experienced (de-)glacial weathering. The specific role of zircon minerals for a more congruent release of Hf (and Pb) during glacial weathering is assessed by dissolution experiments of ground and non-ground zircon mineral separates.

## *3.2 Experimental Setup and Analytical Procedure*

### *3.2.1 Sampling and Material*

In total approximately 20 kg of unweathered and partly weathered (sediments from a small streambed) granite were collected in early September 2014 close to the Damma glacier in Switzerland. All sampled rocks belong to the Central Aar Granite with an age of 298±2 Ma (Schaltegger and Corfu 1992), which is part of a group of Variscan granitoid plutons that intruded an older basement between 350 and 295 Ma ago.

Three different facies of fresh granite (Gf1, 2 and 3) were selected to cover different formation conditions and thus mineral compositions. All three granite samples are metaluminous, calc-alkaline and have experienced a low-grade metamorphic overprint during the Alpine orogeny, which did, however, not strongly alter the original mineralogical composition (Ca-rich garnet and possibly muscovite are most likely of Alpine origin). Sample Gf2 exhibits slight foliation, indicating a higher degree of ductile shearing during Alpine tectonic processes. A detailed description of the mineralogical composition of the analyzed granite samples is provided below in section 3.3.2.

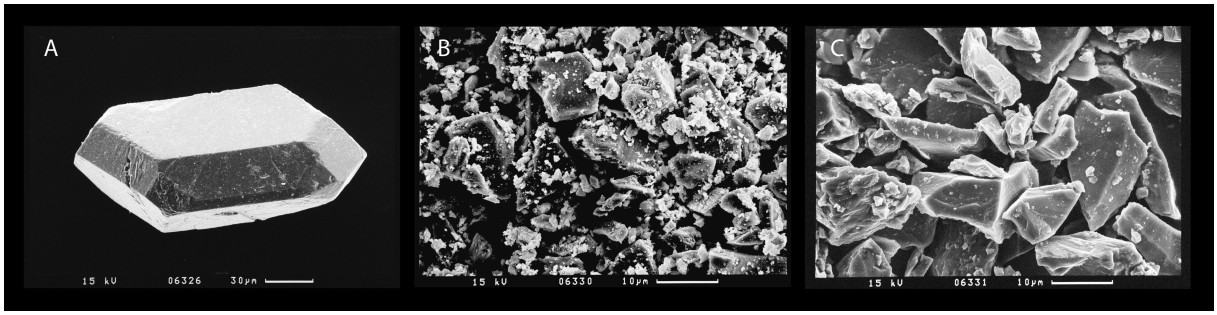


**Figure 3.1: Scanning electron microscope images of different stages in the zircon leaching experiment. (A) shows a pristine zircon mineral grain as leached in subgroup N. (B) depicts ground zircon material directly after grinding and before any leaching. (C) shows ground zircon material after all incomplete leaching steps. Note that the fine fraction (<3µm) was essentially lost completely (either due to dissolution or washed away) during the leaching experiment.**

All collected material was prepared for the leaching experiments in the facilities of the University of Geneva. Granite samples were crushed and milled to grain-sizes smaller than 400µm using a jaw crusher and a steel ring mill. Subsequent mineral separation by density was achieved using a Wilfley-table. The heavy mineral fraction was then further parted by magnetic separation (Frantz magnetic separator) in two steps (0.5 A and 1.5 A current). Minerals that were not magnetic at a current of 1.5 A were further separated by heavy liquids (3.32 g/cm$^2$). Minerals heavier than the heavy liquid mostly comprised zircons, which were kept for the leaching experiment (group Z). Zircon fractions of the three granite facies were kept separate. Aliquots of the zircon fractions were manually milled to a fine powder using an agate mortar directly before the leaching procedure was started. Images of some of the zircon aliquots were taken under large magnification using a scanning electron microscope at the Institute for Geosciences of the University of Kiel (Figure 3.1).

Aliquotes of mixed samples of all three granite facies after crushing (grain-sizes from gravel to clay; termed grains) and fine milling (agate disk mill; grains <125 µm; termed powders) were treated in leaching experiment group G.

The riverbed samples (group S) were dried, sieved and subsequently split into 6 grain-size fractions (>1 mm, 1-0.5 mm, 0.5-0.4 mm, 0.4-0.3 mm, 0.3-0.125 mm and <0.125 mm) that were subjected to leaching without further treatment. Remaining organics (small roots, branches and plants) were removed by picking. Note that the smallest grain size fraction of the riverbed samples did not represent rock powders but also contained fragments of grain sizes up to 0.125 mm.

### *3.2.2 Automated mineralogy (QEMSCAN)*

Thin sections (25 x 37 mm) of the three granite samples (perpendicular to the foliation in sample Gf2) as well as grain mounts of the sediment fractions smaller

than 1 mm were prepared for quantitative evaluation of mineral composition by Quantitative Scanning Electron Microscopy (Qemscan).

Automated mineral analysis and textural imaging of the studied samples were performed using an FEI QEMSCAN® Quanta 650F facility at the Department of Earth Sciences, University of Geneva, Switzerland. The system is equipped with two Bruker QUANTAX light-element energy dispersive X-ray spectrometer (EDS) detectors. Analyses were conducted at high vacuum, accelerating voltage of 25 kV, and a beam current of 10 nA on carbon-coated polished thin sections. FieldImage operating mode (Pirrie et al. 2004) was used for analyses. In total 221 individual fields were measured per sample, with 1500 µm per field, and point spacing of 5 µm. The standard 1000 counts per point were acquired, yielding a limit of detection of approximately 2wt% per element for mineral classifications. Measurements were performed using iMeasure v5.3.2 software and data processing using iDiscover® v5.3.2 software package.

**Table 3.1: Setup scheme, procedure description and sample/group nomenclature of the leaching experiment.**

| Setup: | Step: | Description: | Procedure: | Volume (acid): | pH: | Temperature: |
|---|---|---|---|---|---|---|
| | PD | Pre-Leach | 1.5 hrs in 2M HF | 0.2 ml | 1.42 | Room temperature (RT) |
| incomplete leaches | A | Weak acid leach | 1 week in citric acid (0.05 M) | G/S: 20 ml; Z: 1.5 ml | 2.2 | RT |
| | B | Intermediate acid leach | 1 week in 0.6 M HNO3 w/ 0.05 M citric acid | G/S: 18 ml; Z: 1.5 ml | 0.2 | RT |
| | C | Strong acid leach | 2d in 3M HNO3 w/ 0.05 M citric acid | 15 ml | 0 | RT |
| | Cz | Incomplete zircon digestion | 2d in 6M HNO3 / 0.5 M HF | 1 ml | 0 | RT |
| (semi-) complete leaches | D | Partial dissoltion (Zircon rims) | 3d in 2M HF | 1.5 ml | 1.42 | 120°C |
| | R/WR/WS | Total dissolution (TD) | Grind; Follow TD procedure (supplement) | 1 ml | 0 | see TD procedure in supplement |

| Groups/Material: | G: unweathered granite | | | S: Riverbed Sediment (weathered granite) | | Z: Zircon separates | | |
|---|---|---|---|---|---|---|---|---|
| Subgroups: | P: powder | N: 1-2 mm size fraction | whole rock | 6 grain size fractions P: S1-5; N: S6 | whole Sediment | P: powder | N: grains | fresh zircons |
| Description: | all G samples are mixed aliquots of all three granite facies (Gf 1,2,3) | | | (S1: >1mm, S2: 1-0.5mm, S3: 0.5-0.4mm, S4: 0.4-0.3mm, S5: 0.3-0.125mm, S6: <0.125mm) | equal mixture of all grain-sizes | Z1-3: zircons from different facies (Gf 1-3); Z4: mixture of zircons from 2 facies (Gf 1+2) | | |
| Step: | | | | | | all 13 mg | 13, 11, 11 mg | |
| PD | initial weight | | | initial weight | | Z1p, Z2p, Z3p | Z1g, Z2g, Z3g | |
| | 5000 mg | 5000 mg | | 5000 mg | | | | |
| A | G1, G2 | G3, G4 | | S1, S2, S3, S4, S5, S6 | | Z1p, Z2p, Z3p | Z1g, Z2g, Z3g | |
| B | G1, G2 | G3, G4 | | S1, S2, S3, S4, S5, S6 | | Z1p, Z2p, Z3p | Z1g, Z2g, Z3g | |
| C | G1, G2 | G3, G4 | | S1, S2, S3, S4, S5, S6 | | | | |
| Cz | | | | | | Z1p, Z2p, Z3p | Z1g, Z2g, Z3g | |
| | | | | | | | | 15 mg, 8 mg / 10 mg, 10 mg |
| D | | | | | | Z1p, Z2p, Z3p | Z1g, Z2g, Z3g | Z1pu, Z4pu / Z1gu, Z4gu |
| | 200 mg | 200 mg | 200 mg | 200 mg | 200mg | | | 10 mg |
| R/WR/WS | G1, G2 | G3, G4 | WR1, WR2 | S1, S2, S3, S4, S5, S6 | WS1,WS2 | Z1pR | | Z1RFresh |

### 3.2.3 *Leaching experiments*

Table 3.1 shows the basic scheme and nomenclature of our leaching experiment. All steps are described below. All leaching solutions (termed leachates below)

were centrifuged after each step (twice in the case of Z-P samples), the supernatants were pipetted off and the residual material was rinsed with MQ water between every step.

Step PD: Pre-digestion (PD): Zircon sample powders and grains were pre-digested for 1.5 hours in 0.25 ml 2 M HF at room temperature in order to dissolve remaining fragments of extraneous minerals.

Step A: All samples were leached in 0.05 M citric acid for 1 week at room temperature on a shaking table (18 ml for S and G samples and 1.5 ml for Z samples).

Step B: All samples were leached in 0.6 M $HNO_3$/ 0.016 M citric acid for 1 week at room temperature on a shaking table (18 ml for sediment and granite samples and 1.5 ml for zircon samples).

Step C/Cz: Sediment and granite samples were leached in 15 ml 3 M $HNO_3$ / 0.025 M citric acid for 2 days at room temperature on a shaking table (C). Zircon samples were leached in 1 ml 6 M $HNO_3$ / 0.5 M HF for 2 days at room temperature on a shaking table (Cz).

Step D: All zircon samples were leached in 1.5 ml 2 M HF for 3 days at 110°C on a hotplate.

Step R/Wr: All residual sediment and granite samples as well as two zircon powder samples and two fresh whole rock samples were dried, ground in an agate mortar, and 5% $H_2O_2$ was added to remove organics for 72 hours. Then the samples were further dissolved using aqua regia on a hotplate at 140°C before they were finally completely dissolved in a mixture of concentrated $HNO_3$ and HF in steel jacketed autoclaves at ~180-200°C for 4 days.

All steps were performed consecutively on the same material. In addition, 2 samples of pristine granite and 2 samples of pristine sediment (equally mixed from all grain-size fractions) were digested completely (termed whole rock/sediment; Wr/Ws). One pristine zircon powder sample was added for step D and the total dissolution.

After leaching all supernatants were dried down and re-dissolved in a 4:1 mixture of concentrated $HNO_3$ and 30% $H_2O_2$. Subsequently, all samples were transferred into 2% $HNO_3$ and 10% aliquots were taken for element concentration measurements. The residual solution was brought into HCl form and another 10% of the original volumes were separated for chromatographic cleaning of Pb while the remaining 80% were used for the separation of Hf and Nd.

### 3.2.4 Chemical purification and mass spectrometry

All samples for the analysis of Pb isotopes were purified using ion chromatography following the procedure of Galer and O'Nions (1989). For the separation of HFSEs and REEs a cation exchange resin (AG 50WX8) was used at first. Then the HFSE and REE cuts were each further purified with Ln-spec resin following Münker et al. (2001) and Pin and Zalduegui (1997), respectively.

Most of the isotope analyses were performed on a Thermo Scientific Neptune Plus MC-ICP-MS at GEOMAR, Kiel. Only a set of 9 Nd samples was measured on a Nu Instruments MC-ICP-MS at GEOMAR. Instrumental mass bias was corrected applying an exponential mass fractionation law with a natural $^{176}Hf/^{177}Hf$ ratio of 0.7325 and $^{143}Nd/^{144}Nd$ of 0.7219, respectively. Additionally, mass bias correction during Nd isotope measurements on the Neptune Plus for samples with $^{140}Ce/^{144}Nd < 1$ were carried out following the approach of Vance and Thirlwall (2002). Mass bias correction during Pb isotope analyses was done externally using the Tl-doping technique (Belshaw et al. 1998) via addition of a NIST997 Tl standard solution (Pb:Tl = ~4:1). Given that Tl and Pb fractionate slightly differently during ionisation (cf. Vance and Thirlwall 2002) $^{205}Tl/^{203}Tl$ were determined on a session by session basis so that NBS981 Pb isotope compositions matched published compositions of Baker et al. (2004). Standard concentrations for all analysed elements were adjusted to sample concentrations of each measurement batch and the desolvating unit (Aridus II) was rinsed with a solution of 0.5M $HNO_3$-0-05M HF between samples to ensure proper washout of both Pb and Tl. $^{176}Hf/^{177}Hf$ ratios of all samples were normalized to JMC475 = 0.282160 (Nowell et al. 1998). $^{143}Nd/^{144}Nd$ ratios were normalized to JNdi-1 = 0.512115 (Tanaka et al. 2000). Pb isotope ratios were normalized to NIST NBS981 ($^{206}Pb/^{204}Pb$ = 16.9416, $^{207}Pb/^{204}Pb$ = 15.4998 and $^{208}Pb/^{204}Pb$ = 36.7249; Baker et al. 2004). Isotopic compositions as well as external reproducibilities of Hf and Pb standards with different concentrations are listed in Table 3.2.

**Table 3.2: Standard reproducibilities of Nd, Hf and Pb isotope analyses. The sum of all offsets of our Pb measurements from the values of Baker et al (2004) is always equal to zero for each batch, except for differently concentrated standards of batch 3 where the sum of the offsets of the average of all standards (10 ppb and 1 ppb together) is equal to zero.**

| Nd | JNdi-1; conc. [ppb] | n | $^{143}Nd/^{144}Nd$ | 2σ | $\varepsilon_{Nd}$ | 2σ | | |
|---|---|---|---|---|---|---|---|---|
| | **Neptune Plus ICP-MS** | | | | | | | |
| | single corrected; 5 ppb | 13 | 0.511873 | ± 60 | -14.92 | **1.17** | | |
| | single corrected; 50 ppb; batch 1 | 24 | 0.512056 | ± 18 | -11.35 | **0.34** | | |
| | single corrected; 50 ppb; batch 2 | 11 | 0.512044 | ± 19 | -11.58 | **0.36** | | |
| | double corrected; 50 ppb | 34 | 0.512118 | ± 13 | -10.13 | **0.25** | | |
| | **NU ICP-MS** | | | | | | | |
| | single corrected; 50 ppb | 18 | 0.512115 | ± 15 | -10.20 | **0.29** | | |
| **Hf** | **JMC475; conc. [ppb]** | **n** | $^{176}Hf/^{177}Hf$ | **2σ** | $\varepsilon_{Hf}$ | **2σ** | | |
| | 1 | 7 | 0.282157 | ± 36 | -21.63 | **1.26** | | |
| | 2 | 4 | 0.282157 | ± 17 | -21.65 | **0.60** | | |
| | 3 | 6 | 0.282159 | ± 17 | -21.57 | **0.62** | | |
| | 4 | 5 | 0.282160 | ± 20 | -21.55 | **0.71** | | |
| | 10 | 6 | 0.282159 | ± 14 | -21.56 | **0.50** | | |
| | 20 | 11 | 0.282160 | ± 8 | -21.55 | **0.28** | | |
| | 50 | 11 | 0.282159 | ± 7 | -21.56 | **0.25** | | |
| **Pb** | **NBS981; conc. [ppb]** | **n** | $^{206}Pb/^{204}Pb$ | $^{207}Pb/^{204}P$ | $^{208}Pb/^{204}P$ | $^{208}Pb/^{206}Pb$ | $^{207}Pb/^{206}Pb$ | **calc.** |
| | 1st batch ; 28 ppb | 9 | 16.94185 | 15.49984 | 36.72521 | 2.16772 | 0.91489 | 2.36939 |
| | offset [ppm] from Baker et al. (2004) | | **15** | **2** | **8** | **-13** | **-10** | **-3** |
| | 2nd batch; 28 ppb | 17 | 16.94197 | 15.49994 | 36.72523 | 2.16771 | 0.91488 | 2.36938 |
| | offset [ppm] from Baker et al. (2004) | | **22** | **9** | **9** | **-20** | **-14** | **-6** |
| | 3rd batch; 10 ppb | 15 | 16.94158 | 15.50012 | 36.72575 | 2.16779 | 0.91492 | 2.36939 |
| | offset [ppm] from Baker et al. (2004) | | **-1** | **20** | **23** | **19** | **22** | **-3** |
| | 3rd batch; 1 ppb | 7 | 16.94160 | 15.49980 | 36.72490 | 2.16775 | 0.91490 | 2.36940 |
| | offset [ppm] from Baker et al. (2004) | | **-415** | **-53** | **-152** | **223** | **338** | **-115** |

Major and trace element concentrations were measured in a ten-fold dilution of the original leaching supernatants using an Agilent 7500-CE Quadrupole ICP-MS at GEOMAR (data in Table A1 in the appendix). Two different standard calibrations were employed to cover samples of high and low trace element concentrations with reproducibilities strongly dependent on the respective element. Typically analyses of lighter elements yielded higher uncertainties than those of the heavier ones.

Note that all concentration measurements were converted into yield values (Table A1 in the appendix). The yield is the concentration of particular elements dissolved in the leachates in nanograms divided by the initial concentration of the bulk sample in milligrams (ng/mg = ppm). Bulk rock normalized elemental yields for the respective fractions are plotted in Figure 3.2.

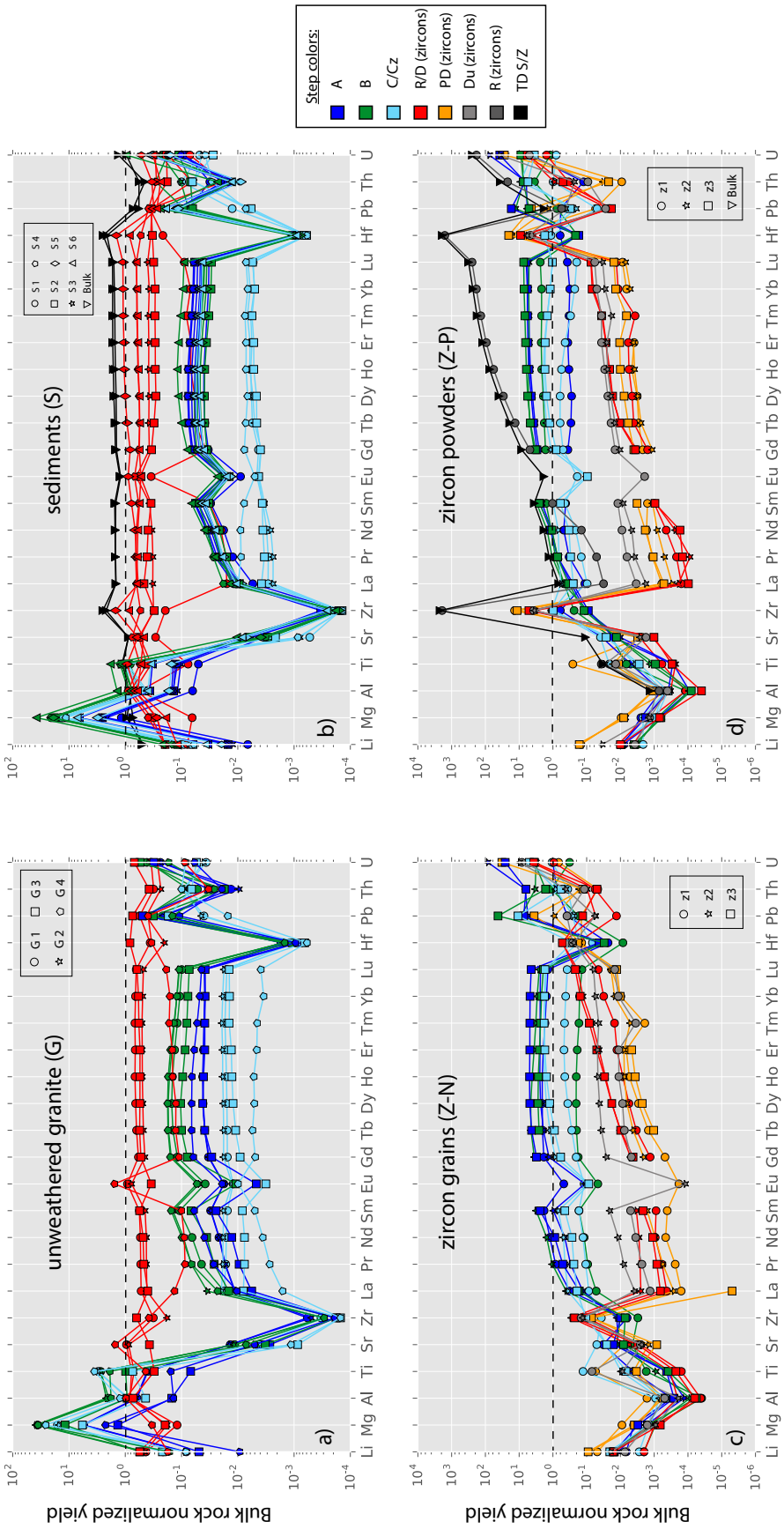


**Figure 3.2: Bulk rock normalized element yields of unweathered granite samples (a), streambed sediments (b), zircon grains (c) and powdered zircons (d). Raw data are provided in the supplementary material. Samples are marked by distinct symbols. The colors refer to the different steps of the experiment.**

## 3.3 Mineral and major element distributions

### 3.3.1 Partial dissolution of pure zircon mineral material

Comparison of electron microscopy images of freshly ground zircons and leached zircon powders indicate that very fine-grained material (<3µm) was lost during leaching (Figure 3.1 B, C). On the other hand, no significant indication of leaching activity (round edges, etch marks etc.) was observed on larger zircon grains and fragments (Figure 3.1 A).

### 3.3.2 Bulk rock and riverine sediment mineral assemblages

Relative abundances (based on area% from the Qemscan analysis) of all major and accessory minerals of the three different granites and all analyzed sediment fractions are listed in Table 3.3. The significance of these mineralogical compositions is, however, difficult to constrain since only a randomly chosen area of 8.75 cm² (Figure 3.3) was analyzed and actual abundances of accessory minerals may vary spatially within the rocks. Thus, the following results are considered as a rough measure of major and accessory mineral compositions in our samples.


**Figure 3.3: QEMSCAN results of analyzed granite samples.**

#### 3.3.2.1 Granite facies classification by mineral composition and zircon abundances

The mineral assemblage of the granite sample Gf1 is monzonitic (monzogranite). Furthermore, compared to the other facies types, Gf1 is enriched in

micas, epidote and accessory minerals. The granite samples Gf2 and Gf3 are typical syenogranites. The slight metamorphic overprint of sample Gf2 is not reflected in its mineral composition. Estimated weight percentages of zircon minerals (based on Qemscan analyses) are 0.06, 0.04 and 0.007 for Gf1, Gf2 and Gf3, respectively, assuming the density of zircon being 4.714 g/cm$^3$ (Anthony et al. 2001) and that of the bulk rock being 2.6 g/cm$^3$ (Schön 2015). The average weight percentage of zircon in the analyzed Aar granite is thus 0.036. Average apatite and sphene percentages are 0.12 and 0.4, respectively (applying density values given in Anthony et al. 2001).

#### *3.3.2.2 Sediment mineral assemblage*

The enrichment/depletion of particular mineral phases as a function of grain size in the sediments is displayed by normalization to the average granitic assemblage (Table 3.3; lower part). All accessory minerals, as well as quartz, biotite and epidote are highly enriched in the finest sediment fraction (S6; <0.125mm), mostly at the cost of K-feldspar and plagioclase, which are depleted by 50 and 30%, respectively. For the sediment grain size fraction between 0.3 and 0.125 mm (S5) a similar although not as pronounced pattern is observed. The coarser fractions (S2, S3 and S4) show a reverse assemblage characterized by enrichment of feldspars and depletion in quartz, glimmers and accessory minerals. Classical sedimentary minerals such as chlorite and hornblendes, however, are enriched in all sediment fractions relative to the unweathered granite material.

**Table 3.3: Mineral distributions in unweathered granite and streambed sediment samples acquired from QemScan analyses. Enrichment/depletion of certain minerals due to mineral sorting processes are emphasized by normalization to the average fresh rock composition.**

| **Area %** | Major minerals | | | | | | Accessory Minerals | | | | | | |
|---|---|---|---|---|---|---|---|---|---|---|---|---|---|
| Sample | Plagioclase | Quartz | K-Feldspar | Biotite | Muscovite | Epidote | Sphene | Apatite | Garnet | Zircon | Amphibole | Chlorite | Monazite |
| Gf1 | 45.3 | 21.7 | 13.9 | 7.6 | 4.7 | 5.4 | 0.624 | 0.220 | 0.011 | 0.034 | 0.017 | 0.003 | |
| Gf2 | 31.7 | 35.0 | 24.2 | 3.0 | 4.8 | 0.6 | 0.156 | 0.041 | 0.036 | 0.022 | 0.004 | | |
| Gf3 | 28.7 | 32.7 | 33.4 | 1.5 | 2.1 | 0.8 | 0.132 | 0.032 | 0.054 | 0.004 | 0.004 | | 0.006 |
| **Average** | **35.2** | **29.8** | **23.8** | **4.0** | **3.9** | **2.2** | **0.304** | **0.098** | **0.033** | **0.020** | **0.008** | **0.003** | **0.006** |
| S2 | 44.6 | 20.2 | 27.3 | 2.3 | 3.5 | 0.9 | 0.290 | 0.070 | 0.024 | 0.012 | 0.051 | 0.156 | |
| S3 | 44.2 | 20.4 | 27.2 | 2.4 | 3.6 | 1.3 | 0.270 | 0.096 | 0.042 | 0.016 | 0.033 | 0.075 | |
| S4 | 44.5 | 23.4 | 24.5 | 2.1 | 3.2 | 1.2 | 0.389 | 0.081 | 0.026 | 0.009 | 0.058 | 0.103 | 0.003 |
| S5 | 34.0 | 42.7 | 16.7 | 1.6 | 2.2 | 1.4 | 0.449 | 0.096 | 0.078 | 0.037 | 0.105 | 0.123 | |
| S6 | 25.9 | 47.8 | 12.2 | 4.8 | 3.7 | 2.8 | 0.615 | 0.429 | 0.179 | 0.141 | 0.113 | 0.631 | 0.001 |
| Normalized area % against average unweathered granite: | | | | | | | | | | | | | |
| Gf1 | 1.3 | 0.7 | 0.6 | 1.9 | 1.2 | 2.4 | 2.1 | 2.3 | 0.3 | 1.7 | 2.0 | 1.0 | |
| Gf2 | 0.9 | 1.2 | 1.0 | 0.7 | 1.2 | 0.3 | 0.5 | 0.4 | 1.1 | 1.1 | 0.5 | | |
| Gf3 | 0.8 | 1.1 | 1.4 | 0.4 | 0.5 | 0.4 | 0.4 | 0.3 | 1.6 | 0.2 | 0.5 | | 1.0 |
| S2 | 1.3 | 0.7 | 1.1 | 0.6 | 0.9 | 0.4 | 1.0 | 0.7 | 0.7 | 0.6 | 6.2 | 57.7 | |
| S3 | 1.3 | 0.7 | 1.1 | 0.6 | 0.9 | 0.6 | 0.9 | 1.0 | 1.3 | 0.8 | 4.1 | 27.9 | |
| S4 | 1.3 | 0.8 | 1.0 | 0.5 | 0.8 | 0.5 | 1.3 | 0.8 | 0.8 | 0.4 | 7.2 | 38.0 | 0.52 |
| S5 | 1.0 | 1.4 | 0.7 | 0.4 | 0.6 | 0.6 | 1.5 | 1.0 | 2.3 | 1.8 | 12.8 | 45.4 | |
| S6 | 0.7 | 1.6 | 0.5 | 1.2 | 0.9 | 1.2 | 2.0 | 4.4 | 5.4 | 7.1 | 13.8 | 233.6 | 0.15 |

### *3.3.3 Major element concentrations*

#### *3.3.3.1 Magnesium and Lithium*

There is a large difference in normalized Mg and Li abundances between leaches of granite/sediment and zircon fractions. While both elements are significantly depleted in zircon leaches (incomplete and complete) Mg is highly enriched

and Li is only slightly depleted in incomplete leaches of groups G and S. The enrichment of Mg (and less pronounced also Li) in the solutions leached from unweathered rocks and sediments during steps B and C are most likely derived from the dissolution of biotite minerals. These observations suggest that biotite was successfully removed from the zircon separates.

#### *3.3.3.2 Aluminum*

Al is also highly depleted in all zircon leaches. Furthermore, there is a clear tendency of Al-depletion in step A leaches of G and S samples. All other leaches are neither particularly enriched nor depleted in Al.

#### *3.3.3.3 Titanium*

Ti is depleted compared to the bulk granite in step A of groups G and S. In solutions of steps B and C in the same groups, however, Ti is slightly enriched. In leaches of zircon material Ti abundances tend to be enriched over other main group elements by an average factor of 50 (in comparison with a factor of 2 for G/S leachates).

#### *3.3.3.4 Strontium*

Sr abundances of incomplete leaches in groups G and S are highly depleted in relation to the bulk rocks. Zircon leaches exhibit relative Sr abundances similar to or slightly enriched compared to those of Al and Ti. The residue of sample G4 is slightly enriched in Sr compared to other residues of the same group.

## *3.4 Trace metal element distributions and mineral mapping*

### *3.4.1 Rare Earth Element (REE) abundances and ratios*

Generally, leaches A and B of groups G and S produced a higher enrichment in REEs than steps C (Figure 3.2). While generally element concentrations of leachates from incomplete leaching steps (A, B and C) in group Z are very low, they are markedly enriched in REEs suggesting the preferred dissolution of REE-rich (easily weatherable) minerals from a contaminant (non-zircon) phase present in the heavy mineral fraction which is not resolved in semi-complete leaching steps D and PD. The total dissolution of zircon material resulted in an inclined pattern from highly depleted LREE to more abundant HREE.

### *3.4.2 REE distribution patterns and normalized ratios*

The shapes of REE distribution patterns were assessed using the following characteristics:

1) LREE: average normalized abundances of La, Pr and Nd.
2) MREE: average normalized abundances of Gd, Tb and Dy.
3) HREE: average normalized abundances of Tm, Yb and Lu.
4) REE bulge: MREE divided by the average of LREE and HREE.
5) REE slope: HREE divided by LREE.
6) Eu anomaly (Eu/Eu*): normalized Eu abundance divided by average normalized abundance of Sm and Gd.

The REE patterns of weak leaches A and B of all groups exhibit a consistent upward convex shape (pronounced REE bulge) which is also visible in C leachates of group Z. Strong and complete leaches of group G and S produced essentially flat REE patterns (shallow REE slope) while, in contrast those of step PD, D and total dissolution in group Z are enriched in HREEs (steep REE slope).

Eu anomalies are highly negative for A and B leaches of groups G and S. Experiment C in groups G and S delivered weakly negative Eu/Eu* with exceptions of positive anomalies for samples G4 and S1, S2, and S3. In group Z all Eu/Eu* were negative with sample Z1 being less negative than samples Z2 and Z3. PD and D values of Eu/Eu* were zero due to the fact, that Eu abundances were below the detection limit of the instrument.

A weak Tm anomaly is observed in some leachates of steps D and PD of group Z, whereas the anomaly is stronger in subgroup N.

### *3.4.3 REE mineral mapping*

By comparison of our experimentally acquired REE patterns with those of published single mineral analyses from the same rock formation (Schaltegger and Krähenbühl 1990) and/or similar rock-types we are able to perform a qualitative estimation of mineral dissolution. For this correlation the numerical coincidence ($R^2$) of the normalized REE patterns of all leachates in our experiment (Figure 3.2) with those of several idealized minerals (Figure 3.4) was calculated using a linear regression algorithm (SciPy, Millman and Aivazis 2011). For each leachate the two minerals with the highest $R^2$ were selected. The results of this mineral mapping are presented in Table A2 in the appendix and are not described in detail here.

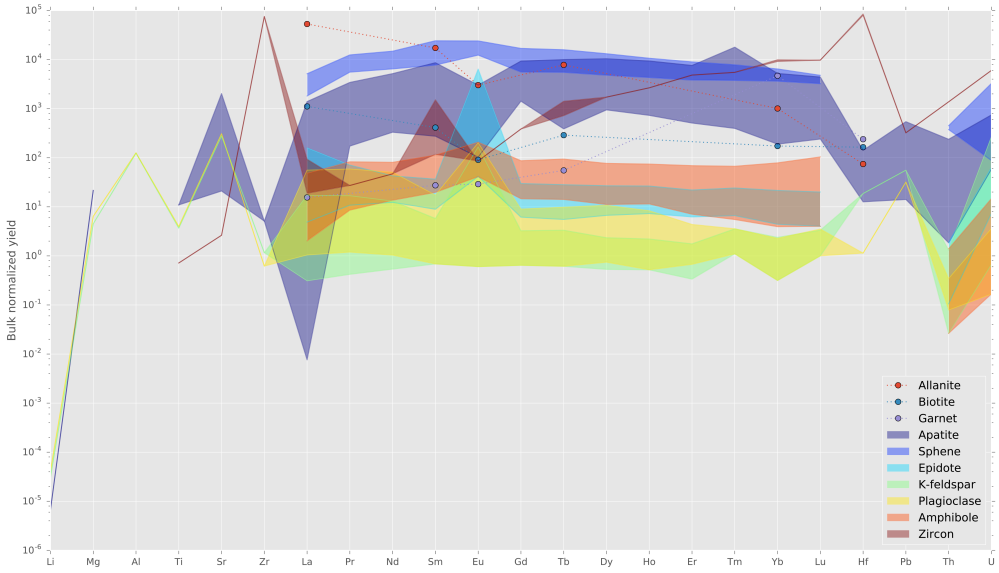


**Figure 3.4: Elemental patterns of selected rock forming and accessory minerals. Colored fields represent typical ranges for I-type granites. Points with dotted line are data from Schaltegger & Krähenbühl (1990). Apatite data from Sha & Chappel (1999). All other mineral data from Bea (1996).**

#### *3.4.3.1 Incomplete sample homogenization in samples with large grain sizes*

The fact that samples of the same origin (such as G3 and G4) delivered different REE patterns suggests that distinct mineral compositions were dissolved during our experiment. We thus conclude that in the case of coarse samples a volume of 5g was not large enough to deliver homogenous mineral composition. This may also apply for the coarse-grained riverbed sediments of group S (S1-4).

## *3.5 The mineral controlled availability of Nd, Hf and Pb to experimental weathering solutions*

As a first measure of mineral availability (for chemical dissolution) based on our results we assume that dissolution processes in our leaching experiment follow the typical sequence of mineral alteration during weathering (Goldich 1938; Harlavan and Erel 2002; Erel et al. 2004) which categorizes the rock-forming and accessory minerals by their resistance to dissolution into easily alterable (e.g. apatite and sphene), moderately resistant (e.g. plagioclase, k-feldspar and biotite) and highly resistant (zircon and garnet). As a more accurate tool for the identification of dominant mineral phases the geochemical properties (normalized REE patterns, mineral specific element ratios and concentrations) of the leachates were monitored in each step of the experiment (section 3.4.3; Table A 2 in the appendix).

Based on these assumptions and due to the fact that the individual minerals in many cases exhibit highly different parent to daughter element ratios, a corresponding degree of fractionation is expected for each radiogenic isotope system as a

consequence of sequential leaching (i.e. Bayon et al. 2006). The different leaching reagents were employed to identify chemical dissolution processes during incipient (A, B) and progressive chemical weathering (C).

Measured radiogenic isotope ratios are shown in Table A 3 in the appendix. Table A 4 in the appendix lists systematic differences in isotopic ratios between leaching experiments of powdered and non-powered samples. Distributions of Hf, Nd and Pb were calculated from the relative yield in one leaching step normalized to the sum of all leaching steps of the same sample including the total dissolution of the residue (Table A 5 in the appendix). Since for practicability reasons only a fraction (200 mg) of the residual material was separated for total dissolution and thus two different volumes of the same sample are compared these normalized distributions are not quantitatively correct but the differences between them allow constraining differences in the budgets semi-quantitatively.

Generally the observations from all three isotope systems are consistent with each other considering the availability of certain minerals to weathering as a function of the intensity of weathering and whether or not the samples were pulverized prior to leaching.

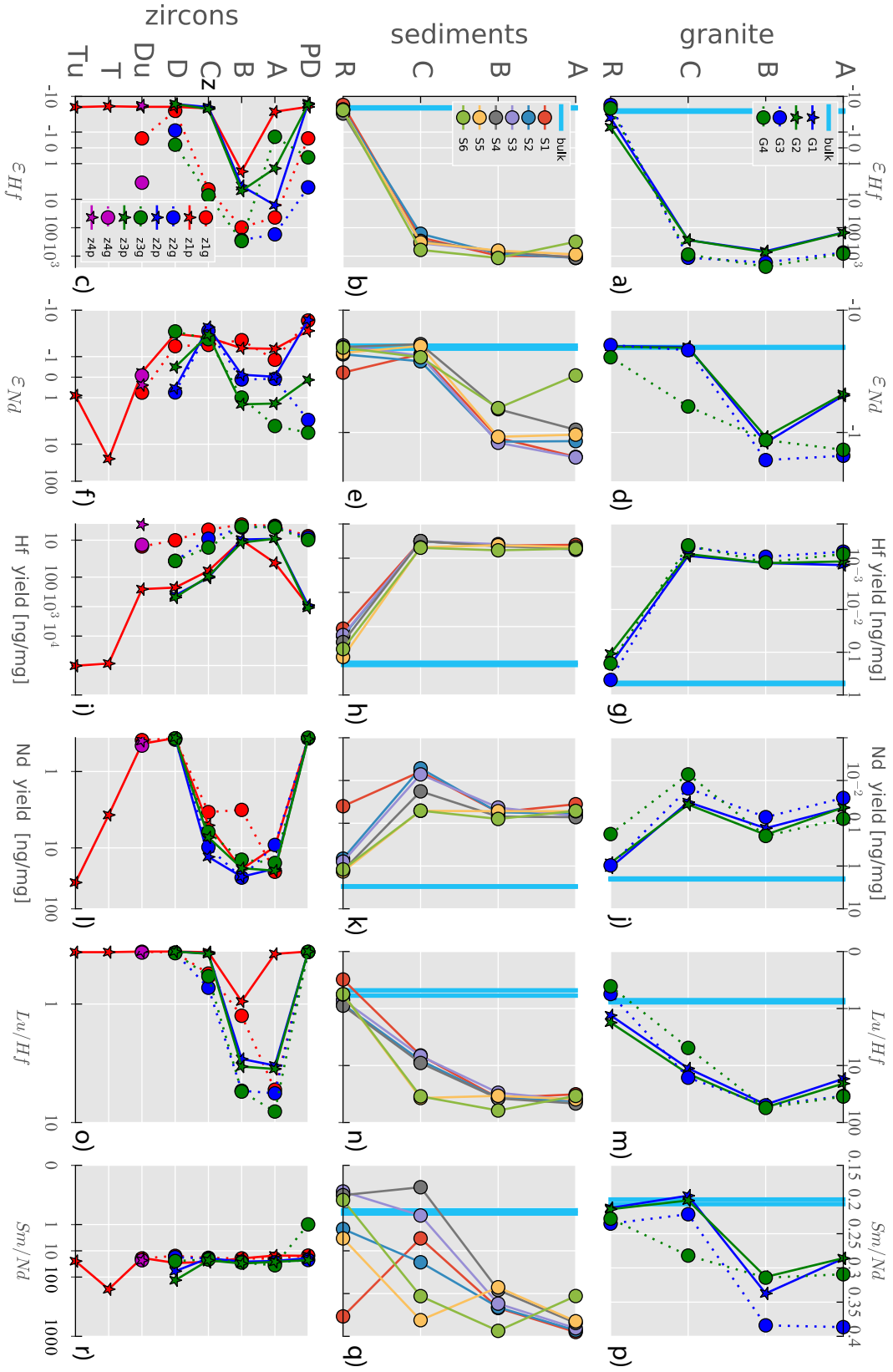


**Figure 3.5: Progress of experimental steps for Hf (a-c) and Nd (d-f) isotope analyses, Hf-yields (g-i), Nd-yields (j-l), Lu-Hf ratios (m-o) and Sm-Nd ratios (p-r). 2σ uncertainties were always smaller than symbol size.**

### 3.5.1 Sm-Nd isotope system

#### 3.5.1.1 Sequential leaching isotope ratios

The ratio of parent to daughter elements of Sm-Nd (Figure 3.5 p-r) is generally higher in weak leaches (A and B). With increasing strength of the leaching reagents (step C and R) Sm/Nd ratios approach the value of the bulk rock composition.

Nd yields, on the other hand, are highest in the residues of groups G and S. However, there are two exceptions (G4 and S1, Figure 3.5 g and f), which released the largest proportions of their Nd during incomplete leaching (61 and 71%; Table A 5 in the appendix). The incomplete leaching experiment step B yielded the largest proportions of all experiments. In group Z the strong leaches D and PD released almost no Nd. Consequently, Nd from zircons was primarily released during experiments A and B, again implying the presence of contaminant accessory minerals. No systematic differences between subgroups N and P are obvious from Nd distribution patterns.

For the unweathered granite and the riverbed sediments experimental steps A and B delivered Nd isotope ratios that were systematically more radiogenic (average $\varepsilon_{Nd}$ = -0.9) than the bulk rock compositions ($\varepsilon_{Nd}$ = -4.1). Average $\varepsilon_{Nd}$ from strong leaching step C and the residues in G and S ($\varepsilon_{Nd}$ ~-4), on the other hand, were close to the bulk rock composition. Only sample G4 showed a significant offset towards a more radiogenic value in step C. Zircon leaches exhibited a wider range in $\varepsilon_{Nd}$ (-5.4 to +25) with generally larger differences between zircons from different granitoid facies in steps PD, A, and B. The range in $\varepsilon_{Nd}$ was widest in PD (-5.4 to +4.9) and became more narrow in A and B (-1.8 to +3.2); while step C produced a narrow range (-3.5 to -1.6). While semi-complete leaches of zircon samples that were already leached (step D) again delivered a wider range of Nd isotope ratios in step D (-2.7 to +0.7), values of fresh zircons in the same experiment were closer to the radiogenic end of this range. The residual zircon material produced the most radiogenic value of +25, which is consistent with enhanced Sm/Nd values for the same sample. The total dissolution of fresh (unleached) zircons, on the other hand, was much less radiogenic (+0.9). The wide range of Nd isotope signatures strongly suggest that Nd in group Z is derived from various of contaminant minerals whereas the zircons themselves only deliver minor amounts of (highly radiogenic) Nd when all other contaminations are fully dissolved.

#### 3.5.1.2 Incongruent weathering of Nd isotopes in the inital stages of the experiment

The Sm-Nd isotope system is expected to be fractionated only very little during weathering processes (e.g. Goldstein et al. 1984) since Sm/Nd ratios do not differ largely between different rock forming and accessory minerals given that both ele-

ments are REEs. Measured Sm/Nd ratios (Figure 3.5 p-r) vary between 0.4 and 0.17 in G and S leachates and show a tendency to higher values in Z leachates (average 0.4; pure zircon 1.5). Easily alterable minerals dissolved during steps A and B in groups G and S generally exhibit Sm/Nd values near the upper end of the observed range (0.3 to 0.4), which is also reflected by more radiogenic Nd $\varepsilon_{Nd}$ signatures between -2 and -0.5 (Figure 3.5 d,e). In step C Sm/Nd and Nd isotope signatures appear to be mainly dominated by the dissolution of plagioclase and k-feldspar (which constitute ~60% of all minerals) as suggested by REE-patterns and further supported by overall more positive Eu-anomalies. Allanite and monazite, which has been demonstrated to contribute significantly to the Nd budget (Garçon et al. 2013) are probably also mainly dissolved in this step. Nevertheless, Nd yield data suggest that the dissolution of easily alterable minerals (apatite and sphene), despite being less abundant, still represent a significant source of more radiogenic Nd under incipient weathering conditions. However, the similarity between Nd isotope signatures of the whole rock and those of the more resistant mineral phases dissolved in step C and R of our study clearly confirms the subordinate role of easily weatherable minerals for the total Nd budget compared with the observed Hf and Pb isotopic trends of the same fractions.

Our experimental data thus indicate that incongruent weathering of Nd isotopes is possible under far-from-equilibrium conditions (step A and B) reflecting the very early stages of chemical weathering of immature rock surfaces. Analogous to Hf and Pb isotopes, this incongruent Nd release is also more radiogenic than bulk rock compositions (see sections 3.5.2 and 3.5.3). Under more corrosive conditions (step C; comparable to progressing chemical weathering) fractionation of Nd isotopes during the dissolution of rocks is only of minor importance. The latter stage likely represents average weathering conditions in natural environments.

Furthermore we cannot confirm the findings of earlier studies suggesting incongruent preferential release of unradiogenic Nd from easily accessible accessory minerals from old cratonic host rocks (Öhlander et al. 2000; Andersson et al. 2001; von Blanckenburg and Nägler 2001). On the contrary, our data support the conclusion that the very easily alterable mineral phases release a significantly more radiogenic Nd isotope signal from the younger host rocks in our experiment, which is in agreement with the results of a recent study revealing incongruent distribution of Nd isotopes within particulate material and the dissolved pool in river waters from the Amazon and its tributaries (Merschel et al. 2017). Considering different crystallization ages and geochemical backgrounds it is very likely that not only the individual mineral assemblage but also the REE distribution in the respective minerals themselves varies significantly between different host rocks. Sm/Nd ratios have been demonstrated to range between well below and well above a ratio of 1 in apa-

tites depending on their geochemical origin (Nagasawa 1970; Bea 1996; Sha and Chappell 1999). A similar variation is possible for sphenes (Bea 1996). We thus expect the Nd isotope compositions released from the labile fraction during dissolution to vary according to the variations of Sm/Nd.

#### *3.5.1.3 Differences between powdered and non-powdered samples*

G-P samples (average $\varepsilon_{Nd}$ = -1.6) released Nd, which is on average about 1 $\varepsilon_{Nd}$ unit less radiogenic than G-N fraction in step A (G3 & G4 average $\varepsilon_{Nd}$ =~-0.6), differences between the subgroups were negligible in step B. Analogously, fine-grained sediment sample S6 was 1.5 $\varepsilon_{Nd}$-units less radiogenic than those of coarse-grained sediments (average S1-S3: $\varepsilon_{Nd}$ ~-0.7) in step A and is not distinguishable from the others in step B.

In group Z PD-leachates of samples Z2p and Z3p yielded $\varepsilon_{Nd}$ values about 7 and 5 $\varepsilon_{Nd}$-units less radiogenic than corresponding N samples. The offset for sample Z1 was only 2.5 $\varepsilon_{Nd}$-units with subsample Z1p being more radiogenic than Z1g. During leaching step A these offsets decrease to a maximum of 2 $\varepsilon_{Nd}$ units (sample Z3). In steps B, C and D offsets between powdered and non-powdered ($\Delta_{P-N}$) samples further decrease to below 1 $\varepsilon_{Nd}$ unit.

Comparing our results of pulverized (P) and non-pulverized (N) fresh rock leachates it is obvious that during mild leaches (steps A and B) the dissolution of very easily alterable minerals (probably apatite) is dominant in subgroup N as manifested in the release of relatively radiogenic Nd isotope signatures ($\varepsilon_{Nd}$ between -0.9 and -0.5), a feature also supported by the $^{176}Hf/^{177}Hf$ and $^{206}Pb/^{204}Pb$ isotopic evolution (described below). In subgroup P the release of more congruently released Nd, probably from a wider variety of minerals (including larger quantities of sphene, as indicated by REE patterns), appears to be dominant over apatite-sourced Nd under the same conditions resulting in a less radiogenic isotope signature ($\varepsilon_{Nd}$ between -1.7 and -0.8).

Moreover, under more intense chemical alteration in step C the two samples of subgroup N diverge significantly pointing to incomplete sample homogenization (see section 3.4.3.1). While sample G4 released Nd incongruently with isotopic signatures more radiogenic than the bulk composition, sample G3 released a congruent composition during step C. It is likely that in sample G3 all radiogenic minerals accessible to dissolution were largely dissolved, they were still abundant in sample G4. Furthermore, sample G4 was likely enriched in minerals with more radiogenic signatures such as sphene, amphibole, and epidote, as indicated by the REE patterns (Table A2 in the appendix) and elevated $\varepsilon_{Nd}$ (-3.3) in step R. Leachates from

subgroup P in step C, in contrast, are identical within errors to whole rock compositions and the residues.

From these observations we conclude that the mechanical disaggregation of a rock substrate, serving as the experimental analogue for glacial abrasion in our study, accelerates the initial dissolution of easily weatherable minerals and leaves more resistant minerals behind. More congruent Nd isotope signatures in incomplete leachates of subgroup P support this finding.

### 3.5.2 *Lu-Hf isotope system*

#### 3.5.2.1 *Abundances and distribution of lutetium, hafnium and zirconium*

Generally, Lu is enriched with respect to Hf (and Zr) in weak leach experiments (steps A, B and C). Especially during step B high amounts of Lu were released to solution. Zr and Hf, on the other hand, were highly depleted in all incomplete leaches of G and S. In the residual material the abundances of Zr and Hf are generally similar to all other elements (including Lu) and even exhibit small peaks in samples G3, S5 and S6.

There is a marked difference in Lu, Zr and Hf yields between all leaches of zircon subgroups P and N (see Figure 3.2 and Table A 4 in the appendix). Incomplete leaches of subgroup N are similar to equivalent leaches of groups G and S, exhibiting relatively high Lu/Hf. On the other hand, incomplete dissolution of powdered zircons yielded on average 25 and 10 times higher Zr and Hf abundances than respective leaches of non-powdered zircons. For steps D and PD the difference is even larger with subgroup P delivering on average 100 times more Zr and 70 times more Hf (Table A 4 in the appendix). The difference between subgroups P and N is also resolvable for incomplete leaches of G and S, however, not as markedly ($Zr_P/Zr_N$=2, $Hf_P/Hf_N$=1.5).

Almost all Hf (and Zr) in samples from groups G and S was contained in the residual material (average = 99.2%). G samples of subgroup P released about 1.5% of their total Hf during incomplete leaching while subgroup N released only 0.55% in the same leaches. Incomplete leaches of samples from group S tend to release smaller amounts of Hf with decreasing grain-size. Hf distribution patterns in Z samples differ strongly between the two subgroups. While a large portion (62-74%) of the total Hf is released during the pre-leach from powdered zircons, the same treatment released only 17 to 33% from zircon grains. On the other hand, Hf contents in incomplete leaches were small (7-8.5%) in subgroup P while they were rather large for subgroup N (23-33%). Consequently, the largest proportion of Hf released from zircon grains was during experiment D, whereas powders that have already suffered severe loss of Hf in step PD discharged only a minor proportion dur-

ing that step (note that absolute concentrations in the leachates of zircon powders were still much larger than those of grains).

#### 3.5.2.2 *Hf isotope compositions*

The range of our experimental Hf isotope ratios (Figure 3.5 a-c) is much wider than that of Nd with $\varepsilon_{Hf}$ values from -5.7 to +2358. Highly radiogenic values between +150 and +2358 were measured in all incomplete leaches (steps A, B, C) of groups G and S, which is consistent with high Lu/Hf ratios in the same leachates. While in group G and for sample S6 leaching step B produced the most radiogenic values, a decreasing trend in $\varepsilon_{Hf}$ was observed during consecutive leaching experiments in group S.

In contrast, leaches of pure zircon samples produced on average less radiogenic $\varepsilon_{Hf}$ close to the whole rock value. However, incomplete leaches of zircon samples also produce radiogenic $\varepsilon_{Hf}$ values of up to +300 (especially in subgroup Z-N).

*Comparison of Hf isotopes in dissolutions of powdered and non-powdered samples*

Incomplete leaches of powdered samples in group G produced Hf isotope compositions that were between 630 and 1300 $\varepsilon_{Hf}$ units less radiogenic than non-powdered samples. In contrast, residual material of powders in group G was 2.8 $\varepsilon_{Hf}$ units more radiogenic than corresponding non-powdered samples. While during leaching step A fine-grained sediments (S6) yielded Hf isotope ratios that were 730 $\varepsilon_{Hf}$ units less radiogenic than those of coarse sediments (S1-S5), steps B and C of the same sample-group produced more radiogenic values (offset by 400 and 330 $\varepsilon_{Hf}$ units) than coarse sediments. Differences between $\varepsilon_{Hf}$ signatures of the residue of fine and coarse sediments are insignificant.

Offsets between powdered and non-powdered zircons were even larger with average $\varepsilon_{Hf}$ values of weak incomplete Z-P leaches being 6-220 $\varepsilon_{Hf}$ units less radiogenic than Z-N leaches. Zircon leaches varied strongly with the presence of hydrofluoric acid (HF) in the leaching reagent. Consequently, strong and semi-complete leaching steps (Cz, D, PD) generally produced smaller offsets between powdered and non-powdered zircon samples (4 - 8 $\varepsilon_{Hf}$ units). Furthermore, a systematically larger offset between Z-P and Z-N (~2 $\varepsilon_{Hf}$ units) was observed for pristine zircon samples in comparison with the respective samples that were already leached. This observation and the fact, that weak leaching steps (A, B and Cz) produce values more radiogenic than expected for zircons (Figure 3.5 c) demonstrates the presence of a contaminant residue of non-zircon minerals in the zircon separates. The occurrence of apatites, which are often included in zircons, may serve to explain these radiogenic Hf isotope compositions in weak leaching steps of group Z.

### 3.5.2.3 The role of mineral sorting

The fact that leachates of step A in experiment S (excluding S6) contained more radiogenic Hf than the same leachates in experiment G suggests that an easily accessible fraction of less radiogenic minerals is missing in the sediments. It is likely that unradiogenic (accessory) mineral phases are depleted in sediment samples S1, S2, S3, S4 and S5, while they are enriched in S6. Based on this, we suggest that mineral sorting processes are responsible for the observed discrepancy between G and S (see also Garçon et al. 2013a). Furthermore, the results obtained from sample S6 are consistent with fresh rock leachates indicating that it best represents the mineral composition of the host rocks.

The observation that the residual material of powdered bulk rock samples is more radiogenic in its Hf isotope composition and less radiogenic in $^{208}Pb/^{204}Pb$ than the bulk rock and residues of non-powdered samples in the same group is most likely an artifact of sample preparation (Figs. 3a,b and 6g, h). Overall decreased Hf-yields of samples G1 and G2 together with a more radiogenic Hf isotope composition strongly suggest the loss of zircon minerals during the leaching process: While whole rock powders for the total dissolution of an untreated aliquot were transferred directly, only a small proportion of the previously leached powder samples G1 and G2 was transferred to the total dissolution procedure. We thus conclude that zircon minerals were not distributed homogeneously within the residual material of G1 and G2 and that the fractions that were transferred to total dissolution were physically depleted in zircon minerals compared to the whole rock.

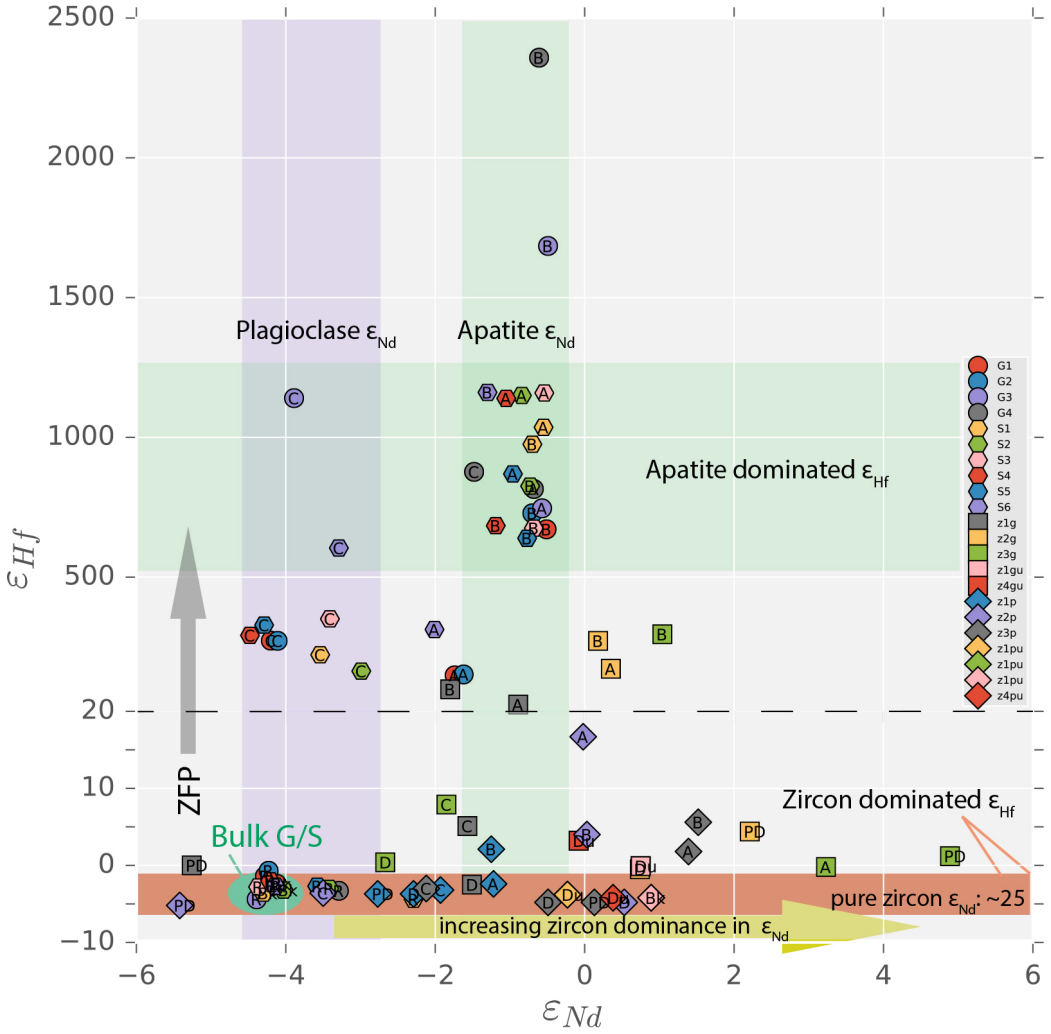


**Figure 3.6: Hf versus Nd isotope results. The letters in the symbols refer to the respective experiment steps. Note that the y-axis scale changes at +20. 2σ uncertainties were always smaller than symbol size.**

### 3.5.2.4 *Preferential release of Hf from easily alterable minerals versus retention in zircons*

The Hf isotope compositions of the incomplete leaches suggest an availability-dependent mixture of multiple end members (Figure 3.6) including at least one ultra-radiogenic phase (with $\varepsilon_{Hf}$ values significantly above +1000) and a less radiogenic mineral phase dissolving during the incipient dissolution. Interestingly, as described for Nd, maximum Hf isotope ratios ($\varepsilon_{Hf}$ > +1000) correlate with REE patterns that most closely resemble those of apatite (Table A 2 in the appendix). On the other hand, leachates with more intermediate $\varepsilon_{Hf}$ values (+150 to +600) exhibit REE patterns that resemble those of sphene. Both minerals have been shown to be extremely radiogenic in $\varepsilon_{Hf}$. Single grain analyses of pure apatites ranged between $\varepsilon_{Hf}$ of +130 and +60,000 while those of a single sphene gave values near +70 (Barfod et al. 2003, 2005). These observations demonstrate that under incipient weathering conditions (steps A and B) but also under more corrosive conditions (step C) disso-

lution of these minerals dominates the Hf isotope budget of the weathering solutions.

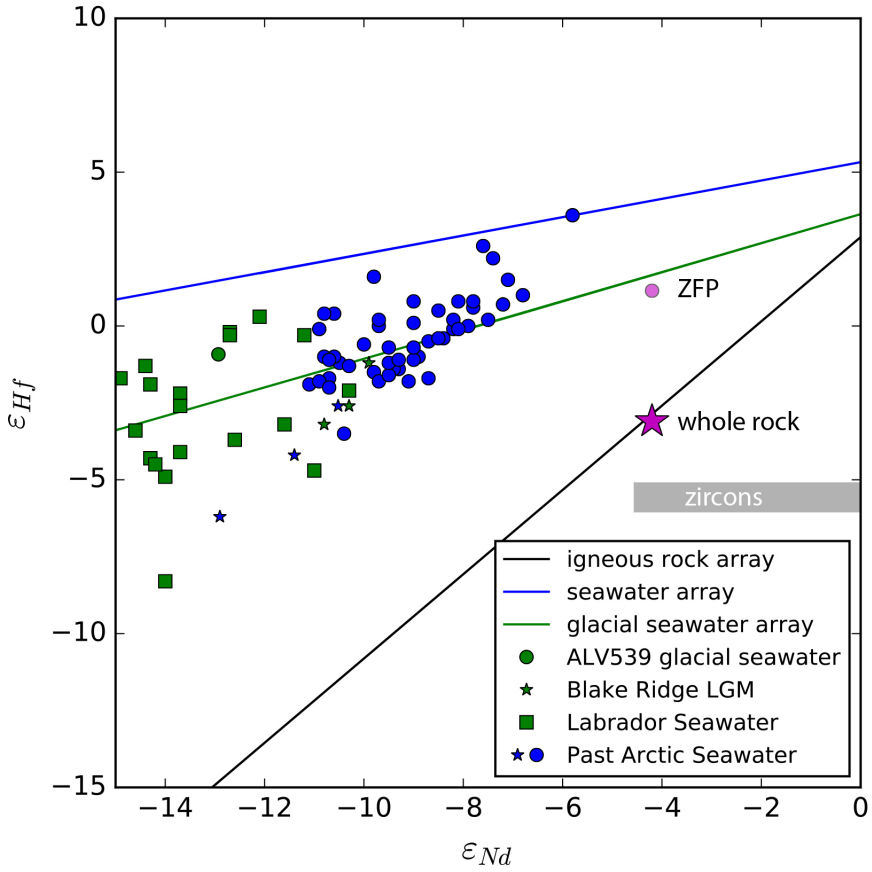


**Figure 3.7: Compilation of Hf versus Nd isotope compositions of glacially affected seawater from the present day Labrador Sea (Filippova et al. 2017) together with data for past seawater from the North Atlantic (Burton et al. 1999; Piotrowski et al. 2000), the Blake Ridge (Gutjahr et al. 2014), the Lomonosov Ridge of the Arctic Ocean (blue circles; Chen et al. 2012) and from the Canada Basin (blue stars; Dausmann et al. 2015). 2σ uncertainties were always smaller than symbol size. The regression line represent to the the seawater data and is referred to as "glacially affected seawater array" ($\varepsilon_{Hf} = 0.46 \cdot \varepsilon_{Nd} + 3.58$). Also depicted are the regression lines of river/seawater and igneous rocks of Bayon et al. (2009).**

While contributions from unradiogenic phases during weak chemical weathering conditions appear to be negligible, these phases clearly dominate the residual material ($\varepsilon_{Hf}$ -5 to -1.9) and the whole rocks ($\varepsilon_{Hf}$ = -3.1), which plot close to the "igneous rock" array (Bayon et al. 2009, Figure 3.7). Consequently, previous studies concluded that the most significant repository of unradiogenic Hf are zircon minerals which are discriminating against Lu during crystallization and can host up to 2 weight percent of Hf (e.g. Patchett et al. 1984; White et al. 1986; van de Flierdt et al. 2007; Chen et al. 2011). In our study, dissolutions of pure zircon mineral fractions from the Aar granite provide a first direct assessment of Hf contributions to the weathering cycle and surface runoff from this unradiogenic phase. While incomplete leaches of these fractions clearly exhibit contributions from remaining contaminant minerals with radiogenic Hf isotope compositions still attached to separated zircons (see section above), strong leaches (PD, D and R) of zircon powders, which are least prone to contamination, range between -4.2 and -5.7. The average

zircon $\varepsilon_{Hf}$ signature of the analyzed Aar granite samples is thus -5.1 (Zircon-dominated $\varepsilon_{Hf}$ in Figure 3.6). This value is in good agreement with the "zircon-bearing sediment" array lying below the igneous rock array in $\varepsilon_{Hf}$-$\varepsilon_{Nd}$ space (Figure 3.7; Bayon et al. 2009) .

#### *3.5.2.5 Additional release of unradiogenic Hf during increasing physical weathering*

The observations presented above raise the question under which conditions the Hf release from highly resistant zircon minerals can be enhanced. There are two basic mechanisms that control weathering regimes in nature: (1) changing physico-chemical conditions controlling dissolution processes (temperature, availability of humic acids, runoff, redox conditions etc.) and (2) changes in mechanical break-down of minerals controlling the surface area of the minerals and disrupting mineral lattices thereby enhancing their availability for dissolution.

In our experiment we tested the differences in isotope signatures that are created by enhancement of the corrosiveness chemical environment (leaching steps A-D) as well as by increasing mechanical stress (powders versus granular material). Differences in the chemical environment have revealed the different availabilities of particular mineral phases according to their relative chemical stability as described above. In addition to that, the grinding of bulk rock samples as well as zircon mineral separates provides clear evidence for the overall enhancement of dissolution processes of the actual zircons with decreasing grain size. Furthermore, the comparison of subgroups P and N in the bulk rock experiment shows that not only more Hf was released from the ground samples but also that the respective isotopic signatures were very different.

The circumstance that pulverized samples in our experiment always delivered a more congruent Hf isotope signature (i.e. less radiogenic) suggests that more resistant minerals, bearing less radiogenic Hf, become accessible to dissolution due to favorable surface to volume ratios. In fact, the results of the leaching of zircon separates demonstrate that a fraction of the very resistant zircon minerals can be dissolved even under very weakly corrosive conditions. While Hf released from contaminant mineral phases ($\varepsilon_{Hf}$ above +40) significantly affects incomplete leachates of zircon grains (estimated 3 to 10% of contamination; Figure 3.8), those of pulverized zircon separates are clearly dominated (only 0.3 to 0.5% of contamination) by zircon-sourced Hf (max $\varepsilon_{Hf}$ = +16).

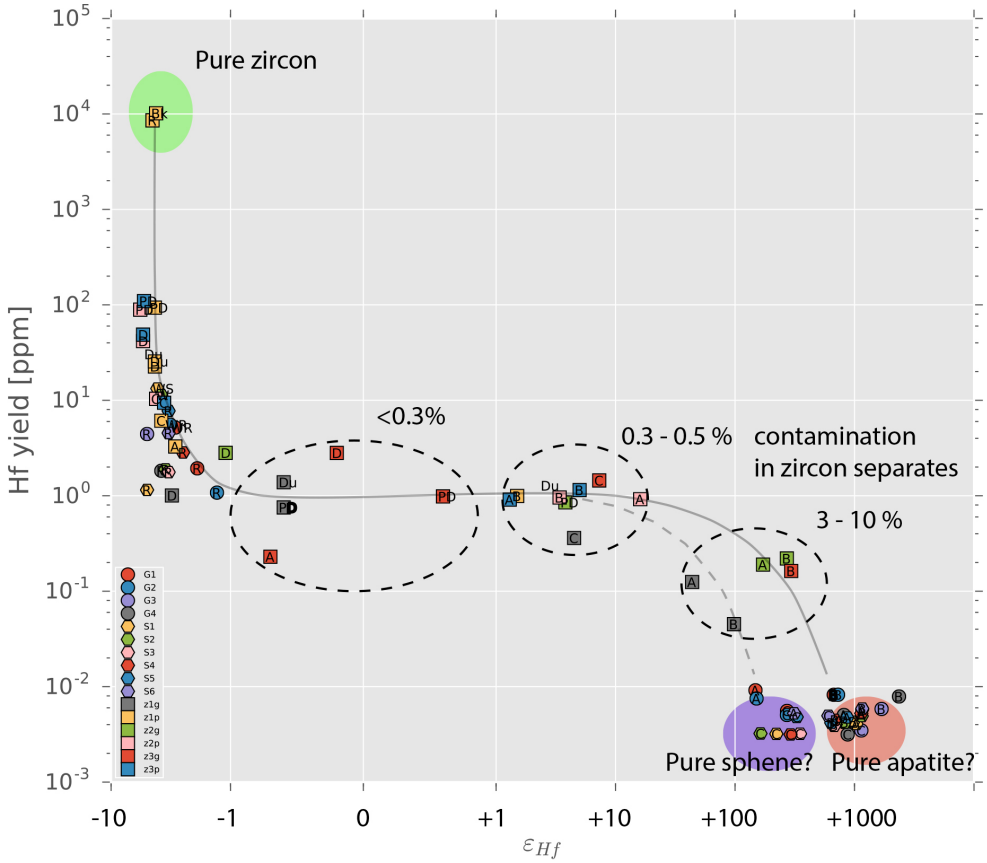


**Figure 3.8: Hf yield plotted against Hf isotope composition. Hypothetical binary mixing between unradiogenic endmember (zircon) and potential radiogenic endmembers (apatite and sphene) is depicted with the gray line. Theoretic proportions of radiogenic contaminations of leachates of zircon separates were calculated via binary mixing of Hf isotope compositions of pure zircon (εHf = -5.1) and the most radiogenic leachate (εHf = +2350).**

On the other hand, Hf from the dissolution of easily alterable minerals is clearly dominant in incomplete leachates of bulk granite samples when considering the whole rock system. However, the predominance of apatite present in samples of subgroup N is less defined in subgroup P indicating that incongruent weathering decreases due to mechanical grinding.

In addition, observations from ground zircon samples in group Z suggest that the zircon-effect is also less intense in these samples given that some zircon-sourced Hf is released to dissolution. This is further supported by increased Zr/Nd in leachates of pulverized granite samples (2.6 fold compared to non-pulverized samples) documenting an enhanced dissolution of a Zr-rich mineral phase even during incomplete leaches. While sphene minerals may hold significant amounts of Zr they are usually highly enriched in REEs (e.g. Garçon et al. 2013b) and can thus not account for the observed higher Zr/Nd ratios. Consequently we conclude that elevated Zr/Nd ratios in leachates of ground, unweathered granite indeed indicate enhanced Zr release from zircon.

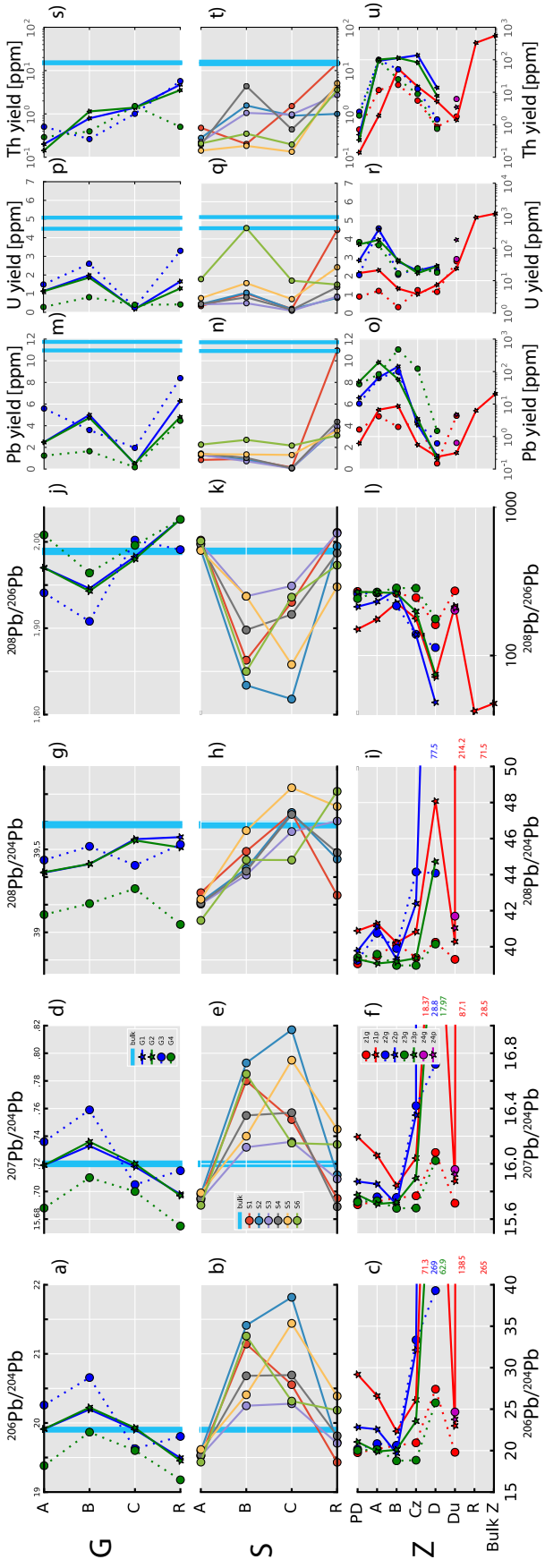


**Figure 3.9: Progress of experimental steps for Pb isotope analyses (a-l), Pb yields (m-o), U-yields (p-r) and Th yields (s-u). 2σ uncertainties were always smaller than symbol size.**

### 3.5.3 U-Th-Pb isotope System

#### 3.5.3.1 Abundances and distributions of Pb, Th and U

Relative to the other leaching steps Pb and U are enriched in the weak leach steps A and B in group G while Th is depleted (Figure 3.9). Experiment C in the same group delivered a reversed pattern with Th being slightly enriched relative to Pb and U. The residue of sample G4 produced a higher depletion in Th than the other three residues, exhibiting a shape similar to steps A and B, though less pronounced.

In group S leaching experiments A and B delivered patterns similar to those of group G. Deviations from these observations emerge for S2-4 during step B. Observations in experiment C are analogous to group G with the exception of samples S5 and S6, which are basically identical to the patterns described for steps A and B. Residues in S show the same patterns as group G with samples S1 and S3 behaving analogous to G4.

Samples of group Z show a large range of different Pb-Th-U patterns. Preleaches in both subgroups yield high amounts of Pb and U, while they are depleted in Th (V-shape in Figure 3.2 c and d). Patterns of weak leaching experiments A and B vary between an essentially flat pattern (U/Th/Pb- ratios close to 1) and a V-shape similar to PD. There is a tendency towards flat shapes in A and B of powdered zircons compared to the same experimental steps for zircon grains. Experiment C generally produced an increasing depletion in Pb and U while Th became more abundant. In leachates of step D and R in both subgroups Pb was highly depleted while Th was at intermediate levels and U was strongly enriched. There is a tendency towards higher enrichment in Th and U in the powdered subgroup.

In contrast to Hf and Nd, large proportions of Pb are released from samples of groups G and S during incomplete leaching. Coarser sediments (S1-S4) tend to retain more Pb during incomplete leaching (63-69%) while more Pb is released in the same leaching procedures from fine-grained sediment fractions S5 and S6. Consistently, larger proportions of Pb were dissolved during step B (18-38%) in pulverized granite samples as well as fine-grained sediment compared to coarse sediment/granite samples (12-22%). Pb release from zircons is largely analogous to observations made for Nd with insignificant amounts of Pb discharged during experiments PD and D, as well as no significant differences between zircon powders and grains.

### 3.5.3.2 Pb isotopes

All Pb isotope data are presented in Figure 3.9. Generally, the variations of the ratios of radiogenic $^{206}Pb$ and $^{207}Pb$ to primordial $^{204}Pb$ (Figure 3.9 a-f) were similar whereas $^{208}Pb/^{204}Pb$ (Figure 3.9 g-i) showed distinct patterns. The trends of $^{208}Pb/^{206}Pb$ (Figure 3.9 j-l) are reversed when compared with corresponding $^{206}Pb/^{204}Pb$. This suggests that variations in $^{206}Pb$ are controlling $^{208}Pb/^{206}Pb$ rather than variations in $^{208}Pb$.

All Group G samples exhibit the same $^{206}Pb/^{204}Pb$ and $^{207}Pb/^{204}Pb$ pattern with consecutive leaching (Figure 3.9 a and d). Radiogenic values, relative to the bulk rock, were obtained during step B, whereas less radiogenic values were released from the total dissolutions of the residual samples. Interestingly both steps A and C produced values identical to the bulk rock composition. $^{208}Pb/^{204}Pb$, on the other hand, peaked in experiment C and was always depleted relative to bulk rock composition in incomplete leachates.

Group S generally exhibited larger variations than group G (Figure 3.9 b, e and h). Leaches of step A delivered the least radiogenic values in all fractions. While samples S1 and S6 reached their peak $^{206}Pb/^{204}Pb$ and $^{207}Pb/^{204}Pb$ in step B (similar to group G) all other samples reached their maximum Pb isotope values in step C. Residual materials were again unradiogenic while those of the whole sediment (mixed aliquots) produced intermediate values. A similar pattern was observed for $^{208}Pb/^{204}Pb$ with values peaking in step C. The only exception was sample S6, which reached its maximum $^{208}Pb/^{204}Pb$ value in the residual material.

Pure zircon leaches produced very large ranges in Pb isotope ratios of up to 1385 for $^{206}Pb/^{204}Pb$, 87 for $^{207}Pb/^{204}Pb$ and 214 for $^{208}Pb/^{204}Pb$ (Figure 3.9 c, f and i). The most radiogenic values were reached in steps with high rates of zircon dissolution (D and R).

*Differences between powdered and non-powdered samples*

All Pb isotope compositions of pulverized G samples were identical in all Pb isotope systems for the respective leaching procedures whereas leaches of non-pulverized G samples produced markedly different values (no systematic trend to more or less radiogenic compositions). In general, leaches of powdered zircon samples delivered Pb isotope ratios significantly more radiogenic than non-powdered zircons.

### 3.5.3.3 Congruent release of $^{206}Pb/^{204}Pb$ and $^{207}Pb/^{204}Pb$ during the initial stage of leaching

Generally higher yields in U and Th during a leaching step should reflect the enhanced dissolution of U-bearing and Th-bearing minerals, respectively. This relationship is clearly documented by an overall similarity of the patterns of U yields to those of $^{206}Pb/^{204}Pb$ and $^{207}Pb/^{204}Pb$, which is also observable for Th yields and $^{208}Pb/^{204}Pb$ ratios (see Figure 3.9).

During the initial stage of the experiment, leachates from pulverized unweathered granite (group G-P) released $^{206}Pb/^{204}Pb$ and $^{207}Pb/^{204}Pb$ congruently with their respective Pb isotope ratios being identical to those of the whole rock (19.9 and 15.72 respectively). Although U yields (Figure 3.2) document the dissolution of U-bearing minerals no increase in radiogenic $^{206}Pb$ and $^{207}Pb$ compared to the whole rock value is recorded. In contrast, less radiogenic $^{208}Pb/^{204}Pb$ signatures and minimal Th yields reflect an apparent resilience of Th-bearing minerals towards dissolution compared with other rock-forming minerals.

The leachates of subgroup G-N, on the other hand, show heterogeneous Pb isotope compositions. This is most likely due to the fact that the two coarse grained samples G3 and G4 were composed of different assemblages of minerals (see section 3.4.3.1). While REE patterns of G4 in step A suggest a significantly increased dissolution of unradiogenic minerals (i.e. epidote,), those of G3 document the dominant dissolution of apatite in the same step (Table A 2 in the appendix). The elevated presence of easily alterable U-bearing minerals in G3 is reflected in more radiogenic $^{206}Pb/^{204}Pb$ and $^{207}Pb/^{204}Pb$ in step A (Figure 3.9) whereas the minerals of G4 release smaller amounts of radiogenic $^{206}Pb/^{204}Pb$ and $^{207}Pb/^{204}Pb$ under the same conditions.

Erel et al. (2004) ascribed this initial phase (step A) of bulk rock weathering to the dissolution of trace amounts of unradiogenic minerals. In fact, the congruency of leachates of pulverized rocks in step A suggests the release of Pb from fresh (reactive) surfaces of many different minerals, representing the average composition of the bulk rock. These reactive mineral surfaces are not available in the following weak leaching steps. It is likely that this unradiogenic pool (needed to compensate for the preferential dissolution of radiogenic minerals) is derived from the dissolution of supposedly more resistant minerals, most likely fragments of feldspars. From this we infer that the fresh mineral surfaces that were generated during the pulverization of many different minerals congruently comprise a highly reactive and consequently congruent source of $^{206}Pb$, $^{207}Pb$ and $^{204}Pb$.

In coarse-grained sample G3 no significant quantities of such mineral surfaces (of unradiogenic minerals) were available and the dissolution of easily accessible accessory minerals such as apatite was dominant. The unradiogenic signature of the initial leach of sample G4, on the other hand, is probably the product of the increased availability of an unradiogenic accessory mineral phase, possibly epidote, as suggested by REE patterns.

#### 3.5.3.4 *Accessory mineral phases causing incongruent weathering*

In step B the release of Pb from U-bearing minerals is documented by peak U yields in almost all G and S samples (Figure 3.9 m and n). Consistently, $^{206}Pb/^{204}Pb$ and $^{207}Pb/^{204}Pb$ signatures also reach their peak radiogenic values. At the same time, the amount of Th released to dissolution only increases slightly accompanied by a small shift towards more radiogenic, but still highly depleted $^{208}Pb/^{204}Pb$ signatures (with the exception of sample G3).

For this stage Erel et al. (2004) argued that the isotopic signal is dominated by dissolution of more radiogenic minerals. REE patterns as well as Nd and Hf isotope signatures (described above) confirm the dominant role of accessory phases such as apatite in step B. Accordingly, leachates that exhibit a larger imprint from apatite dissolution (G3, S1, S2, S6; see Table A 2 in the appendix) also released Pb with more radiogenic $^{206}Pb/^{204}Pb$ and $^{207}Pb/^{204}Pb$ signatures. Th-rich sphene, on the other hand, controls the incongruent release of $^{208}Pb/^{204}Pb$. Consequently, increased yields of Ti (and Th) in step B are also reflected by the release of more radiogenic $^{208}Pb/^{204}Pb$ signatures.

Based on our data we suggest that only insignificant amounts of more resistant minerals (rich in $^{204}Pb$) were dissolved in step B and thus the purest (radiogenic) accessory mineral signature was captured, consistent with the observations from Nd and Hf isotopes. While freshly exposed mineral surfaces lost their reactivity during weathering phase A, various U/Th-rich accessory minerals still preferentially dissolve in phase B leading to less congruent $^{206}Pb/^{204}Pb$ and $^{207}Pb/^{204}Pb$ signals in the runoff during progressive weathering.

#### 3.5.3.5 *The release of unradiogenic $^{206/207}Pb/^{204}Pb$ and radiogenic $^{208}Pb/^{204}Pb$ with progressing weathering*

Principally, we observe two different trends in the Pb leaching experiment. Firstly, in leaching experiment C a general decrease in Pb yields is accompanied by a decrease in radiogenic $^{206}Pb/^{204}Pb$ and $^{207}Pb/^{204}Pb$. More radiogenic $^{208}Pb/^{204}Pb$, in contrast, is enriched in step C compared to steps A and B. These observations suggest that Pb release from easily accessible U-bearing minerals is already exhausted

(with the exception of samples S2 and S5), which is further supported by minimal U yields. The dominant dissolution of more resistant minerals such as plagioclase, however, is reflected by the corresponding REE patterns at this stage of the experiment. These minerals are typically poor in radiogenic Pb (c.f. Erel et al. 1994, 2004) leading to less radiogenic $^{206}Pb/^{204}Pb$ and $^{207}Pb/^{204}Pb$ close to or below the whole rock values (Figure 3.9).

The residual materials (step R) of all samples (with the exception of G3, S5 and S6) exhibit $^{206}Pb/^{204}Pb$ and $^{207}Pb/^{204}Pb$ signatures significantly less radiogenic than the corresponding bulk rock composition. This is due to the fact that radiogenic Pb was preferentially removed from the easily weatherable minerals during the previous steps leaving the residues enriched in unradiogenic Pb. While the U yields indicate that some refractory U-bearing minerals were still left in the residues, $^{206}Pb/^{204}Pb$ and $^{207}Pb/^{204}Pb$ are clearly dominated by unradiogenic lead mainly originating from plagioclase and alkali feldspars (as confirmed by REE patterns; Table A 2 in the appendix). In the case of samples G3, S5 and S6 more radiogenic budgets strongly suggest a higher abundance of accessory minerals carrying radiogenic $^{206}Pb/^{204}Pb$ and $^{207}Pb/^{204}Pb$ signatures. From our data we infer that the increased amounts of radiogenic Pb in these samples are most likely derived from more abundant easily accessible minerals, as well as more abundant radiogenic refractory minerals (possibly zircons as discussed below) in the residual material. In contrast, the negative $^{206}Pb$ and $^{207}Pb$ budgets with respect to the whole rock of sample G4 emphasize the relative depletion of U-rich minerals in this sample.

In agreement with the findings of Erel et al. (2004) that a significant fraction of radiogenic Pb from Th-bearing minerals is less susceptible to dissolution, increasing Th yields with the progressing leaching experiment (Figure 3.9 s and t) reveal contributions of Th-bearing minerals producing more radiogenic $^{208}Pb/^{204}Pb$ signatures in all samples (except G3, which was most likely dominated by the release of common Pb from feldspars in step C). A relatively close correlation ($R^2$ >0.5) with REE patterns of sphene and peak Ti yields in step C leachates suggests that these Th-rich minerals released increased amounts of Th, as well as radiogenic $^{208}Pb$ into dissolution during this stage of the experiment. Correspondingly, increased Th yields from residual materials of most samples in groups G and S reflect the dissolution of Th-rich minerals (most likely also thorite and polycrase; Schaltegger and Krähenbühl 1990). This is particularly pronounced in sample G3. In contrast samples G4, S1 and S2 represent an exception with Th yields being low and $^{208}Pb/^{204}Pb$ being less radiogenic. Both these observations suggest the absence of Th-bearing minerals available in these samples. Furthermore, Sample S4 is unradiogenic although Th yields are relatively high, most likely because the release of common Pb from feldspars dominated the $^{208}Pb/^{204}Pb$ signatures.

Only samples S3, S5 and S6 exhibit $^{208}Pb$ budgets with isotope signatures close to that of the whole rock, whereas all others were depleted in radiogenic $^{208}Pb$ to different degrees. From our Th data we conclude that sample material of G4, S1 and S2 was highly depleted in Th-rich refractory minerals and consequently in $^{208}Pb$ relative to the bulk rock material. Although residual material of G1, G2 and G3 contained significant amounts of Th-rich refractory minerals the sample material was slightly depleted in Th-rich accessory minerals compared with the whole rock. These observations strongly suggest the important role of sorting processes during the sample treatment, e.g. due to the loss of refractory zircons (see also section 3.5.2.3).

#### *3.5.3.6 Radiogenic Pb from zircon minerals and estimation of the alpha recoil-effect*

The analyses of the total digestions of zircon mineral separates confirms their expected highly radiogenic $^{206}Pb/^{204}Pb$, $^{207}Pb/^{204}Pb$ and $^{208}Pb/^{204}Pb$ signatures (up to 1385, 87 and 214 respectively). Furthermore, the release of radiogenic Pb from zircon minerals is clearly controlled by the availability of fresh mineral surfaces.

Analogous to observations from Nd and Hf isotopes, Figure 3.9 c and f illustrate the fact that contaminant minerals (exhibiting a more unradiogenic Pb signature), releasing a Pb isotope signature similar to that of the whole rock composition, dominate the incomplete leachates of non-powdered zircons (circles with dashed lines). The unradiogenic Pb isotope signature suggests that these contaminant minerals are mostly feldspars, which is plausible given that they represent the largest mineral group of the studied rocks.

Weak incomplete leachates of powdered zircon separates, on the other hand, exhibit more radiogenic Pb signatures (except in sample Z3p) suggesting the presence of a labile pool of radiogenic Pb from fresh and reactive mineral surfaces (zircons as well as contaminant minerals) and/or damages of their mineral lattice caused by the recoil of multiple α-decays of the U and Th decay series isotopes (e.g. Silver et al. 1980; Davis and Krogh 2001). These two mechanisms, however, are hard to distinguish since a higher abundance of reactive mineral surfaces increases both the congruent release of Pb during dissolution as well as due to the recoil-effect. Nevertheless, the recoil-effect would have its greatest impact during the initial phase of weathering as proposed in earlier studies (Erel et al. 1994; von Blanckenburg and Nägler 2001). In our zircon leaching experiment, in contrast, increases in leaching intensity even correspond to more radiogenic Pb isotope signatures suggesting a subordinate role of the recoil-effect. This is in coherence with the observations from initial weathering conditions in group G and S, which do not show more radiogenic Pb signatures that would have been expected from a dominant recoil effect.

The fact that experiment B that released most radiogenic $^{206}Pb/^{204}Pb$, $^{207}Pb/^{204}Pb$ during G and S leaching shows the least radiogenic signatures for zircon separates strongly suggests that zircon minerals do not release much of their radiogenic Pb during this step.

Increased Hf and Zr yields in the residual material of sample G3, however, indicate the increased abundance of zircons in this sample. Similarly, S5 and S6 are enriched in zircon minerals as demonstrated from QemScan analyses and high Hf yields in step R. Thus it is not surprising that the budgets of these three samples are shifted towards more radiogenic Pb, which is mainly visible in the total digests of the residual material.

#### *3.5.3.7 Comparison of fresh rock and streambed sediment leaches*

In general, our Pb yield data (Figure 3.9 j-l) demonstrate that fresh granite samples (group G) release Pb more readily from easily alterable minerals, most evidently in step A and BThe sediments contain higher relative proportions of Pb in refractory minerals in step R (Table A 5 in the appendix). This observation suggests that the streambed sediments have experienced some degree of alteration, which is resolvable in our experiment.

Furthermore, leachates of group S provide no evidence for the depletion of (more radiogenic) easily weatherable minerals present in the streambed sediments. This is confirmed by low Pb concentrations in the leachates compared to those of the bulk rock supporting only a small amount of Pb being mobilized. Therefore, in line with the conclusions of Erel et al. (2004) we suggest that weathering processes have not been at work for more than 10,000 years.

In contrast to fresh bulk rock samples in group G, the streambed sediments have likely received significant contributions of unradiogenic Pb of anthropogenic origin. While initial $^{206}Pb/^{204}Pb$ and $^{207}Pb/^{204}Pb$ signatures are in the same range as the residues of the fresh granite samples it is highly likely that anthropogenic contributions are significant. Moreover, fresh (reactive) mineral surfaces have most likely already experienced alteration and are thus not expected to influence Pb isotope signatures.

Other variations between group G and S are most likely based on differences in mineral availability in the respective samples (described above), which is in turn controlled by mineral sorting processes in the stream sediments.

## 3.6 Implications for the decoupling of Hf and Nd isotopes during chemical and physical weathering in the terrestrial regime

The decoupling of Nd and Hf isotope signatures in our experimental data is clearly visible in step C of all groups. In this step Hf isotope signatures stay very radiogenic (except for subgroup Z-P), whereas Nd isotopes are released almost congruently (Figure 3.5 a-f). This clearly demonstrates the different geochemical character of the two isotope systems and serves to explain the observed decoupling in seawater (e.g. Albarède et al. 1998). The highly incongruent isotope compositions of Hf, on the other hand, are pointing out the important role of radiogenic trace minerals for this isotope system, which will be described in the following sections.

### 3.6.1 Chemical weathering of Hf-bearing minerals: incongruent dissolution of the zircon-free portion (ZFP) and the zircon effect

Based on the measured concentrations of Hf in pure zircon mineral analyses (10166 ppm) and on that of the whole rock (5.3 ppm), as well as the average weight percentage of zircon minerals in the bulk rock (0.036%; see section 3.3.2.1) we determine the amount of Hf in the zircon free portion (ZFP) to be 1.7 ppm and consequently the percentage of zircon-bound Hf in our granite samples to be 69% according to:

$$f_{Hf\,in\,zircons} = \frac{[\mathrm{Hf}]_{WR} - [\mathrm{Hf}]_{ZFP}}{[\mathrm{Hf}]_{WR}} \tag{3.1}$$

$$[\mathrm{Hf}]_{ZFP} = \frac{[\mathrm{Hf}]_{WR} - f_{pure\,zircon} \cdot [\mathrm{Hf}]_{pure\,zircon}}{1 - f_{pure\,zircon}} \tag{3.2}$$

where $f_{Hf\,in\,zircons}$ is the percentage of Hf bound in zircon minerals and $f_{pure\,zircon}$ is the weight percentage of zircon minerals in the whole rock. This result agrees well with the conclusions of van de Flierdt et al. (2007) and Chen et al. (2011) who suggested an average crustal percentage of 65% Hf stored in zircons based on model data. With known Hf isotope compositions of the pure zircon material and of the whole rock we calculate the theoretical Hf isotope composition of the ZFP:

$$\varepsilon_{Hf\text{-}ZFP} = \frac{\varepsilon_{Hf\text{-}WR} - f_{Hf\,in\,zircons} \cdot \varepsilon_{Hf\text{-}zircon}}{1 - f_{Hf\,in\,zircons}} \tag{3.3}$$

Applying the above-described results for $f_{Hf\,in\,zircons}$ we calculate the $\varepsilon_{Hf}$ of the ZFP to be +1.3, which corresponds to a bulk rock $\varepsilon_{Hf}$ signature of -3.1. However, given the weight percentages are based on the Qemscan analyses the values for $f_{Hf\,in\,zircons}$ and $\varepsilon_{Hf}$ of the ZFP can only be used as a coarse estimate with uncertainties of up to 100% (section 3.3.2).

Nonetheless, with the calculated $\varepsilon_{Hf}$ of the ZFP being well below the range which is expected for sea and river water at the given Nd isotope composition of the seawater array (see Figure 3.8) and supported by the offset observed between the dissolved and the suspended Hf in a study of four Swiss rivers (Rickli et al. 2013), we conclude that the mere retention of unradiogenic Hf in zircons (zircon effect) cannot alone account for radiogenic Hf isotope compositions found dissolved in natural waters. This confirms conclusions drawn from model-data (Chen et al. 2011) and empirical data defining the zircon-free sediment array (Bayon et al. 2009).

These observations further corroborate earlier suggestions that a significant fraction of the radiogenic Hf responsible for the seawater array must be derived from the preferential dissolution of the ZFP. Apatite and sphene have been shown to carry highly radiogenic Hf isotope signatures (see also Figure 3.6). On the other hand, a large fraction of less radiogenic Hf in the ZFP has to be released in order to compensate for the supply from radiogenic minerals to result in intermediate Hf isotope signatures (close to the zircon free sediment array of Bayon et al. 2009).

Assuming that the total amount of Hf bound to the ZFP fraction in the analyzed rock samples is about 1.7 ppm and an average of 0.015 ppm was dissolved during incomplete leaching we estimate that during our experiment only about one percent of the Hf contained in the ZFP was released. Thus, our leaching experiment data demonstrate that this small preferentially released fraction is dominated by highly radiogenic mineral fractions (apatite and sphene; Figure 3.6), which supports the conclusions of Bayon et al. (2006) that the Hf isotope composition of river waters is primarily controlled by preferential dissolution of accessory phases (i.e., apatite, sphene, allanite) rather than more resistant minerals (e.g., biotite, plagioclase, K-feldspar). This is further supported by observations from Nd and Pb isotopes, which attest a strong influence of radiogenic Nd and Pb most likely originating from apatites.

Considering a weight percentage of apatite minerals of 0.12% (section 3.3.2.1), an assumed $[Hf]_{apatite}$ of 0.06 ppm (Barfod et al. 2003), and an $\varepsilon_{Hf}$ signature as radiogenic as +2358 we infer that in the theoretical case of a complete retention of all Hf in zircon minerals an apatite-sourced fraction of only 0.2% in the released Hf is sufficient to generate a Hf isotope signature on the seawater array. These implications suggest, that the incongruent dissolution of the ZFP ("ZFP effect") alone could in fact account for the generation of the seawater array.

Moreover, if we take into account zircon dissolution on the order of 0.3 % the dissolution of an apatite-sourced fraction of only 0.34% is still sufficient to raise the Hf isotope signature to a typical seawater value. In addition, incomplete leaching of zircon mineral grains (Z-N steps A & B) lends evidence to a significant "zircon

effect" during chemical weathering. Since these leachates are clearly dominated by radiogenic Hf released from contaminant mineral phases (sections 3.5.1.1, 3.5.2.2 and 3.5.3.6) we conclude that no significant amounts of Hf are released from mechanically unaltered zircons under incipient weathering conditions.

Zircon powders, in contrast, clearly release zircon-sourced Hf to solution, which will be highly significant for the Hf isotope composition of weathering solutions, in particular after the retreat of glaciers leaving behind fine-grained rock powders. This feature may become important during glacial maxima or late-glacial stages at ocean margins near major ice sheets.

We conclude that during incipient weathering conditions a combination of both the “zircon effect” as well as the “ZFP effect” controls the Hf isotope composition in the weathering solutions. As weathering progresses these effects are weakening given that increasing amounts of Hf are also released to dissolution from more resistant minerals, which results in the Hf isotope compositions of the solutions becoming increasingly more congruent.

### *3.6.2 Physical weathering: more congruent Hf isotope signatures under glacial weathering conditions from the ZFP?*

The conclusions drawn above suggest that under natural weathering conditions accompanied by glacial grinding the partial dissolution of zircon minerals also constitutes a significant source of unradiogenic Hf to the oceans as proposed in previous studies (Piotrowski et al. 2000; van de Flierdt et al. 2002; Gutjahr et al. 2014; Dausmann et al. 2015). In contrast, the more congruent release of Hf via dissolution of the ZFP-minerals, as demonstrated by far more congruent Hf isotope signatures during incomplete leaches of ground samples in group G (Figure 3.10 A), can also account for more congruent weathering during glacials.

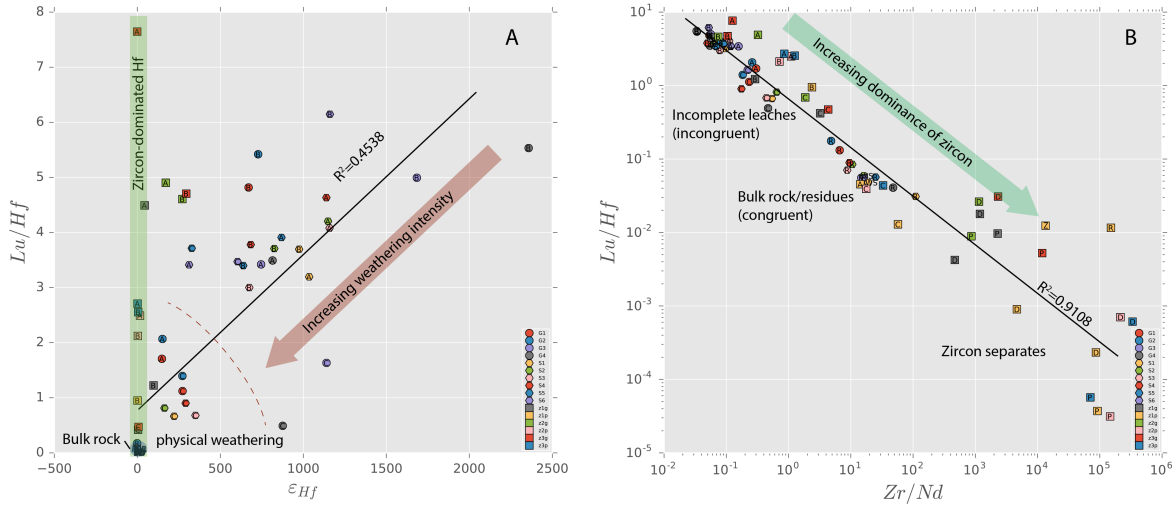


**Figure 3.10: (A) Cross-plot of Lu/Hf and Zr/Nd ratio (Note the logarithmic scale of both axes) illustrating the close relationship between the dissolution of zircon mineral material and the Lu-Hf isotope system, which is closely linked to the relationship between Lu/Hf and Hf-isotope signatures depicted in B. The Zr-Nd ratio is mainly a function of the amount of zircon material dissolved since Zr is highly enriched, whereas Nd is strongly depleted in zircons.**

Figure 3.8 shows a compilation of combined Hf-Nd seawater isotope data from glacially affected regions of the North Atlantic and Arctic Ocean, which appear to define a subdomain of the seawater array. This "glacially affected seawater" array resembles the seawater array but is shifted to less radiogenic Hf isotope values by 2 to 5 $\varepsilon_{Hf}$ units, supporting more congruent weathering under glacial conditions. The slope of this array defined by $\varepsilon_{Hf} = 0.46 \cdot \varepsilon_{Nd} + 3.58$ is almost parallel to that of the seawater array.

Thus within some uncertainty we can calculate the theoretical $\varepsilon_{Hf}$ of seawater controlled by the glacial weathering of continental rocks with the properties of our whole rock to be in the order of +1.6, which is about 3 $\varepsilon_{Hf}$ units lower than the theoretical seawater value generated from these rocks (+4.6 following relations described in Albarède et al. 1998 and Bayon et al. 2009). Below we illustrate why enhanced glacial weathering of zircon alone cannot account for the more congruent Hf-Nd seawater isotope systematics:

The theoretical case that all additional (unradiogenic) Hf released due to glacial activity originates from zircons is highly unlikely, since it is unrealistic that only zircons are weathered more congruently due to glacial grinding. The other extreme case, however, that the unradiogenic Hf discharged due to glacial weathering processes is derived solely from the congruent weathering of the ZFP can theoretically only be achieved if about 90% of the Hf in glacial seawater is derived from congruent dissolution of the ZFP. This implies that while the congruency in the weathering of zircon is unchanged the shift in $\varepsilon_{Hf}$ can be generated by more congrent weathering of the ZFP alone (Figure 3.10 A).

The dominant role of the ZFP-effect due to physically ground minerals is further supported by the fact that while powdered zircon separates deliver about one order of magnitude more Hf than their non-powdered counterparts, the same leaching procedure dissolved only 1.5 times more Hf from subgroup G-P when compared to G-N. If the more efficient dissolution of zircon under enhanced mechanical breakdown were the dominant process for the whole rock dissolution, we would expect the enhancement in the Hf yield to be similar in both experiments, G and Z.

Nonetheless, increased Hf yields from ground zircon separates attest that zircons are in fact weathered more efficiently after mechanical grinding. This suggests that although the more congruent weathering of the ZFP is the dominant factor controlling the Hf budget in dissolution, even the "reduced zircon effect" may still exert significant influence, particularly in the light of extensive continental ice sheets at work during Pleistocene glacial cycles. In experiment G evidence for increased influence from the dissolution of zircon minerals arises from increased Zr/Nd ratios (Figure 3.10 B) documenting an increased Zr output while Nd at the same time remains more or less constant. This validates the aforementioned assumption that mechanical breakdown of zircons enhances their availability for weathering in general. However, our experimental data show that this is not the dominant process leading to more congruent weathering of Hf isotopes under glacial conditions.

In nature, most likely a combination of both processes is responsible for the observed signatures which is probably also controlled by other environmental factors such as different water-rock interaction times as demonstrated in a recent study comparing glacially and non-glacially dominated rivers in Greenland (Rickli et al. 2017). Accordingly contributions from reactive/radiogenic minerals are favored by short interaction times (efficient drainage/run-off) as present under non-glacial conditions. Glacial rivers, on the other hand, receive continuous contributions from waters of distributed sub glacial drainage systems thus exposed to long interaction times and experience a higher influence from zircon-sourced Hf. This temporal factor cannot, however, be resolved in our experiment.

The reduction of 3 $\varepsilon_{Hf}$ units representing the shift to a glacially dominated weathering regime, finally, can have many different reasons. Our new experimental data demonstrate that, together, a decreased zircon-effect and the more congruent weathering of the ZFP are certainly the key processes for these changes in the oceans' Hf isotope compositions.

## 3.7 Summary and Conclusions

In this study, the release of Nd, Hf and Pb from a granitic rock and its minerals during chemical and physical weathering processes was simulated by sequential leaching experiments. These experiments document the systematic preferential release of radiogenic Nd, Hf and Pb isotopes primarily controlled by dissolution characteristics of the host rock's accessory and major minerals. The data demonstrate a high degree of coherence between all isotope systems, which suggests that the preferential digestion of labile accessory minerals, in particular apatite and sphene, dominates the release of radiogenic Nd, Hf and Pb during weak chemical weathering of fresh rock surfaces. The degree of incongruent release of radiogenic Nd is surprising since differences in Sm/Nd between mineral phases are small. The overall effect of mineral-controlled fractionation on Hf isotopes is much larger and also persists under enhanced chemical weathering intensities. Consequently, we find that the about 69% of the total Hf in the analyzed host rocks contained in highly resistant zircons were hardly dissolved or released at all during the incomplete leaching experiments.

The fact that radiogenic $^{206}Pb$ and $^{207}Pb$ in powdered unweathered granite material are dissolved congruently under incipient weathering conditions implies that an easily accessible fraction originating from different minerals (probably mostly feldspars) are available for dissolution at this stage of weathering due to the increased availability of reactive mineral surfaces. This feature is observed despite elevated U release rates during incipient weathering experiments providing clear evidence for preferential U-rich accessory mineral dissolution. With continued weathering/leaching, reactive surfaces of other rock-forming mineral phases appear to decrease leading to enhanced release of radiogenic $^{206}Pb$ and $^{207}Pb$ due to the dissolution of a labile uranogenic mineral phase (probably apatite). Our results also suggest that washout of alpha-recoiled radiogenic Pb during incipient chemical weathering likely does not alter the Pb isotope composition of the runoff to a resolvable degree. In contrast to $^{206}Pb$ and $^{207}Pb$, radiogenic $^{208}Pb$ in the simulated weathering solutions is depleted with respect to the whole rock composition since Th-bearing minerals, the main sources of radiogenic $^{208}Pb$, are generally more resistant to dissolution. Overall, the differences in Pb isotope trends between the subgroups of the experiment are mainly controlled by differences in mineral availability and are probably also controlled by mineral sorting processes.

Mechanical grinding of rocks and their mineral phases clearly reduces the fractionation of Hf and Nd isotopes during dissolution of the host rocks through increasing the fraction of more resistant minerals of the zircon-free fraction accessible to weathering. In addition, more efficient dissolution of zircon minerals is

documented by enhanced release of Hf from ground zircon separates and thus further contributes to the more congruent release of radiogenic Hf isotopes to weathering solutions and ultimately to the ocean under enhanced glacial weathering conditions.

**Acknowledgements**

This study has greatly benefited from discussions with Jörg Rickli. We are grateful to Ana Kolevica who helped by performing concentration measurements. Björn Baresel and Joshua Davies are thanked for helping with sample preparations in Geneva. Jutta Heinze is thanked for help during the conduction of the experiment. We thank Anna Jentzen and Birgit Mohr for the help with the SEM pictures at the University of Kiel. Our special thanks go to the host of the Damma glacier hut for a spectacularly good dinner.

**References**

Albarède, F., Simonetti, A., Vervoort, J.D., Blichert-Toft, J. and Abouchami, W., 1998. A Hf-Nd isotopic correlation in ferromanganese nodules. *Geophysical Research Letters*, 25(20), p.3895. DOI:10.1029/1998GL900008

Anderson, S.P., 2007. Biogeochemistry of glacial landscape systems. *Annual Review of Earth and Planetary Sciences*, 35(1), pp.375–399. DOI:10.1146/annurev.earth.35.031306.140033

Andersson, P.S., Dahlqvist, R., Ingri, J. and Gustafsson, Ö., 2001. The isotopic composition of Nd in a boreal river: A reflection of selective weathering and colloidal transport. *Geochimica et Cosmochimica Acta*, 65(4), pp.521–527. DOI:10.1016/S0016-7037(00)00535-4

Anthony, J.W., Bideaux, R.A.W., Bladh, K., Nichols, M.C. and (Eds.), 2001. Handbook of Mineralogy. *http://www.handbookofmineralogy.org/*, p.1.

Baker, J., Peate, D., Waight, T. and Meyzen, C., 2004. Pb isotopic analysis of standards and samples using a 207Pb–204Pb double spike and thallium to correct for mass bias with a double-focusing MC-ICP-MS. *Chemical Geology*, 211(3), pp.275–303. DOI:10.1016/j.chemgeo.2004.06.030

Balan, E., Trocellier, P., Jupille, J., Fritsch, E., Muller, J.P. and Calas, G., 2001. Surface chemistry of weathered zircons. *Chemical Geology*, 181(1–4), pp.13–22. DOI:10.1016/S0009-2541(01)00271-6

Barfod, G.H., Krogstad, E.J., Frei, R. and Albarède, F., 2005. Lu-Hf and PbSL geochronology of apatites from Proterozoic terranes: A first look at Lu-Hf

isotopic closure in metamorphic apatite. *Geochimica et Cosmochimica Acta*, 69(7), pp.1847–1859. DOI:10.1016/j.gca.2004.09.014

Barfod, G.H., Otero, O. and Albarède, F., 2003. Phosphate Lu-Hf geochronology. *Chemical Geology*, 200(3–4), pp.241–253. DOI:10.1016/S0009-2541(03)00202-X

Bayon, G., Burton, K.W., Soulet, G., Vigier, N., Dennielou, B., Etoubleau, J., Ponzevera, E., German, C.R. and Nesbitt, R.W., 2009. Hf and Nd isotopes in marine sediments: Constraints on global silicate weathering. *Earth and Planetary Science Letters*, 277(3–4), pp.318–326. DOI:10.1016/j.epsl.2008.10.028

Bayon, G., Skonieczny, C., Delvigne, C., Toucanne, S., Bermell, S., Ponzevera, E. and André, L., 2016. Environmental Hf–Nd isotopic decoupling in World river clays. *Earth and Planetary Science Letters*, 438, pp.25–36. DOI:10.1016/j.epsl.2016.01.010

Bayon, G., Vigier, N., Burton, K.W., Brenot, A., Carignan, J., Etoubleau, J. and Chu, N.C., 2006. The control of weathering processes on riverine and seawater hafnium isotope ratios. *Geology*, 34(6), pp.433–436. DOI:10.1130/G22130.1

Bea, F., 1996. Residence of REE, Y, Th and U in Granites and Crustal Protoliths; Implications for the Chemistry of Crustal Melts. *Journal of Petrology*, 37(3), pp.521–552. DOI:10.1093/petrology/37.3.521

Belshaw, N.., Freedman, P.., O'Nions, R.., Frank, M. and Guo, Y., 1998. A new variable dispersion double-focusing plasma mass spectrometer with performance illustrated for Pb isotopes. *International Journal of Mass Spectrometry*, 181(1–3), pp.51–58. DOI:10.1016/S1387-3806(98)14150-7

von Blanckenburg, F. and Nägler, T.F., 2001. Weathering versus circulation controlled changes in radiogenic isotope tracer composition of the Labrador Sea and North Atlantic Deep Water. *Paleoceanography*, 16(4), pp.424–434.

Burton, K.W., Lee, D.C., Christensen, J.N., Halliday, A.N. and Hein, J.R., 1999. Actual timing of neodymium isotopic variations recorded by Fe-Mn crusts in the western North Atlantic. *Earth and Planetary Science Letters*, 171(1), pp.149–156. DOI:10.1016/S0012-821X(99)00138-7

Chen, T.Y., Frank, M., Haley, B. a., Gutjahr, M. and Spielhagen, R.F., 2012. Variations of North Atlantic inflow to the central Arctic Ocean over the last 14 million years inferred from hafnium and neodymium isotopes. *Earth and Planetary Science Letters*, 353–354, pp.82–92. DOI:10.1016/j.epsl.2012.08.012

Chen, T.Y., Ling, H.F., Frank, M., Zhao, K.D. and Jiang, S.Y., 2011. Zircon effect alone

insufficient to generate seawater Nd-Hf isotope relationships. *Geochemistry, Geophysics, Geosystems*, 12(5). DOI:10.1029/2010GC003363

Crocket, K.C., Foster, G.L., Vance, D., Richards, D.A. and Tranter, M., 2013. A Pb isotope tracer of ocean-ice sheet interaction: The record from the NE Atlantic during the Last Glacial/Interglacial cycle. *Quaternary Science Reviews*, 82, pp.133–144. DOI:10.1016/j.quascirev.2013.10.020

Crocket, K.C., Vance, D., Foster, G.L., Richards, D.A. and Tranter, M., 2012. Continental weathering fluxes during the last glacial/interglacial cycle: Insights from the marine sedimentary Pb isotope record at Orphan Knoll, NW Atlantic. *Quaternary Science Reviews*, 38, pp.89–99. DOI:10.1016/j.quascirev.2012.02.004

Dausmann, V., Frank, M., Gutjahr, M. and Rickli, J., 2017. Glacial reduction of AMOC strength and long-term transition in weathering inputs into the Southern Ocean since the mid-Miocene: Evidence from radiogenic Nd and Hf isotopes. *Paleoceanography*, 32(3), pp.265–283. DOI:10.1002/2016PA003056

Dausmann, V., Frank, M., Siebert, C., Christl, M. and Hein, J.R., 2015. The evolution of weathering inputs and deep ocean circulation in the Arctic Ocean since the Late Miocene: Radiogenic isotope evidence. *Earth and Planetary Science Letters*, 419, pp.111–124. DOI:10.1016/j.epsl.2015.03.007

David, K., Frank, M., O'Nions, R.K., Belshaw, N.S. and Arden, J.W., 2001. The Hf isotope composition of global seawater and the evolution of Hf isotopes in the deep Pacific Ocean from Fe-Mn crusts. *Chemical Geology*, 178(1–4), pp.23–42. DOI:10.1016/S0009-2541(00)00427-7

Davis, D.W. and Krogh, T.E., 2001. Preferential dissolution of 234U and radiogenic Pb from α-recoil-damaged lattice sites in zircon: Implications for thermal histories and Pb isotopic fractionation in the near surface environment. *Chemical Geology*, 172(1–2), pp.41–58. DOI:10.1016/S0009-2541(00)00235-7

Erel, Y., Blum, J.D., Roueff, E. and Ganor, J., 2004. Lead and strontium isotopes as monitors of experimental granitoid mineral dissolution. *Geochimica et Cosmochimica Acta*, 68(22), pp.4649–4663. DOI:10.1016/j.gca.2004.04.022

Erel, Y., Harlavan, Y. and Blum, J.D., 1994. Lead isotope systematics of granitoid weathering. *Geochimica et Cosmochimica Acta*, 58(23), pp.5299–5306. DOI:10.1016/0016-7037(94)90313-1

Filippova, A., Frank, M., Kienast, M., Rickli, J., Hathorne, E., Yashayaev, I.M. and Pahnke, K., 2017. Water mass circulation and weathering inputs in the

Labrador Sea based on coupled Hf–Nd isotope compositions and rare earth element distributions. *Geochimica et Cosmochimica Acta*, 199, pp.164–184. DOI:10.1016/j.gca.2016.11.024

Fleischer, R.L., 1982. Alpha-recoil damage and solution effects in minerals: uranium isotopic disequilibrium and radon release. *Geochimica et Cosmochimica Acta*, 46(11), pp.2191–2201. DOI:10.1016/0016-7037(82)90194-6

van de Flierdt, T., Frank, M., Lee, D.-C., Halliday, A.N., Reynolds, B.C. and Hein, J.R., 2004. New constraints on the sources and behavior of neodymium and hafnium in seawater from Pacific Ocean ferromanganese crusts. *Geochimica et Cosmochimica Acta*, 68(19), pp.3827–3843. DOI:10.1016/j.gca.2004.03.009

van de Flierdt, T., Frank, M., Lee, D.C. and Halliday, A.N., 2002. Glacial weathering and the hafnium isotope composition of seawater. *Earth and Planetary Science Letters*, 201(3–4), pp.639–647. DOI:10.1016/S0012-821X(02)00731-8

van de Flierdt, T., Goldstein, S.L., Hemming, S.R., Roy, M., Frank, M. and Halliday, A.N., 2007. Global neodymium–hafnium isotope systematics — revisited. *Earth and Planetary Science Letters*, 259(3–4), pp.432–441. DOI:10.1016/j.epsl.2007.05.003

Foster, G.L. and Vance, D., 2006. Negligible glacial-interglacial variation in continental chemical weathering rates. *Nature*, 444(7121), pp.918–921. DOI:10.1038/nature05365

Galer, S. and O'Nions, R., 1989. Chemical and isotopic studies of ultramafic inclusions from the San Carlos volcanic field, Arizona: A bearing on their petrogenesis. *Journal of Petrology*, 30(4), pp.1033–1064. DOI:10.1093/petrology/30.4.1033

Garçon, M., Chauvel, C., France-Lanord, C., Huyghe, P. and Lavé, J., 2013a. Continental sedimentary processes decouple Nd and Hf isotopes. *Geochimica et Cosmochimica Acta*, 121, pp.177–195. DOI:10.1016/j.gca.2013.07.027

Garçon, M., Chauvel, C., France-Lanord, C., Limonta, M. and Garzanti, E., 2013b. Which minerals control the Nd-Hf-Sr-Pb isotopic compositions of river sediments? *Chemical Geology*, 364, pp.42–55. DOI:10.1016/j.chemgeo.2013.11.018

Godfrey, L. V., Field, M.P. and Sherrell, R.M., 2008. Estuarine distributions of Zr, Hf, and Ag in the Hudson River and the implications for their continental and anthropogenic sources to seawater. *Geochemistry, Geophysics, Geosystems*, 9(12), p.n/a-n/a. DOI:10.1029/2008GC002123

Godfrey, L. V., Zimmermann, B., Lee, D.-C., King, R.L., Vervoort, J.D., Sherrell, R.M. and Halliday, A.N., 2009. Hafnium and neodymium isotope variations in NE Atlantic seawater. *Geochemistry, Geophysics, Geosystems*, 10(8), p.n/a-n/a. DOI:10.1029/2009GC002508

Goldich, S.S., 1938. A Study in Rock-Weathering. *The Journal of Geology*, 46(1), pp.17–58. DOI:10.1086/624619

Goldstein, S.L., O'Nions, R.K. and Hamilton, P.J., 1984. A Sm-Nd isotopic study of atmospheric dusts and particulates from major river systems. *Earth and Planetary Science Letters*, 70(2), pp.221–236. DOI:10.1016/0012-821X(84)90007-4

Gutjahr, M., Frank, M., Halliday, A.N. and Keigwin, L.D., 2009. Retreat of the Laurentide ice sheet tracked by the isotopic composition of Pb in western North Atlantic seawater during termination 1. *Earth and Planetary Science Letters*, 286(3–4), pp.546–555. DOI:10.1016/j.epsl.2009.07.020

Gutjahr, M., Frank, M., Lippold, J. and Halliday, A.N., 2014. Peak Last Glacial weathering intensity on the North American continent recorded by the authigenic Hf isotope composition of North Atlantic deep-sea sediments. *Quaternary Science Reviews*, 99, pp.97–117. DOI:10.1016/j.quascirev.2014.06.022

Harlavan, Y. and Erel, Y., 2002. The release of Pb and REE from granitoids by the dissolution of accessory phases. *Geochimica et Cosmochimica Acta*, 66(5), pp.837–848. DOI:10.1016/S0016-7037(01)00806-7

Harlavan, Y., Erel, Y. and Blum, J.D., 1998. Systematic Changes in Lead Isotopic Composition with Soil Age in Glacial Granitic Terrains. *Geochimica et Cosmochimica Acta*, 62(1), pp.33–46. DOI:10.1016/S0016-7037(97)00328-1

Kurzweil, F., Gutjahr, M., Vance, D. and Keigwin, L., 2010. Authigenic Pb isotopes from the Laurentian Fan: Changes in chemical weathering and patterns of North American freshwater runoff during the last deglaciation. *Earth and Planetary Science Letters*, 299(3–4), pp.458–465. DOI:10.1016/j.epsl.2010.09.031

Ma, J., Wei, G., Xu, Y. and Long, W., 2010. Variations of Sr-Nd-Hf isotopic systematics in basalt during intensive weathering. *Chemical Geology*, 269(3–4), pp.376–385. DOI:10.1016/j.chemgeo.2009.10.012

Merschel, G., Bau, M., Schmidt, K., Münker, C. and Dantas, E.L., 2017. Hafnium and neodymium isotopes and REY distribution in the truly dissolved, nanoparticulate/colloidal and suspended loads of rivers in the Amazon Basin, Brazil. *Geochimica et Cosmochimica Acta*, 213(2017), pp.383–399.

DOI:10.1016/j.gca.2017.07.006

Millman, K.J. and Aivazis, M., 2011. Python for Scientists and Engineers. *Computing in Science & Engineering*, 13(2), pp.9–12. DOI:10.1109/MCSE.2011.36

Münker, C., Weyer, S., Scherer, E. and Mezger, K., 2001. Separation of high field strength elements (Nb, Ta, Zr, Hf) and Lu from rock samples for MC-ICPMS measurements. *Geochemistry, Geophysics, Geosystems*, 2(12). DOI:10.1029/2001GC000183

Nagasawa, H., 1970. Rare earth concentrations in zircons and apatites and their host dacites and granites. *Earth and Planetary Science Letters*, 9(4), pp.359–364. DOI:10.1016/0012-821X(70)90136-6

Nowell, G.M., Kempton, P.D., Noble, S.R., Saunders, A.D., Mahoney, J.J. and Taylor, R.N., 1998. High-precision Hf isotopic measurements of MORB and OIB by thermal ionization mass-spectrometry: insights into the depleted mantle. *Chemical Geology*, 149(3), pp.211–233.

Öhlander, B., Ingri, J., Land, M. and Schöberg, H., 2000. Change of Sm-Nd isotope composition during weathering of till. *Geochimica et Cosmochimica Acta*, 64(5), pp.813–820. DOI:10.1016/S0016-7037(99)00365-8

Öhlander, B., Land, M., Ingri, J. and Widerlund, A., 1996. Mobility of rare earth elements during weathering of till in northern Sweden. *Applied Geochemistry*, 11(1–2), pp.93–99. DOI:10.1016/0883-2927(95)00044-5

Patchett, P.J., White, W.M., Feldmann, H., Kielinczuk, S. and Hofmann, a. W., 1984. Hafnium/rare earth element fractionation in the sedimentary system and crustal recycling into the Earth's mantle. *Earth and Planetary Science Letters*, 69(2), pp.365–378. DOI:10.1016/0012-821X(84)90195-X

Pin, C. and Zalduegui, J.F.S., 1997. Sequential separation of light rare-earth elements, thorium and uranium by miniaturized extraction chromatography: Application to isotopic analyses of silicate rocks. *Analytica Chimica Acta*, 339(1–2), pp.79–89. DOI:10.1016/S0003-2670(96)00499-0

Piotrowski, A.M., Lee, D.-C., Christensen, J.N., Burton, K.W., Halliday, A.N., Hein, J.R. and Günther, D., 2000. Changes in erosion and ocean circulation recorded in the Hf isotopic compositions of North Atlantic and Indian Ocean ferromanganese crusts. *Earth and Planetary Science Letters*, 181(3), pp.315–325. DOI:10.1016/S0012-821X(00)00205-3

Pirrie, D., Butcher, A.R., Power, M.R., Gottlieb, P. and Miller, G.L., 2004. Rapid

quantitative mineral and phase analysis using automated scanning electron microscopy (QemSCAN); potential applications in forensic geoscience. *Geological Society, London, Special Publications*, 232(1), pp.123–136. DOI:10.1144/GSL.SP.2004.232.01.12

Rickli, J., Frank, M., Baker, A.R., Aciego, S., de Souza, G., Georg, R.B. and Halliday, A.N., 2010. Hafnium and neodymium isotopes in surface waters of the eastern Atlantic Ocean: Implications for sources and inputs of trace metals to the ocean. *Geochimica et Cosmochimica Acta*, 74(2), pp.540–557. DOI:10.1016/j.gca.2009.10.006

Rickli, J., Frank, M., Stichel, T., Georg, R.B., Vance, D. and Halliday, A.N., 2013. Controls on the incongruent release of hafnium during weathering of metamorphic and sedimentary catchments. *Geochimica et Cosmochimica Acta*, 101, pp.263–284. DOI:10.1016/j.gca.2012.10.019

Rickli, J., Hindshaw, R.S., Leuthold, J., Wadham, J.L., Burton, K.W. and Vance, D., 2017. Impact of glacial activity on the weathering of Hf isotopes - observations from Southwest Greenland. *Geochimica et Cosmochimica Acta*, 215, pp.295–316. DOI:10.1016/j.gca.2017.08.005

Schaltegger, U. and Corfu, F., 1992. The age and source of late Hercynian magmatism in the central Alps: evidence from precise U-Pb ages and initial Hf isotopes. *Contributions to Mineralogy and Petrology*, 111(3), pp.329–344. DOI:10.1007/BF00311195

Schaltegger, U. and Krähenbühl, U., 1990. Heavy rare-earth element enrichment in granites of the Aar Massif (Central Alps, Switzerland). *Chemical Geology*, 89(1–2), pp.49–63. DOI:10.1016/0009-2541(90)90059-G

Schön, J.H., 2015. *Physical properties of rocks: Fundamentals and principles of geophysics*,

Sha, L.-K. and Chappell, B.W., 1999. Apatite chemical composition, determined by electron microprobe and laser-ablation inductively coupled plasma mass spectrometry, as a probe into granite petrogenesis. *Geochimica et Cosmochimica Acta*, 63(22), pp.3861–3881. DOI:10.1016/S0016-7037(99)00210-0

Silver, L., Williams, I. and Woodhead, J., 1980. *Uranium in granites from the Southwestern United States: actinide parent-daughter systems, sites and mobilization. First year report*,DOI:10.2172/6621099

Tanaka, T., Togashi, S., Kamioka, H., Amakawa, H., Kagami, H., Hamamoto, T.,

Yuhara, M., Orihashi, Y., Yoneda, S., Shimizu, H., Kunimaru, T., Takahashi, K., Yanagi, T., Nakano, T., Fujimaki, H., Shinjo, R., Asahara, Y., Tanimizu, M. and Dragusanu, C., 2000. JNdi-1: A neodymium isotopic reference in consistency with LaJolla neodymium. *Chemical Geology*, 168(3–4), pp.279–281. DOI:10.1016/S0009-2541(00)00198-4

Vance, D. and Burton, K., 1999. Neodymium isotopes in planktonic foraminifera: A record of the response of continental weathering and ocean circulation rates to climate change. *Earth and Planetary Science Letters*, 173(4), pp.365–379. DOI:10.1016/S0012-821X(99)00244-7

Vance, D., Teagle, D. a H. and Foster, G.L., 2009. Variable Quaternary chemical weathering fluxes and imbalances in marine geochemical budgets. *Nature*, 458(7237), pp.493–496. DOI:10.1038/nature07828

Vance, D. and Thirlwall, M., 2002. An assessment of mass discrimination in MC-ICPMS using Nd isotopes. *Chemical Geology*, 185(3), pp.227–240. DOI:10.1016/S0009-2541(01)00402-8

Vervoort, J.D., Plank, T. and Prytulak, J., 2011. The Hf-Nd isotopic composition of marine sediments. *Geochimica et Cosmochimica Acta*, 75(20), pp.5903–5926. DOI:10.1016/j.gca.2011.07.046

White, W.M., Patchett, J. and BenOthman, D., 1986. Hf isotope ratios of marine sediments and Mn nodules: evidence for a mantle source of Hf in seawater. *Earth and Planetary Science Letters*, 79(1–2), pp.46–54. DOI:10.1016/0012-821X(86)90039-7

# 4 Radiogenic neodymium and hafnium isotope compositions of seawater in the Bay of Biscay: Conservative mixing versus non-conservative inputs.

**To be submitted to GCA as:** Dausmann, V., Frank, M. and Zieringer, M.: Radiogenic neodymium and hafnium isotope compositions of seawater in the Bay of Biscay: Conservative mixing versus non-conservative inputs.

## Abstract

We present dissolved neodymium and hafnium concentrations and isotope compositions of surface and deep-water masses from the Bay of Biscay together with Rare Earth Element concentrations. Hafnium and Rare Earth Element concentrations in subsurface waters mainly reflect a nutrient-like increase with depth in the Bay of Biscay. The Nd isotope data acquired in this study range from $\varepsilon_{Nd}$ = -12.9 to -9.4. It is demonstrated that radiogenic Nd isotope signatures in the analyzed surface waters of the Bay of Biscay are dominated by local weathering inputs from the rocks of the surrounding continental margin. Subsurface Eastern North Atlantic Central Water (ENACW) shows a distinct Nd isotope composition of $\varepsilon_{Nd}$ = -12.0 at the southwestern-most station and is significantly diluted on its way along the European margin by mixing with more radiogenic waters from above and below. Furthermore, the Nd isotope data clearly show the declining influence of radiogenic Mediterranean Outflow Water (MOW; $\varepsilon_{Nd}$ = -10.1) at intermediate depths on its way north as it is diluted with ENACW indicating that only 40% to 60% of MOW still present at the Galician margin arrives at the stations further north. A potentially seasonal/temporal feature of Nd isotope changes in MOW is identified when comparing the results of this study with those of earlier studies from the area, which possibly reflects the meandering flow path of MOW. Higher proportions of MOW-like Nd signatures are also manifested in elevated Nd concentrations likely originating from increased terrestrial inputs to the Mediterranean Sea and are then transported as far as the Galician margin. In agreement with observations from Nd isotopes we infer that the Hf isotope composition of MOW was affected by large-scale inputs of dust as can be deduced from elevated Hf concentrations at the Galician margin. The deep-water Nd isotope signatures in the Capbreton region strongly suggest exchange with local shelf sediments. Similarly, Hf isotopes in all water masses of the Bay of Biscay are generally overprinted by local inputs. Therefore, Hf isotope compositions in the Bay of Biscay do not reflect the mixing of respective water masses. Combined with Nd, however, Hf serves as a useful indicator whether a water mass is more proximally affected by inputs from weathering or if it has been advected over long distances.

## 4.1 Introduction

The radiogenic isotopes of neodymium (Nd) and hafnium (Hf) are commonly used tools for the reconstruction of paleoceanographic properties such as water mass circulation and mixing, as well as erosional inputs and related conditions on the continents (e.g. Burton et al. 1997; Piotrowski et al. 2000; Rutberg et al. 2000; Frank 2002; van de Flierdt et al. 2002; Chen et al. 2012). In order to faithfully interpret past isotope records, however, the biogeochemical behavior of Hf and Nd in present-day seawater needs to be understood. Therefore, the water-mass related Hf and Nd isotope distributions in a number of regions of the oceans have been studied (e.g. Piepgras and Wasserburg 1982, 1983; Jeandel 1993; Godfrey et al. 2009; Rickli et al. 2009; Stichel et al. 2012).

The applicability of these radiogenic isotope systems as tracers of ocean circulation is primarily based on their "quasi-conservative" behavior in seawater and residence times similar to the global mixing time of the ocean. This requires that the seawater isotope compositions at a given location principally reflect relative contributions of the respective element from the mixing of water masses. However, non-conservative processes, such as scavenging, vertical regeneration in the water column or inputs from the sediments may obscure advected signals (Goldstein and Hemming 2003; Siddall et al. 2008).

In the case of Nd isotopes it has been demonstrated that in the open ocean the system mostly behaves conservatively with residence times ranging from 500 to 2000 years (e.g. Jeandel et al. 1995; Tachikawa 2003). Nevertheless, a number of studies have observed that Nd can be released or exchanged along continental margins (Lacan and Jeandel 2005a, 2005b; Rickli et al. 2009; Carter et al. 2012; Wilson et al. 2013), implying a non-conservative behavior at least close to the sediment-water interface.

For Hf, on the other hand, there is recent evidence for a much shorter residence time in seawater compared to that of Nd (Rickli et al. 2009, 2014). Rickli et al (2009) argued, that Hf and Nd behave significantly different in the water column, despite that the same processes affect both elements. Accordingly, there is evidence for partial dissolution of terrigenous inputs into surface waters in the case of Nd, while this is not observed to the same extent for Hf. It was thus concluded that scavenging of Hf is more efficient than of Nd while at the same time particulate Hf may be less readily dissolved when introduced into seawater. The mostly non-conservative behavior of Hf in seawater consequently restricts the use of Hf isotopes as tracers of ocean circulation to basin-scales.

The main sources of Hf and Nd in seawater are weathering inputs from the continents. During weathering Nd is released to seawater essentially congruently whereas Hf is released incongruently. This reflects the preferential release of radiogenic Hf from easily weathered minerals (such as apatite and sphene) with high Lu/Hf (Bayon et al. 2006; Rickli et al. 2017; chapter 3) and the efficient retention of unradiogenic Hf in robust zircons (Patchett et al. 1984; chapter 3). These incongruent inputs of Hf explain the offset towards more radiogenic Hf isotope compositions for a given Nd isotope composition observed in seawater and seawater-archives (termed "seawater array"; Albarède et al. 1997) when compared to Hf-Nd compositions measured in continental and igneous rocks (termed "terrestrial array"; Vervoort et al. 1999).

Furthermore, records of past seawater obtained from hydrogenetic sediment phases provide evidence that enhanced physical (glacial) weathering and mechanical grinding of the rocks on land leads to more congruent weathering of Hf. This results from a more efficient release of unradiogenic Hf from more resistant minerals (Piotrowski et al. 2000; van de Flierdt et al. 2002; Gutjahr et al. 2014; Dausmann et al. 2015) pointing to changing continental weathering regimes. In addition to that, local inputs of Hf directly from the continents (riverine, estuarine or atmospheric) or from boundary-exchange with the marginal sediments have been demonstrated to modify the seawater Hf isotope composition (Godfrey et al. 2008; Rickli et al. 2010, 2014; Dausmann et al. 2017). These local inputs reflect environmental conditions on close-by continents (Bayon et al. 2016) and the provenance of suspended particles, such as dust.

In summary, studies applying Nd and Hf isotopes need to evaluate, on a site-by-site basis, to which degree temporal variations of Nd and Hf isotope compositions can either be ascribed to changes in ocean circulation or to non-conservative processes related to inputs from land. The Western European margin and the Bay of Biscay are ideal sites to examine the behavior of the radiogenic isotopes given that the isotopic evolution of the water masses is affected by different continental and sedimentary inputs along their pathway.

Here we present new seawater Hf and Nd isotope composition and concentration data together with rare earth elements (REE) distribution patterns to investigate the modification and mixing of North Atlantic water mass signatures during their advection in the Bay of Biscay.

### 4.1.1 Hydrography

Water samples were taken at five sites along the European continental margin of the Bay of Biscay during German research vessel Meteor cruise M84/5, May 31st - June 21st 2011, from the port of Vigo (Spain) to the port of Brest (France). Deep-water samples were collected in submarine canyons close to the continental slope at four of these sites (the Mugia Canyon, the Pagès Escarpment, the Capbreton Canyon and the St. Nazaire Canyon). Surface water was collected at an additional site close to the port of La Coruña. The sampling sites are referred to as Regions I to V along the cruise track (Figure 4.1).

The Bay of Biscay is characterized by a mixed surface layer depth of about 50 m. It is underlain by cyclonically flowing Eastern North Atlantic Central Water (ENACW; Pollard et al. 1996; Jenkins et al. 2015) extending down to about 500 m depth, which is characterized by a salinity minimum of 35.60 psu in its core. Below that, salinity increases rapidly marking the presence of northward flowing Mediterranean Outflow Water (MOW), which extends down to a depth of around 1500 m. MOW is formed by the admixture of Mediterranean seawater to Atlantic water masses in the Gulf of Cadiz (e.g. Tchernia 1980). Coriolis forcing results in its flow along the continental margin of Western Europe. Along its flow path MOW is diluted by mixing with water masses below and above as reflected by the decreasing salinity maximum at 1100 m depth from 36.17 in Region I to 35.8 in Region V. Below MOW, North Eastern Atlantic Deep Water (NEADW) occupies the deep and bottom waters in the study area. In the uppermost part of NEADW at ~2000 m depth the presence of Labrador Sea Water (LSW) is reflected in a salinity minimum (van Aken 2000).

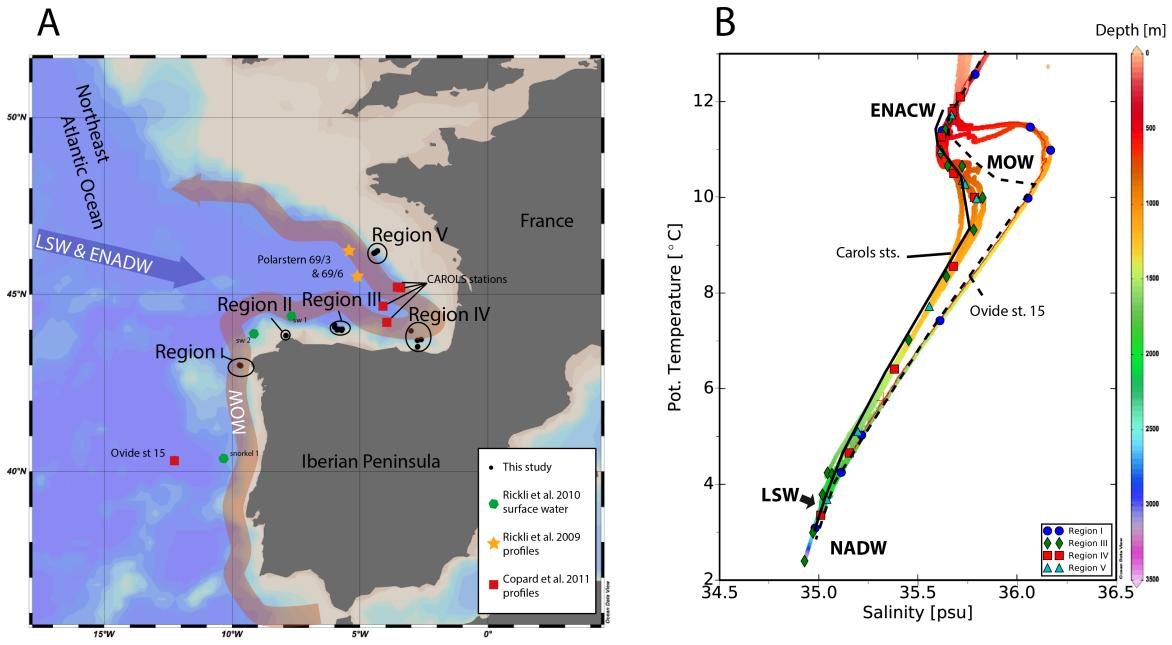


**Figure 4.1: A) Overview map showing the locations of the CTD casts during M84/5 in the Bay of Biscay and other relevant stations in the area (see legend). B) Water masses present in the regions sampled in this study as identified by their potential temperature and salinity. In addition the water mass profiles of Copard et al. (2011) are displayed.**

## 4.2 *Material and Methods*

A set of 6 surface water samples and 42 samples from depths between 124 and 3250 m were taken. In total, 15 profiles were sampled using Niskin bottles mounted to a stainless steel CTD rosette. These profiles are grouped into five geographical regions (see section 4.1.1 and Figure 4.1).

Sample volumes of 20 to 80 l were collected in acid-cleaned 20 l LDPE-collapsible cubitainers and filtered through 0.45 µm Millipore® filters within 12 h after collection. The same happened for the surface water samples (between 20 and 140 l), which were collected using a stainless steel towed fish while the ship was underway. The filtered seawater samples were then acidified to pH ~2 using distilled concentrated nitric acid. For each sample two aliquots of 1 l were separated for the measurement of Hf and Nd concentrations by isotope dilution (ID) and the determination of REE concentrations. All samples were taken and analyzed for REE concentrations and Nd isotope compositions following the GEOTRACES standard protocols (van de Flierdt et al. 2012).

### 4.2.1 *Hf and Nd isotope measurements*

For the analysis of Hf and Nd isotopes 400µl of cleaned $FeCl_3$ solution was added to all samples and Hf and Nd were subsequently coprecipitated with ferric

hydroxide by the addition of ammonia solution raising the pH to 8 (cf. Rickli et al. 2009; Stichel et al. 2012). After settling of the precipitate, most of the supernatant was discarded and the residue was transferred into 2 l PE-bottles for transport to the home laboratory.

In the clean laboratory facilities of GEOMAR the precipitates were then separated from remaining supernatants by centrifugation and further rinsed at least three times with MilliQ water to remove major ions from seawater. Subsequently, the precipitates were dissolved in 4 ml of aqua regia and cooked for at least 24 h at 110 °C in 60ml Teflon vials in order to destroy organic components. After the samples had been dried and brought to chloride-form by dissolution in 6 M HCl the largest proportion of the added Fe was removed by solvent extraction with purified di-ethyl ether.

Some samples formed jelly-like precipitates (containing ~90% of the Hf in the samples) when dissolved in 6M HCl. The precipitates were separated by centrifugation and subsequently dissolved in 2M HF. After evaporation, the jelly separates were dissolved in 6M HCl and added to each sample again.

Hf and Nd were then separated from all other elements following previously established ion exchange chromatographic procedures (Pin and Zalduegui 1997; Münker et al. 2001). The total procedural blank for Hf was negligible at 10 pg compared to typical sample sizes of 2 to 10 ng. For Nd the total procedural blank was below 30 pg and thus considered negligible.

The amounts of Hf and Nd available for measurement varied between 1.4 and 11 ng and between 20 and 200 ng, respectively. All isotope measurements were performed on a Thermo Scientific Neptune Plus at GEOMAR. Measured Hf and Nd isotope compositions were corrected for instrumental mass bias to $^{179}Hf/^{177}Hf$ of 0.7325 and $^{146}Nd/^{144}Nd$ = 0.7219 applying an exponential mass fractionation law. Radiogenic Nd and Hf isotopic compositions are given as ε values, which correspond to the normalized differences of the sample ratio from the one of the chondritic uniform reservoir (CHUR) times 10,000 with $^{143}Nd/^{144}Nd_{CHUR}$ being 0.512638 (Jacobsen and Wasserburg 1980) and $^{176}Hf/^{177}Hf_{CHUR}$ being 0.282785 (Bouvier et al. 2008). The external reproducibility of our Hf isotope analyses was estimated from repeated measurements of the JMC475 standard at concentrations of 1, 2, 5 and 10 ppb and corresponded to 1.18, 0.97, 0.45 and 0.37 $\varepsilon_{Hf}$-units respectively (2 S.D., n = 9 for each beam size, average external reproducibility: 0.74 $\varepsilon_{Hf}$). The external reproducibility of the Nd isotope measurements was estimated based on repeated measurement of the JNdi-1 standard (n = 29) and an in house laboratory standard (n = 14) run at 50 ppb and 30 ppb and gave 0.22 and 0.28 $\varepsilon_{Nd}$ (2 S.D.), respectively. All Nd

and Hf isotope analyses were normalized to the accepted literature values of $^{143}Nd/^{144}Nd$ = 0.512115 for the JNdi-1 standard (Tanaka et al. 2000) and $^{176}Hf/^{177}Hf$ = 0.282160 for the JMC475 standard (Nowell et al. 1998).

### 4.2.2 *Hf and Nd concentration measurements*

Accurate Hf and Nd concentrations were obtained by isotope dilution (ID) following the procedures described in Rickli et al. (2009) and Stichel et al. (2012). Precisely known amounts of Hf single-spike and Nd double-spike solutions, artificially enriched in $^{180}Hf$, $^{149}Sm$ and $^{150}Nd$ respectively, were added to one of the 1l-aliquotes of every sample. Hf and Nd pre-concentration was achieved by iron co-precipitation as described above for the large sample volumes. For Nd sufficient purification was achieved by a single cation chromatographic column separation step (1.4ml BIORAD® AG50W-X8, 200–400 µm mesh-size). The application of a $^{180}Hf$ spike required an additional step of column separation removing interfering $^{180}W$ (1.6ml BIORAD® AG1X-8 resin $Cl^-$ form, 200-400 µm mesh-size) following the protocol of Sahoo et al. (2006). The procedural blank levels were assumed to be similar to those described in Stichel et al. (2012). Analogously blanks of Nd corresponded to less than 1% and no blank corrections were applied. In the same laboratory Stichel et al. (2012) estimated the procedural Hf blank to be 5±0.7 pg (n=11) corresponding to less than 1% of the Hf content of our samples and are thus considered negligible

### 4.2.3 *Rare earth element concentration measurements*

Rare earth element concentration measurements were conducted on an 8 ml sample loop using an online preconcentration technique (OP) ICP-MS at GEOMAR employing an automated "SeaFast" system (Elemental Scientific Inc.) coupled to an Thermo Scientific Element XR analogue to the procedure described by Hathorne et al. (2012). During the measurements, reference seawater from the Bermuda Atlantic Time Series (BATS, 15 m; BATS, 2000 m; van de Flierdt et al. 2012) was used to track the reproducibility and accuracy of the data and are listed for each element in Table A 6 in the appendix. Seawater, from which all the REEs had been removed by Fe-coprecipitation (see above), was used as a procedural blank, which was subtracted from the data.

## 4.3 *Results*

### 4.3.1 *Hf isotope distribution*

A set of 21 deep-water samples and one surface sample was successfully analyzed for Hf isotope compositions (Table A 7 in the appendix and Figure 4.2). The

measured range in $\varepsilon_{Hf}$ between -0.6 and +2.8 agrees well with Hf isotope measurements of seawater samples from nearby stations (RV Polarstern ANT XXIII/1 station 69/3 and station 69/6; $\varepsilon_{Hf}$ ranging between -0.9 and +3.3; Rickli et al. 2009). The surface water sample from Region I shows an $\varepsilon_{Hf}$ value of +1.8, which is within error identical to the nearby surface water measurement sw 2 of Rickli et al. (2010). Shallow water masses above 450 m depth exhibit $\varepsilon_{Hf}$ values within a narrow range close to 0 in all regions (average -0.1 ± 0.5 1 S.D., see Figure 4.2). Below 450 m depth seawater throughout the Bay of Biscay show more variable $\varepsilon_{Hf}$ signatures with a range between -0.6 and +1.4 with an average value of +0.4. Intermediate waters from Region III and a single measurement from Region IV at 511 m depth show relatively radiogenic Hf isotope signatures ($\varepsilon_{Hf}$ between +2.1 and +2.8). A less radiogenic εHf signature between -0.6 and +0.4, however, marks MOW in Region I. The data for Region IV on the other hand, exhibit intermediate $\varepsilon_{Hf}$ values between +0.3 and +1.0 below 500 m in close agreement with the measurements of Rickli et al. (2009). Deeper water masses (below 1500 m) in Regions I and V display a trend towards more radiogenic $\varepsilon_{Hf}$ between +1.4 and +2.2. It is only the deepest sample of Region III (3250 m) that again shows a significantly less radiogenic $\varepsilon_{Hf}$ value of +0.5.

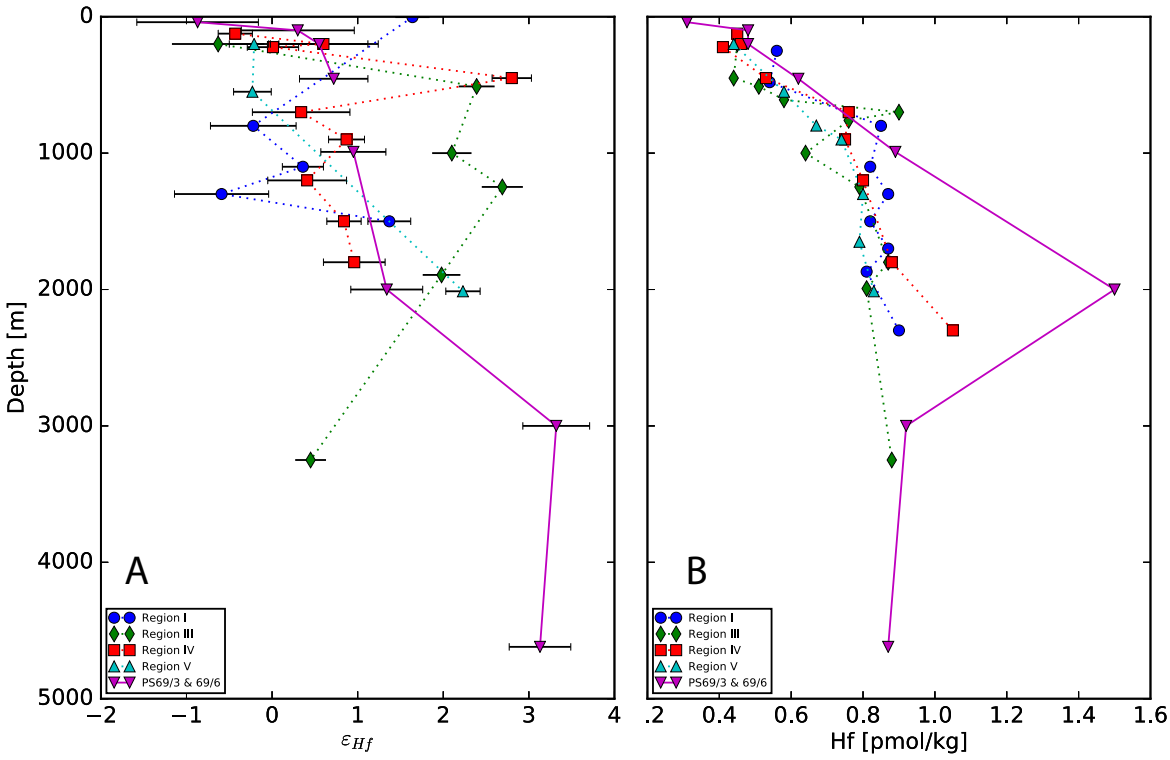


**Figure 4.2: Hafnium isotope compositions (A) and concentration data (B) of all measured samples from the Bay of Biscay plotted together with data from near-by stations of Rickli et al. (2009).**

### 4.3.2 Nd isotope distribution

The Nd isotope data acquired in this study range from $\varepsilon_{Nd}$ = -12.9 to -9.4 (Table A 7 in the appendix). The overall patterns of our Nd isotope signatures agree well with those found in previous studies in the Bay of Biscay (Figure 4.3). The signatures of our Region I and Ovide st.15 (Copard et al. 2011) and those of Region III and the CAROLS stations (Copard et al. 2011) agree particularly well for most depths but also show some distinct differences. The surface waters are characterized by relatively radiogenic $\varepsilon_{Nd}$ values between -10.9 and -9.4 in all five regions, with the most positive values reached in Region II. Nd isotope compositions then decrease with depth to a local minimum ($\varepsilon_{Nd} \approx$ -12 to -11.5) at depths of 500 - 800 m, which is most pronounced and shallowest in most southwesterly Region I. Intermediate water masses between 800 and 1500m water depth (MOW) are again characterized by more radiogenic Nd isotope compositions reaching maximum values (-10.1) at a depth of 1100 m in Region I. The radiogenic maximum at 1000 - 1200 m water depth is also observed in all other regions though less pronounced. Below, the Nd isotope signatures drop again to less radiogenic values between $\varepsilon_{Nd}$ = -13 and -12, reaching minima at depths between 1650 m (Region V) and 1900 m (Region III). This feature is much shallower (1200 m) in Region IV. Bottom water masses below 1800 m (below 1200 m in Region IV) again show a trend towards more radiogenic Nd signatures.

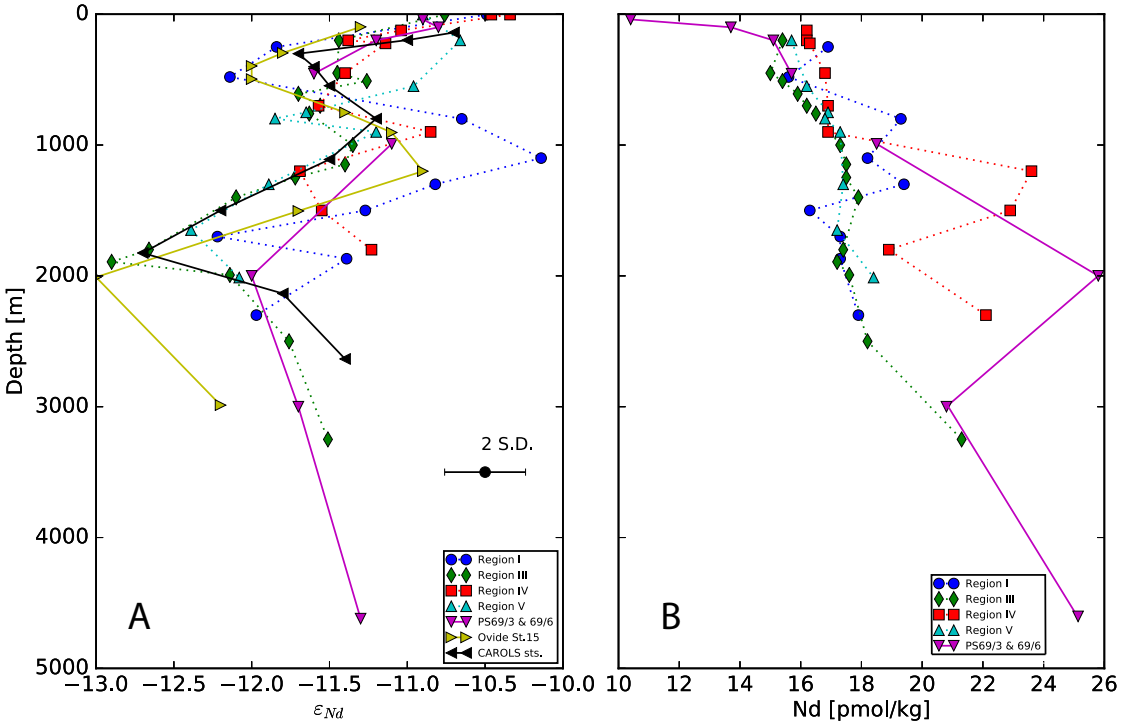


**Figure 4.3: Neodymium isotope compositions (A) and concentration data (B) of all measured samples from the Bay of Biscay plotted together with data from near-by stations of Copard et al. (2011) and Rickli et al. (2009).**

### *4.3.3 Hf and REE concentrations*

All REE analyses acquired from OP-ICP MS measurements are listed in Table A 6 in the appendix. Most elements show relatively homogeneous distributions throughout the water column with a slight trend to low concentrations in the surface and higher concentrations in the deeper water masses (particularly in Region V; see Figure 4.4). Region I and II, however, show slightly enhanced REE concentrations in shallow waters. Cerium, however, shows significantly higher concentrations in shallow water masses compared to deep-water masses. Furthermore, in Region IV Ce concentrations are generally enriched (especially below a depth of 900 m).

Hf and Nd concentration patterns acquired from ID are similar to those of other particle-reactive metals in that lowest concentrations are observed in near surface waters and then grow with depth (Figure 4.2 B and 4.3 B). Hf concentrations (ID) show no large variability throughout the sampled regions in the Bay of Biscay. However, we observe a sudden rise in Hf concentrations between 600 and 800 m water depth from concentrations between 0.4 and 0.6 pmol/kg in the shallow water masses to concentrations between 0.7 and 0.9 pmol/kg below (Figure 4.2 B). This steep increase is most prominent in Regions I and III. Furthermore, Hf concentra-

tions of intermediate waters between 800 and 1500 m water depth are slightly increased in Region I (about 0.05 pmol/kg) compared to the other regions.

The Nd concentrations (ID) show a larger spatial variation in the Bay of Biscay. Prominent features of the Nd concentrations are local maxima in Region I at intermediate depths (between 800 and 1500 m) and in Region IV below 900 m (Figure 4.3 B). The Nd concentrations in intermediate waters of Region I are elevated by 0.5 to 1 pmol/kg compared to the other regions (average at the same depth is ~17 pmol/kg). In Region IV the Nd concentrations below a depth of 900 m are increased more pronouncedly and reach maximum values of up to 23.6 pmol/kg at 1200 m depth. At bottom depth all regions exhibit slightly increased Nd concentrations.


**Figure 4.4: REE concentrations (pmol/kg), HREE/LREE (Er/Nd) ratios and Ce anomalies (Ce/Ce* = 2[Ce]/([La]+[Pr])) versus water depth (m). All shown REE concentrations were obtained by OP-ICP-MS.**

## 4.4 Discussion

### 4.4.1 The elemental distribution of Hf and REE in the Bay of Biscay

The generally homogeneous distribution of Hf and REE concentrations in the uppermost 1000 m throughout the sampled regions in the Bay of Biscay suggests that the concentration of Hf is primarily controlled by particle scavenging at the surface and release in the subsurface waters thus mainly reflecting a nutrient-like increase with depth.

#### 4.4.1.1 Surface water

Surface water in most analyzed regions of the Bay of Biscay is affected by inputs of REE from continental weathering as visible from decreased Ce-anomalies, comparably high REE concentrations (especially Region I and II) and increased La/Yb ratios (Figure 4.4). Only Region V, which is also the remotest of our regions, shows open ocean-like REE concentrations ([Nd] = 10.2 pmol/kg).

#### 4.4.1.2 ENACW and MOW

The sharp rise in Hf concentrations observed at the interface between shallow and intermediate waters in Regions I, III, and IV suggests that the concentration of Hf is related to a water mass boundary. A similar enrichment in intermediate waters of Region I is observed for Nd concentrations (Figure 4.3 B). It is likely that this represents increased amounts of Hf and Nd advected by the plume of MOW, which in the Mediterranean received large inputs via partial dissolution of terrigenous material from the surrounding continents, including Saharan dust (e.g. Meloni et al. 2008). This is further supported by the fact that concentrations are not elevated in the more distal regions (III and V) where the removal of excess (MOW-sourced) Hf and Nd has apparently already been completed. Elevated Ce concentrations in Regions III and IV, on the other hand, suggest the in-situ dissolution of particles. A similar feature, however, is not resolved in Nd or Hf isotope compositions or other REE concentrations.

Nd concentrations below 900 m in Region IV are even higher than in Region I and can thus not be interpreted as Nd inputs from MOW (see below). The fact that the MOW plume is more pronounced in Nd concentrations than in Hf concentrations lends further support to the conclusion of Rickli et al. (2009) that Hf is removed more efficiently from the water column than Nd.

#### 4.4.1.3 Deep water masses

Elevated Nd concentrations (18 to 24 pmol/kg) in the deeper water masses (>900 m) of Region IV (Figure 4.3 B) fall in a similar range as the 'mid-depth' (2000 m) increase in Hf and Nd observed by Rickli et al. (2009). In conjunction with a similar observation of increased amounts of dissolved Fe in nearby water samples (Laës et al. 2003) this enrichment in Nd was interpreted to be sourced by the interaction of LSW with slope sediments before entering the Bay of Biscay from the north. In contrast to the observations of Rickli et al. (2009) we did not find a similar feature in our Hf and Nd concentration profiles suggesting that the enrichment observed by Rickli et al. (2009) may have been linked to a turbidite event. Regarding the confined position of Region IV in the Capbreton canyon, inputs of Nd from local sedimentary sources below 1000 m water depth is more likely. Supported by increased Ce concentrations (Figure 4.4) the high Nd concentrations are interpreted as a reflection of the release of Nd originating from partial dissolution of the detrital fraction of shelf sediments (Lacan and Jeandel 2005a; Rickli et al. 2014) or remineralization in deep waters (cf. Rickli et al. 2009), which is further discussed in section 4.4.3.

### 4.4.2 Hf isotope distribution in the water masses of the Bay of Biscay: conservative versus non-conservative behavior

While the overall range in Hf isotope compositions in this study matches the one obtained by Rickli et al. (2009) the structure of our profiles differs markedly in some regions. It is only the seawater profile from Region IV that agrees quite well with those of stations 69/3 and 69/6 (with the exception of one data point from 450 m water depth; see Figure 4.2 A).

#### 4.4.2.1 Surface water

The surface water Hf isotope composition in Region I is likely affected by local inputs from terrigenous (dust), riverine and/or anthropogenic sources of Hf. Therefore, we assume that the relatively radiogenic $\varepsilon_{Hf}$ value of +1.76 does not reflect surface water mass advection but is rather the product of locally introduced Hf originating from the erosion of rocks from the Galician hinterland which are of Variscan age (e.g. Martínez Catalán et al. 2007; Sánchez Martínez et al. 2011). These rocks are likely to be relatively radiogenic in $\varepsilon_{Hf}$ as can be inferred from radiogenic whole rock $\varepsilon_{Nd}$ values (Sánchez Martínez et al. 2011).

#### 4.4.2.2 ENACW

The ENACW in our study is marked by a distinct Hf isotope composition close to $\varepsilon_{Hf}$ = 0 (-0.1 ± 0.5; 1 S.D.), slightly less radiogenic than measurements or identical within error to those of Rickli et al. (2009) that were in the range from +0.3 to +0.7 albeit with a relatively large uncertainty of ±0.6.

At a water depth near 500 m Hf isotope compositions in the analyzed regions of this study drift apart significantly. While in Region V ENACW stays less radiogenic ($\varepsilon_{Hf}$ = -0.2), it reaches significantly more radiogenic values of up to +2.8 in Regions III and IV. This clearly implies that the same water mass, as demonstrated by their physical properties (Figure 4.1 B), is labeled with distinct Hf isotope signatures in the different regions of the Bay of Biscay and therefore (at least) some of these signatures cannot reflect conservative water mass properties but are the product of local additions of Hf from a different origin. This radiogenic excursion is continued in the intermediate waters of Region III down to a depth of 2000 m. In Region IV, on the other hand, the Hf isotope signatures return to less radiogenic values at 700 m depth. Regarding the fact that most analyzed samples of ENACW (excluding Region III and the 511 m value of Region IV) fall into a range between $\varepsilon_{Hf}$ = -0.6 to +0.9 combining the results of this study and the results of Rickli et al (2009) it is likely, that the Hf isotope composition of ENACW expected from conservative mixing is within this range. Due to the relatively low Hf concentrations in this shallow water mass, however, local inputs of Hf can easily result in a significant alteration of the Hf isotope signature. The increased Hf concentrations in Region III clearly demonstrate this non-conservative process and hence explain the distinct Hf isotope composition in this region.

#### 4.4.2.3 MOW

The intermediate waters of Region I (600 to 1500 m), which show the least diluted hydrographic properties of MOW, exhibit relatively unradiogenic Hf isotope signatures in its core ($\varepsilon_{Hf}$ = -0.6 at 1300 m; Figure 4.5 A). Together with slightly increased Hf concentrations (as well as Nd concentrations as described in section 4.4.1) at the same depth intervals these observations suggest that the measured Hf isotope compositions in Region I mainly reflect conservative admixture of MOW (being slightly less radiogenic than ENACW; see section 4.4.4). This feature, however, is absent or overprinted in all other regions (Figure 4.5 B, C and D) emphasizing the sensitivity of Hf isotope signatures to local inputs. Local additions of Hf, in the case of the analyzed seawater, are most likely derived from interactions with the shelf sediments (e.g. the flanks of the canyons), partial dissolution of lithogenic particles and/or reversible scavenging (e.g. Rickli et al. 2014).

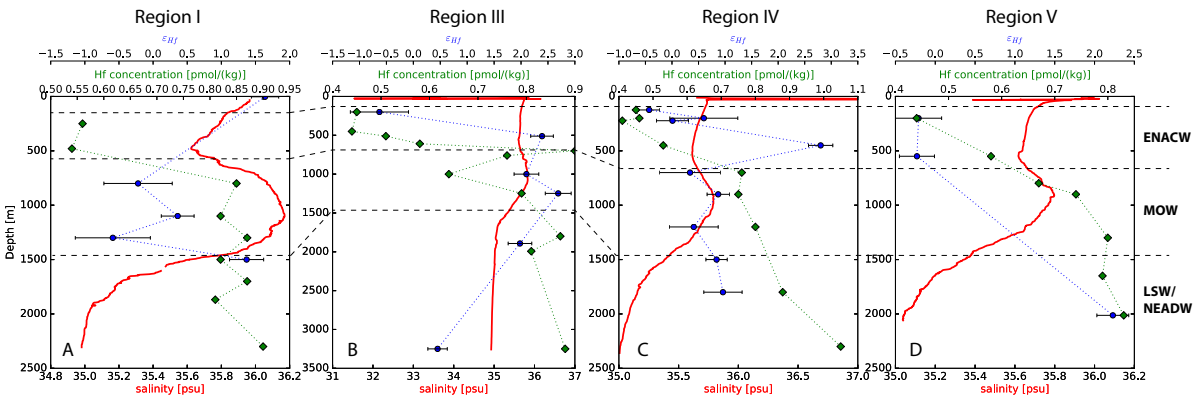


**Figure 4.5: Hafnium isotope and concentration data plotted for each region in the Bay of Biscay plotted together with salinity data for the respective region.**

#### *4.4.2.4 LSW/NADW*

Below 1500 m water depth LSW and NADW occupy the deep Bay of Biscay. In the depth interval between 1500 and 2000 m these water masses are characterized by a Hf isotope signature between +0.8 and +2.2, which agrees with the value of +1.3 of Rickli et al. (2009) at 2000 m water depth. However, similar to the interpretations of Rickli et al (2009) these values are too low for NADW, which has been shown to be more radiogenic in other regions of the Eastern Atlantic (εHf= +3.1 to +3.7; Rickli et al. 2009). Rickli et al. (2009) have argued that less radiogenic Hf was added non-conservatively as a result of the interaction of LSW with shelf sediments as evident by increased Hf concentrations in that depth. In our dataset, however, we cannot find evidence for the addition of Hf from a sediment-source suggesting that the non-conservative behavior observed by Rickli et al. (2009) was a short-term event. Furthermore, a more recent study revealed the less radiogenic Hf isotope composition (by about 2 to 3 $\varepsilon_{Hf}$-units relative to NEADW/NADW) of LSW in the Labrador Sea (Filippova et al. 2017). Consequently, it is plausible that the isotopic structure of deep-waters in the Northwest Atlantic is transferred quasi-conservatively to the Northeast Atlantic Ocean and to the Bay of Biscay.

The relatively unradiogenic Hf isotope signature of one measurement at a depth of 3250 m ($\varepsilon_{Hf}$ = +0.4) in Region III is not in agreement with the values found by Rickli et al. (2009) for these water masses ($\varepsilon_{Hf}$ = +3.1 to +3.3). The influence of LSW seems unlikely in these water depths making the quasi-conservative admixture of less radiogenic water unrealistic. Thus we infer that this value also reflects non-conservative behavior, likely due to interactions with shelf sediments or from the partial dissolution of particles.

### 4.4.3 Nd isotope distribution in the water masses of the Bay of Biscay

The structure of our Nd isotopic compositions (Figure 4.6 A) acquired for the Bay of Biscay is consistent with those found by the studies of Copard et al. (2011) and Rickli et al. (2009). Variations in $\varepsilon_{Nd}$ along the European margin arise from the mixing of Mediterranean waters with those of the Northeast Atlantic and some local inputs from the continents and the shelfs. Copard et al. (2011) already described the evolution of MOW along the Iberian Peninsula. Consequently Nd isotope data from this study is aimed to complement their record as well as reveal possible short-term variations in $\varepsilon_{Nd}$ as were recently observed at near margin sites in the Panama Basin (Grasse et al. 2017) and in the Bay of Bengal (Yu et al. 2017).

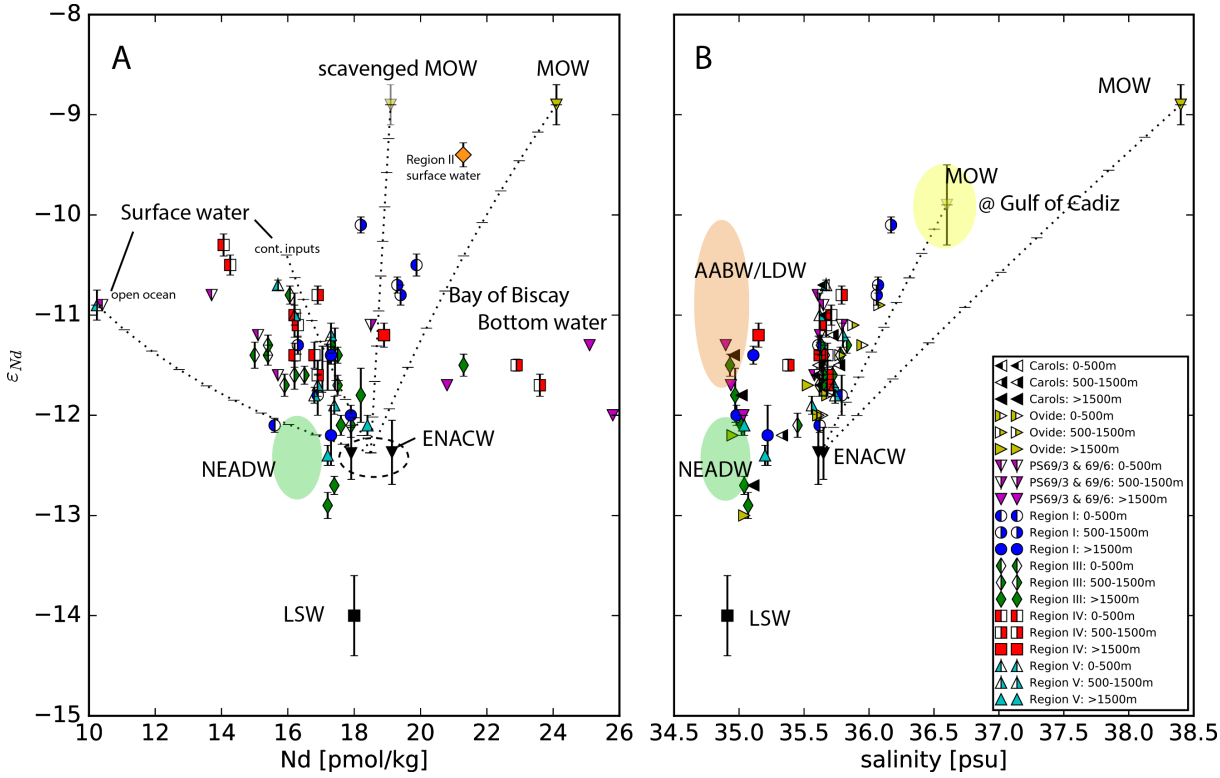


**Figure 4.6: Neodymium isotope compositions plotted against Nd concentration (A) and salinity (B). Dotted lines represent conservative mixing trends between MOW ($\varepsilon_{Nd}$ = -8.9; [Nd] = 24.1 pmol/kg; sal = 38.4 psu; Tachikawa et al. 2004) and ENACW ($\varepsilon_{Nd}$ = -12.4; [Nd] = 17.9 to 19.1 pmol/kg; sal = 35.61 to 35.65 psu; Stichel et al. 2015). Scavenged MOW represents an endmember, which lost 5 pmol/kg due to the removal of Nd with sinking particles following the conclusions of Tachikawa et al. (2004) and Stichel et al. (2015). Two different surface seawater endmembers are displayed (see text for description). LSW endmember data ($\varepsilon_{Nd}$ = -14; [Nd] = 18 pmol/kg; sal = 34.9) is derived from measurements in the Labrador Sea (Filipova et al. 2017).**

#### 4.4.3.1 Surface water

The relatively radiogenic Nd isotope compositions in the surface mixed-layer of the Bay of Biscay (average $\varepsilon_{Nd}$ = -10.4) are most likely derived from radiogenic regional weathering inputs (dissolved and particulate) mixed with less radiogenic Nd

from the water masses below. The rock formations on the surrounding continents are mostly part of the Variscan Belt, which in nearby Galicia have a Nd isotope composition ranging from $\varepsilon_{Nd}$ = +5.9 to +9.9 (Sánchez Martínez et al. 2011). These whole rock values from the Cabo Ortegal Complex are in the direct vicinity of Region II and are reflected by strongly increased Nd concentrations and the most radiogenic surface water value of the entire dataset ($\varepsilon_{Nd}$ = -9.4). A more unradiogenic Nd isotope composition was observed in the most depleted surface water ([Nd]=10.2) in Region V. This agrees well with surface water Nd composition of Rickli et al. 2009.

#### *4.4.3.2 ENACW*

The core of ENACW at a depth of 400-500 m off the coast of Portugal is marked by an $\varepsilon_{Nd}$ value of -12.0 while further north in the Bay of Biscay it is -11.7 at a depth of ~300 m (Copard et al. 2011). Consistently, our new data for the minima in $\varepsilon_{Nd}$ related to ENACW range between -12.1 in Region I and -11.6 in Region IV. Nevertheless, our data disagree with those of Copard et al. (2011) in that these minimum $\varepsilon_{Nd}$ values are reached at greater depth further north in the Bay of Biscay than at the Galician margin. In Region I, where the ENACW is least diluted, the minimum value of -12.1 is reached at a depth of 480 m. Further north ENACW is generally characterized by slightly more radiogenic Nd isotope compositions at depths between 200 and 500 m, while the minimum is reached in a depth of about 600 m, 700 m and 800m in Region III, IV and V, respectively. Furthermore, the upper 500 m in Region V are more radiogenic and reach $\varepsilon_{Nd}$ signatures of -10.7 to -11.0. The general interpretation of Copard et al. (2011) that ENACW loses some of its unradiogenic imprint while it travels along the Iberian Peninsula due to dilution is also reflected in our dataset. Moreover, the data from the stations further along the way into the Bay of Biscay (especially in Region V) indicate that more radiogenic Nd isotope signatures are transferred vertically to ENACW from the weathering-affected surface layer (Figure 4.6).

#### *4.4.3.3 MOW*

Similar to ENACW, MOW is diluted along its way north as has been demonstrated by Copard et al. (2011). In Region I more radiogenic Nd isotope signatures together with enhanced Nd-concentrations are recorded from 800 to 1300 m depth with its core at a depth of 1100 m showing a radiogenic $\varepsilon_{Nd}$ peak of -10.1 demonstrating the presence of a large proportion of MOW (also inferred from the mixing diagram in Figure 4.6 A). Further north the "radiogenic plume" of MOW only occupies a thinner and shallower layer peaking between -11.2 and -10.8 near 900 m.

The maximum value in Region I is even more radiogenic than the value of Copard et al. (2011) for their station off the coast of Portugal (Ovide st. 15; -10.9 at 1200 m). Furthermore, in comparison with Ovide st. 15 the overall more radiogenic signatures of our data set in Region I suggest that MOW had a stronger influence and was less diluted than in the study of Copard et al. (2011). This is in agreement with potential temperature and salinity (T-S) data where the peak of MOW (36.08 psu) at Ovide st. 15 is exceeded by the peak value of 36.17 psu in our Region I profile (Figure 4.1 B and Figure 4.6 B). Together, our Nd isotope data and T-S relations clearly demonstrate the presence of a thicker layer of MOW in our dataset, in comparison with the data of Copard et al. (2011).

$$\varepsilon_{Nd-mix} = \frac{\varepsilon_{Nd-MOW} \times [Nd]_{MOW} \times S_{MOW} \times f + \varepsilon_{Nd-ENACW} \times [Nd]_{ENACW} \times S_{ENACW} \times (1-f)}{[Nd]_{MOW} \times S_{MOW} + [Nd]_{ENACW} \times S_{ENACW}} \quad (4.1)$$

Taking into account the "pure" MOW characteristics of $\varepsilon_{Nd\text{-}MOW}$ = –8.9 to -9.4 $[Nd]_{MOW}$ = 24.1 pmol/kg and $S_{MOW}$ = 38.5 psu determined in the region of its inflow at the Strait of Gibraltar (Spivack and Wasserburg 1988; Tachikawa et al. 2004) and those of ENACW being $\varepsilon_{Nd\text{-}ENACW}$ = –12.4, $[Nd]_{ENACW} \cong$ 18.5 pmol/kg and $S_{ENACW}$ = 35.6 psu (Stichel et al. 2015) we estimate that MOW in Region I ($\varepsilon_{Nd}$ = –10.1) is produced by conservative mixing of 58 to 72% MOW and 42 to 28% ENACW (depending on the Nd isotope composition of the MOW endmember). Calculating the mixing proportions solely based on the salinity budgets of both these water masses, on the other hand, results in a very different proportion of approximately 20% MOW and 80% ENACW. Similar to the conclusions drawn by Copard et al. (2011) we suggest that MOW is already diluted with a third low salinity water mass before it arrives in Region I. In support of this, salinity data of Piepgras and Wasserburg (1983) demonstrate that the highly saline outflow of Mediterranean-source water is already diluted to a salinity of 36.6 psu in the Gulf of Cadiz, resulting in a mixture of approximately 57% MOW and 43% ENACW in Region I. This agrees well with the lower end of mixing proportion of MOW calculated from Nd isotope compositions.

Taking water masses present in Region I as endmembers only about 40% of the MOW present in Region I arrive in Regions III and V, whereas in Region IV the same water mass constitutes about 60%. This suggests that the dilution of MOW along the Iberian margin does not occur in linear relation with distance from its origin but that the flow path of the water mass much rather meanders (as indicated in Figure 4.1 A), therefore explaining spatial and temporal differences in mixing proportions (such as the discrepancy between the data of Ovide St. 15 and those of Region I).

#### 4.4.3.4 LSW/NADW

Nd isotopic compositions in the Bay of Biscay (with the exception of Region IV) are strictly decreasing towards a minimum between -12.9 and -12.2 at a depth of about 1700 -1900 m. The same feature was already observed by Rickli et al. (2009) and Copard et al. (2011) and was interpreted to reflect the presence of LSW in the Bay of Biscay, which is labeled with a unradiogenic Nd isotope composition of around -15 at its origin in the Labrador Sea (Lacan and Jeandel 2004). The greatest influence of LSW in our new data was found in Region III (see Figure 4.6 A and B).

Below the LSW Nd isotope signatures rise again ($\varepsilon_{Nd}$ = -12.4 to $\varepsilon_{Nd}$ = -11.8), which Copard et al. (2011) attributed to the presence of a mixture of NEADW (-12.1 to -12.7; Filippova et al. 2016) and LDW (a derivative of AABW; -10.6 to -11.7; Jeandel 1993). This interpretation is supported by the new Nd data from Regions I, III and V. In Region III (the deepest profile) contributions of LDW grow with depth from a proportion of about 75-25 NEADW-LDW at a depth of 2000 m to 28-72 NEADW-LDW at a depth of 3250 m.

Furthermore, two deep-water (below 1500 m) measurements in Region IV and one in Region I (~1900 m) are significantly more radiogenic than in corresponding depths of the other regions. Since there is no evidence for different water masses from T-S characteristics the addition of Nd with a more radiogenic signature is most likely affecting these sites. Particularly the fact that Nd concentrations (Figure 4.5 A and 4.7 B) are also significantly increased at these depths in Region IV (see section 4.4.1) supports this hypothesis. Remineralization and/or boundary exchange with the close-by shelf sediments (cf. Lacan and Jeandel 2005; Rickli et al. 2014) in the confined canyon systems and their higher likelihood of increased turbidity are the most likely processes explaining these additions. The latter process is supported by sediments along the margin of the Bay of Biscay having mean $\varepsilon_{Nd}$ values of near –10 (e.g. Parra et al. 1998).

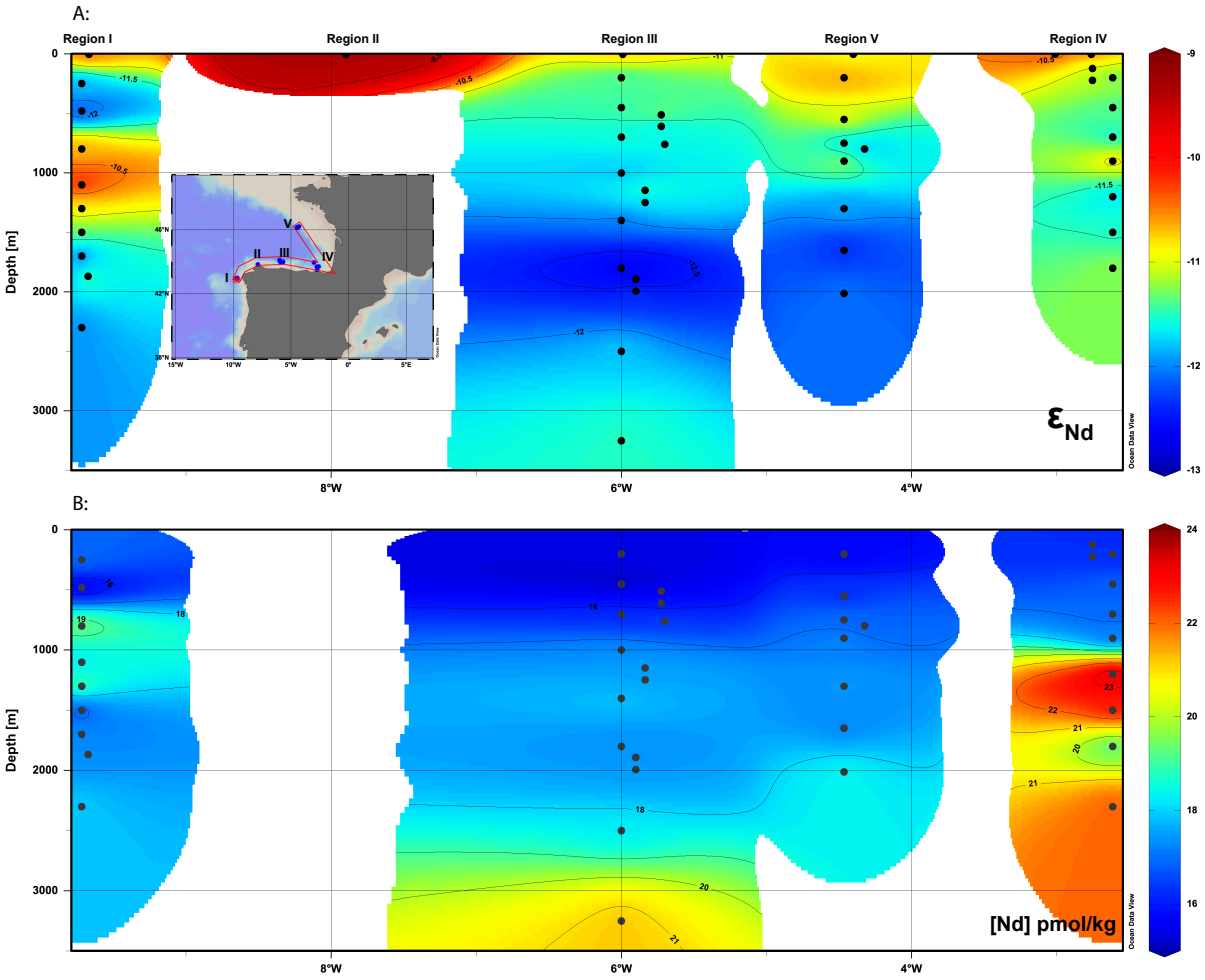


**Figure 4.7: West to East section through the Bay of Biscay showing the distribution of Nd isotope (A) and concentration (B) data of all measured samples in this study. Note that Region V is more to the west of Region IV.**

### *4.4.4 Combined Hf and Nd isotopes*

As described in section 4.4.2, Hf isotopes alone are of limited use as a water mass tracer since Hf isotope signatures may vary significantly within the same water masses. This is due to the fact that Hf is easily affected by local inputs as overall concentrations are low and residence times in seawater are short (due to extensive scavenging, e.g. Rickli et al. 2009). Nevertheless, if combined with Nd isotope analyses, Hf isotopes provide valuable information about the weathering and/or climatic conditions on the continents that the water masses pick up on their way along the continental margins. Our Hf-Nd data all plot close to the well defined seawater-array in Hf-Nd space (Figure 4.8) which was first determined for Fe-Mn hydroxide records (Albarède et al. 1997) and was confirmed by later studies of seawater samples (Godfrey et al. 2009; Rickli et al. 2009; Zimmermann et al. 2009; Stichel et al. 2012).

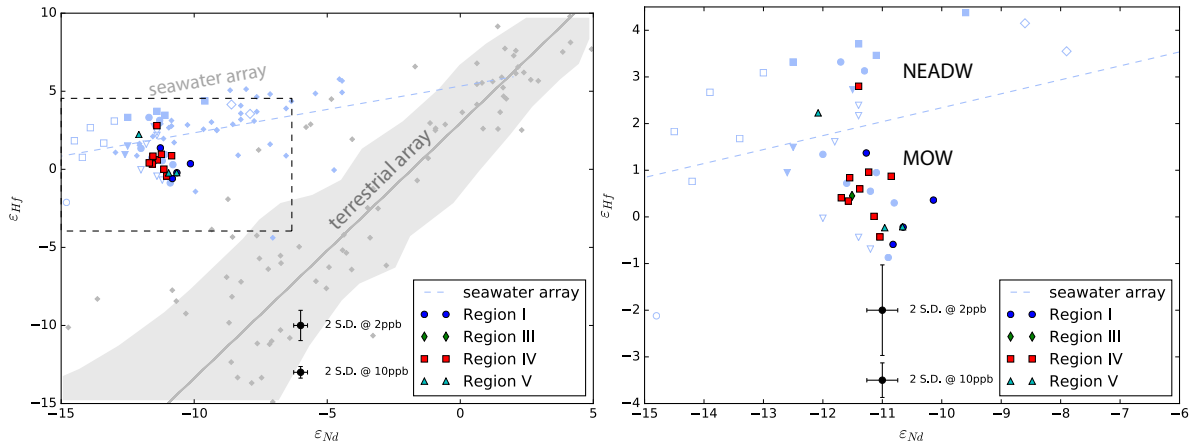


**Figure 4.8: Cross-plot of Hf isotope versus Nd isotope data together with the data from the Eastern Atlantic of Rickli et al. (2009) and the arrays of seawater or seawater-archives (Albarède et al. 1997) and terrestrial rocks (Vervoort et al. 1999).**

Accordingly, Hf isotopes are released incongruently exhibiting more radiogenic values in seawater when compared to the whole rock composition, while Nd isotope show only negligible degrees of incongruence. This incongruent release of Hf, moreover, can be modified by the style of weathering (predominantly chemical versus physical weathering; e.g. Piotrowski et al. 2000; van de Flierdt et al. 2002) on the continent of origin or the mode of influx in which Hf was introduced into the ocean (dust inputs, estuarine activity, hydrothermal activity; e.g. Bau and Koschinsky 2006; Godfrey et al. 2008; Rickli et al. 2010). On the other hand, the degree of congruency is strongly dependent on the age and type of the weathered source-rock. Hence, older rocks typically release Hf of highly incongruent compositions to weathering solutions as they exhibit a wider range of different Hf isotope signatures in their different mineral phases (their radiogenic minerals, which are typically weathered more easily become more radiogenic over time; see chapter 3). By implication, younger igneous rocks (such as present at the European margin and in the Mediterranean region) typically release a more congruent Hf weathering signal. Therefore, we argue that "proximally affected" water masses are characterized by a more congruent Hf isotope composition (below the seawater-array in Figure 4.8) since they carry mostly Hf derived from Mesozoic rocks from the European continent. Water masses from more distal regions (e.g. NEADW from the Western Atlantic or NEACW from remote regions), on the other hand, exhibit distinct properties (more incongruent in the case of NEADW, since it is derived from a region affected by weathering of old continental rocks). In addition, it is likely, that MOW is strongly affected by the in situ dissolution of Hf from Saharan dust deposited in the Mediterranean sea by local wind systems as deduced from increased Hf concentrations in this water mass.

## 4.5 Conclusions

New Hf and Nd isotopic compositions and concentrations are presented for seawater from five regions in the Bay of Biscay. The overall water mass structure found agrees with and confirms the data from nearby stations in the Bay of Biscay.

Radiogenic Nd isotope signatures in the surface waters of the Bay of Biscay are explained by local weathering inputs from the surrounding rocks. ENACW is significantly diluted on its way along the European margin by mixing with more radiogenic waters from above and below. Similarly, the influence of MOW at intermediate depths decreases on its way north as it is diluted with ENACW, as was already shown in earlier studies. By comparison with the data of Copard et al. (2011) we identify a potentially seasonal/temporal feature of Nd isotope changes in MOW. A higher proportion of MOW-like Nd signatures is also manifested in elevated Nd concentrations. These likely originate from increased dust inputs to the Mediterranean Sea and are then transported as far as the Galician margin but not to the other regions of this study further north.

Our interpretations of deep-water Nd compositions in the Bay of Biscay mostly follow those of the studies of Copard et al. (2011) and Rickli et al. (2009). However, we find seawater in the Cap Breton region most likely affected by exchange with shelf sediments.

Hafnium isotopes are generally found not to be a conservative water mass property but are often overprinted by local inputs. This lends support to the hypothesized more efficient removal of Hf (compared with Nd) from the water column as the water masses travel along the continental margin. Combined with Nd, however, it may be a useful indicator if a water mass is more proximally affected by inputs or if it has been advected over long distances. Similar to Nd we infer that the Hf isotope composition of MOW was affected by large-scale inputs of dust as can be deduced from elevated Hf concentrations at the Galician margin.

**Acknowledgements**

We would like to thank the crew of RV Meteor during cruise M84/5. Sascha Flögel is thanked for scientific organization of the cruise and providing hydrographic data. Jutta Heinze, Peer Rahlf and Georgi Laukert are acknowledged for help during the chemical treatment of the samples in the lab. Marcus Gutjahr and Ed Hathorne are thanked for help during the analysis of the isotope and REE concentration measurements.

**References**

van Aken, H.M., 2000. *The hydrography of the mid-latitude northeast Atlantic Ocean: I: The deep water masses*,DOI:10.1016/S0967-0637(99)00092-8

Albarède, F., Goldstein, S.L. and Dautel, D., 1997. The neodymium isotopic composition of manganese nodules from the Southern and Indian oceans, the global oceanic neodymium budget, and their bearing on deep ocean circulation. *Geochimica et Cosmochimica Acta*, 61(6), pp.1277–1291.DOI:10.1016/S0016-7037(96)00404-8

Bau, M. and Koschinsky, A., 2006. Hafnium and neodymium isotopes in seawater and in ferromanganese crusts: The "element perspective." *Earth and Planetary Science Letters*, 241(3–4), pp.952–961.DOI:10.1016/j.epsl.2005.09.067

Bayon, G., Skonieczny, C., Delvigne, C., Toucanne, S., Bermell, S., Ponzevera, E. and André, L., 2016. Environmental Hf–Nd isotopic decoupling in World river clays. *Earth and Planetary Science Letters*, 438, pp.25–36.DOI:10.1016/j.epsl.2016.01.010

Bayon, G., Vigier, N., Burton, K.W., Brenot, A., Carignan, J., Etoubleau, J. and Chu, N.C., 2006. The control of weathering processes on riverine and seawater hafnium isotope ratios. *Geology*, 34(6), pp.433–436.DOI:10.1130/G22130.1

Bouvier, A., Vervoort, J.D. and Patchett, P.J., 2008. The Lu-Hf and Sm-Nd isotopic composition of CHUR: Constraints from unequilibrated chondrites and implications for the bulk composition of terrestrial planets. *Earth and Planetary Science Letters*, 273(1–2), pp.48–57.DOI:10.1016/j.epsl.2008.06.010

Burton, K.W., Ling, H.-F. and O'Nions, R.K., 1997. Closure of the Central American Isthmus and its effect on deep-water formation in the North Atlantic. *Nature*, 386(6623), pp.382–385.DOI:10.1038/386382a0

Carter, P., Vance, D., Hillenbrand, C.D., Smith, J.A. and Shoosmith, D.R., 2012. The neodymium isotopic composition of waters masses in the eastern Pacific sector of the Southern Ocean. *Geochimica et Cosmochimica Acta*, 79, pp.41–59.DOI:10.1016/j.gca.2011.11.034

Chen, T.Y., Frank, M., Haley, B. a., Gutjahr, M. and Spielhagen, R.F., 2012. Variations of North Atlantic inflow to the central Arctic Ocean over the last 14 million years inferred from hafnium and neodymium isotopes. *Earth and Planetary Science Letters*, 353–354, pp.82–92.DOI:10.1016/j.epsl.2012.08.012

Copard, K., Colin, C., Frank, N., Jeandel, C., Montero-Serrano, J.-C., Reverdin, G.

and Ferron, B., 2011. Nd isotopic composition of water masses and dilution of the Mediterranean outflow along the southwest European margin. *Geochemistry, Geophysics, Geosystems*, 12(6).DOI:10.1029/2011GC003529

Dausmann, V., Frank, M., Gutjahr, M. and Rickli, J., 2017. Glacial reduction of AMOC strength and long-term transition in weathering inputs into the Southern Ocean since the mid-Miocene: Evidence from radiogenic Nd and Hf isotopes. *Paleoceanography*, 32(3), pp.265–283.DOI:10.1002/2016PA003056

Dausmann, V., Frank, M., Siebert, C., Christl, M. and Hein, J.R., 2015. The evolution of weathering inputs and deep ocean circulation in the Arctic Ocean since the Late Miocene: Radiogenic isotope evidence. *Earth and Planetary Science Letters*, 419, pp.111–124.DOI:10.1016/j.epsl.2015.03.007

Filippova, A., Frank, M., Kienast, M., Rickli, J., Hathorne, E., Yashayaev, I.M. and Böning, P., 2016. Water mass circulation and weathering inputs in the Labrador Sea based on coupled Hf-Nd isotope compositions and rare earth element distributions. *Geochimica et Cosmochimica Acta*.

Filippova, A., Frank, M., Kienast, M., Rickli, J., Hathorne, E., Yashayaev, I.M. and Pahnke, K., 2017. Water mass circulation and weathering inputs in the Labrador Sea based on coupled Hf–Nd isotope compositions and rare earth element distributions. *Geochimica et Cosmochimica Acta*, 199, pp.164–184.DOI:10.1016/j.gca.2016.11.024

van de Flierdt, T., Frank, M., Lee, D.C. and Halliday, A.N., 2002. Glacial weathering and the hafnium isotope composition of seawater. *Earth and Planetary Science Letters*, 201(3–4), pp.639–647.DOI:10.1016/S0012-821X(02)00731-8

van de Flierdt, T., Pahnke, K., Amakawa, H., Andersson, P., Basak, C., Coles, B., Colin, C., Crocket, K., Frank, M., Frank, N., Goldstein, S.L., Goswami, V., Haley, B.A., Hathorne, E.C., Hemming, S.R., Henderson, G.M., Jeandel, C., Jones, K., Kreissig, K., Lacan, F., Lambelet, M., Martin, E.E., Newkirk, D.R., Obata, H., Pena, L., Piotrowski, A.M., Pradoux, C., Scher, H.D., Schöberg, H., Singh, S.K., Stichel, T., Tazoe, H., Vance, D. and Yang, J., 2012. GEOTRACES intercalibration of neodymium isotopes and rare earth element concentrations in seawater and suspended particles. Part 1: reproducibility of results for the international intercomparison. *Limnology and Oceanography: Methods*, 10(4), pp.234–251.DOI:10.4319/lom.2012.10.234

Frank, M., 2002. Radiogenic isotopes: Tracers of past ocean circulation and erosional input. *Reviews of Geophysics*, 40(1).DOI:10.1029/2000RG000094

Godfrey, L. V., Field, M.P. and Sherrell, R.M., 2008. Estuarine distributions of Zr, Hf, and Ag in the Hudson River and the implications for their continental and anthropogenic sources to seawater. *Geochemistry, Geophysics, Geosystems*, 9(12), p.n/a-n/a.DOI:10.1029/2008GC002123

Godfrey, L. V., Zimmermann, B., Lee, D.-C., King, R.L., Vervoort, J.D., Sherrell, R.M. and Halliday, A.N., 2009. Hafnium and neodymium isotope variations in NE Atlantic seawater. *Geochemistry, Geophysics, Geosystems*, 10(8), p.n/a-n/a.DOI:10.1029/2009GC002508

Goldstein, S.L. and Hemming, S.R., 2003. *Long-lived Isotopic Tracers in Oceanography, Paleoceanography, and Ice-sheet Dynamics*, Elsevier.DOI:10.1016/B0-08-043751-6/06179-X

Grasse, P., Bosse, L., Hathorne, E.C., Böning, P., Pahnke, K. and Frank, M., 2017. Short-term variability of dissolved rare earth elements and neodymium isotopes in the entire water column of the Panama Basin. *Earth and Planetary Science Letters*, 475, pp.242–253.DOI:10.1016/j.epsl.2017.07.022

Gutjahr, M., Frank, M., Lippold, J. and Halliday, A.N., 2014. Peak Last Glacial weathering intensity on the North American continent recorded by the authigenic Hf isotope composition of North Atlantic deep-sea sediments. *Quaternary Science Reviews*, 99, pp.97–117.DOI:10.1016/j.quascirev.2014.06.022

Hathorne, E.C., Haley, B., Stichel, T., Grasse, P., Zieringer, M. and Frank, M., 2012. Online preconcentration ICP-MS analysis of rare earth elements in seawater. *Geochemistry, Geophysics, Geosystems*, 13(1), pp.1–12.DOI:10.1029/2011GC003907

Jacobsen, S.B. and Wasserburg, G.J., 1980. Sm-Nd isoopic evolution of chondrites. *Earth and Planetary Science Letters*, 50(1), pp.139–155.

Jeandel, C., 1993. Concentration and isotopic composition of Nd in the South Atlantic Ocean. *Earth and Planetary Science Letters*, 117(3–4), pp.581–591.DOI:10.1016/0012-821X(93)90104-H

Jeandel, C., Bishop, J.K. and Zindler, A., 1995. Exchange of neodymium and its isotopes between seawater and small and large particles in the Sargasso Sea. *Geochimica et Cosmochimica Acta*, 59(3), pp.535–547.DOI:10.1016/0016-7037(94)00367-U

Jenkins, W.J., Smethie, W.M., Boyle, E.A. and Cutter, G.A., 2015. Water mass analysis for the U.S. GEOTRACES (GA03) North Atlantic sections. *Deep-Sea*

*Research Part II: Topical Studies in Oceanography*, 116, pp.6–20.DOI:10.1016/j.dsr2.2014.11.018

Lacan, F. and Jeandel, C., 2004. Subpolar mode water formation traced by neodymium isotopic composition. *Geophysical Research Letters*, 31(14), pp.1–5.DOI:10.1029/2004GL019747

Lacan, F. and Jeandel, C., 2005a. Neodymium isotopes as a new tool for quantifying exchange fluxes at the continent-ocean interface. *Earth and Planetary Science Letters*, 232(3–4), pp.245–257.DOI:10.1016/j.epsl.2005.01.004

Lacan, F. and Jeandel, C., 2005b. Acquisition of the neodymium isotopic composition of the North Atlantic Deep Water. *Geochemistry, Geophysics, Geosystems*, 6(12).DOI:10.1029/2005GC000956

Laës, A., Blain, S., Laan, P., Achterberg, E.P., Sarthou, G. and de Baar, H.J.W., 2003. Deep dissolved iron profiles in the eastern North Atlantic in relation to water masses. *Geophysical Research Letters*, 30(17), p.1902 doi:10.1029/2003GL017902.DOI:10.1029/2003GL017902

Martínez Catalán, J.R., Arenas, R., Díaz García, F., González Cuadra, P., Gómez-Barreiro, J., Abati, J., Castiñeiras, P., Fernández-Suárez, J., Martínez Sánchez, S. and Andonaegui, P., 2007. Space and time in the tectonic evolution of the northwestern Iberian Massif: Implications for the Variscan belt. *Geological Society of America*, Memoir 200(21), pp.403–423.DOI:10.1130/2007.1200(21).

Meloni, D., di Sarra, A., Monteleone, F., Pace, G., Piacentino, S. and Sferlazzo, D.M., 2008. Seasonal transport patterns of intense Saharan dust events at the Mediterranean island of Lampedusa. *Atmospheric Research*, 88(2), pp.134–148.DOI:10.1016/j.atmosres.2007.10.007

Münker, C., Weyer, S., Scherer, E. and Mezger, K., 2001. Separation of high field strength elements (Nb, Ta, Zr, Hf) and Lu from rock samples for MC-ICPMS measurements. *Geochemistry, Geophysics, Geosystems*, 2(12).DOI:10.1029/2001GC000183

Nowell, G.M., Kempton, P.D., Noble, S.R., Saunders, A.D., Mahoney, J.J. and Taylor, R.N., 1998. High-precision Hf isotopic measurements of MORB and OIB by thermal ionization mass-spectrometry: insights into the depleted mantle. *Chemical Geology*, 149(3), pp.211–233.

Parra, M., Castaing, P., Jouanneau, J.M., Grousset, F. and Latouche, C., 1998. Nd-Sr

isotopic composition of present-day sediments from the Gironde Estuary, its draining basins and the WestGironde mud patch (SW France). *Continental Shelf Research*, 19(1), pp.135–150.DOI:10.1016/S0278-4343(98)00083-1

Patchett, P.J., White, W.M., Feldmann, H., Kielinczuk, S. and Hofmann, a. W., 1984. Hafnium/rare earth element fractionation in the sedimentary system and crustal recycling into the Earth's mantle. *Earth and Planetary Science Letters*, 69(2), pp.365–378.DOI:10.1016/0012-821X(84)90195-X

Piepgras, D. and Wasserburg, G., 1982. Isotopic Composition of Neodymium in Waters from the Drake Passage. *Science*, 217(4556), pp.207–214.DOI:10.1126/science.217.4556.207

Piepgras, D.J. and Wasserburg, G.J., 1983. Influence of the Mediterranean Outflow on the isotopic composition of neodymium in waters of the North Atlantic. *Journal of Geophysical Research*, 88(C10), p.5997.DOI:10.1029/JC088iC10p05997

Pin, C. and Zalduegui, J.F.S., 1997. Sequential separation of light rare-earth elements, thorium and uranium by miniaturized extraction chromatography: Application to isotopic analyses of silicate rocks. *Analytica Chimica Acta*, 339(1–2), pp.79–89.DOI:10.1016/S0003-2670(96)00499-0

Piotrowski, A.M., Lee, D.-C., Christensen, J.N., Burton, K.W., Halliday, A.N., Hein, J.R. and Günther, D., 2000. Changes in erosion and ocean circulation recorded in the Hf isotopic compositions of North Atlantic and Indian Ocean ferromanganese crusts. *Earth and Planetary Science Letters*, 181(3), pp.315–325.DOI:10.1016/S0012-821X(00)00205-3

Pollard, R.T., Griffttths, M.J., Cunningham, S.A., Read, J.F., Pérez, F.F. and Ríos, A.F., 1996. Vivaldi 1991 - A study of the formation, circulation and ventilation of Eastern North Atlantic Central Water. *Progress in Oceanography*, 37(2), pp.167–192.DOI:10.1016/S0079-6611(96)00008-0

Rickli, J., Frank, M., Baker, A.R., Aciego, S., de Souza, G., Georg, R.B. and Halliday, A.N., 2010. Hafnium and neodymium isotopes in surface waters of the eastern Atlantic Ocean: Implications for sources and inputs of trace metals to the ocean. *Geochimica et Cosmochimica Acta*, 74(2), pp.540–557.DOI:10.1016/j.gca.2009.10.006

Rickli, J., Frank, M. and Halliday, A.N., 2009. The hafnium–neodymium isotopic composition of Atlantic seawater. *Earth and Planetary Science Letters*, 280(1–4), pp.118–127.DOI:10.1016/j.epsl.2009.01.026

Rickli, J., Gutjahr, M., Vance, D., Fischer-Gödde, M., Hillenbrand, C.-D. and Kuhn, G., 2014. Neodymium and hafnium boundary contributions to seawater along the West Antarctic continental margin. *Earth and Planetary Science Letters*, 394, pp.99–110.DOI:10.1016/j.epsl.2014.03.008

Rickli, J., Hindshaw, R.S., Leuthold, J., Wadham, J.L., Burton, K.W. and Vance, D., 2017. Impact of glacial activity on the weathering of Hf isotopes - observations from Southwest Greenland. *Geochimica et Cosmochimica Acta*, 215, pp.295–316.DOI:10.1016/j.gca.2017.08.005

Rutberg, R., Hemming, S. and Goldstein, S., 2000. Reduced North Atlantic Deep Water flux to the glacial Southern Ocean inferred from neodymium isotope ratios. *Nature*, 405(6789), pp.935–8.DOI:10.1038/35016049

Sahoo, Y. V, Nakai, S. and Ali, A., 2006. Modified ion exchange separation for tungsten isotopic measurements from kimberlite samples using multi-collector inductively coupled plasma mass spectrometry. *Analyst*, 131(3), pp.434–439.DOI:10.1039/b511557d

Sánchez Martínez, S., Arenas, R., Gerdes, A., Castiñeiras, P., Potrel, A. and Fernández-Suárez, J., 2011. Isotope geochemistry and revised geochronology of the Purrido Ophiolite (Cabo Ortegal Complex, NW Iberian Massif): Devonian magmatism with mixed sources and involved Mesoproterozoic basement. *Journal of the Geological Society*, 168(3), pp.733–750.DOI:10.1144/0016-76492010-065

Siddall, M., Khatiwala, S., van de Flierdt, T., Jones, K., Goldstein, S.L., Hemming, S. and Anderson, R.F., 2008. Towards explaining the Nd paradox using reversible scavenging in an ocean general circulation model. *Earth and Planetary Science Letters*, 274(3–4), pp.448–461.DOI:10.1016/j.epsl.2008.07.044

Spivack, A.J. and Wasserburg, G.J., 1988. Neodymium isotopic composition of the Mediterranean outflow and the eastern North Atlantic. *Geochimica et Cosmochimica Acta*, 52(12), pp.2767–2773.DOI:10.1016/0016-7037(88)90144-5

Stichel, T., Frank, M., Rickli, J. and Haley, B. a., 2012. The hafnium and neodymium isotope composition of seawater in the Atlantic sector of the Southern Ocean. *Earth and Planetary Science Letters*, 317–318, pp.282–294.DOI:10.1016/j.epsl.2011.11.025

Stichel, T., Hartman, A.E., Duggan, B., Goldstein, S.L., Scher, H. and Pahnke, K., 2015. Separating biogeochemical cycling of neodymium from water mass

mixing in the Eastern North Atlantic. *Earth and Planetary Science Letters*, 412, pp.245–260.DOI:10.1016/j.epsl.2014.12.008

Tachikawa, K., 2003. Neodymium budget in the modern ocean and paleo-oceanographic implications. *Journal of Geophysical Research*, 108(C8).DOI:10.1029/1999JC000285

Tachikawa, K., Roy-Barman, M., Michard, A., Thouron, D., Yeghicheyan, D. and Jeandel, C., 2004. Neodymium isotopes in the Mediterranean Sea: Comparison between seawater and sediment signals. *Geochimica et Cosmochimica Acta*, 68(14), pp.3095–3106.DOI:10.1016/j.gca.2004.01.024

Tanaka, T., Togashi, S., Kamioka, H., Amakawa, H., Kagami, H., Hamamoto, T., Yuhara, M., Orihashi, Y., Yoneda, S., Shimizu, H., Kunimaru, T., Takahashi, K., Yanagi, T., Nakano, T., Fujimaki, H., Shinjo, R., Asahara, Y., Tanimizu, M. and Dragusanu, C., 2000. JNdi-1: A neodymium isotopic reference in consistency with LaJolla neodymium. *Chemical Geology*, 168(3–4), pp.279–281.DOI:10.1016/S0009-2541(00)00198-4

Tchernia, P., 1980. *Descriptive regional oceanography*, Pergamon Press.

Vervoort, J.D., Patchett, P.J., Blichert-Toft, J. and Albarède, F., 1999. Relationships between Lu-Hf and Sm-Nd isotopic systems in the global sedimentary system. *Earth and Planetary Science Letters*, 168(1–2), pp.79–99.DOI:10.1016/S0012-821X(99)00047-3

Wilson, D.J., Piotrowski, A.M., Galy, A. and Clegg, J. a., 2013. Reactivity of neodymium carriers in deep sea sediments: Implications for boundary exchange and paleoceanography. *Geochimica et Cosmochimica Acta*, 109, pp.197–221.DOI:10.1016/j.gca.2013.01.042

Yu, Z., Colin, C., Meynadier, L., Douville, E., Dapoigny, A., Reverdin, G., Wu, Q., Wan, S., Song, L., Xu, Z. and Bassinot, F.C., 2017. Seasonal variations in dissolved neodymium isotope composition in the Bay of Bengal. *Earth and Planetary Science Letters*, 479, pp.310–321.DOI:http://dx.doi.org/10.1016/jepsl.2017.09.022

Zimmermann, B., Porcelli, D., Frank, M., Andersson, P.S., Baskaran, M., Lee, D.C. and Halliday, A.N., 2009. Hafnium isotopes in Arctic Ocean water. *Geochimica et Cosmochimica Acta*, 73(11), pp.3218–3233.DOI:10.1016/j.gca.2009.02.028

# 5 Glacial reduction of AMOC strength and long term transition in weathering inputs into the Southern Ocean since the Mid Miocene: Evidence from radiogenic Nd and Hf isotopes

**Published as:** Dausmann, V., Frank, M., Gutjahr, M. and Rickli, J., 2017. Glacial reduction of AMOC strength and long-term transition in weathering inputs into the Southern Ocean since the mid-Miocene: Evidence from radiogenic Nd and Hf isotopes. *Paleoceanography*, 32(3), pp.265–283. DOI:10.1002/2016PA003056

## Abstract

Combined seawater radiogenic hafnium (Hf) and neodymium (Nd) isotope compositions were extracted from bulk sediment leachates and foraminifera of Site 1088, ODP Leg 177, 2082 m water depth on the Agulhas Ridge. The new data provide a continuous reconstruction of long and short-term changes in ocean circulation and continental weathering inputs since the Mid-Miocene. Due to its intermediate water depth the sediments of this core sensitively recorded changes in admixture of North Atlantic Deep Water (NADW) to the Antarctic Circumpolar Current (ACC) as a function of the strength of the Atlantic Meridional Overturning Circulation (AMOC).

Nd isotope compositions ($\varepsilon_{Nd}$) range from -7 to -11 with glacial values generally 1 to 3 units more radiogenic than during the interglacials of the Quaternary. The data reveal episodes of significantly increased AMOC strength during late Miocene and Pliocene warm periods whereas peak radiogenic $\varepsilon_{Nd}$ values mark a strongly diminished AMOC during the major intensification of Northern Hemisphere Glaciation near 2.8 Ma and in the Pleistocene after 1.5 Ma.

In contrast, the Hf isotope compositions ($\varepsilon_{Hf}$) show an essentially continuous evolution from highly radiogenic values of up to +11 during the Miocene to less radiogenic present day values (+2 to +4) during the late Quaternary. The data document a long-term transition in dominant weathering inputs, where inputs from the South America are replaced by those from Southern Africa. Moreover, radiogenic peaks provide evidence for the supply of radiogenic Hf originating from Patagonian rocks to the Atlantic sector of the Southern Ocean via dust inputs.

## *5.1 Introduction*

It has been demonstrated by numerous studies that global climate has been closely linked to the strength of the meridional overturning circulation in the Atlantic Ocean (AMOC) (e.g. Broecker et al. 1985; Enfield et al. 2001; Sutton and Hodson 2005). In this context it is important to understand the processes governing present and past changes in the strength and flow paths of the water masses of the AMOC.

Variations of AMOC strength have been monitored directly during the last decade and have been attributed to adjustments of water mass density in the Labrador Sea due to changes in temperature and salinity in the North Atlantic (e.g. Robson et al. 2015; Jackson et al. 2016). Furthermore, variations in the net heat transfer from the southern to the northern hemisphere via the Agulhas Leakage are thought to contribute to fluctuations in AMOC strength (Biastoch et al. 2008). The export of heat and salt from the Southern Ocean (SO) and Indian Ocean regulates chemical and physical properties of water masses in the Atlantic, especially in the formation region of the North Atlantic Deep Water (NADW) (Gordon et al. 1992).

There is general consensus that millennial-scale and glacial-interglacial (G-I) climate oscillations have been linked to a seesaw between a 'warm' and a 'cold' mode of NADW export to the Southern Ocean and thus AMOC strength (e.g. Boyle & Keigwin 1982; Curry & Lohmann 1982; Oppo & Fairbanks 1987; Rutberg et al. 2000; Piotrowski 2005; Lynch-Stieglitz et al. 2007). From North Atlantic records it is evident that NADW was less dense and was exported at shallower depths during peak glacial conditions in late MIS 3 and MIS 2 to be replaced by southern sourced waters but that the AMOC was at the same time vigorous (Böhm et al. 2015). Pronounced glacial perturbations (such as freshwater inputs from iceberg discharge during Heinrich events), however, were strong enough to diminish or even shut down the AMOC (McManus et al. 2004; Lippold et al. 2012; Böhm et al. 2015), while during interstadials the AMOC remained strong (Henry et al. 2016). In the SO, in contrast, shallower and reduced import of warm and saline NADW has been inferred to have led to a higher degree of stratification, which likely acted as a positive feedback mechanism for global cooling during glacial episodes due to enhanced carbon sequestration to the deep ocean (e.g. Adkins 2013; Yu et al. 2016).

Weathering inputs to the oceans from the continents, on the other hand, have also responded to climatic changes on similar time scales. Changes in the hydrological conditions, for instance, influence weathering style and transport mechanisms (aeolian, fluvial, ice-rafted), while source regions of weathering inputs have changed on both geological and shorter time scales (e.g. Petschick et al. 1996; Walter et al. 2000; Diekmann et al. 2003). Moreover, there is evidence that increased dust supply may act as a feedback mechanism to climatic changes, serving as fertilizer for marine productivity in the high southern latitudes leading to enhanced $CO_2$ draw-down (e.g. Martin 1990; Jaccard et al. 2013). Changes in sources and mechanisms delivering continental inputs to the ocean are thus not only considered to react to changes in climate but also to modify these.

### 5.1.1 Background

Combined radiogenic isotope signatures of neodymium (Nd) and hafnium (Hf) have been applied as reliable tracers of water mass mixing, provenance of weathering inputs and changes in continental weathering regimes (e.g. Frank 2002; Goldstein and Hemming 2003). In dissolved form, Nd is moderately particle-reactive and has an average oceanic residence time between 360 and 1500 years (Jeandel et al. 1995; Tachikawa 2003; Siddall et al. 2008; Arsouze et al. 2009; Rempfer et al. 2011). A longer residence time of Hf compared to Nd has been proposed based on relatively homogenous Hf isotope ratios across different ocean basins and its speciation in seawater (e.g. White et al. 1986; Godfrey et al. 2008). However, more recently evidence emerged that Hafnium is more efficiently adsorbed to particles (Stichel et al. 2012a) and that its residence time in seawater is likely shorter than that of Nd (Rickli et al. 2009; Firdaus et al. 2011; Stichel et al. 2012a; Chen et al. 2013b; Filippova et al. 2016).

Seawater is labelled with the Nd and Hf isotope composition of rocks on the surrounding continents via dissolved weathering inputs by rivers, exchange with particulate material in the water column or with shelf sediments (e.g. Lacan and Jeandel 2005; Bayon et al. 2006; van de Flierdt et al. 2007; Rickli et al. 2009, 2010) and potentially also via hydrothermal inputs in the case of Hf (Bau and Koschinsky 2006). Radiogenic Nd and Hf isotopic compositions are given as ε values, which correspond to the normalized differences of the sample ratio from the one of the chondritic uniform reservoir (CHUR) times 10,000 ($^{143}Nd/^{144}Nd_{CHUR}$ = 0.512638 (Jacobsen and Wasserburg 1980) and $^{176}Hf/^{177}Hf_{CHUR}$ = 0.282769 (Nowell et al. 1998)). The seawater derived isotopic composition of Nd and Hf extracted from marine sediments has been applied to reconstruct water mass mixing-processes and local weathering inputs to the oceans (e.g. Piepgras and Wasserburg 1982; Ling et al. 1997; Burton et al. 1999; Piotrowski et al. 2000; Rutberg et al. 2000; Chen et al. 2012). In fact, while Nd isotopes in the intermediate and deep SO essentially reflect water mass mixing, Hf isotopes were demonstrated to be homogenous in the entire Atlantic sector of the SO (Stichel et al. 2012a) and thus are not suitable to trace water mass mixing in this ocean basin.

The modern hydrography of the Atlantic Sector of the Southern Ocean is dominated by northward flowing Antarctic Intermediate Water (AAIW) at intermediate depths (500 to 1000 m, $\varepsilon_{Nd}$ = -8.5) and Antarctic Bottom Water (AABW) at abyssal ($\varepsilon_{Nd}$ = ~-9), whereas depths between 2000 and 3500m are affected by the admixture of less radiogenic northern sourced NADW ($\varepsilon_{Nd}$ = ~-11) (Stichel et al. 2012a; see Figure 5.1). The well-mixed Circumpolar Deep Water (CDW) of the ACC

also has an $\varepsilon_{Nd}$ signature of ~-9. At the surface, warm and saline water masses entering from the tropical Indian Ocean (Agulhas Current AC; $\varepsilon_{Nd}$ between -7 and -8; Stichel et al. 2012a) are separated from cold southern sourced surface waters at the sub-polar front (Figure 5.1). The Agulhas Ridge rising more than 2500 m from the surrounding seafloor is a part of the Agulhas-Falkland Fracture Zone (AFFZ). The ridge basement is of tectono-magmatic origin and was uplifted at least until the early Oligocene (cf. Uenzelmann-Neben and Gohl 2004). It forms a natural barrier for northward flowing bottom water masses and its top is located in the mixing zone of modern CDW and NADW.

Seawater Nd isotope records obtained from Fe-Mn crusts and authigenic Fe-Mn oxyhydroxide coatings of bulk sediments and of foraminifera in the deep SO revealed a significantly decreased influence of unradiogenic North Atlantic sourced water masses (Northern Component Water NCW) during the last glacial cycle (Rutberg et al. 2000; Piotrowski et al. 2004, 2008; Piotrowski 2005; Skinner et al. 2013) and during the Mid Pleistocene Transition (MPT: 1.2 to 0.7 Ma) (Pena and Goldstein 2014).

Previous studies have also demonstrated that the Lu-Hf and the Sm-Nd isotope-systems behave differently during continental (silicate) weathering and may thus deliver important information on sources and mechanisms of weathering when combined. Distinct relationships for different reservoirs formed during weathering processes such as the 'seawater array' (Albarède et al. 1998) and the 'clay array' (e.g. Bayon et al. 2009, 2016) emerge when directly comparing radiogenic Nd and Hf isotope signatures. These relationships are based on the fact, that very large proportions of a rocks' Hf is bound in zircon minerals, which are very resistant to chemical weathering (e.g. Balan et al. 2001). Intensified physical weathering (e.g. due to glacial erosion) destroying mineral lattices and increasing mineral surface area available for weathering likely enhances the release of less radiogenic Hf from zircons, causing a higher congruency between bulk rock and dissolved Hf isotope compositions (Piotrowski et al. 2000; van de Flierdt et al. 2002). Partial dissolution of aeolian and fluvial transported particles, on the other hand, leads to a particularly incongruent release of Hf isotopes as heavy zircon minerals are lost during transport (e.g. Rickli et al. 2010; Chen et al. 2013b). Spatial and temporal variations in Hf isotope compositions in seawater have thus been modified by changes in inputs from physical and chemical weathering processes on the close by continents.

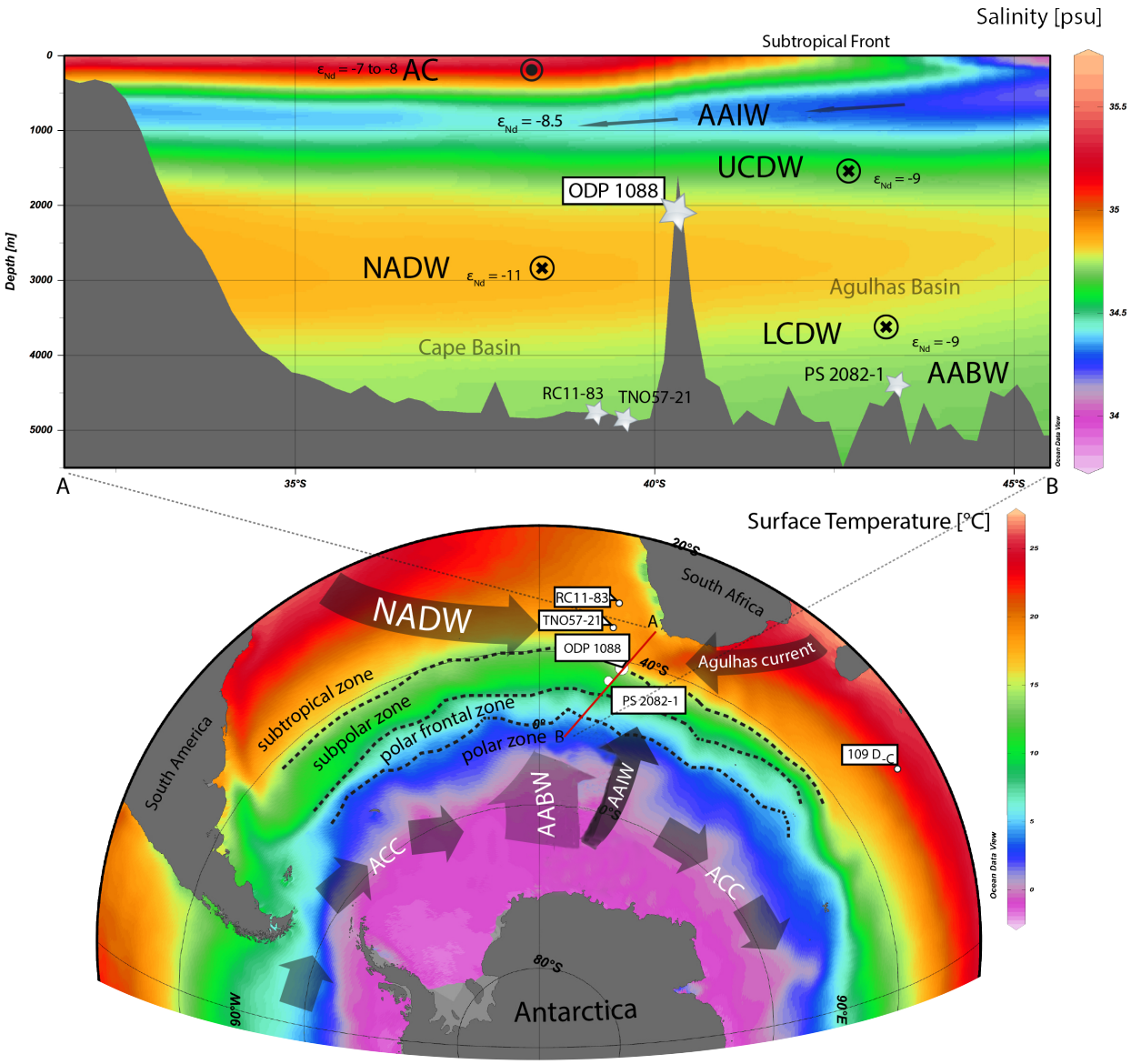


**Figure 5.1: Section and map of the study area showing the locations of ODP Site 1088 and nearby sediment cores and ferromanganese crust samples. Schematic pathways of major water masses of the modern Southern Ocean (Reid 1996) are displayed by grey arrows. Black dashed lines represent approximate locations of oceanic frontal zones (Orsi et al. 1995). Abbreviations: AABW: Antarctic Bottom Water; AAIW: Antarctic Intermediate Water; AC: Agulhas Current; ACC: Antarctic Circumpolar Current; U/L/CDW: Upper/Lower Circumpolar Deep Water; NADW: North Atlantic Deep Water. Produced using Ocean Data View (Schlitzer, R., Ocean Data View, http://odv.awi.de, 2016).**

Here we present the first dataset reconstructing mid Miocene to Holocene water-mass mixing and continental weathering inputs using seawater Nd and Hf isotope signatures obtained from sediments on the Agulhas Ridge in the Atlantic sector of the Southern Ocean. This location is ideal to study variations in intermediate depth water mass mixing between the North Atlantic, the Southern Ocean, and the Indian Ocean. These data are further complemented by detrital Nd and Hf isotope signatures reflecting changes in continental weathering inputs. The new data provide the first continuous record of changes in intermediate depth ocean

circulation and continental inputs in the Atlantic Sector of the Southern based on radiogenic isotopes since the mid Miocene, which includes major climatic transitions such as the onset of Northern Hemisphere Glaciation.

## *5.2 Material and Methods*

### *5.2.1 Sedimentology*

The studied core of Site 1088 (ODP, Leg 177, December 1997), located on the Agulhas Ridge at 41°8.163′S, 13°33.770′E, was recovered from a water depth of ~2082 m reaching a length of 223.4 m. The sediments predominantly consist of carbonate nannofossil foraminiferal ooze with carbonate contents ranging between 80 and 95%, which increase downcore (Gersonde et al. 1999). While relative abundances of foraminifers are high in the topmost 20 m they decrease progressively downhole and nannofossil percentages increase accordingly. In the section younger than ~2.8 Ma interbeds of darker, less foraminifera-rich sediment (up to 80% foraminifers) commonly incorporate ice-rafted debris (IRD), rare drop stones, and occasionally diatoms. Some of these darker beds also show erosional contacts with the underlying pale nannofossil ooze (cf. Gersonde et al. 1999).

In total, 118 depth intervals were sampled spanning the entire length of the core. However, 80% of all samples were taken in the section younger than 4 Ma while the remainder of the samples have ages between 14 and 4 Ma.

### *5.2.2 Age model*

The initial age model based on calcareous nannofossil biostratigraphy for the entire core was published in the Initial Report of the Shipboard Scientific Party (Gersonde et al. 1999) and was later refined by Censarek and Gersonde (2002) and Marino and Flores (2002). The biostratigraphy was extended by tuning benthic foraminiferal (*Cibicidoides*) $\delta^{18}O$ records to the records of Bassinot et al. (1994) and Mix et al. (1995) for the interval covering the uppermost 1.2 Ma (Hodell et al. 2003a). In addition, tuning of $\delta^{13}C$ and $\delta^{18}O$ records of planktonic (*G. bulloides*) and benthic (*Cibicidoides*) foraminifers to the records of Mix et al. (1995) support the nanofossil stratigraphy for the interval between 2.5 and 8.6 Ma (Billups 2002; Billups et al. 2008). Sedimentation rates decrease towards the younger part with an overall range between 30 and 7 m per Myr (Diekmann et al. 2003). In addition, a hiatus was identified between 12.3 and 12.7 Ma.

### 5.2.3 Sample preparation and radiogenic isotope analysis

#### 5.2.3.1 Extraction of bottom water signatures from ferromanganese oxyhydroxide coatings of bulk sediments

Seawater Nd and Hf isotope signatures (84 samples and 63 samples, respectively) were extracted from authigenic ferromanganese oxyhydroxides of bulk sediment samples (approx. 3 g; freeze-dried) following the leaching protocol of Gutjahr et al. (2007). The carbonate fraction was partly removed by adding 20 ml 2.8 M acetic acid - 1 M Na-acetate (pH ~4) on a shaking table for 2.5 hours in order to reduce the amount of the disturbing carbonate matrix (which can result in a less efficient removal of Yb during element separation). The authigenic Fe-Mn oxyhydroxide fraction was subsequently dissolved in 25 ml 0.005 M hydroxylamine hydrochloride, 1.5% acetic acid and 0.03 M Na-EDTA solution (HH) buffered to pH 4 with suprapure NaOH for 90 minutes at room temperature (i.e., ten times diluted relative to concentrations used by Gutjahr et al. 2007). Subsequently, the samples were centrifuged and the supernatants were dried and re-dissolved for ion exchange chromatography.

#### 5.2.3.2 Extraction of bottom water signatures from planktonic foraminifera

On average 125 mg of mixed species planktonic foraminifera tests were hand picked from the size fraction >315 µm under a light microscope from 60 freeze-dried and clay-free (wet-sieved) sediment samples. The microfossil shells were subsequently cracked between glass plates, to ensure that all chambers were opened and were ultrasonicated several times in deionized water and then in ethanol to ensure the removal of most of the clays and other silicate particles. The carbonates and associated ferromanganese coatings of the samples were then progressively dissolved by stepwise addition of dilute nitric acid. The solution was then centrifuged to ensure removal of smallest detrital particles and subsequently the Nd was chemically purified using the same chromatographic method as above.

#### 5.2.3.3 Detrital material

A total of sixteen samples were selected for measurement of the detrital Nd-Hf isotope compositions. Bulk sample residues processed to extract seawater signatures (section 2.3.1) were further treated with a stronger reductive leaching solution for one day to ensure complete removal of remaining Fe-Mn oxyhydroxides. Afterwards, these samples were dried, ground, and 5% $H_2O_2$ was added for 72 hours to oxidize organics that might otherwise disturb chemical purification. The samples were then further treated in aqua regia on a hotplate at 140°C preceding digestion in

a mixture of concentrated $HNO_3$ and HF in steel jacketed high-pressure bombs at ~180-200°C for 4 days.

#### 5.2.3.4 *Chemical purification and mass spectrometry*

A cation exchange resin (AG50W-X8) was used to first separate HFSEs and REEs. Subsequently, the HFSE and REE cuts were further purified with Ln-spec resin following Münker et al. (2001) and Pin and Zalduegui (1997), respectively. Hf and Nd isotope compositions were measured at GEOMAR in Kiel on a Nu Instruments MC-ICP-MS (all Nd samples, 20 Hf leachates and all detrital Hf samples) or on a Thermo Scientific Neptune Plus MC-ICP-MS and on a Thermo Scientific Neptune Plus MC-ICP-MS at the ETH in Zurich (43 Hf leachate samples). Instrumental mass bias was corrected applying an exponential mass fractionation law using a natural $^{179}Hf/^{177}Hf$ ratio of 0.7325 and $^{146}Nd/^{144}Nd$ of 0.7219, respectively. While average Nd yields were ~900 ng in bulk sediment leachates and ~30 ng from foraminifers, Hf yields from sediment leachates were quite low with an average of 13 ng. Blanks were at an average of 0.93 ng for Nd and 0.18 ng for Hf. Respective isotope standards were measured at similar concentrations as samples during each measurement batch. $^{176}Hf/^{177}Hf$ ratios of all samples were normalized to the literature value of JMC475 (0.282160, Nowell et al. 1998) while $^{143}Nd/^{144}Nd$ was normalized to the literature value of JNdi-1 (0.512115, Tanaka et al. 2000). 2σ external reproducibilities of the Hf and Nd isotope measurements were in the range of 0.2 to 0.4 ε units (for 50 and 10 ng Hf standards, respectively) and 0.1 to 0.34 ε units (for 50 and 20 ng Nd standards, respectively), respectively.

Since Hf beam intensities were very low for some samples internal uncertainties exceeded the external reproducibility for some of the sediment leachates (see Table A 8 in the appendix). The reliability of data produced from these measurements is addressed in section 5.3.1. Using a jet sampler and x skimmer cone interface, the sensitivity of the Neptune Plus MC-ICP-MS was sufficient to perform precise and accurate Hf isotope measurements even for solutions containing as little as 1.4 ng Hf. $^{176}Yb$ interferences on $^{176}Hf$ were negligible for the samples measured on the Neptune. Nevertheless, Yb doped standards were used to assure adequate interference correction was applied. The addition of 1% Yb and 1% Lu (not exceeded in sample solutions) to some of the standards produced an average deviation from the standard value (2σ) 0.14 ε-units smaller than the pure Hf standard, hence within measurement uncertainty. An additional correction of Yb interferences was therefore not applied.

## 5.3 Results

All $\varepsilon_{Nd}$ and $\varepsilon_{Hf}$ signatures presented in this study were not corrected for radiogenic ingrowth since deposition. Maximum contribution of decay to both radiogenic isotope systems was calculated to be 0.2 ε-units in the oldest samples, which is within analytical uncertainty. Results of all seawater Hf and Nd isotope measurements and their respective uncertainties are presented in Figure 5.2 C and F and are summarized in Supplementary Table A 8 in the appendix. Detrital Hf and Nd isotope measurements and their respective uncertainties are presented in Figure 5.2 D and G and in Table A 8 in the appendix.

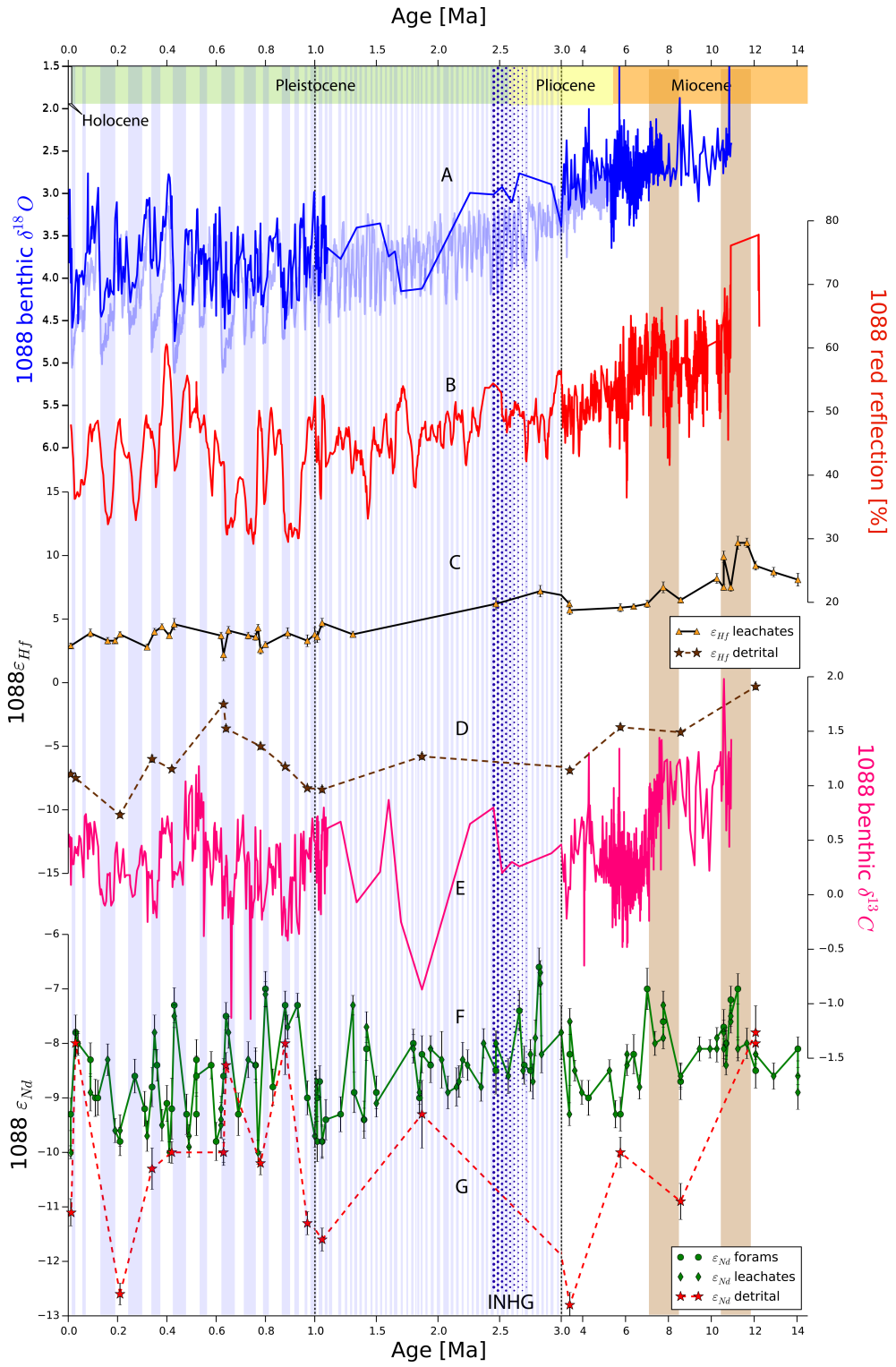


**Figure 5.2: Temporal evolution of geochemical proxies in ODP Site 1088 from the Agulhas Ridge. A: Benthic oxygen isotope time series obtained from *Cibicidoides* (Billups 2002; Hodell et al. 2003; Billups et al. 2008). In the background the global benthic oxygen isotope evolution is plotted and global marine isotope stages are displayed as blue bars (Lisiecki and Raymo 2005). B: Sediment color expressed as reflectance of red visible light with wavelength of 650-750 nm (Gersonde et al. 1999). C: Seawater Hf isotope time series from ODP 1088 (this study). D: Detrital Hf isotope time series from ODP 1088 (this study). E: Benthic carbon isotope time series *Cibicidoides* (Billups 2002; Hodell et al. 2003; Billups et al. 2008). F: Seawater Nd isotope time series from ODP 1088 (this study). G: Detrital Nd isotope time series from ODP Site 1088 (this study). The error bars denote the 2σ external reproducibility of the $\varepsilon_{Hf}$ and $\varepsilon_{Nd}$ measurements. Note that the age scale on the x-axis changes at 3 and 1 Ma.**

### 5.3.1 Seawater Nd isotope signatures

The $\varepsilon_{Nd}$ values of all samples ranged between -10 and -6.6 at an average external reproducibility of 0.29 (2σ) (Figure 5.2, 5.3). The $\varepsilon_{Nd}$ values of samples older than ~1 Ma varied within a narrower range of -8 ± 1.5. Thereafter, values dropped to less radiogenic values averaging -9 ±1. The Holocene $\varepsilon_{Nd}$ values of our record (-10) matched modern seawater from a nearby location (-9.9; Station 101 of Stichel et al. 2012a). In general, our $\varepsilon_{Nd}$ time series oscillated in harmony with marine isotope stages (MIS) (Lisiecki and Raymo 2005) in that more radiogenic values prevailed during glacial stages than during interglacial stages. For samples older than 1 Ma it was more difficult to unambiguously assign particular MIS. The covariation of $\varepsilon_{Nd}$ with colour reflectance, however, was still very clear and served to identify glacial and interglacial period. A pronounced maximum ($\varepsilon_{Nd}$ = -6.6) consisting of two data points occurred at about 2.8 Ma. Furthermore, we observed two pronounced positive $\varepsilon_{Nd}$ peaks during the mid to late Miocene (around 11 Ma and between 7.7 and 7 Ma, marked with brown dashed fields in Figure 5.2).

The Nd isotope data of bulk sediment leachates and foraminifera were identical within the 2σ uncertainties. Only one sample from the mid Miocene corresponding to an age of 11.2 Ma showed a larger offset of 1.1 $\varepsilon_{Nd}$-units, with the foraminiferal $\varepsilon_{Nd}$ being more radiogenic than that of the bulk sediment leachate, which is likely caused by inhomogeneity of the sediment material of this one sample. The data obtained from the leachate and foraminifera thus both reliably reflect past bottom water signatures.

### 5.3.2 Detrital Nd isotope signatures

All detrital $\varepsilon_{Nd}$ values ranged between -13 and - 8, with only 5 of the 16 samples being more radiogenic than -10, and thus were generally less radiogenic than the respective seawater fractions. However, in particular during the Pleistocene, the detrital $\varepsilon_{Nd}$ signatures varied with the climatic stages similar to the seawater Nd isotopes in that more radiogenic signatures reflected glacial stages (Figure 5.2).

### 5.3.3 Seawater Hf isotope signatures

The seawater $\varepsilon_{Hf}$ signatures ranged from highly radiogenic +12.5) to unradiogenic +1.9. There was a clear secular trend from more radiogenic compositions (+5.5 to +12.5) in the Miocene and early Pleistocene (3 to 13 Ma) to a relatively uniform Hf isotope composition between +2 and +5 over the last 3 Myr. While the $\varepsilon_{Hf}$ signatures exhibited three radiogenic peaks at ~11.2 Ma, 7.3 Ma, and 2.8 Ma interrupted the otherwise steady decline in the Miocene and Pliocene, they reached values 1.5 Myrs

ago. The average $\varepsilon_{Hf}$ composition of this stable episode (+3.5 ±0.9) agreed with that of the nearest measured modern seawater sample (+3.5 ±0.8, 2000m water depth, St. 104; Stichel et al. 2012a).

### *5.3.4 Detrital Hf isotope signatures*

The contrasts between detrital and authigenic $\varepsilon_{Hf}$ values were more pronounced than those of $\varepsilon_{Nd}$. Although the detrital Hf isotope signature was generally much less radiogenic than seawater with values ranging from -10.4 to -0.3, its evolution has been parallel to seawater with the exception of an excursion to more radiogenic detrital values between 1 and 0.4 Ma.

## *5.4 Discussion*

### *5.4.1 The role of non-conservative Nd behaviour*

Before we interpret our data in terms of bottom seawater variability controlled by deep water mass mixing we have to consider that non-conservative effects may have biased the isotopic compositions of bottom waters. Boundary exchange in shelf and/or continental rise settings (Lacan and Jeandel 2005; Arsouze et al. 2009; Rempfer et al. 2012) or the presence of easily dissolvable volcanic ashes and/or high amounts of IRD in the sediment (e.g. Wilson et al. 2013; Roberts and Piotrowski 2015; Blaser et al. 2016) can potentially alter seawater isotopic compositions and, hence, authigenic sedimentary signatures. While the key controls driving the effects and strength of boundary exchange at a given location are still not well understood, it is likely that the resulting effects were stronger during phases of sluggish AMOC (e.g. Lang et al. 2016) and may thus have modified seawater $\varepsilon_{Nd}$ to variable degrees across G-I cycles. Considering that detrital and authigenic Nd signatures varied in parallel during some periods of time of our record we cannot fully exclude slight shifts of the extracted seawater signatures originating from exchange with the detrital fraction of the sediments or even contributions from the pore waters (Abbott et al. 2015). We stress, however, that modern ambient deep-water $\varepsilon_{Nd}$ were successfully captured supporting our bulk sediment leaching approach. In addition, the Nd isotope signatures of the bulk sediment leachates and corresponding foraminifera agree for most of the data. This is consistent with the location of our core site at a large distance to continental landmasses and reactive sediment input from land.

Volcanic ash was mainly observed in the interval between 6.3 and 7.3 Ma but is present in small amounts in many sections of this core (Gersonde et al. 1999). Even though it is unlikely that the seawater Nd isotope composition was altered by instantaneous release of Nd from volcanic ash over an extended period of time it is

possible that volcanic-ash derived Nd was released during the bulk sediment leaching (Wilson et al. 2013; Blaser et al. 2016). However, we expect such contamination by volcanic material to be negligible as indicated by our measurements performed on foraminifera tests which are clearly not influenced by volcanic ash particles.

### 5.4.2 *Variations in AMOC strength during the last 14 Ma inferred from Nd isotope evolution*

At present, the Nd isotope signature of the waters above the Agulhas Ridge reflects essentially conservative mixing between NCW (NADW) and CDW, the Nd composition of which is ultimately controlled by admixture of both Pacific and Atlantic sourced waters with negligible contributions from boundary exchange with the Antarctic continent (Carter et al. 2012; Stichel et al. 2012a). We therefore assume binary mixing between water masses delivered from the North Atlantic (NCW) with water mass delivered from the Pacific (Southern component water; SCW) to have prevailed over the past 14 Myr.

Following the binary mixing model of Piotrowski et al. (2004) modern SO seawater $\varepsilon_{Nd}$ is the product of a NCW-SCW mixture of about 3:1. These calculations are based on $\varepsilon_{Nd}$ signatures of modern NCW of -13.5 and -4.5 for SCW together with Nd concentrations $[Nd]_{NCW}$ = 22 pmol and $[Nd]_{SCW}$ = 42 pmol (Goldstein and Hemming 2003). In the present study it is assumed that water masses with these compositions have been mixed conservatively in the SO and inputs from exchange processes with the ocean boundary on their respective pathways did not significantly affect NCW and SCW Nd isotope ratios and concentrations (c.f. Piotrowski et al. 2004 and references therein). Holocene samples in our record ($\varepsilon_{Nd}$ = -10 to -9.3) agree very well with the modern seawater composition of the SO of ~-9.9 measured at a depth of 2000m in the Cape Basin close to the Agulhas Ridge (Stichel et al. 2012a), indicating that the location experienced no resolvable addition from preformed ferromanganese phases of continental origin. This is in contrast, for instance, to the Angola Basin where Congo-derived ferromanganese phases have been shown to contribute significantly to the authigenic fraction of the sediments (Bayon et al. 2009).

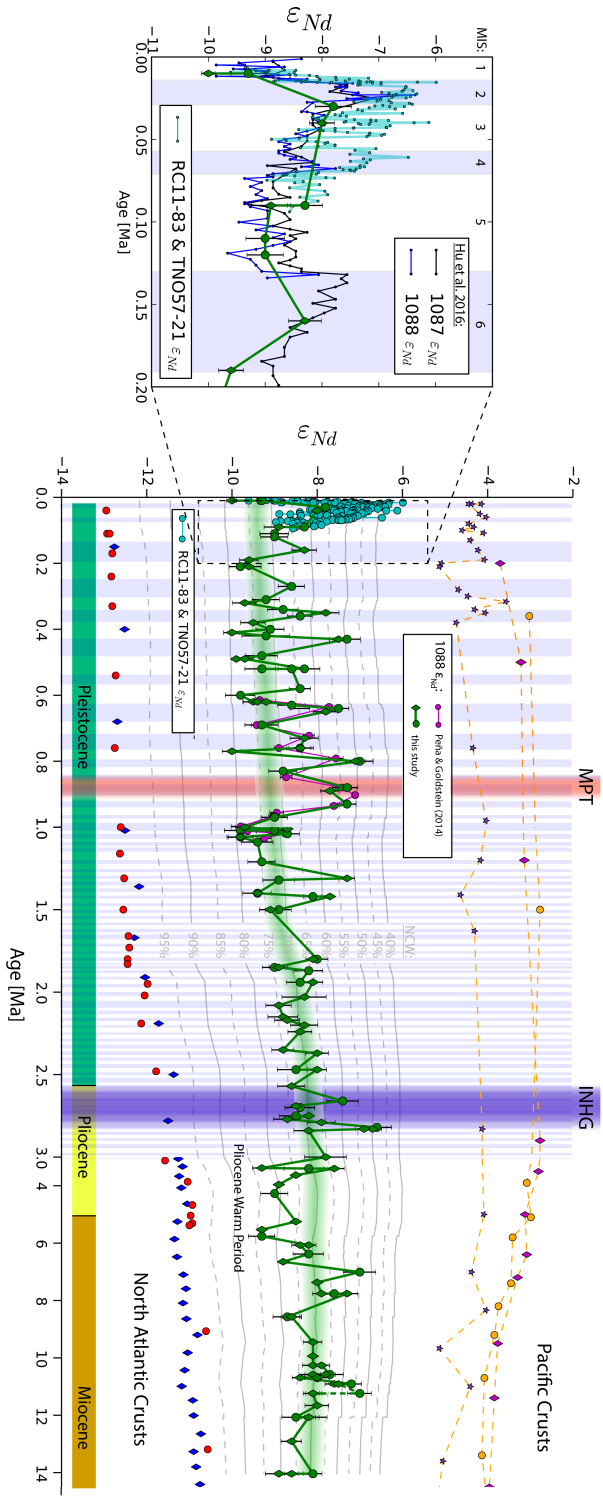


**Figure 5.3: Comparison between the seawater Nd isotope evolution of the intermediate depth Southern Ocean at ODP Site 1088 (this study, Pena and Goldstein 2014; Hu et al. 2016) and compositions of the North Atlantic (O'Nions et al. 1998; Burton et al. 1999) and Pacific Ocean (Abouchami et al. 1997; Ling et al. 1997) endmembers, as well as near-by Late Quaternary records of cores RC11-83 and TNO57-21 from the deep Cape Basin (Piotrowski et al. 2008). Grey lines represent calculated mixing proportions of North Atlantic sourced water (NCW) with Pacific sourced water (SCW) according to the variable end-member Nd compositions and constant Nd concentrations of $[Nd]_{NCW}$ = 22 pmol/kg and $[Nd]_{SCW}$ = 42 pmol/kg (Goldstein and Hemming 2003). The error bars denote the 2σ external reproducibility of the $\varepsilon_{Nd}$ measurements. Note that the age scale changes at 3 and 1 Ma.**

In order to reconstruct changes in the Nd isotope compositions of Pacific and Atlantic sourced waters through time, Fe-Mn crust data from the North Atlantic (O'Nions et al. 1998; Burton et al. 1999) and Pacific (Abouchami et al. 1997; Ling et al. 1997) were used to assess the evolution of the end-member Nd isotopic compositions at a coarse (>100 kyr) temporal resolution (Figure 5.3). Past variations in end-member Nd concentrations, however, cannot be constrained given that there is currently no proxy for past seawater Nd concentrations. Systematic changes in the concentrations over time cannot be ruled out and have to be considered as a source of uncertainty. In order to quantify these uncertainties, we have tested the impact of changes $[Nd]_{SCW}/[Nd]_{NCW}$ on our calculations by simulating deviations from the current concentration ratio by up to 20%. These simulations show that an increase in $[Nd]_{SCW}$ by 20% translates into a 4% increase of NCW advection; while an increase of the Nd concentration in NCW by 20% translates into a 5% decrease in NCW advection.

Our reconstructions show that the mid Miocene to Holocene proportions of NCW oscillated between a minimum of 49% and a maximum of 84%. The average of the entire time series of 69% NCW is close to the Holocene composition ranging between 72-78% NCW, suggesting that general oceanographic configuration has remained similar to today. This 69% NCW contribution is thus considered the baseline of similar-to-modern SO water mass mixing at the Agulhas ridge. These records hence corroborate earlier suggestions (e.g. Scher and Martin 2008) that water masses from the North Atlantic have been advected to the SO in significant amounts since at least the mid Miocene. Clearly, however, there were pronounced glacial/interglacial differences in AMOC strength over the past 3 Myr and distinct episodes with significantly different mixing proportions stand out in our record and will be discussed in chronological order in the following sections.

#### *5.4.2.1 Miocene to Pliocene AMOC variability*

During the mid Miocene (14 to 6 Ma; orange background in Figure 5.2) the intermediate depth SO Nd isotope composition only showed a relatively small variability of ±0.6 $\varepsilon_{Nd}$-units (1 SD) around a mean value of -8.1. The Oligocene and early Miocene long-term trend of decreasing $\varepsilon_{Nd}$ described by Scher and Martin (2008) did not continue until the older parts of our record. Consistent with interpretations of Scher and Martin (2004), who measured an $\varepsilon_{Nd}(t)$ of ~-8.5 for the Early Miocene in fossil fish teeth from ODP Site 689 from the Maud Rise, the resemblance of our Miocene data to modern SO mixing proportions suggests an Atlantic circulation pattern similar to modern conditions. Maximum NCW contributions (minimum $\varepsilon_{Nd}$ values in Figure 5.3) in the mid to late Miocene were of the same order as during the

Pleistocene interglacials and the Holocene. Analogous to observations of Scher and Martin (2008) we did not find any correlation of our data with potentially changing weathering inputs during major drops in eustatic sealevel, which are attributed to Antarctic glaciation events (cf. Miller et al. 1998).

Moreover, radiogenic $\varepsilon_{Nd}$ peaks at 11.2 Ma and between 7.7 and 7 Ma, which translate into intervals of low NCW admixture of about 60%, are in the same range as $\varepsilon_{Nd}$ peaks throughout the entire section and are thus considered robust evidence for reduced NCW import during these episodes. Low NCW admixture between 8 and 7 Ma is consistent with conclusions drawn from $\delta^{13}C$ gradients between the SO, the North Atlantic and the Pacific (Billups 2002).

Similar to the observations of Billups (2002), our record suggests a stronger late Miocene AMOC preceding a global warm period at 6 Ma that was possibly amplified by the shoaling of the Central American Seaway (CAS; Haug and Tiedemann 1998) and/or by the widening of the Arctic-Atlantic gateway (Knies et al. 2014).

Between 6 and 3 Ma enhanced NCW export to the Southern Ocean resulted in an average of $76\%_{NCW}$ and was thus up to 10% stronger than the modern interglacial circulation mode. More radiogenic $\varepsilon_{Nd}$ values above -8 indicating weaker NCW export were only reached again close to the end of this period. These observations are in good agreement with interpretations of Billups (2002) who, based on a compilation of benthic $\delta^{13}C$ records from the North Atlantic, Pacific and SO, inferred enhanced admixture of a northern sourced water mass similar to modern NCW near 6.0 Ma and in excess of the modern admixed proportions during the early Pliocene at ODP Site 1088. With global mean temperatures of up to 3.5 °C warmer and atmospheric $CO_2$ levels about 35% higher than the pre-industrial value the early and mid Pliocene have been identified as a time of prolonged warmth associated with a vigorous AMOC (e.g. Raymo et al. 1996; Martínez-Botí et al. 2015).

In contrast to the benthic $\delta^{13}C$ record of the same core, our Nd isotope time series suggests a return to reduced AMOC strength in the late Pliocene (around 3 Ma) as indicated by a trend to more radiogenic $\varepsilon_{Nd}$ marking the transition into an episode of global cooling.

#### *5.4.2.2 The intensification of Northern Hemispheric Glaciation*

At 2.8 Ma maximum $\varepsilon_{Nd}$ values of -6.6 (Figure 5.4 B) mark a pronounced weakening of the AMOC with NCW percentages below 50%. Consequently, the relative fraction of SCW in the SO increased by about a factor of 2 compared to its average proportion (from $25\%_{SCW}$ to more than $50\%_{SCW}$). At this time, the Northern

Hemisphere experienced a major acceleration in the build up of continental ice shields (see Figure 5.4 E) known as the Intensification of Northern Hemispheric Glaciation (INHG; ~3.6-2.4 Ma; Raymo 1994). An age control point at 2.84 Ma for 27.54 mcd (Billups et al. 2008) decreases the age uncertainty (control point spacing 300-400 kyr; Billups et al. 2008) to only a few thousand years for the $\varepsilon_{Nd}$ peak at 2.82-2.83 Ma (27.3-27.4 mcd), Furthermore, colour reflection data from the same core (Figure 5.4 A) clearly document glacial or interglacial stages (low reflections and low carbonate content typically marks glacial stage conditions and vice versa). Consequently we are confident to assign the observed $\varepsilon_{Nd}$ peak to glacial MIS G10, which has previously been identified as the first glacial marked by build-up of large ice sheets in the Northern Hemisphere (Jansen et al. 2000).

Comparison of evidence for marked incursions of SCW to the North Atlantic based on Nd isotope data obtained from core U1313 (situated in the core of modern NADW at 41°N, 32.5°W and a depth of 3426 m) shows that the shift of 1.6 $\varepsilon_{Nd}$-units (from -13.1 to -11.5; Figure 5.4 C; Lang et al. 2016) triggered by the incursion of SCW into the North Atlantic during MIS G10 was identical to that observed in our $\varepsilon_{Nd}$ record (from -8.2 to -6.6; Figure 5.4 B). This supports rapid SCW expansion delivering more radiogenic Nd signatures to the North Atlantic accompanied by a reduction of NCW. Lang et al. (2016) have argued for a connection of changes in deep water circulation and global climate to be driven by the interplay of Southern Ocean conditions, notably deep-water densification through increased sea-ice formation (Ferrari et al., 2014) versus northern forcing agents such as a reduction in NCW formation during the glacials due to its sensitivity to freshwater forcing in the North Atlantic (Böhm et al. 2015).

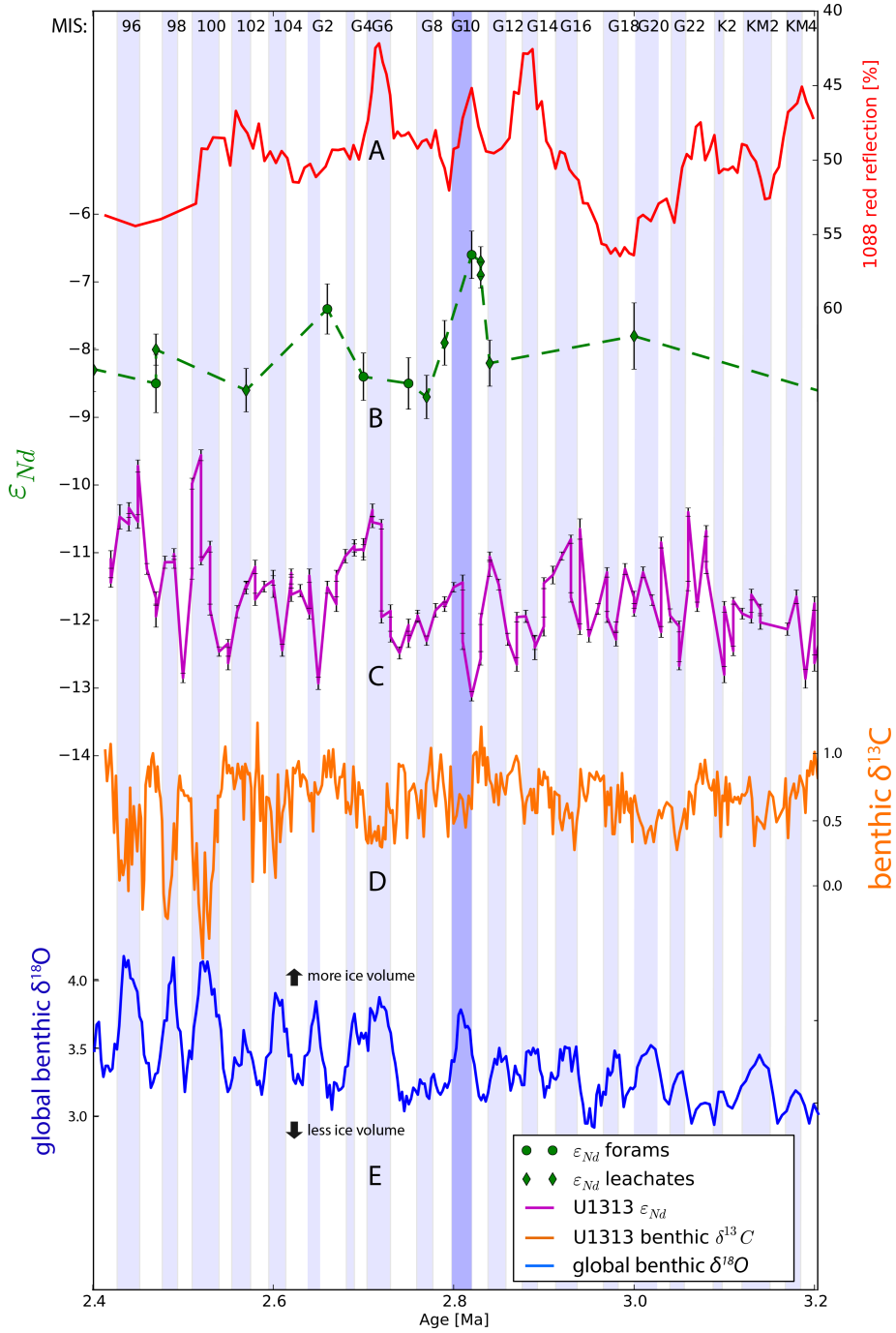


**Figure 5.4: Late Pliocene to early Pleistocene (3.4-2.2 Ma) comparison of sediment color (A); Nd isotope data from Southern Ocean ODP Site 1088 (B, this study) and North Atlantic IODP Site U1313(C; Lang et al. 2016), the benthic carbon isotope record (D) of U1313 (Lang et al. 2014) and the global benthic oxygen isotope stack (E; Lisiecki and Raymo 2005). The error bars denote the 2σ external reproducibility of the $\varepsilon_{Nd}$ measurements.**

### 5.4.2.3 *The transition to the modern Icehouse World*

Between 2.8 and 1.5 Ma the variability of the $\varepsilon_{Nd}$ signatures was limited around a mean value of -8.4 ± 0.4, corresponding to a NCW percentage of 71±6%. The invariance observed in our $\varepsilon_{Nd}$ record suggests a time of a stable and strong AMOC in this section on glacial interglacial time scales. This further indicates that

glacial conditions during this episode did not significantly reduce the export of northern sourced water masses, consistent with a strong but shallow deep-water formation cell suggested by benthic carbon isotope data in the North Atlantic covering the latest Pliocene/early Pleistocene (Venz and Hodell 2002).

After 1.55 Ma a marked decline of glacial $\delta^{13}C$ values was recorded in the Southern Ocean (Hodell and Venz 1992; Venz and Hodell 2002) as well as in the deep North Atlantic (Raymo et al. 1990). These shifts were attributed to a major reorganization in deep circulation patterns of the North Atlantic, also documented by $\varepsilon_{Nd}$ records from the northeast Atlantic (Khélifi and Frank 2014). Based on a significant shift of interglacial bottom water $\varepsilon_{Nd}$ Khélifi and Frank (2014) suggested a diminished production of well-ventilated deep waters in the Nordic Seas between 1.6 and 1.4 Ma. This in turn may have lead to a major reduction in NCW production and export to the SO. Revealing first major cyclic radiogenic excursions directly after 1.5 Ma, our $\varepsilon_{Nd}$ record adds new evidence for diminished glacial NCW admixture (resulting in SO proportions as low as $50\%_{NCW}$) after 1.5 Ma, marking the transition to Late Quaternary glacial-interglacial variability.

Between 1.2 and 0.9 Ma, our Nd isotope record confirms a phase of strong AMOC during both glacials and interglacials consistent with previous observations by Peña and Goldstein (2014). The Nd isotope data translate into high NCW proportions of 70-80% in the intermediate-depth SO at the time (Figure 5.2 F, 5.3). This is consistent with $\delta^{13}C$ records from the North Atlantic indicating that the glacial-interglacial variability in AMOC strength was very low from ~1.1 to 0.9 Ma (Venz and Hodell 2002).

From the "Thermohaline Circulation Crisis" described by Peña and Goldstein (2014) to the present, the AMOC-system operated in the modern G-I oscillation mode including strong reductions in NCW export to the SO by up to 40% during glacials (cf. Rutberg et al. 2000; Piotrowski et al. 2004; Piotrowski 2005; Peña and Goldstein 2014).

In coherence with a recent study by Hu et al. (2016) that includes higher resolution Nd isotope data of the same core, our new MIS 2 $\varepsilon_{Nd}$ value of intermediate waters from the Agulhas Ridge was less radiogenic by up to ~2 $\varepsilon_{Nd}$ units than records from the deep Cape Basin (RC11-83 and TNO57-21; see insertion in Figure 5.3) indicating a higher glacial contribution of NCW to the intermediate waters at the Agulhas Ridge relative to the deep waters in the surrounding deep basins. The Holocene and MIS 3 interglacial $\varepsilon_{Nd}$ values, on the other hand, were identical in the deep Cape Basin and the intermediate waters at the Agulhas Ridge. These observations reflect the (modern) interglacial state of vigorous mixing of essentially the

entire water column of the SO. Moreover, this confirms previous findings pointing towards reduced glacial NCW advection to shallower depths and a more persistent influence of NCW in the upper circulation cell (above ~3,500 m) in the Southeast Atlantic (Hodell et al. 2003b; Adkins 2013; Hu et al. 2016).

### 5.4.3 *Changes in regional oceanography and weathering conditions on the surrounding continents*

#### 5.4.3.1 *Invigoration of regional circulation and long term change in sediment provenance*

Terrestrial material supplied to the Southern Ocean from Antarctica, Southern Africa and South America is redistributed by ocean currents at all depths (Hegner et al. 2007). Understanding sources and pathways thus helps to reconstruct regional ocean current patterns and inputs, which have been related to enhancements of micronutrient release and thus of the fuelling of the biological pump (e.g. Martin 1990; Jaccard et al. 2013).

Radiogenic isotopes of Nd, Sr and Pb together with other proxies such as clay mineral composition (e.g. Petschick et al. 1996; Diekmann et al. 2003) are commonly used to determine detrital provenance and have been applied to identify shifts in sediment provenance in the Atlantic sector of the SO over the last glacial cycle (e.g. Walter et al. 2000; Noble et al. 2012). In general, the less radiogenic Nd isotope end-member represents inputs from South Africa and eastern Antarctica, while the more radiogenic end-member mainly originates from Patagonia/South America and western Antarctica. More radiogenic detrital $\varepsilon_{Nd}$ during glacial stages have been interpreted as increased glaciogenic continental inputs from Patagonia and West Antarctica imported via the strong ACC or via dust deposition whereas during interglacial stages sediment inputs from Southern Africa supplied mainly via the Agulhas Current were clearly dominant (Franzese et al. 2006). The ODP Site 1088 detrital $\varepsilon_{Nd}$ signal younger than 1 Ma shows a G-I cyclicity analogous to the observations for the last glacial cycle (Noble et al. 2012) with more radiogenic values during phases of relatively weak AMOC (see Figure 5.2 G) lending further support to the above-mentioned climate-dependant variations in regional scale circulation dynamics. Changes in detrital Nd isotope signatures recorded by the Pliocene and Miocene sediments, on the other hand, do not correlate well with AMOC variability suggesting that a different mode of detrital sediment transport prevailed at that time.

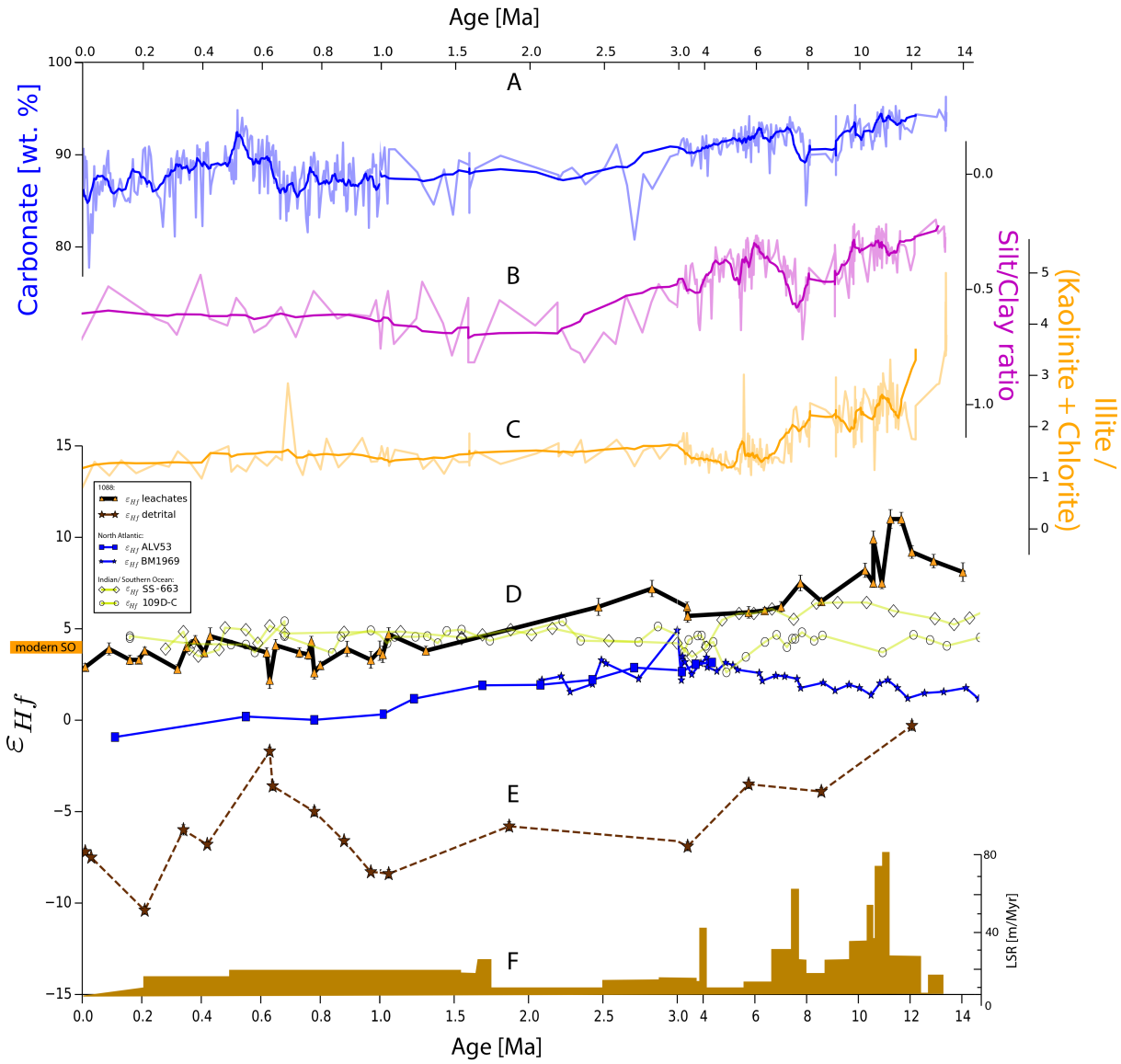


**Figure 5.5: Variability of ODP Site 1088 sedimentary components (A-C, Diekmann et al. 2003) and the Hf isotope record (D and E). Authigenic Hf isotope records from crusts from the North Atlantic, equatorial Indian Ocean and the Indian sector of the Southern Ocean (Piotrowski et al. 2000, 2009) are also shown in (D). The linearly interpolated sedimentation rate record (LSR) of ODP Site 1088 (Diekmann et al. 2003) is shown in (F). The error bars denote the 2σ external reproducibility of the $\varepsilon_{Hf}$ and $\varepsilon_{Nd}$ measurements. Note that the age scale changes at 3 and 1 Ma.**

In addition to that, detrital Hf isotope signatures (Figure 5.5 E), can also be applied as a sensitive proxy for changes in grain size and thus transport pathways. A trend towards more radiogenic Hf is commonly expected with decreasing grain size in marine sediments, mainly caused by zircon loss during (long distance) sediment transport (e.g. Vervoort et al. 1999, 2011, Bayon et al. 2009, 2016; Chen et al. 2013a). In agreement with increasing amounts of silt in 1088 sediments over time (Diekmann et al. 2003, Figure 5.5 B) we observe a continuously decreasing trend in our detrital $\varepsilon_{Hf}$ record across the Miocene and Pliocene, which is reflected by a change from the clay array towards the terrestrial array in $\varepsilon_{Hf}$-$\varepsilon_{Nd}$ space (green arrow in Fig-

ure 5.6; cf. Bayon et al. 2016). For the age interval between 1 and 0.6 Ma the general trend in Figure 5.5 E is reversed before it declines again until the Holocene, which is also reflected in the grain-size record although not as pronounced.

Accordingly, it is highly likely that variations in the admixture of sediment sources represent the first order control on detrital $\varepsilon_{Hf}$. Analogous to Nd isotopes, the radiogenic compositions in the older parts of the record (detrital $\varepsilon_{Hf}$ = -1 to -3) is in theoretic agreement with a distant South American/Patagonian provenance (also more radiogenic due to the presence of relatively young volcanic rocks from the Andean Belt), while the less radiogenic compositions in the younger sections (detrital $\varepsilon_{Hf}$ = -12 to -10) represents a proximal South African provenance (predominantly old cratonic rocks with unradiogenic Hf signatures).

Consequently, we infer that the evolution of detrital Hf isotopes represents a combination of the effect of coarsening sediments (Figure 5.5 B) induced by the invigoration of regional ocean circulation (namely the Agulhas current, Diekmann et al. 2003) and hence a simultaneous transition in sediment provenance from South America/Patagonia to the African craton, which was also inferred from clay mineral assemblages of the same core (Figure 5.5 C, Diekmann et al. 2003).

#### *5.4.3.2 Sources and implications of seawater Hf isotope changes*

Previous studies have focussed on marine Hf isotopes as indicators of changes in climatic conditions and thus weathering regimes on nearby continents (van de Flierdt et al. 2002; Gutjahr et al. 2014; Dausmann et al. 2015; Bayon et al. 2016). Consequently the presence of ice sheets on the surrounding continents is expected to lead to decreases of the marine $\varepsilon_{Hf}$ signatures, which has been observed in Fe-Mn crust records from the Arctic Ocean (Dausmann et al. 2015), as well as in Fe-Mn crust records (Piotrowski et al. 2000) and Late Quaternary sedimentary records from the North Atlantic (Gutjahr et al. 2014). Moreover, recent work by Bayon et al. (2016) demonstrated the relationship between climatic conditions (temperature and precipitation) and congruency in Hf weathering. Accordingly, a large scale global cooling potentially favours the release of more unradiogenic Hf.

In the modern SO, however, there is no evidence for the predominant release of unradiogenic Hf from the close-by glaciated regions of Eastern Antarctica (Stichel et al. 2012b) and Western Antarctica (Rickli et al. 2014). In addition, there is no indication for the presence of large ice sheets and glaciers on the nearby Southern African continent over the past 14 million years. Considering the relatively short residence time of Hf in the SO, as inferred from recent seawater studies in the Atlantic Ocean pointing to high rates of scavenging and the lack of enrichment in

deep water Hf concentrations (Rickli et al. 2009, 2010, 2014), the admixture of distal sourced Hf (e.g. from South American runoff) is unlikely.

In agreement with this evidence, our seawater Hf isotope record from the Agulhas Ridge does not exhibit systematic G-I variations during the Pleistocene, clearly showing that seawater Hf isotope signatures have not been sensitive to glacial to interglacial variations of circulation or weathering inputs in the Atlantic sector of the SO over the past 14 Myr. Furthermore, there is no evidence for climatic variations (temperature and precipitation) related to global cooling during glacials on the close-by continents.

Instead the Hf isotopic compositions (Figure 5.5 D) continuously decreased from highly radiogenic values of up to + 11 and an average of +8 during the Miocene and early Pliocene to reach stable conditions in the Pleistocene near the modern day $\varepsilon_{Hf}$ of seawater above the Agulhas Ridge (+3.5; 2000m St. 104; Stichel et al. 2012a).

Based on these observations we infer that the SO seawater evolution towards less radiogenic dissolved Hf isotopic ratios was not caused by the evolution of a more congruent mode of weathering. The highly radiogenic Hf isotope compositions in the early part of the record, which apparently indicate strongly incongruent weathering conditions (Fig. 6), were most likely caused by aeolian supply and partial dissolution of young volcanogenic particles supplied from Patagonia, which decreased over time as indicated by decreasing sedimentation rates (Figure 5.5 F) and increasing grain sizes (Figure 5.5 B). The radiogenic Hf isotope signature was amplified by the prevailing fine-grained material dominated by labile minerals with highly radiogenic Hf isotope signatures (cf. chapter 3 and described below).

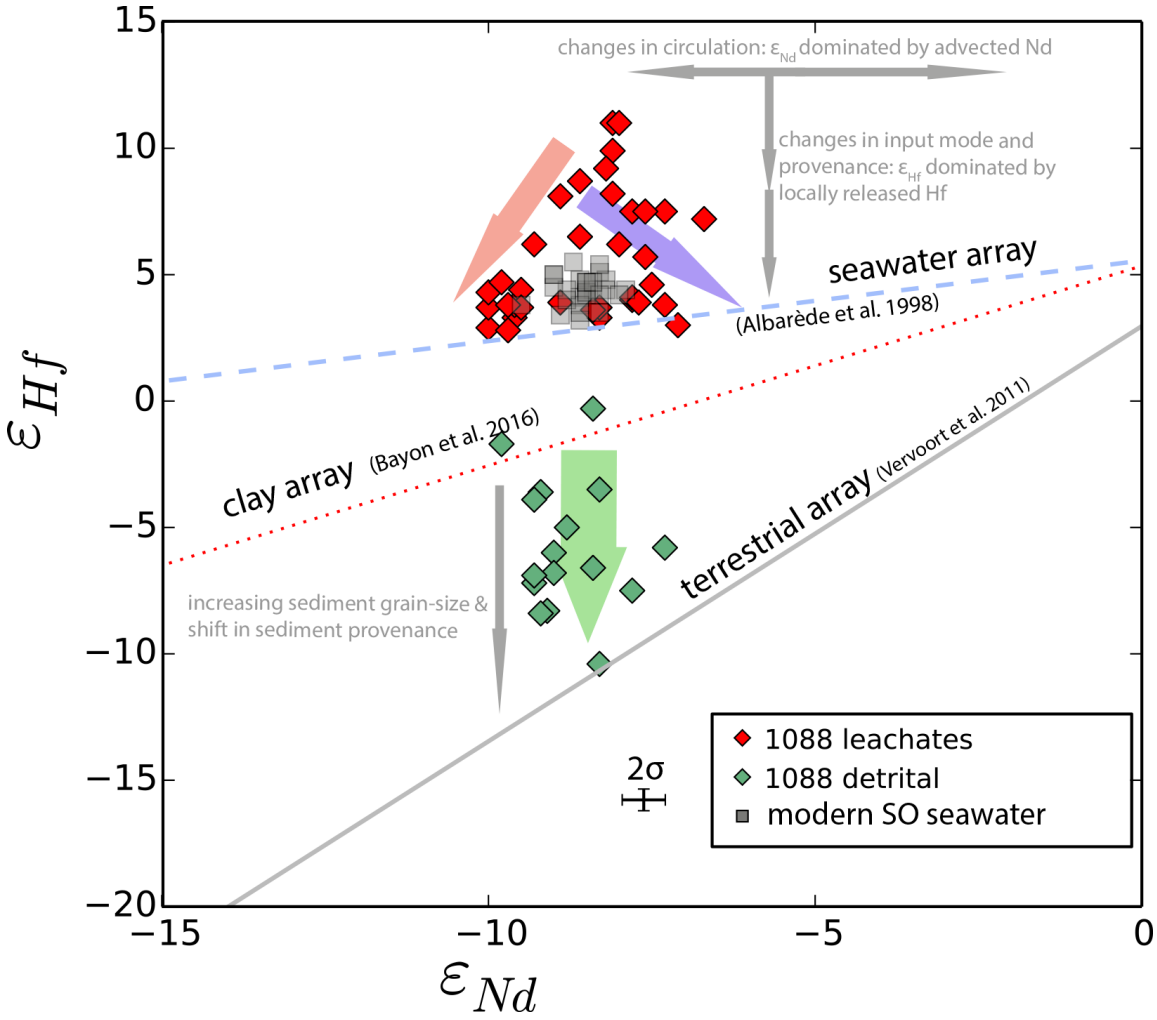


**Figure 5.6: Cross-plot of seawater and detrital Hf and Nd isotope compositions from the Southern Ocean of the past 14 Myr. The dashed line represents the global seawater array defined by Fe–Mn crust and seawater data (Albarède et al. 1998). The solid grey line represents the global terrestrial array (Vervoort et al. 1999). The red dotted line represents the clay array (Bayon et al. 2016). The red arrow represents the temporal evolution of weathering inputs from the surrounding continents during interglacial conditions from highly incongruent in the Miocene to more congruent in the Pleistocene. The blue arrow expresses the development during glacials reflecting the changes in NCW advection affecting the seawater Nd isotope compositions. The green arrow represents the evolution of the detrital material related to both changes in grain-size distributions and provenance of the sediment. Error bars denote the 2σ external reproducibility of the $\varepsilon_{Hf}$ and $\varepsilon_{Nd}$ measurements.**

*The evolution of dissolved Hf in the Atlantic sector of the Southern Ocean*

Based on the results discussed above we interpret more radiogenic Hf isotope ratios ($\varepsilon_{Hf}$ above +5) in the Miocene and Pliocene (see Figure 5.5 D) to be derived from partial dissolution of young volcanogenic particles of South American provenance. Although large contributions from this source are not evident in present-day seawater in the SO (Stichel et al. 2012a; Rickli et al. 2014) it is likely that different wind fields in the past (e.g. westerly wind field further polewards in the warmer Miocene and Pliocene, cf. Toggweiler et al. 2006) delivered larger amounts of South American sourced dust to the Agulhas Ridge. While in the modern SO Hf

concentrations in seawater close to the Agulhas Ridge are extremely low, unradiogenic Nd isotope compositions show that terrigenous inputs from the Southern African continent are significant (Stichel et al. 2012b). This shows that inputs from an additional external source may have altered the seawater Hf isotope composition easily. Thus it is likely that South American dust-derived Hf dominated the seawater signature when atmospheric import of dust from the west were enhanced and lead to more radiogenic Hf isotope ratios at the Agulhas Ridge without significantly affecting the detrital and dissolved Nd isotope compositions.

With the end of the Pliocene the influence of South American dust particles on dissolved Hf ceased and the predominance of (less radiogenic) Hf of Southern African origin was established. Although ice-core and sedimentary records from Antarctica and the SO show that dust from South America was also exported to the region during the Pleistocene (e.g. Basile et al. 1997; Diekmann et al. 2000) and even strengthened during glacial episodes (Lambert et al. 2008) it did not exert significant influence on the dissolved Hf in seawater above the Agulhas Ridge any more. These interpretations are in agreement with progressively increasing abundances of kaolinite minerals (from tropical and subtropical Africa; Figure 5.5 C) mirroring the gradual strengthening of the Agulhas leakage until it stabilized in the latest Pliocene (Diekmann et al. 2003). Subsequently, the stronger Agulhas current largely prevented radiogenic Hf from partial dissolution of South American dust particles to reach the surface waters at the Agulhas Ridge.

Accordingly, the apparently parallel evolution of our Agulhas ridge seawater $\varepsilon_{Hf}$ record and those of North Atlantic crusts ALV539 and BM1969 (Figure 5.5 D) after 3 Ma is the result of the long term evolution in particle provenance due to changes of atmospheric and oceanic circulation in the Southern Hemisphere. The similarity in the records does thus not reflect a causal relationship.

*Tracing inputs of Patagonian dust in the Southern Ocean*

Radiogenic peaks of 2-3 ε units in our seawater $\varepsilon_{Hf}$ record at ~12 to 10.6 Ma and at ~7 Ma, as well as at 2.8 Ma in the late Pliocene reaching values above +8 were likely the result of highly incongruent dissolution of erosional products of the South American continent. Partial dissolution of the mostly volcanogenic dust likely acted as a significant source of highly radiogenic Hf given that other detrital inputs at the Agulhas Ridge have been very low. The isotopic composition of dust itself varied with atmospheric loading and likely amplified highly incongruent Hf isotope compositions (e.g. due to zircon loss during aeolian transport, Rickli et al. 2010).

Increased input and partial dissolution of dust particles from arid regions was demonstrated to be an important source of radiogenic Hf to the ocean as reflected by elevated Hf concentrations for surface waters west of the Sahara, which are up to 10 $\varepsilon_{Hf}$ units more radiogenic than the bulk dust composition (Rickli et al. 2010). Consequently, the dominating westerly winds in the region that have delivered large amounts of South America sourced dust to the SO have contributed significantly to the oceanic Hf budget. Phases of increased dust deposition from South America were a consequence of past environmental conditions (e.g. Sugden et al. 2009), which were probably also linked to the uplift of the Andean mountain range since the Miocene, which reached elevations severely altering South American climate between 4 and 3 Ma (e.g. Hartley 2003).

## *5.5 Conclusions*

(1) Past mixing proportions between precursors of modern NADW and CDW/Pacific waters are reconstructed using seawater Nd isotope compositions. An average of 69%$_{NCW}$ similar to modern SO water mass mixing at the Agulhas ridge suggests that the general configuration of the circulation system has prevailed for the past 14 Myr, which was, however, interrupted by short-term perturbations throughout the entire investigated period of time.

(2) The continuous evolution from highly radiogenic to less radiogenic Hf isotope signatures between 14 Ma and at the Pliocene indicates the gradual increase in the supply Hf originating from partial dissolution of particles from Southern Africa, which were transported by a stronger Agulhas current at the expense of South American sourced Hf, which prevailed during the Miocene and early Pliocene. Hf isotopes in the SO do not reflect variations due to glacial activity and subsequent changes of the AMOC.

(3) We attribute Miocene/Pliocene excursions around 11 Ma, from 8 to 7 Ma, and near 2.8 Ma present in both Hf and Nd isotope signatures to phases of substantially decreased NCW admixture. Switches to more arid conditions in South America causing increased inputs of highly radiogenic Hf via aeolian dust occurred at a similar timing.

(4) A period of early Pliocene warmth was accompanied by enhanced AMOC strength and NADW inflow into the Southern Ocean.

(5) At 2.8 Ma, during MIS G10, the first large-scale glaciation in the Northern Hemisphere was accompanied by a pronounced weakening of the AMOC and a subsequent expansion of SCW, which was also notable in the North Atlantic.

(6) A phase of stable and relatively strong AMOC between 2.5 and 1.5 Ma was finally followed by the Late Pleistocene icehouse conditions, during which major glacial drops in NADW supply occurred. Analogously, increased glacial AMOC strength is evident in our records for roughly 200 kyr before the 900 ka trans-glacial event (Pena and Goldstein 2014) which marked the transition to the modern mode of G-I oscillations in AMOC strength at the 100 kyr periodicity.

(7) A comparison of $\varepsilon_{Nd}$ values of intermediate waters from the Agulhas Ridge and the deep Cape and Agulhas Basin points to a less well-mixed SO during the last glacial. This is in agreement with recent findings of Hu et al. (2016).

**Acknowledgments, Samples, and Data**

All data are available at https://doi.pangaea.de/10.1594/PANGAEA.871943. The ODP/IODP core repository in Bremen provided sediment material for this study. Walter Hale and Alex Wülbers are thanked for their assistance during the sampling of ODP core 1088.

We thank Tianyu Chen who helped to develop an appropriate leaching method for the sediment samples. Chris Siebert and Anne Osbourne are thanked for help with chemical separation and MC-ICP-MS measurements. We thank Jutta Heinze, Peer Rahlf, Ingmar Schindlbeck and Julia Langer for help with sample preparation and assistance in the lab. We are grateful to Ellen Thomas and Christopher Reinhard, for editorial handling. We acknowledge the comments from two anonymous reviewers that helped to improve the manuscript.

**References**

Abbott, A.N., Haley, B.A. and McManus, J., 2015. Bottoms up: Sedimentary control of the deep North Pacific Ocean's ε Nd signature. *Geology*, 43(11), p.G37114.1, doi: 10.1130/G37114.1.

Abouchami, W., Goldstein, S.L., Gazer, S.J.G., Eisenhauer, A. and Mangini, A., 1997. Secular changes of lead and neodymium in central Pacific seawater recorded by a Fe-Mn crust. *Geochimica et Cosmochimica Acta*, 61(18), pp.3957–3974, doi: 10.1016/S0016-7037(97)00218-4.

Adkins, J.F., 2013. The role of deep ocean circulation in setting glacial climates. *Paleoceanography*, 28(3), pp.539–561, doi: 10.1002/palo.20046.

Albarède, F., Simonetti, A., Vervoort, J.D., Blichert-Toft, J. and Abouchami, W., 1998. A Hf-Nd isotopic correlation in ferromanganese nodules. *Geophysical Re-*

*search Letters*, 25(20), p.3895, doi: 10.1029/1998GL900008.

Arsouze, T., Dutay, J.-C., Lacan, F. and Jeandel, C., 2009. Reconstructing the Nd oceanic cycle using a coupled dynamical – biogeochemical model. *Biogeosciences Discussions*, 6(3), pp.5549–5588, doi: 10.5194/bgd-6-5549-2009.

Balan, E., Trocellier, P., Jupille, J., Fritsch, E., Muller, J.P. and Calas, G., 2001. Surface chemistry of weathered zircons. *Chemical Geology*, 181(1–4), pp.13–22, doi: 10.1016/S0009-2541(01)00271-6.

Basile, I., Grousset, F.E., Revel, M., Petit, J.R., Biscaye, P.E. and Barkov, N.I., 1997. Patagonian origin of glacial dust deposited in East Antarctica (Vostok and Dome C) during glacial stages 2, 4 and 6. *Earth and Planetary Science Letters*, 146(3), pp.573–589, doi: 10.1016/S0012-821X(96)00255-5.

Bassinot, F.C., Labeyrie, L.D., Vincent, E., Quidelleur, X., Shackleton, N.J. and Lancelot, Y., 1994. The astronomical theory of climate and the age of the Brunhes-Matuyama magnetic reversal. *Earth and Planetary Science Letters*, 126(1–3), pp.91–108, doi: 10.1016/0012-821X(94)90244-5.

Bau, M. and Koschinsky, A., 2006. Hafnium and neodymium isotopes in seawater and in ferromanganese crusts: The "element perspective." *Earth and Planetary Science Letters*, 241(3–4), pp.952–961, doi: 10.1016/j.epsl.2005.09.067.

Bayon, G., Burton, K.W., Soulet, G., Vigier, N., Dennielou, B., Etoubleau, J., Ponzevera, E., German, C.R. and Nesbitt, R.W., 2009. Hf and Nd isotopes in marine sediments: Constraints on global silicate weathering. *Earth and Planetary Science Letters*, 277(3–4), pp.318–326, doi: 10.1016/j.epsl.2008.10.028.

Bayon, G., Skonieczny, C., Delvigne, C., Toucanne, S., Bermell, S., Ponzevera, E. and André, L., 2016. Environmental Hf–Nd isotopic decoupling in World river clays. *Earth and Planetary Science Letters*, 438, pp.25–36, doi: 10.1016/j.epsl.2016.01.010.

Bayon, G., Vigier, N., Burton, K.W., Brenot, A., Carignan, J., Etoubleau, J. and Chu, N.C., 2006. The control of weathering processes on riverine and seawater hafnium isotope ratios. *Geology*, 34(6), pp.433–436, doi: 10.1130/G22130.1.

Biastoch, A., Böning, C.W. and Lutjeharms, J.R.E., 2008. Agulhas leakage dynamics affects decadal variability in Atlantic overturning circulation. *Nature*, 456(7221), pp.489–492, doi: 10.1038/nature07426.

Billups, K., 2002. Late Miocene through early Pliocene deep water circulation and

climate change viewed from the sub-Antarctic South Atlantic. *Palaeogeography, Palaeoclimatology, Palaeoecology*, 185(3–4), pp.287–307, doi: 10.1016/S0031-0182(02)00340-1.

Billups, K., Kelly, C. and Pierce, E., 2008. The late Miocene to early Pliocene climate transition in the Southern Ocean. *Palaeogeography, Palaeoclimatology, Palaeoecology*, 267(1–2), pp.31–40, doi: 10.1016/j.palaeo.2008.05.013.

Blaser, P., Lippold, J., Gutjahr, M., Frank, N., Link, J.M. and Frank, M., 2016. Extracting foraminiferal seawater Nd isotope signatures from bulk deep sea sediment by chemical leaching. *Chemical Geology*, 439, pp.189–204, doi: 10.1016/j.chemgeo.2016.06.024.

Böhm, E., Lippold, J., Gutjahr, M., Frank, M., Blaser, P., Antz, B., Fohlmeister, J., Frank, N., Andersen, M.B. and Deininger, M., 2015. Strong and deep Atlantic meridional overturning circulation during the last glacial cycle. *Nature*, 517(7534), pp.73–76, doi: 10.1038/nature14059.

Boyle, E.A. and Keigwin, L.D., 1982. Deep Circulation of the North Atlantic over the Last 200,000 Years: Geochemical Evidence. *Science (New York, N.Y.)*, 218(4574), pp.784–7, doi: 10.1126/science.218.4574.784.

Broecker, W.S., Peteet, D.M. and Rind, D., 1985. Does the ocean-atmosphere system have more than one stable mode of operation? *Nature*, 315(2), pp.21–26, doi: 10.1038/315021a0.

Burton, K.W., Lee, D.C., Christensen, J.N., Halliday, A.N. and Hein, J.R., 1999. Actual timing of neodymium isotopic variations recorded by Fe-Mn crusts in the western North Atlantic. *Earth and Planetary Science Letters*, 171(1), pp.149–156, doi: 10.1016/S0012-821X(99)00138-7.

Carter, P., Vance, D., Hillenbrand, C.D., Smith, J.A. and Shoosmith, D.R., 2012. The neodymium isotopic composition of waters masses in the eastern Pacific sector of the Southern Ocean. *Geochimica et Cosmochimica Acta*, 79, pp.41–59, doi: 10.1016/j.gca.2011.11.034.

Censarek, B. and Gersonde, R., 2002. Miocene diatom biostratigraphy at ODP sites 689, 690, 1088, 1092 (Atlantic sector of the Southern Ocean). *Marine Micropaleontology*, 45(3–4), pp.309–356, doi: 10.1016/S0377-8398(02)00034-8.

Chen, T.Y., Frank, M., Haley, B. a., Gutjahr, M. and Spielhagen, R.F., 2012. Variations of North Atlantic inflow to the central Arctic Ocean over the last 14 million

years inferred from hafnium and neodymium isotopes. *Earth and Planetary Science Letters*, 353–354, pp.82–92, doi: 10.1016/j.epsl.2012.08.012.

Chen, T.Y., Li, G., Frank, M. and Ling, H.F., 2013a. Hafnium isotope fractionation during continental weathering: Implications for the generation of the seawater Nd-Hf isotope relationships. *Geophysical Research Letters*, 40(5), pp.916–920, doi: 10.1002/grl.50217.

Chen, T.Y., Stumpf, R., Frank, M., Beldowski, J. and Staubwasser, M., 2013b. Contrasting geochemical cycling of hafnium and neodymium in the central Baltic Sea. *Geochimica et Cosmochimica Acta*, 123, pp.166–180, doi: 10.1016/j.gca.2013.09.011.

Curry, W.B. and Lohmann, G.P., 1982. Carbon isotopic changes in benthic foraminifera from the western South Atlantic: Reconstruction of glacial abyssal circulation patterns. *Quaternary Research*, 18(2), pp.218–235, doi: 10.1016/0033-5894(82)90071-0.

Dausmann, V., Frank, M., Siebert, C., Christl, M. and Hein, J.R., 2015. The evolution of weathering inputs and deep ocean circulation in the Arctic Ocean since the Late Miocene : Radiogenic isotope evidence. *Earth and Planetary Science Letters*, 419, pp.111–124, doi: 10.1016/j.epsl.2015.03.007.

Diekmann, B., Fälker, M. and Kuhn, G., 2003. Environmental history of the southeastern South Atlantic since the Middle Miocene: evidence from the sedimentological records of ODP Sites 1088 and 1092. *Sedimentology*, 50(3), pp.511–529, doi: 10.1046/j.1365-3091.2003.00562.x.

Diekmann, B., Kuhn, G., Rachold, V., Abelmann, A., Brathauer, U., Fütterer, D.K., Gersonde, R. and Grobe, H., 2000. Terrigenous sediment supply in the Scotia Sea (Southern Ocean): response to Late Quaternary ice dynamics in Patagonia and on the Antarctic Peninsula. *Palaeogeography, Palaeoclimatology, Palaeoecology*, 162(3), pp.357–387, doi: 10.1016/S0031-0182(00)00138-3.

Enfield, D.B., Mestas-Nuñez, A.M. and Trimble, P.J., 2001. The Atlantic Multidecadal Oscillation and its relation to rainfall and river flows in the continental U.S. *Geophysical Research Letters*, 28(10), pp.2077–2080, doi: 10.1029/2000GL012745.

Ferrari, R., Jansen, M.F., Adkins, J.F., Burke, A., Stewart, A.L. and Thompson, A.F., 2014. Antarctic sea ice control on ocean circulation in present and glacial climates. *Proceedings of the National Academy of Sciences of the United States of*

*America*, 111(24), pp.8753–8758, doi: 10.1073/pnas.1323922111.

Filippova, A., Frank, M., Kienast, M., Rickli, J., Hathorne, E., Yashayaev, I.M. and Böning, P., 2016. Water mass circulation and weathering inputs in the Labrador Sea based on coupled Hf-Nd isotope compositions and rare earth element distributions. *Geochimica et Cosmochimica Acta*.

Firdaus, M.L., Minami, T., Norisuye, K. and Sohrin, Y., 2011. Strong elemental fractionation of Zr–Hf and Nb–Ta across the Pacific Ocean. *Nature Geoscience*, 4(4), pp.227–230, doi: 10.1038/ngeo1114.

Frank, M., 2002. Radiogenic isotopes: Tracers of past ocean circulation and erosional input. *Reviews of Geophysics*, 40(1), doi: 10.1029/2000RG000094.

Franzese, A.M., Hemming, S.R., Goldstein, S.L. and Anderson, R.F., 2006. Reduced Agulhas Leakage during the Last Glacial Maximum inferred from an integrated provenance and flux study. *Earth and Planetary Science Letters*, 250(1–2), pp.72–88, doi: 10.1016/j.epsl.2006.07.002.

Gersonde, R., Hodell, D. a., Blum, P. and others, 1999. Site 1088 Initial Report. *Proceedings of the Ocean Drilling Program, Initial Reports*, 177.

Godfrey, L. V., Field, M.P. and Sherrell, R.M., 2008. Estuarine distributions of Zr, Hf, and Ag in the Hudson River and the implications for their continental and anthropogenic sources to seawater. *Geochemistry, Geophysics, Geosystems*, 9(12), p.n/a-n/a, doi: 10.1029/2008GC002123.

Goldstein, S.L. and Hemming, S.R., 2003. *Long-lived Isotopic Tracers in Oceanography, Paleoceanography, and Ice-sheet Dynamics*, Elsevier.

Gordon, A.L., Weiss, R.F., Smethie, W.M. and Warner, M.J., 1992. Thermocline and intermediate water communication between the south Atlantic and Indian oceans. *Journal of Geophysical Research*, 97(C5), p.7223, doi: 10.1029/92JC00485.

Gutjahr, M., Frank, M., Lippold, J. and Halliday, A.N., 2014. Peak Last Glacial weathering intensity on the North American continent recorded by the authigenic Hf isotope composition of North Atlantic deep-sea sediments. *Quaternary Science Reviews*, 99, pp.97–117, doi: 10.1016/j.quascirev.2014.06.022.

Gutjahr, M., Frank, M., Stirling, C.H., Klemm, V., van de Flierdt, T. and Halliday, A.N., 2007. Reliable extraction of a deepwater trace metal isotope signal from Fe-Mn oxyhydroxide coatings of marine sediments. *Chemical Geology*, 242(3–4), pp.351–370, doi: 10.1016/j.chemgeo.2007.03.021.

Hartley, A.J., 2003. Andean uplift and climate change. *Journal of the Geological Society*, 160(1), pp.7–10, doi: 10.1144/0016-764902-083.

Haug, G.H. and Tiedemann, R., 1998. Effect of the formation of the Isthmus of Panama on Atlantic Ocean thermohaline circulation. *Nature*, 393(6686), pp.673–676, doi: 10.1038/31447.

Hegner, E., Dauelsberg, H.J., Rutgers Van Der Loeff, M.M., Jeandel, C. and De Baar, H.J.W., 2007. Nd isotopic constraints on the origin of suspended particles in the Atlantic Sector of the Southern Ocean. *Geochemistry, Geophysics, Geosystems*, 8(10), doi: 10.1029/2007GC001666.

Henry, L.G., Henry, L.G., Mcmanus, J.F., Curry, W.B., Roberts, N.L., Piotrowski, A.M. and Keigwin, L.D., 2016. North Atlantic ocean circulation and abrupt climate change during the last glaciation. , 5529, doi: 10.1126/science.aaf5529.

Hodell, D.A., Charles, C.D., Curtis, J.H., Mortyn, P.G., Ninnemann, U.S. and Venz, K. a, 2003a. Data Report: Oxygen Isotope Stratigraphy of ODP Leg 177 Sites 1088, 1089, 1090, 1093, and 1094. *Proceedings of the Ocean Drilling Program, Scientific Results*, 177(October 2001), pp.1–26.

Hodell, D.A. and Venz, K., 1992. Toward a high-resolution stable isotopic reord of the southern ocean during the pliocene-pleistocene (4.8 to 0.8 Ma). In *Antarctic Research Series*. American Geophysical Union, pp. 265–310.

Hodell, D. a., Venz, K. a., Charles, C.D. and Ninnemann, U.S., 2003b. Pleistocene vertical carbon isotope and carbonate gradients in the South Atlantic sector of the Southern Ocean. *Geochemistry, Geophysics, Geosystems*, 4(1), pp.1–19, doi: 10.1029/2002GC000367.

Hu, R., Noble, T.L., Piotrowski, A.M., McCave, I.N., Bostock, H.C. and Neil, H.L., 2016. Neodymium isotopic evidence for linked changes in Southeast Atlantic and Southwest Pacific circulation over the last 200 kyr. *Earth and Planetary Science Letters*, 455, pp.106–114, doi: 10.1016/j.epsl.2016.09.027.

Jaccard, S.L., Hayes, C.T., Martínez-García, A., Hodell, D.A., Anderson, R.F., Sigman, D.M. and Haug, G.H., 2013. Two modes of change in Southern Ocean productivity over the past million years. *Science (New York, N.Y.)*, 339(6126), pp.1419–23, doi: 10.1126/science.1227545.

Jackson, L.C., Peterson, K.A., Roberts, C.D. and Wood, R.A., 2016. Recent slowing of Atlantic overturning circulation as a recovery from earlier strengthening. *Natu-*

*re Geoscience*, 9(May), doi: 10.1038/ngeo2715.

Jacobsen, S.B. and Wasserburg, G.J., 1980. Sm-Nd isoopic evolution of chondrites. *Earth and Planetary Science Letters*, 50(1), pp.139–155.

Jansen, E., Fronval, T., Rack, F. and Channell, J.E.T., 2000. Pliocene-Pleistocene ice rafting history and cyclicity in the Nordic Seas during the last 3.5 Myr. *Paleoceanography*, 15(6), pp.709–721, doi: 10.1029/1999PA000435.

Jeandel, C., Bishop, J.K. and Zindler, A., 1995. Exchange of neodymium and its isotopes between seawater and small and large particles in the Sargasso Sea. *Geochimica et Cosmochimica Acta*, 59(3), pp.535–547, doi: 10.1016/0016-7037(94)00367-U.

Khélifi, N. and Frank, M., 2014. A major change in North Atlantic deep water circulation during the Early Pleistocene transition 1.6 million years ago. *Climate of the Past Discussions*, 9(6), pp.6495–6513, doi: 10.5194/cpd-9-6495-2013.

Knies, J., Mattingsdal, R., Fabian, K., Grøsfjeld, K., Baranwal, S., Husum, K., De Schepper, S., Vogt, C., Andersen, N., Matthiessen, J., Andreassen, K., Jokat, W., Nam, S. Il and Gaina, C., 2014. Effect of early Pliocene uplift on late Pliocene cooling in the Arctic-Atlantic gateway. *Earth and Planetary Science Letters*, 387, pp.132–144, doi: 10.1016/j.epsl.2013.11.007.

Lacan, F. and Jeandel, C., 2005. Neodymium isotopes as a new tool for quantifying exchange fluxes at the continent-ocean interface. *Earth and Planetary Science Letters*, 232(3–4), pp.245–257, doi: 10.1016/j.epsl.2005.01.004.

Lambert, F., Delmonte, B., Petit, J.R., Bigler, M., Kaufmann, P.R., Hutterli, M.A., Stocker, T.F., Ruth, U., Steffensen, J.P. and Maggi, V., 2008. Dust-climate couplings over the past 800,000 years from the EPICA Dome C ice core. *Nature*, 452(7187), pp.616–619, doi: 10.1038/nature06763.

Lang, D.C., Bailey, I., Wilson, P.A., Beer, C.J., Bolton, C.T., Friedrich, O., Newsam, C., Spencer, M.R., Gutjahr, M., Foster, G.L., Cooper, M.J. and Milton, J.A., 2014. The transition on North America from the warm humid Pliocene to the glaciated Quaternary traced by eolian dust deposition at a benchmark North Atlantic Ocean drill site. *Quaternary Science Reviews*, 93, pp.125–141, doi: 10.1016/j.quascirev.2014.04.005.

Lang, D.C., Bailey, I., Wilson, P.A., Chalk, T.B., Foster, G.L. and Gutjahr, M., 2016. Incursions of southern-sourced water into the deep North Atlantic during late

Pliocene glacial intensification. *Nature Geoscience*, (April), pp.1–6, doi: 10.1038/ngeo2688.

Ling, H.F., Burton, K.W., O'Nions, R.K., Kamber, B.S., von Blanckenburg, F., Gibb, A.J. and Hein, J.R., 1997. Evolution of Nd and Pb isotopes in Central Pacific seawater from ferromanganese crusts. *Earth and Planetary Science Letters*, 146(1–2), pp.1–12, doi: 10.1016/S0012-821X(96)00224-5.

Lippold, J., Luo, Y., Francois, R., Allen, S.E., Gherardi, J., Pichat, S., Hickey, B. and Schulz, H., 2012. Strength and geometry of the glacial Atlantic Meridional Overturning Circulation. *Nature Geoscience*, 5(11), pp.813–816, doi: 10.1038/ngeo1608.

Lisiecki, L.E. and Raymo, M.E., 2005. A Pliocene-Pleistocene stack of 57 globally distributed benthic δ18O records. *Paleoceanography*, 20(1), pp.1–17, doi: 10.1029/2004PA001071.

Lynch-Stieglitz, J., Adkins, J.F., Curry, W.B., Dokken, T., Hall, I.R., Herguera, J.C., Hirschi, J.J.-M., Ivanova, E. V, Kissel, C., Marchal, O., Marchitto, T.M., McCave, I.N., McManus, J.F., Mulitza, S., Ninnemann, U., Peeters, F., Yu, E.-F. and Zahn, R., 2007. Atlantic meridional overturning circulation during the Last Glacial Maximum. *Science (New York, N.Y.)*, 316(5821), pp.66–69, doi: 10.1126/science.1137127.

Marino, M. and Flores, J.A., 2002. Miocene to Pliocene calcareous nannofossil biostratigraphy at ODP Leg 177 Sites 1088 and 1090. *Marine Micropaleontology*, 45(3–4), pp.291–307, doi: 10.1016/S0377-8398(02)00033-6.

Martin, J.H., 1990. Glacial-Interglacial CO2 changes: The Iron Hypothesis. *Paleoceanography*, 5(1), pp.1–13, doi: doi:10.1029/PA005i001p00001.

Martínez-Botí, M.A., Foster, G.L., Chalk, T.B., Rohling, E.J., Sexton, P.F., Lunt, D.J., Pancost, R.D., Badger, M.P.S. and Schmidt, D.N., 2015. Plio-Pleistocene climate sensitivity evaluated using high-resolution CO2 records. *Nature*, 518(7537), pp.49–54, doi: 10.1038/nature14145.

McManus, J.F., Francois, R., Gherardi, J.-M., Keigwin, L.D. and Brown-Leger, S., 2004. Collapse and rapid resumption of Atlantic meridional circulation linked to deglacial climate changes. *Nature*, 428(6985), pp.834–837, doi: 10.1038/nature02494.

Miller, K.G., Mountain, G.S., Browning, J. V., Kominz, M., Sugarman, P.J., Christie-

Blick, N., Katz, M.E. and Wright, J.D., 1998. Cenozoic global sea level, sequences, and the New Jersey Transect: Results From coastal plain and continental slope drilling. *Reviews of Geophysics*, 36(98), p.569, doi: 10.1029/98RG01624.

Mix, A.C., Pisias, N.G., Rugh, W., Wilson, J., Morey, A. and Hagelberg, T.K., 1995. Benthic foraminifer stable isotope record from Site 849 (0-5 Ma): local and global climate changes. *Proceedings of the Ocean Drilling Program, Scientific Results*, 138, pp.371–412.

Münker, C., Weyer, S., Scherer, E. and Mezger, K., 2001. Separation of high field strength elements (Nb, Ta, Zr, Hf) and Lu from rock samples for MC-ICPMS measurements. *Geochemistry Geophysics Geosystems*, 1(12), p.n/a-n/a, doi: 10.1029/2001GC000183.

Noble, T.L., Piotrowski, A.M., Robinson, L.F., McManus, J.F., Hillenbrand, C.D. and Bory, A.J.M., 2012. Greater supply of Patagonian-sourced detritus and transport by the ACC to the Atlantic sector of the Southern Ocean during the last glacial period. *Earth and Planetary Science Letters*, 317–318, pp.374–385, doi: 10.1016/j.epsl.2011.10.007.

Nowell, G.M., Kempton, P.D., Noble, S.R., Saunders, A.D., Mahoney, J.J. and Taylor, R.N., 1998. High-precision Hf isotopic measurements of MORB and OIB by thermal ionization mass-spectrometry: insights into the depleted mantle. *Chemical Geology*, 149(3), pp.211–233.

O'Nions, R.., Frank, M., von Blanckenburg, F. and Ling, H.-F., 1998. Secular variation of Nd and Pb isotopes in ferromanganese crusts from the Atlantic, Indian and Pacific Oceans. *Earth and Planetary Science Letters*, 155(1–2), pp.15–28, doi: 10.1016/S0012-821X(97)00207-0.

Oppo, D.W. and Fairbanks, R.G., 1987. Variability in the deep and intermediate water circulation of the Atlantic Ocean during the past 25,000 years: Northern Hemisphere modulation of the Southern Ocean. *Earth and Planetary Science Letters*, 86(1), pp.1–15, doi: 10.1016/0012-821X(87)90183-X.

Orsi, A.H., Whitworth, T. and Nowlin, W.D., 1995. On the meridional extent and fronts of the Antarctic Circumpolar Current. *Deep Sea Research Part I: Oceanographic Research Papers*, 42(5), pp.641–673, doi: 10.1016/0967-0637(95)00021-W.

Pena, L.D. and Goldstein, S.L., 2014. Thermohaline circulation crisis and impacts during the mid-Pleistocene transition. *Science*, 345(6194), pp.318–322, doi:

10.1126/science.1249770.

Petschick, R., Kuhn, G. and Gingele, F., 1996. Clay mineral distribution in surface sediments of the South Atlantic: sources, transport, and relation to oceanography. *Marine Geology*, 130(3–4), pp.203–229, doi: 10.1016/0025-3227(95)00148-4.

Piepgras, D. and Wasserburg, G., 1982. Isotopic Composition of Neodymium in Waters from the Drake Passage. *Science*, 217(4556), pp.207–214, doi: 10.1126/science.217.4556.207.

Pin, C. and Santos Zalduegui, J.F., 1997. Sequential separation of light rare-earth elements, thorium and uranium by miniaturized extraction chromatography: Application to isotopic analyses of silicate rocks. *Analytica Chimica Acta*, 339(1–2), pp.79–89, doi: 10.1016/S0003-2670(96)00499-0.

Piotrowski, A.M., 2005. Temporal Relationships of Carbon Cycling and Ocean Circulation at Glacial Boundaries. *Science*, 307(5717), pp.1933–1938, doi: 10.1126/science.1104883.

Piotrowski, A.M., Banakar, V.K., Scrivner, A.E., Elderfield, H., Galy, A. and Dennis, A., 2009. Indian Ocean circulation and productivity during the last glacial cycle. *Earth and Planetary Science Letters*, 285(1–2), pp.179–189, doi: 10.1016/j.epsl.2009.06.007.

Piotrowski, A.M., Goldstein, S.L., Hemming, Sidney, R., Fairbanks, R.G. and Zylberberg, D.R., 2008. Oscillating glacial northern and southern deep water formation from combined neodymium and carbon isotopes. *Earth and Planetary Science Letters*, 272(1–2), pp.394–405, doi: 10.1016/j.epsl.2008.05.011.

Piotrowski, A.M., Goldstein, S.L., Hemming, S.R. and Fairbanks, R.G., 2004. Intensification and variability of ocean thermohaline circulation through the last deglaciation. *Earth and Planetary Science Letters*, 225(1–2), pp.205–220, doi: 10.1016/j.epsl.2004.06.002.

Piotrowski, A.M., Lee, D.-C., Christensen, J.N., Burton, K.W., Halliday, A.N., Hein, J.R. and Günther, D., 2000. Changes in erosion and ocean circulation recorded in the Hf isotopic compositions of North Atlantic and Indian Ocean ferromanganese crusts. *Earth and Planetary Science Letters*, 181(3), pp.315–325, doi: 10.1016/S0012-821X(00)00205-3.

Raymo, M., 1994. The Initiation of Northern Hemisphere Glaciation. *Annual Review*

*of Earth and Planetary Sciences*, 22(1), pp.353–383, doi: 10.1146/annurev.earth.22.1.353.

Raymo, M.E., Grant, B., Horowitz, M. and Rau, G.H., 1996. Mid-Pliocene warmth: stronger greenhouse and stronger conveyor. *Marine Micropaleontology*, 27(1–4), pp.313–326, doi: 10.1016/0377-8398(95)00048-8.

Raymo, M.E., Ruddiman, W.F., Shackleton, N.J. and Oppo, D.W., 1990. Evolution of Atlantic-Pacific d13C gradients over the last 2.5 m.y. *Earth and Planetary Science Letters*, 97(3–4), pp.353–368, doi: 10.1016/0012-821X(90)90051-X.

Reid, J., 1996. On the circulation of the South Atlantic Ocean. In *The South Atlantic*. Berlin, Heidelberg: Springer Berlin Heidelberg, pp. 13–44.

Rempfer, J., Stocker, T.F., Joos, F. and Dutay, J.-C., 2012. Sensitivity of Nd isotopic composition in seawater to changes in Nd sources and paleoceanographic implications. *Journal of Geophysical Research: Oceans*, 117(C12), p.n/a-n/a, doi: 10.1029/2012JC008161.

Rempfer, J., Stocker, T.F., Joos, F., Dutay, J.C. and Siddall, M., 2011. Modelling Nd-isotopes with a coarse resolution ocean circulation model: Sensitivities to model parameters and source/sink distributions. *Geochimica et Cosmochimica Acta*, 75(20), pp.5927–5950, doi: 10.1016/j.gca.2011.07.044.

Rickli, J., Frank, M., Baker, A.R., Aciego, S., de Souza, G., Georg, R.B. and Halliday, A.N., 2010. Hafnium and neodymium isotopes in surface waters of the eastern Atlantic Ocean: Implications for sources and inputs of trace metals to the ocean. *Geochimica et Cosmochimica Acta*, 74(2), pp.540–557, doi: 10.1016/j.gca.2009.10.006.

Rickli, J., Frank, M. and Halliday, A.N., 2009. The hafnium-neodymium isotopic composition of Atlantic seawater. *Earth and Planetary Science Letters*, 280(1–4), pp.118–127, doi: 10.1016/j.epsl.2009.01.026.

Rickli, J., Gutjahr, M., Vance, D., Fischer-Gödde, M., Hillenbrand, C.D. and Kuhn, G., 2014. Neodymium and hafnium boundary contributions to seawater along the West Antarctic continental margin. *Earth and Planetary Science Letters*, 394, pp.99–110, doi: 10.1016/j.epsl.2014.03.008.

Roberts, N.L. and Piotrowski, A.M., 2015. Radiogenic Nd isotope labeling of the northern NE Atlantic during MIS 2. *Earth and Planetary Science Letters*, 423, pp.125–133, doi: 10.1016/j.epsl.2015.05.011.

Robson, J., Ortega, P. and Sutton, R., 2015. A recent reversal of climatic trends in the North Atlantic. , 9(June), pp.1–15, doi: 10.1038/ngeo2727.

Rutberg, R., Hemming, S. and Goldstein, S., 2000. Reduced North Atlantic Deep Water flux to the glacial Southern Ocean inferred from neodymium isotope ratios. *Nature*, 405(6789), pp.935–8, doi: 10.1038/35016049.

Scher, H.D. and Martin, E.E., 2004. Circulation in the Southern Ocean during the Paleogene inferred from neodymium isotopes. *Earth and Planetary Science Letters*, 228(3–4), pp.391–405, doi: 10.1016/j.epsl.2004.10.016.

Scher, H.D. and Martin, E.E., 2008. Oligocene deep water export from the North Atlantic and the development of the Antarctic Circumpolar Current examined with neodymium isotopes. *Paleoceanography*, 23(1), pp.1–12, doi: 10.1029/2006PA001400.

Siddall, M., Khatiwala, S., van de Flierdt, T., Jones, K., Goldstein, S.L., Hemming, S. and Anderson, R.F., 2008. Towards explaining the Nd paradox using reversible scavenging in an ocean general circulation model. *Earth and Planetary Science Letters*, 274(3–4), pp.448–461, doi: 10.1016/j.epsl.2008.07.044.

Skinner, L.C., Scrivner, A.E., Vance, D., Barker, S., Fallon, S. and Waelbroeck, C., 2013. North atlantic versus southern ocean contributions to a deglacial surge in deep ocean ventilation. *Geology*, 41(6), pp.667–670, doi: 10.1130/G34133.1.

Stichel, T., Frank, M., Rickli, J. and Haley, B. a., 2012a. The hafnium and neodymium isotope composition of seawater in the Atlantic sector of the Southern Ocean. *Earth and Planetary Science Letters*, 317–318, pp.282–294, doi: 10.1016/j.epsl.2011.11.025.

Stichel, T., Frank, M., Rickli, J., Hathorne, E.C., Haley, B. a., Jeandel, C. and Pradoux, C., 2012b. Sources and input mechanisms of hafnium and neodymium in surface waters of the Atlantic sector of the Southern Ocean. *Geochimica et Cosmochimica Acta*, 94, pp.22–37, doi: 10.1016/j.gca.2012.07.005.

Sugden, D.E., McCulloch, R.D., Bory, A.J.-M. and Hein, A.S., 2009. Influence of Patagonian glaciers on Antarctic dust deposition during the last glacial period. *Nature Geoscience*, 2(4), pp.281–285, doi: 10.1038/ngeo474.

Sutton, R.T. and Hodson, D.L.R., 2005. Atlantic Ocean forcing of North American and European summer climate. *Science (New York, N.Y.)*, 309(5731), pp.115–8, doi: 10.1126/science.1109496.

Tachikawa, K., 2003. Neodymium budget in the modern ocean and paleo-oceanographic implications. *Journal of Geophysical Research*, 108(C8), doi: 10.1029/1999JC000285.

Tanaka, T., Togashi, S., Kamioka, H., Amakawa, H., Kagami, H., Hamamoto, T., Yuhara, M., Orihashi, Y., Yoneda, S., Shimizu, H., Kunimaru, T., Takahashi, K., Yanagi, T., Nakano, T., Fujimaki, H., Shinjo, R., Asahara, Y., Tanimizu, M. and Dragusanu, C., 2000. JNdi-1: A neodymium isotopic reference in consistency with LaJolla neodymium. *Chemical Geology*, 168(3–4), pp.279–281, doi: 10.1016/S0009-2541(00)00198-4.

Toggweiler, J.R., Russell, J.L. and Carson, S.R., 2006. Midlatitude westerlies, atmospheric CO2, and climate change during the ice ages. *Paleoceanography*, 21(2), pp.1–15, doi: 10.1029/2005PA001154.

Uenzelmann-Neben, G. and Gohl, K., 2004. The Agulhas Ridge, South Atlantic: The peculiar structure of a fracture zone. *Marine Geophysical Researches*, 25(3–4), pp.305–319, doi: 10.1007/s11001-005-1338-8.

van de Flierdt, T., Frank, M., Lee, D.C. and Halliday, A.N., 2002. Glacial weathering and the hafnium isotope composition of seawater. *Earth and Planetary Science Letters*, 201(3–4), pp.639–647, doi: 10.1016/S0012-821X(02)00731-8.

van de Flierdt, T., Goldstein, S.L., Hemming, S.R., Roy, M., Frank, M. and Halliday, A.N., 2007. Global neodymium-hafnium isotope systematics - revisited. *Earth and Planetary Science Letters*, 259(3–4), pp.432–441, doi: 10.1016/j.epsl.2007.05.003.

Venz, K. a. and Hodell, D. a., 2002. New evidence for changes in Plio–Pleistocene deep water circulation from Southern Ocean ODP Leg 177 Site 1090. *Palaeogeography, Palaeoclimatology, Palaeoecology*, 182(3–4), pp.197–220, doi: 10.1016/S0031-0182(01)00496-5.

Vervoort, J.D., Patchett, P.J., Blichert-Toft, J. and Albarède, F., 1999. Relationships between Lu-Hf and Sm-Nd isotopic systems in the global sedimentary system. *Earth and Planetary Science Letters*, 168(1–2), pp.79–99, doi: 10.1016/S0012-821X(99)00047-3.

Vervoort, J.D., Plank, T. and Prytulak, J., 2011. The Hf-Nd isotopic composition of marine sediments. *Geochimica et Cosmochimica Acta*, 75(20), pp.5903–5926, doi: 10.1016/j.gca.2011.07.046.

Walter, H.J., Hegner, E., Diekmann, B., Kuhn, G. and Rutgers Van Der Loeff, M.M., 2000. Provenance and transport of terrigenous sediment in the South Atlantic Ocean and their relations to glacial and interglacial cycles: Nd and Sr isotopic evidence. *Geochimica et Cosmochimica Acta*, 64(22), pp.3813–3827, doi: 10.1016/S0016-7037(00)00476-2.

White, W.M., Patchett, J. and BenOthman, D., 1986. Hf isotope ratios of marine sediments and Mn nodules: evidence for a mantle source of Hf in seawater. *Earth and Planetary Science Letters*, 79(1–2), pp.46–54, doi: 10.1016/0012-821X(86)90039-7.

Wilson, D.J., Piotrowski, A.M., Galy, A. and Clegg, J. a., 2013. Reactivity of neodymium carriers in deep sea sediments: Implications for boundary exchange and paleoceanography. *Geochimica et Cosmochimica Acta*, 109, pp.197–221, doi: 10.1016/j.gca.2013.01.042.

Yu, J., Menviel, L., Jin, Z.D., Thornalley, D.J.R., Barker, S., Marino, G., Rohling, E.J., Cai, Y., Zhang, F., Wang, X., Dai, Y., Chen, P. and Broecker, W.S., 2016. Sequestration of carbon in the deep Atlantic during the last glaciation. *Nature Geoscience*, 9(4), pp.319–324, doi: 10.1038/ngeo2657.

# 6 Summary, conclusions and outlook

## *6.1 Summary and conclusions*

An integrated view of different geochemical aspects for the application of radiogenic isotopes in paleoceanography is presented in the three main chapters of this thesis. In principle, the different topics presented here accompany the evolution of radiogenic isotopes of Nd and Hf in the hydrosphere from the first release into solution during continental weathering (chapter 3; including Pb isotopes) via the cycling in present day seawater (chapter 4) and finally to the marine sediments where the information about past ocean circulation is stored (chapter 5).

**Chapter 3** aims at improving the understanding of the mechanisms releasing distinct isotope signatures to weathering solutions, which is essential when relating e.g. combined Nd-Hf isotope data of modern and paleoceanographic studies to present and past continental weathering conditions. The particularly important role of differential weathering of both highly resistant minerals (such as zircon) as well as highly reactive minerals (such as apatite) was studied by simulating different weathering conditions with a special focus on the effect of glacial processes on the continents. The experiments performed during this study document the systematic preferential release of radiogenic Nd, Hf and Pb isotopes to weathering solutions in agreement with the resistance of the rocks' minerals to weathering. The results show that the digestion of labile accessory minerals, in particular apatite and sphene, dominates the release of more radiogenic Nd, Hf and Pb during weak chemical weathering of fresh rock surfaces. The degree of incongruent release of radiogenic Nd observed during this study is surprisingly high since differences in Sm/Nd between mineral phases are typically small. The overall effect of mineral-controlled fractionation on Hf isotopes is much larger and also persists under enhanced chemical weathering intensities given that variations in Lu/Hf ratios in rocks are comparably large. Furthermore, it is demonstrated that, similar to previous estimates, about 69% of the host rocks' Hf is contained in highly resistant zircons, which were hardly dissolved during the weak leaching experiments. Mechanical grinding of rocks and their mineral phases, on the other hand, clearly reduces the fractionation of Hf and Nd isotopes during dissolution of the host rocks. Primarily this is achieved by an increase of the fraction of non-zircon minerals that are accessible to weathering. In addition to that, a more efficient dissolution of zircon minerals is documented by enhanced release of Hf from ground zircon separates, which thus also contributes to the more congruent release of radiogenic Hf isotopes

to weathering solutions and ultimately to the ocean under enhanced glacial weathering conditions.

Furthermore, it is demonstrated that radiogenic $^{206}Pb$ and $^{207}Pb$ in ground granite material are dissolved congruently under incipient weathering conditions. This implies that an easily accessible mélange of all kinds of different minerals (probably mostly feldspars) is available for dissolution at this stage of weathering due to the increased availability of reactive mineral surfaces. This feature is observed despite elevated U release rates, providing clear evidence for preferential U-rich accessory mineral dissolution. Therefore, the results from the granite samples in this study indicate that the washout of radiogenic Pb released due to alpha recoil during incipient chemical weathering likely does not alter the Pb isotope composition of the weathering liquids to a resolvable degree. With continued weathering/leaching, reactive surfaces of other rock-forming mineral phases appear to disappear leading to enhanced release of more radiogenic $^{206}Pb$ and $^{207}Pb$ due to the dissolution of labile U-bearing mineral phases (such as apatite). Radiogenic $^{208}Pb$ in the simulated weathering solutions, in contrast, is depleted with respect to the whole rock composition, since Th-bearing minerals, the main sources of radiogenic $^{208}Pb$, are generally more resistant to dissolution. Overall, the differences in Pb isotope trends between the subgroups of the experiment were mainly controlled by differences in mineral availability and were probably also controlled by mineral sorting processes.

**Chapter 4** focused on the better understanding of quantitative water mass mixing and the relative impact of non-conservative behavior along the European margin in the Bay of Biscay. It is demonstrated that radiogenic Nd isotope signatures in the analyzed surface waters of the Bay of Biscay are dominated by local weathering inputs from the rocks of the surrounding continental margin. Subsurface ENACW shows a distinct Nd isotope composition of $\varepsilon_{Nd}$ = -12.0 at the south-western-most station and is significantly diluted on its way along the European margin by mixing with more radiogenic waters from above and below. Furthermore, the Nd isotope data clearly show the declining influence of MOW at intermediate depths on its way north as it is diluted with ENACW indicating that only 40% to 60% of MOW still present at the Galician margin arrives at the stations further north. A potentially seasonal/temporal feature of Nd isotope changes in MOW is identified when comparing the results of this study with those of earlier studies from the area, which possibly reflects the meandering flow path of MOW. Higher proportions of MOW-like Nd signatures are also manifested in elevated Nd concentrations likely originating from increased terrestrial inputs to the Mediterranean Sea and are then transported as far as the Galician margin. In agreement with observa-

tions from Nd isotopes we infer that the Hf isotope composition of MOW was affected by large-scale inputs of dust as can be deduced from elevated Hf concentrations at the Galician margin. The deep-water Nd isotope signatures in the Capbreton region strongly suggest exchange with local shelf sediments. Similarly, Hf isotopes in all water masses of the Bay of Biscay are generally overprinted by local inputs. This lends support to the hypothesized more efficient removal of Hf from the water column as the water masses travel along the continental margin. Combined with Nd, however, Hf serves as a useful indicator whether a water mass is more proximally affected by inputs from weathering or if it has been advected over long distances.

**Chapter 5** reconstructs past mixing proportions between precursors of modern NADW and CDW/Pacific waters using seawater Nd isotope compositions extracted from the sediments of the Agulhas Ridge. Furthermore, the Hf isotope evolution from the same sediments was established, reflecting changing weathering contributions to the region. The data suggest that a long-term average of 69% of northern sourced water was admixed to Southern Ocean (SO) water masses over the last 14 Myr. This is similar to modern SO water mass mixing ratios at the Agulhas ridge, which suggests that the general configuration of the circulation system has prevailed for the past 14 Myr. Furthermore, however, the Nd isotope data document that this configuration was interrupted by short-term perturbations throughout the entire investigated period of time. Miocene/Pliocene excursions to more radiogenic Nd isotope signatures around 11 Ma, from 8 to 7 Ma, and near 2.8 Ma are for example attributed to phases of substantially decreased admixture of northern sourced water. Switches to more arid conditions in South America causing increased inputs of highly radiogenic Hf via aeolian dust are, in contrast, suggested to be responsible for excursions in the Hf isotope signatures that occurred at a similar timing. The period of early Pliocene warmth (~7-3 Ma) was accompanied by enhanced AMOC strength and northern sourced inflow into the Southern Ocean reflected by less radiogenic Nd isotope compositions of around $\varepsilon_{Nd}$ = -9. In contrast, peak radiogenic Nd isotope signatures ($\varepsilon_{Nd}$ = -6.7) during MIS G10 (~2.8 Ma) reflect a pronounced weakening of the AMOC and the subsequent expansion of southern sourced water masses, which accompanied the first large-scale glaciation of the Northern Hemisphere. This was followed by a phase of relatively stable and strong AMOC (with 65 to 75% northern sourced water) between 2.5 and 1.5 Ma. Finally, the Late Pleistocene icehouse conditions were established after 1.5 Ma, which introduced major drops in NADW supply (reflected by radiogenic peaks in the order of $\varepsilon_{Nd}$ from -7 to -8) during glacials. Moreover, a relatively strong glacial AMOC is evident in our records for roughly 200 kyr before the 900 ka trans-glacial event, which was introduced by Pena and Goldstein (2014) and marked the transition to the

modern mode of glacial-interglacial oscillations in AMOC strength at the 100 kyr periodicity.

Hf isotopes in the SO, on the other hand, do not reflect variations caused by glacial activity and/or changes in overturning circulation. The essentially continuous evolution from highly radiogenic to less radiogenic Hf isotope signatures between 14 Ma and at the Pliocene is interpreted as the gradual increase in the supply of Hf originating from partial dissolution of particles from Southern Africa, which were transported by a stronger Agulhas current at the expense of South American sourced Hf, which prevailed during the Miocene and early Pliocene.

In summary, the following conclusions can be drawn from this thesis:

(1) The quantification of present and past water mass mixing can be reliably achieved using Nd isotope signatures for the sites studied in this thesis. Incongruent weathering during continental weathering was observed in chapter 3. Its influence on the total budget of Nd isotopes in seawater, however, is insignificant. In the case of the Bay of Biscay, the distribution of Nd isotopes can mostly be attributed to conservative water mass mixing. Only in confined locations close to the continent and to the sediment-seawater interface non-conservative inputs were observed. The seawater Nd isotope extracted from the sediments of the Agulhas Ridge reliably track variations in the admixture of northern sourced water masses as a measure of AMOC strength on glacial-interglacial timescales.

(2) Hafnium isotopes, on the other hand, are less well suited as a tracer of water mass circulation. Chapters 4 and 5 demonstrate that regional non-conservative processes easily overprint Hf isotope signatures of water masses. Thus Hf isotope variations are generally not suitable to investigate water mass mixing. Chapter 3, however, clearly suggests that Hf isotopes serve as a sensitive tracer of changes in weathering style/strength. Furthermore, observations of Hf isotope data in chapter 5 imply that the changing provenance of regional weathering inputs can be traced.

(3) Similar to Hf isotopes Pb isotopes are well suited as a tool of tracking weathering intensities. Radiogenic $^{206}Pb$ and $^{207}Pb$ are released congruently under incipient weathering conditions of freshly ground material but show distinct signatures for non-ground material. Under progressing weathering conditions the dissolution of labile U-bearing minerals leads to incongruent weathering, releasing more radiogenic $^{206}Pb/^{204}Pb$ and $^{207}Pb/^{204}Pb$ signatures. Radiogenic $^{208}Pb$, on the other hand, is released incongruently under most weathering conditions since Th-rich minerals are typically very resistant to dissolution.

## 6.2 Outlook and perspective of future work

From the new insights presented in this thesis new questions arise. Some issues that should be addressed in future work include:

A more comprehensive isotopic characterization of different mineral phases of the zircon-free portion in future studies will help to better quantify fractionation processes that occur during chemical and physical weathering. Analyzing several different lithological backgrounds of host rocks (e.g. basalts, metamorphic rocks, sedimentary rocks) would provide further insight into the control of variable lithology on Nd, Hf and Pb isotopes in weathering solutions. Moreover, repeated dry and wet climatic cycles (Ganor et al. 2005), the residence time of weathering agents (Hindshaw et al. 2011; Rickli et al. 2017), as well as the role of colloids (i.e. Merschel et al. 2017) should be considered as important factors for future experiments. Furthermore, the important role of transport and removal mechanisms of dissolved trace metals has to be investigated in order to understand the cycling of radiogenic isotopes. Especially the influence of climatic conditions on these mechanisms needs to be understood, when applying these tracers for the reconstruction of paleoclimate. Continuous-flow experiments simulating accelerated natural processes similar to those carried out by Erel et al. (2004) for Pb isotopes could be realized for Nd and Hf isotopes. More field experiments (spanning several years/seasons) such as those of Rickli et al. (2013; 2017) will also help to estimate these factors when analyzing weathering solution for different species of dissolved trace metals.

Another important factor is the behavior of radiogenic isotopes during and after burial in the sediments as well as their cycling within and between different sedimentary phases. In this context, also the differences in removal and sedimentation mechanisms of Nd and Hf in seawater need to be investigated in more detail in order to apply combined Hf-Nd isotope evolution in studies reconstructing changes in past weathering regimes and connected environmental conditions more reliably.

The comparison of $\varepsilon_{Nd}$ values of intermediate waters from the Agulhas Ridge and the deep Cape and Agulhas Basin points to a less well-mixed Southern Ocean during the last glacial. This is in agreement with recent findings of Hu et al. (2016). Further studies with higher sampling resolution investigating these differences are needed to elucidate the vertical water mass structure over glacial-interglacial cycles and during shorter term climatic changes in the Southern Ocean and will help to better constrain possible feedback mechanisms between circulation changes and glacial $CO_2$ draw down.

**References**

Erel, Y., Blum, J.D., Roueff, E. and Ganor, J., 2004. Lead and strontium isotopes as monitors of experimental granitoid mineral dissolution. *Geochimica et Cosmochimica Acta*, 68(22), pp.4649–4663.DOI:10.1016/j.gca.2004.04.022

Ganor, J., Roueff, E., Erel, Y. and Blum, J.D., 2005. The dissolution kinetics of a granite and its minerals—Implications for comparison between laboratory and field dissolution rates. *Geochimica et Cosmochimica Acta*, 69(3), pp.607–621.DOI:10.1016/j.gca.2004.08.006

Hindshaw, R.S., Tipper, E.T., Reynolds, B.C., Lemarchand, E., Wiederhold, J.G., Magnusson, J., Bernasconi, S.M., Kretzschmar, R. and Bourdon, B., 2011. Hydrological control of stream water chemistry in a glacial catchment (Damma Glacier, Switzerland). *Chemical Geology*, 285(1), pp.215–230.DOI:10.1016/j.chemgeo.2011.04.012

Merschel, G., Bau, M., Schmidt, K., Münker, C. and Dantas, E.L., 2017. Hafnium and neodymium isotopes and REY distribution in the truly dissolved, nanoparticulate/colloidal and suspended loads of rivers in the Amazon Basin, Brazil. *Geochimica et Cosmochimica Acta*, 213(2017), pp.383–399.DOI:10.1016/j.gca.2017.07.006

Pena, L.D. and Goldstein, S.L., 2014. Thermohaline circulation crisis and impacts during the mid-Pleistocene transition. *Science*, 345(6194), pp.318–322.DOI:10.1126/science.1249770

Rickli, J., Frank, M., Stichel, T., Georg, R.B., Vance, D. and Halliday, A.N., 2013. Controls on the incongruent release of hafnium during weathering of metamorphic and sedimentary catchments. *Geochimica et Cosmochimica Acta*, 101, pp.263–284. DOI:10.1016/j.gca.2012.10.019

Rickli, J., Hindshaw, R.S., Leuthold, J., Wadham, J.L., Burton, K.W. and Vance, D., 2017. Impact of glacial activity on the weathering of Hf isotopes - observations from Southwest Greenland. *Geochimica et Cosmochimica Acta*, 215, pp.295–316.DOI:10.1016/j.gca.2017.08.005

## DANKSAGUNG

Danke, Martin dafür, dass du ein super Betreuer warst und mir in den letzten vier Jahren immer mit Rat und Tat zur Seite gestanden bist und mich immer wieder für diese Arbeit motiviert und inspiriert hast.

An dieser Stelle möchte ich mich auch bei Marcus Gutjahr bedanken: Du hast mir sehr geholfen, nicht nur mit den vielen Messungen am MS sondern auch durch immer hilfreiche Kommentaren und Anregungen.

A big "Mercí" goes to Germain Bayon for his agreement to be the second examiner of this thesis. Thank you very much!

Weiterhin möchte ich mich bei den vielen Personen bedanken, die mir in der Zeit am GEOMAR geholfen haben: Ed, Chris, Mario, Moritz, Georgi, Clauschi, Paddy, Steffie, Kristin, Kristin, Roland, Claudia, Anne, Chris, Anna, Zeynep, Jacek, Tianyu, Stefan, Daniel, David, Jackie, Janine… Vielen Dank euch allen für die großartige Hilfe besonders am Anfang der Arbeit. Außerdem will ich natürlich auch den HiWis danken, die auch maßgeblich an der Arbeit beteiligt waren: Julia, Theresa, Ingmar und Peer Danke für eure Zeit und eure Geduld! Besonders Peer möchte ich auch für seinen Rat und die Hilfe später im Labor danken.

A propos Labor: Jutta is the best! Danke, danke, danke.

Außerdem, hat natürlich auch Urs Schaltegger und seine Arbeitsgruppe in Genf meine besondere Dankbarkeit eure die große Hilfe bei der Durchführung des Verwitterungsexperiments verdient. Danke euch Björn, Hervé, Jörn, Kalin und Josh! Auch die externen sollen nicht vergessen bleiben: Jörg Rickli, Torben Stichel, Tina van de Flierdt, Patrick Blaser, Marcus Christl und Jim Hein. Vielen Dank euch allen!

Einen besonderen Dank möchte ich an meinen Spezl und zeitweise sogar Vorgesetzten Jan Taucher aussprechen, du hast mir im letzten Jahr viel Raum gegeben um gleichzeitig an der Thesis und einem spannenden neuen Projekt arbeiten zu können. Daran möchte ich mit Dank an Ulf Riebesell und die gesamte Arbeitsgruppe BI anschließen: Danke für die Unterstützung und die nette Ablenkung in den Mittagspausen Allanah, Judith, Lenni, Tim, Paul, Matze, Janina, Till, Micha, Carsten und Silvana.

Zu guter Letzt möchte ich mich natürlich auch bei meinen Eltern, meinen Freunden und meiner Tanja bedanken, ihr habt immer an mich geglaubt und mich bedingungslos unterstützt: ohne euch wäre das hier nichts geworden!

# APPENDIX

**Table A 1: (Chapter 3) Elemental yields of all leachates. All yields are given in ppm.**

| Step | Group/Sample | Subgroup | Calibration | Li | RSD% | Mg | RSD% | Al | RSD% | Ti | RSD% | Sr 86 | RSD% | Sr 88 | RSD% | Zr 90 | RSD% | La 139 | RSD% | Pr 141 | RSD% | Nd 144 | RSD% | Nd 146 | RSD% | Sm 147 | RSD% | Eu 153 | RSD% |
|---|---|---|---|---|---|---|---|---|---|---|---|---|---|---|---|---|---|---|---|---|---|---|---|---|---|---|---|---|---|
| WR | WR1 | | high | 32.82 | 0.89 | 1.88 | 37 | 1.75 | 1555 | 1.99 | 77.98 | 1.35 | 112.12 | 0.57 | 109.56 | 1.06 | 236.40 | 0.95 | 24.34 | 0.77 | 5.60 | 0.30 | 19.66 | 0.37 | 21.42 | 0.05 | 4.25 | 0.44 | 0.68 | 1.00 |
| WR | WR2 | | high | 31.04 | 0.39 | 1.88 | 38 | 1.17 | 1612 | 1.39 | 73.90 | 0.87 | 109.88 | 0.17 | 109.36 | 0.78 | 236.40 | 0.82 | 24.62 | 0.93 | 5.60 | 0.13 | 18.76 | 0.53 | 20.44 | 0.08 | 3.92 | 0.71 | 0.64 | 0.69 |
| A | G1 | P | high | 2.63 | 1.34 | 2.31 | 231 | 1.23 | 978 | 1.38 | 30.14 | 0.92 | 1.50 | 0.63 | 1.50 | 0.68 | 0.28 | 0.84 | 0.10 | 0.24 | 0.53 | 0.63 | 0.45 | 0.01 | 0.12 | 0.01 | 0.01 | 0.50 |
| B | G1 | P | high | 13.87 | 2.31 | 1522 | 1.73 | 3141 | 2.05 | 0.42 | 207.44 | 1.13 | 1.24 | 0.24 | 1.25 | 0.54 | 0.43 | 0.37 | 0.25 | 0.23 | 1.26 | 0.36 | 1.35 | 0.00 | 0.44 | 0.43 | 0.03 | 0.12 |
| C | G1 | P | high | 6.89 | 0.75 | 678 | 2.48 | 1455 | 0.44 | 0.76 | 102.22 | 0.48 | 0.68 | 0.58 | 0.68 | 0.54 | 0.07 | 0.27 | 0.09 | 0.06 | 0.31 | 0.24 | 0.34 | 0.01 | 0.12 | 0.01 | 0.01 | 0.15 |
| A | G2 | P | high | 2.76 | 0.81 | 241 | 0.78 | 1017 | 0.93 | 0.40 | 15.52 | 0.42 | 0.10 | 0.14 | 0.10 | 0.43 | 0.37 | 0.42 | 0.10 | 0.04 | 0.41 | 0.44 | 0.01 | 0.00 | 0.43 | 0.01 | 0.01 | 0.38 |
| B | G2 | P | high | 14.80 | 1.55 | 1638 | 1.63 | 3459 | 1.72 | 1.28 | 208.64 | 2.07 | 1.28 | 0.74 | 1.29 | 1.34 | 0.66 | 0.96 | 0.86 | 1.40 | 0.38 | 0.98 | 1.79 | 1.92 | 0.01 | 0.89 | 0.03 | 0.75 |
| C | G2 | P | high | 6.10 | 0.65 | 637 | 0.41 | 1373 | 1.02 | 0.49 | 73.64 | 0.99 | 0.16 | 0.51 | 0.33 | 0.97 | 0.48 | 0.51 | 0.33 | 0.11 | 0.85 | 0.35 | 0.51 | 0.38 | 0.01 | 0.42 | 0.01 | 0.25 |
| A | G3 | P | high | 14.43 | 1.00 | 98 | 1.20 | 1358 | 1.33 | 0.28 | 52.81 | 0.97 | 97.24 | 0.15 | 98.10 | 0.33 | 40.82 | 0.54 | 10.11 | 0.14 | 0.40 | 0.61 | 2.40 | 0.62 | 8.13 | 0.61 | 8.81 | 0.05 | 1.81 |
| B | G3 | N | high | 1.56 | 1.11 | 57 | 0.78 | 237 | 0.28 | 0.53 | 5.23 | 0.97 | 0.28 | 0.59 | 0.30 | 0.14 | 0.04 | 0.45 | 0.32 | 0.35 | 0.57 | 0.15 | 0.35 | 0.70 | 0.25 | 0.57 | 0.26 | 0.01 | 0.10 |
| C | G3 | N | high | 6.99 | 0.28 | 244 | 0.66 | 690 | 0.40 | 0.34 | 56.06 | 0.34 | 0.07 | 0.43 | 0.10 | 0.52 | 0.20 | 0.34 | 0.04 | 0.04 | 0.67 | 0.15 | 0.74 | 0.74 | 0.16 | 0.00 | 0.03 | 0.19 | 0.00 |
| A | G4 | N | high | 17.47 | 0.45 | 497 | 0.34 | 1470 | 0.62 | 0.40 | 74.74 | 1.18 | 0.34 | 0.38 | 0.36 | 0.45 | 0.04 | 0.32 | 0.35 | 0.57 | 0.35 | 0.70 | 0.71 | 0.74 | 0.01 | 0.28 | 0.01 | 0.02 | 0.01 |
| B | G4 | N | high | 17.73 | 1.17 | 8 | 1.15 | 1154 | 1.14 | 0.18 | 23.16 | 1.84 | 40.98 | 0.88 | 40.98 | 1.18 | 142.44 | 1.17 | 9.75 | 0.25 | 0.51 | 0.15 | 0.99 | 0.75 | 0.89 | 0.60 | 10.08 | 0.06 | 2.28 |
| C | G4 | N | high | 6.99 | 0.30 | 220 | 1.18 | 1179 | 1.08 | 0.54 | 0.76 | 0.55 | 0.53 | 0.04 | 0.76 | 0.25 | 0.25 | 0.51 | 0.15 | 0.99 | 0.75 | 0.89 | 0.81 | 0.04 | 0.03 | 1.36 | 0.00 | 5.55 |
| A | G4 | N | high | 5.23 | 1.68 | 1498 | 1.62 | 2832 | 1.90 | 143.04 | 2.10 | 0.78 | 0.13 | 0.78 | 0.62 | 0.07 | 0.56 | 0.58 | 0.84 | 1.91 | 0.04 | 2.05 | 0.01 | 0.00 | 0.17 | 0.11 | 0.01 | 0.61 |
| B | G4 | N | high | 2.43 | 1.11 | 629 | 1.38 | 830 | 1.27 | 89.68 | 1.02 | 0.06 | 0.61 | 0.09 | 0.85 | 0.03 | 0.63 | 0.06 | 0.44 | 0.01 | 0.27 | 0.05 | 0.80 | 0.05 | 0.00 | 0.01 | 3.08 | 0.00 | 0.00 |
| C | G4 | N | high | 2.67 | 0.82 | 1093 | 0.21 | 1964 | 0.98 | 268.48 | 0.41 | 0.10 | 1.91 | 0.12 | 0.40 | 0.03 | 0.58 | 0.04 | 0.61 | 0.02 | 0.31 | 0.07 | 1.05 | 0.08 | 0.01 | 0.02 | 2.21 | 0.01 | 0.67 |
| R | G4 | N | high | 5.62 | 1.73 | 14 | 2.03 | 1558 | 1.46 | 32.82 | 1.46 | 170.56 | 0.74 | 166.52 | 1.01 | 85.44 | 1.05 | 3.26 | 0.93 | 0.49 | 0.97 | 1.71 | 0.46 | 1.87 | 0.24 | 0.41 | 1.03 | 1.03 | 1.08 |
| A | S1 | N | high | 0.21 | 0.36 | 50 | 1.42 | 101 | 0.89 | 3.82 | 0.32 | 0.36 | 0.80 | 0.38 | 0.40 | 0.13 | 0.31 | 0.07 | 0.28 | 0.07 | 0.37 | 0.76 | 0.37 | 0.00 | 0.12 | 0.50 | 0.01 | 2.40 |
| B | S1 | N | high | 3.37 | 1.52 | 587 | 1.51 | 937 | 1.43 | 61.78 | 1.32 | 0.30 | 0.71 | 0.31 | 0.34 | 0.46 | 0.26 | 0.46 | 0.11 | 0.62 | 0.53 | 0.52 | 0.57 | 0.00 | 0.12 | 0.44 | 0.01 | 0.87 |
| C | S1 | N | high | 2.89 | 1.60 | 552 | 1.47 | 792 | 1.63 | 81.60 | 1.16 | 0.03 | 2.21 | 0.06 | 0.70 | 0.03 | 0.27 | 0.07 | 0.10 | 0.02 | 0.40 | 0.06 | 0.62 | 0.06 | 0.01 | 0.21 | 0.00 | 0.78 |
| R | S1 | N | high | 2.52 | 1.71 | 3 | 1.01 | 876 | 0.27 | 5.81 | 0.06 | 32.08 | 0.26 | 31.86 | 0.39 | 43.84 | 0.46 | 0.38 | 0.72 | 0.09 | 1.84 | 0.38 | 2.45 | 0.42 | 0.86 | 0.13 | 1.33 | 0.23 | 0.41 |
| A | S2 | N | high | 0.40 | 1.30 | 91 | 0.98 | 187 | 0.47 | 7.85 | 0.63 | 0.61 | 0.77 | 0.62 | 0.70 | 0.04 | 1.22 | 0.23 | 0.35 | 0.58 | 0.80 | 0.62 | 0.01 | 0.21 | 0.00 | 0.80 | 0.78 | 0.05 |
| B | S2 | N | high | 4.44 | 0.56 | 891 | 0.68 | 1364 | 0.32 | 92.08 | 1.00 | 0.28 | 0.81 | 0.30 | 0.43 | 0.04 | 0.52 | 0.29 | 0.41 | 0.11 | 0.36 | 0.53 | 0.22 | 0.57 | 0.00 | 0.17 | 0.11 | 0.01 |
| C | S2 | N | high | 2.43 | 1.11 | 629 | 1.38 | 830 | 1.27 | 89.68 | 1.02 | 0.06 | 0.61 | 0.09 | 0.85 | 0.03 | 0.63 | 0.06 | 0.44 | 0.01 | 0.27 | 0.05 | 0.80 | 0.05 | 0.00 | 0.01 | 3.08 | 0.00 | 0.00 |
| R | S2 | N | high | 6.39 | 1.46 | 12 | 2.02 | 1096 | 1.82 | 26.26 | 1.35 | 61.06 | 0.43 | 60.26 | 1.08 | 70.94 | 0.97 | 7.94 | 0.37 | 1.84 | 0.26 | 6.43 | 0.50 | 7.00 | 0.06 | 1.51 | 1.17 | 0.42 | 1.20 |
| A | S3 | N | high | 1.30 | 107 | 1.85 | 219 | 9.78 | 0.72 | 1.01 | 0.70 | 0.89 | 0.25 | 0.59 | 0.13 | 1.14 | 0.66 | 0.27 | 0.13 | 0.49 | 0.23 | 0.71 | 0.00 | 0.23 | 0.18 | 0.01 | 0.29 |
| B | S3 | N | high | 3.76 | 0.75 | 767 | 1.17 | 1176 | 0.92 | 81.52 | 0.82 | 0.31 | 0.80 | 0.33 | 0.26 | 0.03 | 0.29 | 0.09 | 0.23 | 0.06 | 0.49 | 0.41 | 0.73 | 0.44 | 0.01 | 0.13 | 0.55 | 0.01 | 1.13 |
| C | S3 | N | high | 1.99 | 1.92 | 529 | 2.07 | 700 | 2.20 | 76.26 | 1.83 | 0.22 | 1.08 | 0.24 | 1.03 | 0.03 | 0.26 | 0.03 | 0.09 | 0.85 | 0.02 | 1.06 | 0.07 | 0.47 | 0.07 | 0.01 | 0.02 | 2.28 | 0.00 |
| R | S3 | N | high | 6.23 | 0.10 | 14 | 0.85 | 1271 | 0.53 | 31.38 | 0.77 | 64.46 | 0.11 | 63.40 | 1.09 | 69.02 | 0.41 | 11.38 | 0.57 | 2.35 | 0.23 | 7.52 | 0.36 | 8.23 | 0.09 | 1.42 | 0.78 | 0.36 | 1.44 |
| A | S4 | N | high | 0.48 | 0.87 | 106 | 0.76 | 225 | 0.91 | 8.97 | 0.42 | 0.79 | 0.43 | 0.80 | 0.10 | 0.04 | 0.57 | 0.29 | 0.31 | 0.14 | 0.69 | 0.69 | 0.15 | 0.75 | 0.00 | 0.24 | 1.13 | 0.01 | 0.05 |
| B | S4 | N | high | 4.59 | 1.98 | 898 | 1.47 | 1391 | 0.69 | 93.84 | 0.86 | 0.34 | 0.58 | 0.35 | 0.74 | 0.03 | 0.10 | 0.44 | 0.56 | 0.16 | 0.54 | 0.67 | 0.30 | 0.72 | 0.01 | 0.21 | 0.48 | 0.01 | 2.10 |
| C | S4 | N | high | 1.92 | 1.07 | 481 | 0.79 | 647 | 0.30 | 69.66 | 0.30 | 0.07 | 2.62 | 0.09 | 0.38 | 0.03 | 0.30 | 0.24 | 0.74 | 0.05 | 1.28 | 0.17 | 0.30 | 0.19 | 0.00 | 0.03 | 1.71 | 0.00 | 2.25 |
| R | S4 | N | high | 6.27 | 0.67 | 17 | 1.60 | 1417 | 1.31 | 83.78 | 0.24 | 83.78 | 0.37 | 121.24 | 0.44 | 15.46 | 0.55 | 3.72 | 0.14 | 12.20 | 0.76 | 13.30 | 0.17 | 2.26 | 0.52 | 0.45 | 0.50 |
| A | S5 | P | high | 0.54 | 0.31 | 115 | 0.97 | 236 | 1.16 | 10.66 | 0.86 | 0.76 | 1.22 | 0.77 | 0.76 | 0.21 | 0.63 | 0.10 | 0.24 | 0.50 | 0.49 | 0.50 | 0.45 | 0.54 | 0.00 | 0.17 | 1.30 | 0.01 | 1.71 |
| B | S5 | P | high | 3.93 | 0.80 | 794 | 0.90 | 1203 | 1.52 | 83.28 | 0.92 | 0.41 | 0.24 | 0.43 | 0.23 | 0.04 | 0.27 | 0.32 | 0.56 | 0.11 | 0.44 | 0.50 | 0.39 | 0.54 | 0.01 | 0.15 | 0.20 | 0.01 | 0.80 |
| C | S5 | P | high | 0.74 | 0.63 | 105 | 1.10 | 1017 | 0.79 | 11.42 | 0.25 | 0.76 | 0.83 | 0.77 | 0.22 | 0.05 | 0.15 | 0.76 | 0.10 | 0.23 | 0.49 | 0.58 | 0.33 | 0.53 | 0.01 | 0.17 | 0.87 | 0.01 | 1.69 |
| R | S5 | P | high | 6.44 | 0.57 | 92 | 1.17 | 1057 | 1.34 | 70.62 | 1.08 | 66.98 | 0.71 | 66.18 | 1.08 | 33.20 | 0.78 | 14.42 | 0.13 | 3.81 | 0.54 | 12.87 | 0.33 | 13.96 | 0.15 | 3.16 | 0.83 | 0.59 | 0.81 |
| A | S6 | P | high | 2.09 | 0.59 | 277 | 0.47 | 581 | 0.42 | 24.98 | 0.82 | 0.90 | 0.47 | 0.91 | 0.07 | 0.06 | 0.37 | 0.11 | 0.84 | 0.49 | 0.36 | 0.53 | 0.00 | 0.16 | 0.01 | 0.41 | 0.01 | 0.21 |
| B | S6 | P | high | 7.12 | 1.24 | 1604 | 0.97 | 2211 | 0.90 | 139.52 | 1.94 | 1.14 | 0.91 | 1.16 | 1.20 | 0.04 | 0.25 | 0.23 | 0.08 | 0.15 | 0.16 | 0.77 | 0.30 | 0.82 | 0.00 | 0.27 | 0.63 | 0.02 | 0.21 |
| C | S6 | P | high | 3.20 | 0.36 | 301 | 1.33 | 631 | 1.54 | 26.58 | 0.92 | 0.69 | 0.49 | 0.93 | 1.20 | 0.06 | 0.40 | 0.26 | 0.49 | 0.11 | 0.74 | 0.49 | 0.04 | 0.53 | 0.00 | 0.09 | 1.00 | 0.01 | 1.09 |
| R | S6 | P | high | 15.15 | 0.68 | 31 | 1.00 | 1366 | 1.30 | 84.40 | 1.06 | 96.08 | 0.43 | 96.24 | 1.44 | 565.80 | 0.95 | 35.76 | 0.75 | 8.47 | 0.27 | 28.68 | 0.34 | 31.10 | 0.06 | 6.04 | 1.25 | 0.30 | 0.43 |
| WS | WS2 | | high | 15.60 | 0.80 | 40 | 0.34 | 1194 | 1.21 | 86.64 | 1.32 | 97.64 | 0.32 | 97.14 | 0.70 | 492.60 | 1.02 | 36.04 | 1.09 | 8.88 | 0.59 | 29.12 | 0.16 | 31.82 | 0.05 | 6.29 | 1.48 | 0.43 | 0.76 |
| PD | Z1g | N | low | 1.55 | 0.80 | 0.38 | 2.60 | 0.12 | 4.16 | 0.10 | 0.84 | 0.63 | 0.14 | 0.70 | 0.49 | 20.44 | 0.40 | 0.00 | 8.20 | 0.00 | 26.90 | 0.01 | 2.94 | 0.07 | 4.08 | 0.09 | 91.29 | 0.00 | >100 |
| Du | Z1g | N | low | 0.21 | 2.56 | 0.17 | 0.85 | 0.48 | 0.93 | 0.18 | 3.56 | 0.18 | 1.43 | 7.80 | 0.59 | 0.26 | 0.37 | 0.11 | 0.84 | 0.49 | 0.36 | 0.53 | 0.03 | 0.16 | 0.00 | 0.03 | 1.19 | 0.22 | 1.73 |
| A | Z1g | N | low | 0.07 | 1.39 | 0.04 | 0.99 | 0.06 | 0.71 | 0.13 | 1.04 | 0.48 | 0.45 | 0.48 | 1.20 | 0.04 | 0.25 | 0.23 | 0.08 | 0.15 | 0.16 | 0.77 | 0.30 | 0.82 | 0.00 | 0.27 | 0.63 | 0.02 | 0.21 |
| B | Z1g | N | low | 0.09 | 5.25 | 0.06 | 3.60 | 1.44 | 2.70 | 9.75 | 2.23 | 0.86 | 8.31 | 1.33 | 2.13 | 0.60 | 0.61 | 0.45 | 2.47 | 1.34 | 2.70 | 0.44 | 0.69 | 1.93 | 0.08 | 0.77 | 41.51 |
| C | Z1g | N | low | 0.06 | 2.17 | 0.04 | 0.80 | 0.61 | 0.01 | 0.84 | 0.28 | 2.14 | 22.11 | 1.37 | 0.01 | 3.83 | 0.00 | 5.00 | 0.02 | 5.57 | 0.02 | 4.15 | 0.00 | 18.54 | 0.00 | 18.15 |
| Du | Z1g | N | low | 0.24 | 3.15 | 0.07 | 3.75 | 0.78 | 4.09 | 5.29 | 3.19 | 0.28 | 1.62 | 33.06 | 1.29 | 0.03 | 3.10 | 0.01 | 1.11 | 1.50 | 0.07 | 1.32 | 0.07 | 2.24 | 4.68 | 0.00 | 18.15 |
| PD | Z1p | P | low | 4.74 | 12.38 | 0.40 | 8.18 | 0.65 | 7.24 | 19.52 | 5.05 | 0.25 | 3.18 | 3093.08 | 1.05 | 2.78 | 0.65 | 4.04 | 1.09 | 0.01 | 13.63 | 0.03 | 11.44 | 0.03 | 2.92 | 0.01 | 25.23 | 0.00 | 43.05 |
| A | Z1p | P | low | 0.25 | 3.36 | 0.10 | 2.48 | 0.99 | 1.68 | 0.38 | 1.25 | 3.89 | 0.40 | 135.96 | 1.89 | 0.77 | 9.08 | 0.78 | 10.03 | 0.38 | 1.71 | 0.04 | 2.88 | | | | | | |
| B | Z1p | P | low | 0.10 | 1.10 | 0.03 | 1.09 | 0.19 | 0.75 | 0.51 | 0.68 | 2.00 | 0.16 | 53.27 | 0.69 | 11.41 | 0.17 | 4.83 | 0.36 | 21.42 | 0.13 | 6.50 | 0.47 | 0.31 | 2.33 | | | | |
| C | Z1p | P | low | 0.07 | 1.96 | 0.09 | 1.15 | 0.69 | 1.10 | 1.63 | 1.21 | 4.30 | 0.95 | 243.19 | 0.95 | 2.37 | 0.96 | 0.82 | 4.10 | 0.65 | 1.89 | 0.77 | 4.40 | 0.42 | 1.80 | 0.07 | 2.38 | | |
| D | Z1p | P | low | 0.13 | 1.04 | 0.05 | 0.76 | 0.19 | 0.86 | 0.04 | 0.47 | 0.30 | 0.75 | 766.92 | 0.60 | 0.00 | 35.01 | 0.00 | 64.46 | 0.01 | 31.51 | 0.01 | 9.63 | 0.00 | 43.86 | 0.00 | 9.06 | | |
| Du | Z1pu | P | low | 0.12 | 1.68 | 0.06 | 0.98 | 0.64 | 0.29 | 1.04 | 0.18 | 0.19 | 0.07 | 839.33 | 0.31 | 0.08 | 0.63 | 0.04 | 0.90 | 0.17 | 2.31 | 0.19 | 0.71 | 0.05 | 4.06 | 0.00 | 35.36 | | |
| R | Z1p | P | high | 25.90 | 1.08 | -0.42 | 3.22 | 1.14 | 63.42 | 2.80 | 1.30 | -4.66 | 12.85 | 1.96 | 32.56 | 434769.23 | 1.03 | 0.77 | 23.59 | 0.39 | 10.35 | 2.89 | 1.22 | 2.86 | 7.82 | 3.60 | 0.62 | 2.12 | |
| TD | Z1pu | P | high | 32.13 | 0.38 | -0.35 | 10.75 | 2.08 | 8.07 | 2.49 | 2.12 | 2.94 | 11.10 | 11.93 | 5.29 | 499280.00 | 0.99 | 16.48 | 0.58 | 7.40 | 0.99 | 35.94 | 0.73 | 38.25 | 4.52 | 14.56 | 1.22 | 3.93 | |
| PD | Z2g | N | low | 2.71 | 0.41 | 0.13 | 0.41 | 1.09 | 0.82 | 0.31 | 0.74 | 0.16 | 2.22 | 16.32 | 2.69 | 0.01 | 9.25 | 0.00 | 6.87 | 0.02 | 5.19 | 0.02 | 1.03 | 0.01 | 12.21 | 0.00 | 35.11 | | |
| A | Z2g | N | low | 0.38 | 0.79 | 0.07 | 0.49 | 0.20 | 0.99 | 0.03 | 0.09 | 1.29 | 0.32 | 2.88 | 0.63 | 0.03 | 3.17 | 0.26 | 1.71 | 0.44 | 8.62 | 0.80 | 9.24 | 0.05 | 3.95 | 0.58 | 0.08 | 1.12 | |
| B | Z2g | N | low | 0.52 | 0.84 | 0.05 | 0.30 | 0.14 | 0.28 | 0.07 | 0.39 | 1.41 | 0.53 | 2.28 | 0.19 | 9.89 | 0.28 | 5.96 | 0.20 | 29.61 | 0.10 | 31.93 | 0.05 | 12.77 | 0.18 | 0.13 | 1.87 | | |
| C | Z2g | N | low | 0.74 | 0.63 | 0.05 | 0.61 | 1.10 | 0.79 | 0.73 | 1.12 | 2.79 | 0.75 | 18.00 | 0.44 | 8.74 | 0.50 | 2.51 | 0.55 | 9.29 | 0.36 | 10.16 | 0.25 | 2.85 | 1.06 | 0.06 | 2.21 | | |
| D | Z2g | N | low | 0.55 | 0.30 | 0.05 | 0.36 | 0.32 | 0.75 | 0.03 | 2.35 | 0.60 | 1.01 | 64.68 | 0.88 | 0.06 | 0.73 | 0.01 | 4.70 | 0.06 | 2.37 | 0.06 | 3.15 | 0.01 | 15.16 | 0.00 | 26.90 | | |
| PD | Z2p | P | low | 5.98 | 0.21 | 0.29 | 1.12 | 1.66 | 1.11 | 1.27 | 0.50 | 0.32 | 0.37 | 2382.69 | 0.97 | 0.01 | 4.07 | 0.00 | 10.35 | 0.02 | 3.58 | 0.02 | 3.63 | 0.00 | 16.34 | 0.00 | 10.98 | | |
| A | Z2p | P | low | 0.26 | 0.53 | 0.03 | 0.75 | 0.14 | 0.52 | 0.02 | 0.95 | 1.12 | 0.48 | 24.12 | 0.27 | 7.20 | 0.07 | 4.20 | 0.45 | 21.10 | 0.34 | 22.83 | 0.12 | 8.51 | 0.15 | 0.12 | 1.72 | | |
| B | Z2p | P | low | 0.12 | 1.38 | 0.03 | 0.75 | 0.15 | 0.45 | 0.10 | 0.98 | 1.43 | 0.20 | 21.27 | 0.51 | 11.92 | 0.15 | 6.02 | 0.07 | 28.64 | 0.37 | 30.92 | 0.20 | 12.30 | 0.37 | 0.14 | 1.07 | | |
| C | Z2p | P | low | 0.37 | 0.91 | 0.04 | 0.38 | 0.84 | 0.68 | 0.28 | 0.46 | 2.37 | 0.44 | 247.85 | 0.81 | 14.16 | 0.53 | 3.76 | 0.45 | 13.38 | 0.59 | 14.68 | 0.12 | 3.96 | 1.09 | 0.07 | 3.62 | | |
| D | Z2p | P | low | 1.72 | 0.08 | 1.86 | 0.52 | 1.17 | 0.02 | 9.05 | 0.13 | 1.29 | 1028.85 | 0.33 | 0.00 | 8.80 | 0.00 | >100 | 0.00 | 0.00 | 34.72 | 0.01 | 10.38 | 0.00 | 2.67 | 0.00 | 57.77 | 0.00 | 24.17 |
| PD | Z3g | N | low | 2.88 | 1.12 | 0.16 | 0.23 | 0.86 | 0.19 | 0.26 | 0.71 | 0.09 | 3.37 | 16.21 | 1.40 | 0.00 | 0.00 | 0.00 | 40.87 | 0.00 | 3.20 | 0.00 | #WERT! | 0.00 | 91.44 | 0.00 | 9.26 | | |
| A | Z3g | N | low | 0.48 | 1.42 | 0.13 | 1.33 | 0.41 | 1.02 | 0.03 | 0.98 | 0.27 | 2.22 | 4.03 | 0.43 | 4.25 | 0.15 | 2.91 | 0.81 | 17.17 | 0.54 | 18.22 | 0.16 | 9.77 | 0.18 | 0.15 | 1.84 | | |
| B | Z3g | N | low | 0.50 | 1.73 | 0.07 | 2.40 | 0.09 | 1.03 | 0.03 | 2.03 | 0.89 | 4.82 | 6.18 | 4.25 | 0.44 | 2.80 | 0.32 | 15.05 | 0.87 | 16.17 | 0.24 | 6.99 | 1.34 | 0.07 | 3.72 | | | |
| C | Z3g | N | low | 0.66 | 0.36 | 0.06 | 0.12 | 0.75 | 0.60 | 0.52 | 0.40 | 2.83 | 23.70 | 0.90 | 1.36 | 1.35 | 5.22 | 0.75 | 5.72 | 0.15 | 1.81 | 0.49 | 0.06 | 3.54 | | | | | |
| D | Z3g | N | low | 0.53 | 1.42 | 0.03 | 0.75 | 0.10 | 1.43 | 0.02 | 0.33 | 0.34 | 1.37 | 51.86 | 1.46 | 0.02 | 1.76 | 0.00 | 3.75 | 0.02 | 10.04 | 0.02 | 7.34 | 0.01 | 23.91 | 0.00 | 12.27 | | |
| PD | Z5p | P | low | 5.28 | 0.10 | 0.34 | 0.21 | 1.72 | 0.28 | 0.87 | 0.41 | 0.34 | 2.74 | 2599.23 | 0.45 | 0.01 | 0.92 | 0.01 | 6.52 | 0.04 | 1.84 | 0.06 | 0.99 | 0.01 | 13.01 | 0.00 | 17.75 | | |
| A | Z5p | P | low | 0.30 | 2.82 | 0.08 | 1.39 | 0.61 | 1.68 | 0.02 | 2.67 | 1.75 | 1.44 | 30.23 | 0.55 | 6.21 | 0.55 | 4.13 | 0.52 | 22.73 | 0.89 | 24.61 | 0.35 | 9.93 | 0.50 | 0.13 | 1.13 | | |
| B | Z5p | P | low | 0.76 | 1.76 | 0.03 | 1.55 | 0.13 | 1.32 | 0.07 | 1.07 | 2.93 | 0.57 | 27.00 | 0.69 | 6.10 | 0.41 | 4.14 | 0.48 | 20.74 | 0.65 | 22.52 | 0.43 | 10.39 | 1.16 | 0.15 | 1.65 | | |
| C | Z5p | P | low | 0.30 | 0.49 | 0.04 | 0.77 | 0.63 | 0.86 | 0.21 | 0.77 | 0.56 | 0.56 | 221.42 | 0.30 | 0.00 | 1.70 | 0.90 | 6.42 | 0.48 | 7.00 | 0.27 | 2.44 | 1.26 | 0.06 | 1.65 | | | |
| Du | Z5p | P | low | 0.32 | 0.78 | 0.03 | 0.65 | 0.38 | 0.82 | 0.38 | 0.85 | 0.11 | 2.67 | 1167.77 | 1.07 | 0.05 | 1.73 | 0.48 | 6.31 | 0.23 | 6.87 | 0.40 | 6.80 | 0.17 | 1.83 | 0.00 | 34.72 | | |
| Du | Z5p | P | low | 0.29 | 1.27 | 0.06 | 0.43 | 1.27 | 0.47 | 2.17 | 0.74 | 0.29 | 0.86 | 791.88 | 0.58 | 0.04 | 4.61 | 0.02 | 3.70 | 0.09 | 3.18 | 0.09 | 4.08 | 0.03 | 7.63 | 0.00 | 34.72 | | |

**Table A 1 (continued): Elemental yields of all leachates. All yields are given in ppm.**

| Step | Gd 157 | RSD% | Tb 159 | RSD% | Dy 163 | RSD% | Ho 165 | RSD% | Er 166 | RSD% | Tm 169 | RSD% | Yb 172 | RSD% | Lu 175 | RSD% | Hf 178 | RSD% | Hf 179 | RSD% | Pb 207 | RSD% | Pb 208 | RSD% | Th 232 | RSD% | U 138 | RSD% | $^{176}Lu/^{177}Hf$ | $^{147}Sm/^{144}Nd$ |
|---|---|---|---|---|---|---|---|---|---|---|---|---|---|---|---|---|---|---|---|---|---|---|---|---|---|---|---|---|---|---|
| WR | 4.48 | 0.85 | 0.67 | 0.52 | 3.82 | 0.65 | 0.78 | 1.11 | 2.41 | 0.77 | 0.37 | 0.46 | 2.57 | 0.80 | 0.40 | 0.70 | 5.17 | 0.88 | 5.19 | 0.28 | 11.63 | 0.85 | 11.86 | 0.79 | 15.57 | 0.83 | 5.07 | 1.37 | 0.011 | 0.130 |
| WR | 4.23 | 0.22 | 0.63 | 0.51 | 3.71 | 0.17 | 0.75 | 1.04 | 2.34 | 0.44 | 0.36 | 0.57 | 2.51 | 1.02 | 0.40 | 1.83 | 5.57 | 0.46 | 5.54 | 0.30 | 10.90 | 0.46 | 11.00 | 0.61 | 14.78 | 0.66 | 4.48 | 1.02 | 0.010 | 0.126 |
| A | 0.14 | 0.31 | 0.03 | 0.60 | 0.16 | 0.27 | 0.03 | 0.42 | 0.10 | 0.32 | 0.01 | 1.35 | 0.10 | 0.76 | 0.02 | 0.31 | 0.01 | 3.50 | 0.01 | 6.41 | 2.47 | 0.77 | 2.50 | 0.79 | 0.20 | 0.59 | 1.14 | 0.62 | 0.238 | 0.180 |
| B | 0.52 | 0.50 | 0.09 | 0.62 | 0.56 | 0.12 | 0.11 | 0.10 | 0.32 | 0.51 | 0.04 | 0.42 | 0.27 | 0.27 | 0.04 | 0.46 | 0.01 | 4.13 | 0.01 | 2.14 | 4.95 | 0.66 | 5.05 | 0.71 | 0.79 | 0.77 | 1.98 | 0.28 | 0.671 | 0.213 |
| C | 0.07 | 0.47 | 0.01 | 0.73 | 0.06 | 0.58 | 0.01 | 0.72 | 0.04 | 0.55 | 0.01 | 1.86 | 0.04 | 2.61 | 0.01 | 0.42 | 0.01 | 5.59 | 0.01 | 4.23 | 0.45 | 0.52 | 0.46 | 0.96 | 1.39 | 0.50 | 0.17 | 1.87 | 0.156 | 0.122 |
| R | 2.54 | 1.18 | 0.41 | 0.83 | 2.47 | 1.53 | 0.52 | 0.58 | 1.58 | 1.82 | 0.25 | 0.63 | 1.67 | 0.72 | 0.26 | 1.21 | 1.93 | 0.33 | 1.94 | 1.91 | 6.30 | 0.41 | 6.28 | 0.94 | 4.75 | 1.63 | 1.65 | 1.55 | 0.018 | 0.134 |
| A | 0.14 | 1.02 | 0.03 | 2.14 | 0.15 | 1.37 | 0.03 | 1.64 | 0.10 | 1.09 | 0.01 | 1.79 | 0.10 | 1.40 | 0.02 | 2.35 | 0.01 | 11.33 | 0.01 | 11.03 | 2.45 | 0.78 | 2.47 | 0.76 | 0.14 | 4.28 | 1.12 | 1.00 | 0.288 | 0.180 |
| B | 0.66 | 1.18 | 0.11 | 1.32 | 0.65 | 0.82 | 0.13 | 0.92 | 0.35 | 0.98 | 0.05 | 0.71 | 0.31 | 0.89 | 0.04 | 1.91 | 0.01 | 0.19 | 0.01 | 0.11 | 4.68 | 1.11 | 4.78 | 1.21 | 1.14 | 1.35 | 1.86 | 1.82 | 0.755 | 0.197 |
| C | 0.08 | 0.99 | 0.01 | 1.16 | 0.07 | 1.35 | 0.01 | 0.93 | 0.04 | 0.43 | 0.01 | 0.80 | 0.05 | 1.11 | 0.01 | 0.37 | 0.00 | 0.32 | 0.01 | 2.57 | 0.50 | 0.49 | 0.51 | 0.40 | 1.40 | 0.59 | 0.19 | 0.66 | 0.194 | 0.127 |
| R | 1.95 | 0.18 | 0.31 | 0.87 | 1.84 | 0.25 | 0.38 | 1.23 | 1.19 | 1.78 | 0.18 | 1.17 | 1.25 | 1.42 | 0.19 | 1.79 | 1.08 | 2.28 | 1.08 | 1.99 | 4.82 | 0.70 | 4.80 | 0.30 | 3.54 | 1.03 | 1.28 | 1.68 | 0.025 | 0.135 |
| A | 0.13 | 1.66 | 0.03 | 0.09 | 0.16 | 0.77 | 0.03 | 0.66 | 0.09 | 0.70 | 0.01 | 1.12 | 0.10 | 0.88 | 0.02 | 0.66 | 0.00 | 2.04 | 0.01 | 1.42 | 5.55 | 0.63 | 5.63 | 0.34 | 0.50 | 0.50 | 1.49 | 0.75 | 0.476 | 0.244 |
| B | 0.34 | 0.97 | 0.07 | 0.96 | 0.39 | 0.94 | 0.07 | 0.71 | 0.20 | 0.46 | 0.03 | 1.26 | 0.20 | 0.60 | 0.03 | 1.05 | 0.00 | 1.77 | 0.01 | 2.21 | 3.58 | 0.62 | 3.62 | 0.65 | 0.26 | 0.23 | 2.60 | 0.83 | 0.695 | 0.242 |
| C | 0.04 | 0.49 | 0.01 | 1.03 | 0.05 | 1.23 | 0.01 | 0.66 | 0.03 | 0.44 | 0.01 | 0.17 | 0.04 | 0.39 | 0.01 | 2.07 | 0.00 | 1.70 | 0.00 | 4.01 | 1.94 | 0.22 | 1.97 | 0.43 | 1.01 | 0.82 | 0.26 | 0.13 | 0.227 | 0.140 |
| R | 2.30 | 1.37 | 0.36 | 0.77 | 2.07 | 0.66 | 0.42 | 0.96 | 1.30 | 0.29 | 0.21 | 1.95 | 1.48 | 2.06 | 0.25 | 1.58 | 4.43 | 0.83 | 4.44 | 2.18 | 8.34 | 0.84 | 8.45 | 0.47 | 5.72 | 0.59 | 3.30 | 1.02 | 0.008 | 0.148 |
| A | 0.27 | 0.96 | 0.04 | 1.09 | 0.25 | 0.71 | 0.05 | 0.82 | 0.14 | 1.16 | 0.02 | 1.44 | 0.12 | 0.56 | 0.02 | 0.50 | 0.00 | 2.71 | 0.01 | 2.18 | 1.23 | 1.60 | 1.24 | 1.20 | 0.29 | 1.24 | 0.28 | 1.45 | 0.486 | 0.195 |
| B | 0.69 | 0.24 | 0.11 | 0.42 | 0.67 | 0.99 | 0.13 | 0.91 | 0.37 | 0.52 | 0.05 | 1.70 | 0.31 | 0.16 | 0.04 | 0.97 | 0.01 | 2.50 | 0.01 | 0.60 | 1.64 | 0.52 | 1.65 | 0.44 | 0.40 | 1.23 | 0.81 | 1.37 | 0.770 | 0.198 |
| C | 0.02 | 2.98 | 0.00 | 0.85 | 0.02 | 0.88 | 0.00 | 2.56 | 0.01 | 2.70 | 0.00 | 2.75 | 0.01 | 0.37 | 0.00 | 2.80 | 0.00 | 1.56 | 0.00 | 1.52 | 0.17 | 0.67 | 0.17 | 0.46 | 1.52 | 0.40 | 0.40 | 0.46 | 0.068 | 0.178 |
| R | 0.48 | 0.19 | 0.08 | 1.30 | 0.47 | 2.73 | 0.11 | 2.42 | 0.35 | 0.97 | 0.06 | 0.18 | 0.41 | 1.26 | 0.07 | 0.31 | 1.83 | 0.42 | 1.83 | 1.34 | 4.47 | 0.58 | 4.44 | 0.78 | 0.50 | 0.93 | 0.42 | 1.27 | 0.006 | 0.144 |
| A | 0.15 | 0.91 | 0.03 | 0.25 | 0.15 | 0.22 | 0.03 | 0.79 | 0.09 | 1.56 | 0.01 | 1.01 | 0.08 | 1.10 | 0.01 | 0.64 | 0.00 | 1.91 | 0.00 | 1.53 | 0.84 | 1.29 | 0.85 | 0.35 | 0.48 | 0.90 | 0.38 | 0.71 | 0.445 | 0.210 |
| B | 0.20 | 0.55 | 0.03 | 0.88 | 0.21 | 0.67 | 0.04 | 0.55 | 0.12 | 0.90 | 0.02 | 0.90 | 0.11 | 1.39 | 0.02 | 1.40 | 0.00 | 1.24 | 0.00 | 1.73 | 0.93 | 0.23 | 0.94 | 0.43 | 0.20 | 0.87 | 1.05 | 0.55 | 0.515 | 0.200 |
| C | 0.02 | 1.84 | 0.00 | 0.82 | 0.02 | 1.86 | 0.00 | 2.61 | 0.01 | 2.88 | 0.00 | 2.83 | 0.01 | 1.11 | 0.00 | 0.84 | 0.00 | 1.03 | 0.00 | 2.28 | 0.14 | 1.08 | 0.14 | 1.32 | 1.51 | 0.75 | 0.23 | 0.77 | 0.093 | 0.148 |
| R | 0.16 | 2.09 | 0.04 | 2.25 | 0.22 | 3.37 | 0.05 | 2.89 | 0.16 | 2.25 | 0.03 | 0.21 | 0.18 | 1.88 | 0.04 | 2.19 | 1.15 | 1.30 | 1.15 | 1.15 | 4.14 | 0.81 | 4.11 | 1.33 | 0.28 | 2.42 | 0.34 | 1.17 | 0.004 | 0.206 |
| A | 0.24 | 0.74 | 0.04 | 0.42 | 0.25 | 0.18 | 0.05 | 0.36 | 0.15 | 0.54 | 0.02 | 0.45 | 0.13 | 1.10 | 0.02 | 1.03 | 0.00 | 1.34 | 0.01 | 3.36 | 1.30 | 0.94 | 1.32 | 1.40 | 0.28 | 1.07 | 0.49 | 1.69 | 0.586 | 0.216 |
| B | 0.20 | 0.66 | 0.03 | 0.76 | 0.20 | 0.71 | 0.04 | 0.66 | 0.11 | 0.26 | 0.02 | 1.34 | 0.10 | 0.61 | 0.02 | 1.53 | 0.00 | 1.64 | 0.00 | 1.33 | 0.85 | 0.45 | 0.85 | 0.93 | 1.56 | 0.41 | 1.10 | 0.40 | 0.516 | 0.199 |
| C | 0.02 | 0.89 | 0.00 | 0.66 | 0.02 | 0.31 | 0.00 | 1.02 | 0.01 | 0.27 | 0.00 | 5.16 | 0.02 | 0.29 | 0.00 | 0.52 | 0.00 | 2.57 | 0.00 | 1.87 | 0.08 | 0.54 | 0.07 | 0.64 | 0.91 | 0.50 | 0.21 | 0.85 | 0.113 | 0.166 |
| R | 1.63 | 0.79 | 0.25 | 1.33 | 1.42 | 0.90 | 0.30 | 1.33 | 0.91 | 0.78 | 0.14 | 1.09 | 0.95 | 0.33 | 0.16 | 1.19 | 1.88 | 0.45 | 1.89 | 2.19 | 3.85 | 0.48 | 3.83 | 0.84 | 1.00 | 0.94 | 0.82 | 0.82 | 0.012 | 0.141 |
| A | 0.27 | 0.72 | 0.05 | 0.90 | 0.28 | 0.71 | 0.06 | 0.93 | 0.17 | 0.64 | 0.02 | 1.02 | 0.15 | 0.71 | 0.02 | 1.01 | 0.00 | 3.02 | 0.01 | 1.95 | 1.30 | 0.38 | 1.30 | 0.22 | 0.22 | 0.46 | 0.47 | 0.25 | 0.568 | 0.215 |
| B | 0.15 | 0.43 | 0.03 | 0.42 | 0.15 | 0.50 | 0.03 | 0.33 | 0.09 | 0.44 | 0.01 | 0.16 | 0.08 | 1.34 | 0.01 | 0.35 | 0.00 | 1.22 | 0.00 | 2.49 | 0.72 | 0.10 | 0.72 | 0.23 | 1.05 | 0.31 | 0.54 | 1.15 | 0.418 | 0.196 |
| C | 0.02 | 2.60 | 0.00 | 3.16 | 0.02 | 0.92 | 0.00 | 2.19 | 0.01 | 0.93 | 0.00 | 3.11 | 0.01 | 1.78 | 0.00 | 0.51 | 0.00 | 1.74 | 0.00 | 0.86 | 0.07 | 1.42 | 0.06 | 0.58 | 0.97 | 0.41 | 0.13 | 0.98 | 0.095 | 0.132 |
| R | 1.49 | 0.97 | 0.20 | 1.31 | 1.07 | 2.31 | 0.22 | 1.50 | 0.70 | 0.99 | 0.11 | 1.07 | 0.75 | 0.87 | 0.12 | 1.73 | 1.75 | 1.88 | 1.79 | 0.48 | 3.93 | 0.30 | 3.95 | 0.81 | 2.73 | 1.04 | 0.88 | 0.95 | 0.010 | 0.114 |
| A | 0.29 | 0.32 | 0.05 | 0.19 | 0.29 | 0.09 | 0.06 | 1.14 | 0.17 | 0.64 | 0.02 | 1.41 | 0.16 | 0.88 | 0.02 | 1.30 | 0.00 | 2.42 | 0.01 | 0.74 | 1.43 | 0.71 | 1.43 | 0.56 | 0.19 | 0.37 | 0.49 | 0.23 | 0.645 | 0.211 |
| B | 0.23 | 0.53 | 0.04 | 0.59 | 0.22 | 0.54 | 0.04 | 0.77 | 0.13 | 1.33 | 0.02 | 0.52 | 0.11 | 1.40 | 0.02 | 1.53 | 0.00 | 2.64 | 0.01 | 2.08 | 1.03 | 0.95 | 1.03 | 0.83 | 4.37 | 0.56 | 0.85 | 1.45 | 0.526 | 0.186 |
| C | 0.03 | 1.09 | 0.00 | 1.40 | 0.03 | 0.97 | 0.01 | 1.06 | 0.02 | 0.93 | 0.00 | 0.91 | 0.02 | 2.72 | 0.00 | 0.57 | 0.00 | 0.47 | 0.00 | 2.29 | 0.08 | 1.62 | 0.08 | 0.69 | 0.44 | 0.54 | 0.18 | 0.11 | 0.126 | 0.111 |
| R | 2.50 | 1.46 | 0.36 | 0.84 | 2.13 | 0.74 | 0.46 | 0.32 | 1.45 | 1.49 | 0.23 | 2.07 | 1.58 | 0.72 | 0.25 | 0.43 | 2.82 | 0.35 | 2.86 | 1.90 | 4.35 | 0.43 | 4.39 | 1.19 | 4.23 | 0.99 | 1.40 | 0.55 | 0.012 | 0.117 |
| A | 0.21 | 0.48 | 0.04 | 0.04 | 0.22 | 0.62 | 0.04 | 0.41 | 0.13 | 0.71 | 0.02 | 0.26 | 0.12 | 0.64 | 0.02 | 0.32 | 0.00 | 2.69 | 0.01 | 1.64 | 1.37 | 0.62 | 1.38 | 0.28 | 0.14 | 0.25 | 0.81 | 0.03 | 0.544 | 0.209 |
| B | 0.18 | 0.50 | 0.03 | 0.79 | 0.18 | 1.64 | 0.04 | 0.52 | 0.10 | 0.77 | 0.01 | 0.97 | 0.09 | 0.43 | 0.01 | 0.74 | 0.00 | 1.87 | 0.00 | 3.10 | 1.34 | 0.75 | 1.36 | 0.19 | 0.18 | 0.68 | 1.62 | 0.89 | 0.473 | 0.184 |
| C | 0.20 | 0.89 | 0.03 | 0.38 | 0.21 | 0.61 | 0.04 | 1.20 | 0.12 | 0.89 | 0.02 | 0.86 | 0.12 | 0.51 | 0.02 | 2.04 | 0.00 | 2.52 | 0.01 | 3.64 | 1.30 | 0.51 | 1.30 | 1.00 | 0.13 | 1.34 | 0.75 | 1.41 | 0.517 | 0.209 |
| R | 3.56 | 0.39 | 0.61 | 0.15 | 3.77 | 0.57 | 0.80 | 0.26 | 2.51 | 0.11 | 0.40 | 0.57 | 2.78 | 0.53 | 0.44 | 0.99 | 7.75 | 0.49 | 7.74 | 0.17 | 3.54 | 0.71 | 3.56 | 0.29 | 5.09 | 0.49 | 2.47 | 0.21 | 0.008 | 0.148 |
| A | 0.18 | 0.94 | 0.03 | 0.52 | 0.19 | 0.79 | 0.04 | 1.00 | 0.12 | 0.55 | 0.02 | 1.58 | 0.11 | 0.86 | 0.02 | 0.58 | 0.00 | 2.29 | 0.01 | 3.14 | 2.25 | 0.93 | 2.26 | 1.30 | 0.21 | 0.82 | 1.83 | 0.63 | 0.475 | 0.191 |
| B | 0.34 | 0.59 | 0.07 | 0.19 | 0.43 | 0.55 | 0.09 | 0.61 | 0.27 | 0.51 | 0.04 | 0.90 | 0.24 | 0.54 | 0.04 | 0.23 | 0.00 | 1.74 | 0.01 | 2.93 | 2.67 | 0.51 | 2.71 | 0.74 | 0.35 | 0.19 | 4.58 | 0.33 | 0.856 | 0.217 |
| C | 0.18 | 0.28 | 0.03 | 0.38 | 0.18 | 0.27 | 0.04 | 0.36 | 0.11 | 0.66 | 0.02 | 0.54 | 0.11 | 0.32 | 0.02 | 1.29 | 0.00 | 1.35 | 0.01 | 1.58 | 2.16 | 0.38 | 2.17 | 0.88 | 0.20 | 0.65 | 1.75 | 0.29 | 0.483 | 0.191 |
| R | 2.45 | 0.34 | 0.36 | 0.74 | 2.11 | 0.29 | 0.45 | 0.35 | 1.42 | 0.54 | 0.22 | 1.85 | 1.58 | 0.45 | 0.25 | 0.63 | 4.53 | 0.23 | 4.55 | 0.16 | 3.10 | 0.64 | 3.10 | 0.42 | 3.58 | 0.31 | 1.54 | 0.94 | 0.008 | 0.120 |
| WS | 6.25 | 1.11 | 0.94 | 0.56 | 5.48 | 0.46 | 1.15 | 0.88 | 3.62 | 0.78 | 0.56 | 0.47 | 3.97 | 0.37 | 0.64 | 1.06 | 13.27 | 0.56 | 13.28 | 0.54 | 8.16 | 0.82 | 8.24 | 0.48 | 6.82 | 0.99 | 6.33 | 0.73 | 0.007 | 0.128 |
| WS | 6.52 | 0.96 | 1.00 | 1.51 | 6.01 | 1.10 | 1.26 | 0.83 | 3.97 | 0.50 | 0.61 | 0.70 | 4.26 | 0.53 | 0.67 | 1.14 | 11.34 | 0.50 | 11.36 | 0.73 | 6.45 | 0.26 | 6.53 | 1.03 | 8.65 | 0.48 | 4.57 | 0.59 | 0.008 | 0.130 |
| PD | 0.00 | 61.76 | 0.00 | 10.70 | 0.01 | 8.63 | 0.00 | 5.75 | 0.02 | 4.87 | 0.00 | 46.12 | 0.02 | 5.99 | 0.01 | 4.76 | 0.76 | 2.11 | 0.75 | 0.92 | 1.64 | 0.67 | 1.65 | 1.27 | 0.71 | 0.22 | 3.23 | 0.66 | 0.001 | 0.115 |
| A | 8.10 | 0.88 | 1.32 | 0.76 | 7.80 | 1.44 | 1.59 | 1.24 | 4.58 | 1.22 | 0.62 | 1.13 | 3.94 | 1.86 | 0.56 | 1.28 | 0.11 | 0.68 | 0.14 | 2.18 | 4.18 | 1.85 | 4.23 | 1.68 | 11.65 | 2.03 | 4.83 | 2.27 | 0.625 | 0.190 |
| B | 0.78 | 1.15 | 0.13 | 0.54 | 0.77 | 0.86 | 0.16 | 1.45 | 0.45 | 1.22 | 0.06 | 1.79 | 0.41 | 0.95 | 0.06 | 1.68 | 0.05 | 0.93 | 0.04 | 6.21 | 1.93 | 1.26 | 2.03 | 1.13 | 16.85 | 1.03 | 1.53 | 1.24 | 0.170 | 0.182 |
| C | 0.89 | 1.51 | 0.18 | 1.52 | 1.37 | 0.99 | 0.34 | 1.66 | 1.12 | 2.29 | 0.16 | 3.20 | 1.06 | 3.52 | 0.15 | 2.90 | 0.36 | 4.42 | 0.36 | 2.07 | 2.84 | 3.80 | 2.88 | 3.84 | 5.51 | 4.49 | 5.08 | 4.64 | 0.058 | 0.169 |
| D | 0.01 | 18.69 | 0.00 | 7.29 | 0.02 | 11.93 | 0.01 | 0.28 | 0.03 | 2.00 | 0.01 | 14.88 | 0.08 | 1.46 | 0.02 | 1.99 | 1.01 | 1.24 | 1.01 | 2.29 | 0.13 | 1.82 | 0.17 | 2.08 | 0.86 | 0.44 | 4.51 | 0.91 | 0.002 | 0.122 |
| Du | 0.02 | 8.98 | 0.00 | 7.25 | 0.03 | 6.05 | 0.01 | 3.19 | 0.03 | 5.62 | 0.00 | >100 | 0.03 | 6.00 | 0.01 | 8.23 | 1.38 | 2.72 | 1.39 | 2.08 | 4.30 | 1.56 | 4.40 | 3.22 | 1.79 | 4.14 | 39.44 | 3.21 | 0.001 | 0.182 |
| PD | 0.01 | 3.23 | 0.00 | 11.91 | 0.01 | 14.78 | 0.00 | 3.75 | 0.01 | 34.02 | 0.00 | >100 | 0.02 | 13.37 | 0.00 | 5.17 | 92.96 | 6.54 | 94.08 | 6.48 | 0.60 | 8.74 | 0.63 | 8.89 | 0.14 | 9.38 | 17.13 | 10.48 | 0.000 | 0.121 |
| A | 1.57 | 1.90 | 0.19 | 0.90 | 1.05 | 2.24 | 0.26 | 1.61 | 0.86 | 2.05 | 0.12 | 2.56 | 0.80 | 2.02 | 0.15 | 1.83 | 3.28 | 1.59 | 3.29 | 2.01 | 6.54 | 2.21 | 6.80 | 2.66 | 1.88 | 2.50 | 21.01 | 2.47 | 0.006 | 0.113 |
| B | 7.22 | 0.45 | 1.17 | 0.37 | 7.25 | 0.74 | 1.65 | 0.69 | 5.27 | 0.83 | 0.79 | 0.82 | 5.50 | 0.97 | 0.94 | 1.11 | 0.99 | 1.49 | 1.00 | 2.45 | 8.48 | 1.53 | 8.78 | 1.52 | 53.12 | 1.87 | 5.70 | 1.98 | 0.132 | 0.183 |
| C | 2.19 | 1.21 | 0.40 | 1.35 | 2.31 | 0.93 | 0.43 | 1.17 | 1.03 | 1.50 | 0.11 | 1.76 | 0.57 | 2.83 | 0.08 | 0.86 | 6.12 | 1.28 | 6.10 | 1.23 | 0.54 | 9.34 | 0.58 | 9.44 | 14.95 | 2.90 | 3.83 | 3.64 | 0.002 | 0.268 |
| D | 0.01 | 28.15 | 0.00 | 28.22 | 0.02 | 12.33 | 0.00 | 8.98 | 0.01 | 11.85 | 0.00 | 43.71 | 0.03 | 9.12 | 0.01 | 10.22 | 22.60 | 0.61 | 22.65 | 0.35 | 0.22 | 9.31 | 0.26 | 8.00 | 5.20 | 0.67 | 7.40 | 0.29 | 0.000 | 0.291 |
| Du | 0.06 | 5.26 | 0.01 | 4.35 | 0.09 | 1.73 | 0.02 | 4.45 | 0.09 | 2.62 | 0.01 | 6.39 | 0.13 | 1.78 | 0.02 | 1.56 | 25.53 | 0.28 | 25.56 | 0.55 | 0.30 | 2.42 | 0.33 | 2.67 | 1.40 | 0.45 | 23.74 | 0.41 | 0.000 | 0.170 |
| R | 20.94 | 1.19 | 8.58 | 0.51 | 110.34 | 0.36 | 43.91 | 0.85 | 223.94 | 0.71 | 49.85 | 0.87 | 469.85 | 0.63 | 99.26 | 1.07 | 8676.92 | 0.96 | 8464.62 | 1.39 | 7.01 | 2.19 | 5.58 | 2.72 | 332.92 | 0.50 | 876.92 | 0.70 | 0.002 | 0.922 |
| TD | 36.83 | 0.83 | 12.43 | 0.99 | 149.20 | 0.81 | 57.68 | 0.76 | 289.24 | 0.35 | 64.12 | 0.25 | 597.60 | 0.09 | 125.68 | 0.33 | 10308.90 | 0.77 | 10024.00 | 0.74 | 21.34 | 0.63 | 20.02 | 0.22 | 554.40 | 0.58 | 1161.69 | 0.20 | 0.002 | 0.247 |
| PD | 0.01 | 16.33 | 0.00 | 17.07 | 0.02 | 5.44 | 0.01 | 8.61 | 0.02 | 9.42 | 0.00 | 16.84 | 0.04 | 1.97 | 0.01 | 5.46 | 0.85 | 2.80 | 0.85 | 1.36 | 10.29 | 0.48 | 10.33 | 0.55 | 2.50 | 0.64 | 14.85 | 0.42 | 0.001 | 0.220 |
| A | 5.71 | 0.41 | 1.24 | 0.09 | 8.72 | 0.25 | 1.87 | 0.19 | 5.74 | 0.19 | 0.87 | 0.18 | 6.05 | 0.60 | 0.93 | 0.39 | 0.18 | 1.14 | 0.20 | 2.75 | 61.86 | 0.43 | 63.64 | 0.74 | 99.68 | 0.73 | 405.50 | 0.84 | 0.683 | 0.279 |
| B | 15.47 | 0.23 | 2.92 | 0.06 | 17.10 | 0.24 | 3.16 | 0.17 | 8.56 | 0.18 | 1.17 | 0.59 | 7.43 | 0.85 | 1.01 | 0.54 | 0.19 | 0.46 | 0.25 | 3.28 | 99.55 | 0.46 | 99.91 | 0.51 | 50.59 | 0.26 | 15.18 | 0.68 | 0.641 | 0.262 |
| C | 3.75 | 0.15 | 0.80 | 0.34 | 5.84 | 0.48 | 1.36 | 0.90 | 4.36 | 0.43 | 0.65 | 0.86 | 4.30 | 0.30 | 0.63 | 1.03 | 0.90 | 0.64 | 0.92 | 0.79 | 2.77 | 2.51 | 3.03 | 0.56 | 12.57 | 0.20 | 23.62 | 0.13 | 0.096 | 0.185 |
| D | 0.02 | 8.08 | 0.01 | 3.83 | 0.07 | 5.05 | 0.02 | 1.32 | 0.10 | 3.04 | 0.03 | 5.37 | 0.33 | 1.11 | 0.07 | 3.44 | 2.82 | 1.50 | 2.81 | 0.71 | 0.58 | 1.67 | 0.65 | 1.23 | 1.46 | 0.99 | 20.30 | 0.87 | 0.004 | 0.153 |
| PD | 0.00 | 24.53 | 0.00 | 6.81 | 0.01 | 4.49 | 0.00 | 2.79 | 0.01 | 10.06 | 0.00 | 43.70 | 0.01 | 9.50 | 0.00 | 24.03 | 88.73 | 0.55 | 89.54 | 0.94 | 15.46 | 0.80 | 15.67 | 1.33 | 0.49 | 2.61 | 41.92 | 1.34 | 0.000 | 0.176 |
| A | 11.18 | 0.23 | 2.20 | 0.41 | 15.18 | 0.67 | 3.59 | 0.60 | 11.85 | 0.32 | 1.87 | 0.14 | 13.32 | 0.10 | 2.29 | 0.11 | 0.90 | 0.58 | 0.94 | 3.68 | 64.31 | 0.71 | 67.23 | 0.50 | 93.00 | 0.41 | 369.58 | 0.59 | 0.347 | 0.244 |
| B | 15.54 | 0.30 | 3.13 | 0.47 | 19.92 | 0.46 | 4.08 | 0.91 | 12.31 | 0.43 | 1.86 | 0.20 | 13.15 | 0.66 | 2.03 | 0.67 | 0.92 | 1.30 | 1.00 | 1.22 | 142.88 | 1.03 | 143.85 | 1.05 | 112.38 | 1.02 | 38.50 | 1.13 | 0.296 | 0.260 |
| C | 4.94 | 0.17 | 1.00 | 0.29 | 6.79 | 0.38 | 1.47 | 0.69 | 4.24 | 0.52 | 0.54 | 0.42 | 3.05 | 0.45 | 0.41 | 0.97 | 10.33 | 0.73 | 10.40 | 0.83 | 2.24 | 0.71 | 2.38 | 0.83 | 138.04 | 1.09 | 20.22 | 0.27 | 0.005 | 0.178 |
| D | 0.01 | 5.51 | 0.01 | 4.64 | 0.07 | 0.01 | 0.02 | 4.76 | 0.06 | 8.53 | 0.01 | 13.46 | 0.16 | 2.98 | 0.03 | 13.27 | 41.65 | 2.60 | 41.73 | 2.79 | 0.23 | 3.40 | 0.28 | 6.31 | 13.84 | 3.19 | 28.51 | 3.86 | 0.000 | 0.489 |
| PD | 0.00 | 76.98 | 0.00 | 8.40 | 0.01 | 19.93 | 0.00 | 15.54 | 0.01 | 7.58 | 0.00 | >100 | 0.03 | 7.51 | 0.01 | 5.79 | 0.99 | 1.65 | 0.98 | 1.39 | 40.80 | 0.62 | 41.28 | 0.75 | 1.92 | 0.53 | 154.95 | 0.76 | 0.001 | -0.635 |
| A | 13.40 | 0.33 | 2.78 | 0.60 | 18.22 | 0.73 | 3.78 | 0.66 | 11.49 | 0.43 | 1.75 | 1.42 | 12.05 | 1.27 | 1.76 | 0.73 | 0.19 | 2.06 | 0.26 | 2.32 | 82.45 | 0.72 | 82.82 | 0.66 | 95.18 | 0.76 | 123.64 | 0.74 | 1.065 | 0.348 |
| B | 8.87 | 1.24 | 1.68 | 1.10 | 10.40 | 1.22 | 2.08 | 1.23 | 5.96 | 0.77 | 0.84 | 1.00 | 5.54 | 1.31 | 0.77 | 2.20 | 0.14 | 8.52 | 0.18 | 6.66 | 481.36 | 2.36 | 478.18 | 2.19 | 25.07 | 2.37 | 16.70 | 2.66 | 0.655 | 0.282 |
| C | 2.57 | 1.01 | 0.59 | 0.95 | 4.68 | 1.21 | 1.19 | 0.24 | 4.13 | 0.61 | 0.66 | 0.96 | 4.51 | 0.93 | 0.68 | 0.63 | 1.44 | 0.35 | 1.45 | 2.11 | 123.23 | 0.49 | 122.36 | 1.21 | 8.83 | 0.49 | 23.80 | 0.05 | 0.066 | 0.208 |
| D | 0.02 | 9.27 | 0.01 | 3.17 | 0.07 | 3.20 | 0.02 | 0.72 | 0.12 | 2.11 | 0.03 | 4.55 | 0.39 | 2.52 | 0.09 | 1.62 | 2.80 | 1.14 | 2.81 | 0.42 | 1.47 | 1.20 | 1.51 | 0.79 | 0.75 | 0.83 | 17.62 | 1.61 | 0.004 | 0.246 |
| PD | 0.02 | 3.64 | 0.00 | 4.02 | 0.03 | 5.51 | 0.01 | 2.09 | 0.03 | 2.17 | 0.00 | 18.03 | 0.04 | 3.23 | 0.01 | 8.05 | 109.23 | 0.28 | 109.92 | 0.47 | 49.15 | 0.90 | 49.31 | 0.49 | 0.34 | 1.67 | 131.15 | 0.60 | 0.000 | 0.225 |
| A | 12.92 | 0.96 | 2.43 | 0.64 | 16.56 | 0.80 | 3.93 | 0.51 | 13.04 | 1.13 | 2.07 | 1.00 | 14.50 | 0.94 | 2.47 | 1.13 | 0.88 | 1.23 | 0.95 | 1.20 | 195.12 | 1.31 | 192.69 | 1.38 | 101.38 | 1.98 | 179.27 | 2.00 | 0.377 | 0.264 |
| B | 14.27 | 1.09 | 3.04 | 0.94 | 21.05 | 1.19 | 4.69 | 1.42 | 15.30 | 1.36 | 2.46 | 1.39 | 18.19 | 1.51 | 2.93 | 1.39 | 1.11 | 1.72 | 1.19 | 1.81 | 57.62 | 2.15 | 58.15 | 1.40 | 113.73 | 2.34 | 42.50 | 2.74 | 0.356 | 0.304 |
| C | 3.51 | 1.01 | 0.80 | 0.43 | 5.83 | 0.47 | 1.32 | 0.42 | 4.01 | 0.41 | 0.53 | 0.98 | 3.05 | 0.22 | 0.41 | 0.41 | 9.40 | 0.18 | 9.45 | 0.44 | 3.48 | 0.20 | 3.47 | 1.36 | 82.92 | 0.25 | 16.90 | 0.56 | 0.006 | 0.229 |
| D | 0.02 | 8.04 | 0.01 | 2.99 | 0.06 | 1.56 | 0.02 | 4.71 | 0.06 | 3.15 | 0.01 | 3.02 | 0.17 | 2.50 | 0.03 | 1.76 | 48.65 | 1.38 | 48.77 | 1.28 | 0.20 | 2.83 | 0.22 | 1.04 | 7.71 | 1.89 | 27.42 | 1.96 | 0.000 | 0.707 |
| Du | 0.11 | 0.22 | 0.02 | 3.19 | 0.16 | 2.24 | 0.04 | 2.77 | 0.11 | 1.60 | 0.02 | 4.70 | 0.14 | 2.27 | 0.03 | 4.85 | 1.28 | 1.33 | 1.28 | 1.06 | 0.60 | 2.39 | 0.68 | 0.51 | 6.20 | 0.30 | 46.13 | 0.58 | 0.003 | 0.227 |
| Du | 0.04 | 6.62 | 0.01 | 8.18 | 0.07 | 6.04 | 0.02 | 2.79 | 0.06 | 4.15 | 0.01 | 10.88 | 0.07 | 1.93 | 0.01 | 3.07 | 30.53 | 0.28 | 30.47 | 0.28 | 4.57 | 0.72 | 4.84 | 0.34 | 3.48 | 0.67 | 179.75 | 0.38 | 0.000 | 0.230 |

**Table A 2: (Chapter 3) Coincidence factors (R2) of leachate REE patterns with those of selected rock-forming and accessory minerals. Colors indicate the coincidence (Red: no coincidence to Green: high coincidence)**

| **Bulk unweathered Granite:** | **Whole rock** | | **G1** | | | | **G2** | | | | **G3** | | | | **G4** | | | |
|---|---|---|---|---|---|---|---|---|---|---|---|---|---|---|---|---|---|---|
| Experiment: | WR1 | WR2 | A | B | C | R | A | B | C | R | A | B | C | R | A | B | C | R |
| Apatite | -0.07 | -0.09 | 0.38 | 0.86 | -0.09 | -0.13 | 0.38 | 0.65 | -0.07 | -0.14 | 0.71 | 0.80 | -0.04 | 0.02 | 0.74 | 0.78 | 0.07 | -0.75 |
| Sphene | 0.66 | 0.63 | 0.69 | 0.54 | 0.61 | 0.64 | 0.69 | 0.78 | 0.62 | 0.64 | 0.03 | 0.36 | 0.51 | 0.70 | 0.77 | 0.73 | 0.94 | 0.21 |
| Epidote | 0.19 | 0.20 | -0.32 | -0.69 | 0.18 | 0.25 | -0.32 | -0.41 | 0.17 | 0.27 | -0.91 | -0.76 | 0.03 | 0.09 | -0.47 | -0.51 | 0.36 | 0.96 |
| K-Feldspar | 0.59 | 0.60 | 0.10 | -0.50 | 0.58 | 0.64 | 0.10 | -0.10 | 0.57 | 0.66 | -0.70 | -0.51 | 0.45 | 0.50 | -0.24 | -0.32 | 0.61 | 0.98 |
| Plagioclase | 0.86 | 0.86 | 0.47 | -0.22 | 0.85 | 0.89 | 0.47 | 0.23 | 0.84 | 0.90 | -0.40 | -0.20 | 0.75 | 0.79 | 0.05 | -0.05 | 0.77 | 0.82 |
| Amphibole | 0.64 | 0.61 | 0.64 | 0.46 | 0.59 | 0.62 | 0.64 | 0.71 | 0.60 | 0.63 | -0.06 | 0.27 | 0.47 | 0.67 | 0.71 | 0.66 | 0.94 | 0.28 |
| Zircon | -0.41 | -0.39 | -0.29 | -0.32 | -0.37 | -0.41 | -0.29 | -0.48 | -0.38 | -0.42 | 0.21 | -0.18 | -0.23 | -0.37 | -0.45 | -0.44 | -0.74 | -0.37 |

| **Sediment fractions:** | **Whole sediment** | | **S1** | | | | **S2** | | | | **S3** | | | | **S4** | | | | **S5** | | | | **S6** | | | |
|---|---|---|---|---|---|---|---|---|---|---|---|---|---|---|---|---|---|---|---|---|---|---|---|---|---|---|
| Experiment: | WS1 | WS2 | A | B | C | R | A | B | C | R | A | B | C | R | A | B | C | R | A | B | C | R | A | B | C | R |
| Apatite | -0.06 | -0.07 | 0.83 | 0.68 | -0.06 | -0.81 | 0.82 | 0.59 | -0.08 | -0.14 | 0.83 | 0.55 | -0.12 | -0.16 | 0.79 | 0.42 | -0.09 | -0.10 | 0.79 | 0.47 | 0.78 | -0.06 | 0.59 | 0.86 | 0.57 | -0.10 |
| Sphene | 0.64 | 0.65 | 0.51 | 0.72 | 0.54 | -0.10 | 0.56 | 0.75 | 0.41 | 0.65 | 0.55 | 0.78 | 0.55 | 0.61 | 0.59 | 0.79 | 0.62 | 0.65 | 0.56 | 0.76 | 0.58 | 0.61 | 0.70 | 0.04 | 0.71 | 0.62 |
| Epidote | 0.16 | 0.17 | -0.74 | -0.50 | 0.12 | 0.95 | -0.70 | -0.40 | 0.02 | 0.28 | -0.70 | -0.35 | 0.17 | 0.27 | -0.67 | -0.22 | 0.19 | 0.21 | -0.70 | -0.30 | -0.67 | 0.12 | -0.49 | -0.95 | -0.47 | 0.19 |
| K-Feldspar | 0.56 | 0.57 | -0.52 | -0.18 | 0.53 | 0.76 | -0.46 | -0.05 | 0.44 | 0.66 | -0.48 | 0.01 | 0.58 | 0.66 | -0.41 | 0.17 | 0.59 | 0.61 | -0.43 | 0.09 | -0.41 | 0.54 | -0.13 | -0.88 | -0.10 | 0.59 |
| Plagioclase | 0.84 | 0.84 | -0.21 | 0.17 | 0.81 | 0.45 | -0.15 | 0.30 | 0.73 | 0.90 | -0.17 | 0.35 | 0.84 | 0.90 | -0.08 | 0.51 | 0.85 | 0.87 | -0.10 | 0.44 | -0.07 | 0.82 | 0.24 | -0.65 | 0.26 | 0.86 |
| Amphibole | 0.62 | 0.63 | 0.43 | 0.65 | 0.52 | -0.01 | 0.48 | 0.68 | 0.39 | 0.64 | 0.47 | 0.71 | 0.53 | 0.60 | 0.51 | 0.73 | 0.60 | 0.63 | 0.48 | 0.69 | 0.51 | 0.59 | 0.63 | -0.05 | 0.65 | 0.60 |
| Zircon | -0.37 | -0.38 | -0.19 | -0.41 | -0.35 | -0.13 | -0.25 | -0.44 | -0.15 | -0.42 | -0.25 | -0.46 | -0.32 | -0.41 | -0.27 | -0.48 | -0.39 | -0.39 | -0.24 | -0.43 | -0.25 | -0.32 | -0.28 | 0.12 | -0.30 | -0.37 |

| **Zircon fractions:** | **Pure Z1** | **Z1g** | | | | | **Z1p** | | | | **Z2g** | | | | **Z2p** | | | | **Z3g** | | | | | **Z3p** | | | | | |
|---|---|---|---|---|---|---|---|---|---|---|---|---|---|---|---|---|---|---|---|---|---|---|---|---|---|---|---|---|---|
| Experiment: | R | PD | A | B | C | D | PD | A | B | C | D | PD | A | B | C | D | PD | A | B | C | D | PD | A | B | C | D | PD | A | B | C | D |
| Apatite | -0.25 | -0.33 | 0.75 | 0.53 | 0.16 | -0.62 | -0.67 | 0.37 | 0.49 | 0.67 | -0.60 | -0.61 | 0.46 | 0.89 | 0.26 | -0.62 | -0.65 | 0.37 | 0.70 | 0.27 | -0.57 | -0.57 | 0.54 | 0.84 | 0.10 | -0.59 | -0.56 | 0.40 | 0.31 | 0.45 | -0.56 |
| Sphene | -0.64 | -0.53 | 0.76 | 0.79 | 0.00 | -0.58 | -0.32 | 0.90 | 0.61 | 0.54 | -0.69 | -0.64 | -0.59 | 0.31 | 0.00 | -0.56 | -0.68 | -0.50 | -0.20 | 0.49 | -0.70 | -0.65 | -0.55 | -0.07 | -0.56 | -0.58 | -0.69 | -0.52 | -0.63 | -0.21 | -0.69 |
| Epidote | -0.34 | -0.32 | -0.51 | -0.34 | -0.51 | -0.31 | -0.12 | -0.15 | -0.54 | -0.35 | -0.44 | -0.42 | -0.87 | -0.76 | -0.60 | -0.28 | -0.40 | -0.86 | -0.98 | -0.23 | -0.42 | -0.44 | -0.86 | -0.90 | -0.66 | -0.33 | -0.52 | -0.86 | -0.81 | -0.71 | -0.42 |
| K-Feldspar | -0.42 | -0.37 | -0.27 | 0.03 | -0.15 | -0.30 | -0.10 | 0.12 | -0.17 | -0.14 | -0.45 | -0.41 | -0.92 | -0.64 | -0.24 | -0.26 | -0.39 | -0.87 | -0.89 | 0.19 | -0.41 | -0.43 | -0.95 | -0.88 | -0.55 | -0.32 | -0.52 | -0.90 | -0.85 | -0.46 | -0.41 |
| Plagioclase | -0.46 | -0.39 | 0.03 | 0.38 | 0.17 | -0.35 | -0.12 | 0.40 | 0.20 | 0.09 | -0.49 | -0.45 | -0.83 | -0.40 | 0.09 | -0.31 | -0.43 | -0.76 | -0.68 | 0.54 | -0.46 | -0.47 | -0.90 | -0.71 | -0.41 | -0.36 | -0.56 | -0.82 | -0.79 | -0.18 | -0.46 |
| Amphibole | -0.61 | -0.49 | 0.69 | 0.73 | -0.06 | -0.51 | -0.24 | 0.89 | 0.56 | 0.46 | -0.64 | -0.58 | -0.65 | 0.22 | -0.07 | -0.49 | -0.62 | -0.54 | -0.27 | 0.42 | -0.65 | -0.56 | -0.61 | -0.15 | -0.60 | -0.52 | -0.64 | -0.56 | -0.67 | -0.31 | -0.64 |
| Zircon | 0.98 | 0.89 | -0.41 | -0.45 | 0.29 | 0.96 | 0.83 | -0.39 | -0.06 | -0.64 | 0.94 | 0.94 | 0.65 | -0.23 | 0.28 | 0.96 | 0.95 | 0.78 | 0.41 | -0.35 | 0.98 | 0.99 | 0.54 | 0.11 | 0.79 | 0.97 | 0.92 | 0.76 | 0.80 | 0.15 | 0.99 |

| **Fresh zircon fractions:** | **fresh zircon** | **Z1g** | **Z1p** | **Z4g** | **Z4p** |
|---|---|---|---|---|---|
| Experiment: | Rfresh | Du | Du | Du | Du |
| Apatite | -0.24 | -0.68 | -0.01 | 0.31 | -0.58 |
| Sphene | -0.64 | -0.14 | -0.41 | -0.44 | -0.68 |
| Epidote | -0.35 | -0.07 | -0.60 | -0.85 | -0.48 |
| K-Feldspar | -0.42 | -0.07 | -0.54 | -0.81 | -0.48 |
| Plagioclase | -0.46 | -0.07 | -0.43 | -0.67 | -0.52 |
| Amphibole | -0.60 | -0.08 | -0.41 | -0.47 | -0.63 |
| Zircon | 0.98 | 0.52 | 0.91 | 0.78 | 0.92 |

**Table A 3: (Chapter 3) Summary of all isotope analyses conducted from leachates and total dissolutions. Sample and step nomenclature according to Table 3.1. For a more details the reader is referred to the supplementary dataset.**

| Step | Sample | $^{143}Nd/^{144}Nd$ | | $\varepsilon_{Nd}$ | 2σ | | $^{176}Hf/^{177}Hf$ | | $\varepsilon_{Hf}$ | 2σ | $^{206}Pb/^{204}Pb$ | 2σ | $^{207}Pb/^{204}Pb$ | 2σ | $^{208}Pb/^{204}Pb$ | 2σ | [Pb batch] |
|---|---|---|---|---|---|---|---|---|---|---|---|---|---|---|---|---|---|
| WR | WR1 | 0.512226 | ± 5 | -4.1 | 0.1 | [a] | 0.282491 | ± 2 | -2.9 | 0.1 | 19.889 | 0.001 | 15.719 | 0.000 | 39.591 | 0.001 | [II] |
| WR | WR2 | 0.512219 | ± 6 | -4.2 | 0.1 | [a] | 0.282461 | ± 2 | -3.2 | 0.1 | 19.917 | 0.000 | 15.721 | 0.000 | 39.567 | 0.001 | [II] |
| A | G1 | 0.512470 | ± 6 | -1.7 | 0.1 | | 0.297606 | ± 7 | 148.2 | 0.2 | 19.912 | 0.001 | 15.719 | 0.000 | 39.232 | 0.001 | [I] |
| B | G1 | 0.512557 | ± 5 | -0.8 | 0.1 | | 0.349833 | ± 7 | 670.5 | 0.2 | 20.196 | 0.001 | 15.733 | 0.000 | 39.294 | 0.001 | [I] |
| C | G1 | 0.512218 | ± 10 | -4.2 | 0.2 | | 0.310021 | ± 6 | 272.4 | 0.2 | 19.905 | 0.001 | 15.718 | 0.000 | 39.474 | 0.001 | [II] |
| R | G1 | 0.512210 | ± 5 | -4.3 | 0.1 | [a] | 0.282592 | ± 2 | -1.9 | 0.1 | 19.493 | 0.000 | 15.698 | 0.000 | 39.489 | 0.001 | [II] |
| A | G2 | 0.512467 | ± 5 | -1.7 | 0.1 | | 0.297926 | ± 5 | 151.4 | 0.2 | 19.913 | 0.001 | 15.719 | 0.001 | 39.235 | 0.002 | [I] |
| B | G2 | 0.512546 | ± 5 | -0.9 | 0.1 | | 0.355579 | ± 8 | 727.9 | 0.3 | 20.224 | 0.001 | 15.736 | 0.000 | 39.295 | 0.002 | [I] |
| C | G2 | 0.512227 | ± 8 | -4.1 | 0.2 | | 0.309946 | ± 6 | 271.6 | 0.2 | 19.930 | 0.001 | 15.720 | 0.000 | 39.465 | 0.001 | [II] |
| R | G2 | 0.512215 | ± 6 | -4.2 | 0.1 | [a] | 0.282658 | ± 2 | -1.3 | 0.1 | 19.453 | 0.001 | 15.697 | 0.000 | 39.414 | 0.001 | [II] |
| A | G3 | 0.512581 | ± 8 | -0.6 | 0.2 | | 0.357341 | ± 9 | 745.6 | 0.3 | 20.259 | 0.001 | 15.736 | 0.000 | 39.323 | 0.001 | [II] |
| B | G3 | 0.512589 | ± 7 | -0.5 | 0.1 | | 0.451191 | ± 16 | 1684.1 | 0.6 | 20.657 | 0.001 | 15.759 | 0.001 | 39.422 | 0.002 | [I] |
| C | G3 | 0.512249 | ± 8 | -3.9 | 0.2 | | 0.396755 | ± 13 | 1139.7 | 0.4 | 19.628 | 0.001 | 15.705 | 0.000 | 39.285 | 0.001 | [II] |
| R | G3 | 0.512199 | ± 6 | -4.4 | 0.1 | [a] | 0.282284 | ± 2 | -5.0 | 0.1 | 19.805 | 0.001 | 15.715 | 0.001 | 39.436 | 0.002 | [II] |
| A | G4 | 0.512570 | ± 8 | -0.7 | 0.2 | | 0.364255 | ± 8 | 814.7 | 0.3 | 19.382 | 0.001 | 15.688 | 0.001 | 38.928 | 0.001 | [I] |
| B | G4 | 0.512552 | ± 5 | -0.9 | 0.1 | | 0.518535 | ± 14 | 2357.5 | 0.5 | 19.867 | 0.001 | 15.710 | 0.001 | 39.008 | 0.002 | [I] |
| C | G4 | 0.512490 | ± 5 | -1.5 | 0.1 | | 0.370384 | ± 17 | 876.0 | 0.6 | 19.601 | 0.001 | 15.700 | 0.001 | 39.116 | 0.001 | [II] |
| R | G4 | 0.512309 | ± 8 | -3.3 | 0.2 | [a] | 0.282403 | ± 3 | -3.8 | 0.1 | 19.177 | 0.001 | 15.675 | 0.001 | 38.857 | 0.002 | [II] |
| A | S1 | 0.512583 | ± 7 | -0.5 | 0.1 | | 0.386327 | ± 20 | 1035.4 | 0.7 | 19.524 | 0.001 | 15.695 | 0.000 | 39.087 | 0.001 | [II] |
| B | S1 | 0.512548 | ± 6 | -0.9 | 0.1 | | 0.380262 | ± 19 | 974.8 | 0.7 | 21.142 | 0.001 | 15.780 | 0.001 | 39.386 | 0.001 | [I] |
| C | S1 | 0.512284 | ± 6 | -3.5 | 0.1 | | 0.304950 | ± 15 | 221.7 | 0.5 | 20.554 | 0.001 | 15.752 | 0.000 | 39.663 | 0.001 | [II] |
| R | S1 | 0.512409 | ± 9 | -2.3 | 0.2 | [a] | 0.282287 | ± 2 | -5.0 | 0.1 | 19.431 | 0.001 | 15.695 | 0.000 | 39.068 | 0.001 | [II] |
| A | S2 | 0.512554 | ± 8 | -0.8 | 0.2 | | 0.397696 | ± 9 | 1149.1 | 0.3 | 19.596 | 0.001 | 15.698 | 0.001 | 39.021 | 0.001 | [I] |
| B | S2 | 0.512555 | ± 4 | -0.8 | 0.1 | | 0.365308 | ± 23 | 825.2 | 0.8 | 21.413 | 0.001 | 15.793 | 0.001 | 39.262 | 0.001 | [II] |
| C | S2 | 0.512339 | ± 6 | -3.0 | 0.1 | | 0.299116 | ± 8 | 163.3 | 0.3 | 21.819 | 0.001 | 15.817 | 0.001 | 39.667 | 0.001 | [II] |
| R | S2 | 0.512285 | ± 6 | -3.5 | 0.1 | | 0.282431 | ± 3 | -3.5 | 0.1 | 19.717 | 0.001 | 15.712 | 0.000 | 39.330 | 0.001 | [II] |
| A | S3 | 0.512584 | ± 10 | -0.5 | 0.2 | | 0.398598 | ± 11 | 1158.1 | 0.4 | 19.525 | 0.001 | 15.694 | 0.001 | 39.004 | 0.001 | [II] |
| B | S3 | 0.512557 | ± 5 | -0.8 | 0.1 | | 0.350244 | ± 21 | 674.6 | 0.7 | 20.249 | 0.000 | 15.732 | 0.000 | 39.215 | 0.001 | [II] |
| C | S3 | 0.512297 | ± 9 | -3.4 | 0.2 | | 0.317795 | ± 21 | 350.1 | 0.8 | 20.279 | 0.001 | 15.736 | 0.000 | 39.529 | 0.001 | [II] |
| R | S3 | 0.512203 | ± 5 | -4.3 | 0.1 | | 0.282451 | ± 2 | -3.3 | 0.1 | 19.706 | 0.000 | 15.709 | 0.000 | 39.605 | 0.001 | [III] |
| A | S4 | 0.512533 | ± 8 | -1.0 | 0.2 | | 0.396682 | ± 194 | 1139.0 | 6.9 | 19.539 | 0.001 | 15.695 | 0.001 | 39.011 | 0.002 | [I] |
| B | S4 | 0.512495 | ± 6 | -1.4 | 0.1 | | 0.351136 | ± 76 | 683.5 | 2.7 | 20.682 | 0.001 | 15.755 | 0.001 | 39.243 | 0.002 | [I] |
| C | S4 | 0.512190 | ± 10 | -4.5 | 0.2 | | 0.311901 | ± 14 | 291.2 | 0.5 | 20.693 | 0.001 | 15.757 | 0.001 | 39.653 | 0.001 | [II] |
| R | S4 | 0.512219 | ± 4 | -4.2 | 0.1 | | 0.282532 | ± 2 | -2.5 | 0.1 | 19.814 | 0.001 | 15.689 | 0.001 | 39.377 | 0.004 | [II] |
| A | S5 | 0.512542 | ± 9 | -1.0 | 0.2 | | 0.369642 | ± 14 | 868.6 | 0.5 | 19.616 | 0.001 | 15.699 | 0.001 | 39.039 | 0.002 | [I] |
| B | S5 | 0.512546 | ± 4 | -0.9 | 0.1 | | 0.346633 | ± 15 | 638.5 | 0.5 | 20.408 | 0.001 | 15.740 | 0.000 | 39.536 | 0.001 | [I] |
| C | S5 | 0.512209 | ± 8 | -4.3 | 0.2 | | 0.315591 | ± 234 | 328.1 | 8.3 | 21.441 | 0.001 | 15.795 | 0.001 | 39.846 | 0.001 | [III] |
| R | S5 | 0.512273 | ± 3 | -3.6 | 0.1 | | 0.282459 | ± 2 | -3.3 | 0.1 | 20.389 | 0.001 | 15.745 | 0.000 | 39.711 | 0.001 | [II] |
| A | S6 | 0.512424 | ± 5 | -2.1 | 0.1 | | 0.313991 | ± 51 | 312.1 | 1.8 | 19.434 | 0.001 | 15.690 | 0.001 | 38.886 | 0.001 | [I] |
| B | S6 | 0.512493 | ± 6 | -1.5 | 0.1 | | 0.398815 | ± 11 | 1160.3 | 0.4 | 21.258 | 0.001 | 15.785 | 0.001 | 39.324 | 0.002 | [I] |
| C | S6 | 0.512309 | ± 8 | -3.3 | 0.2 | | 0.343143 | ± 15 | 603.6 | 0.5 | 20.316 | 0.001 | 15.735 | 0.001 | 39.323 | 0.002 | [II] |
| R | S6 | 0.512225 | ± 3 | -4.1 | 0.1 | | 0.282457 | ± 3 | -3.3 | 0.1 | 20.184 | 0.001 | 15.734 | 0.001 | 39.820 | 0.002 | [II] |
| WS | WS1 | 0.512205 | ± 5 | -4.3 | 0.1 | | 0.282370 | ± 3 | -4.1 | 0.1 | 21.067 | 0.001 | 15.782 | 0.000 | 39.753 | 0.001 | [III] |
| WS | WS2 | 0.512235 | ± 8 | -4.0 | 0.2 | | 0.282408 | ± 2 | -3.8 | 0.1 | 20.322 | 0.001 | 15.734 | 0.001 | 39.753 | 0.002 | [II] |
| PD | Z1g | 0.512112 | ± 76 | -5.3 | 1.5 | | 0.282725 | ± 10 | -0.6 | 0.4 | 19.752 | 0.004 | 15.704 | 0.003 | 39.053 | 0.009 | [III] |
| A | Z1g | 0.512553 | ± 5 | -0.8 | 0.1 | | 0.287155 | ± 10 | 43.7 | 0.4 | 20.186 | 0.001 | 15.728 | 0.001 | 39.467 | 0.003 | [III] |
| B | Z1g | 0.512458 | ± 3 | -1.8 | 0.1 | | 0.292578 | ± 798 | 97.9 | 28.2 | 20.620 | 0.002 | 15.753 | 0.002 | 40.186 | 0.004 | [I] |
| C | Z1g | 0.512481 | ± 3 | -1.6 | 0.1 | | 0.283235 | ± 15 | 4.5 | 0.5 | 20.932 | 0.002 | 15.768 | 0.001 | 39.396 | 0.004 | [III] |
| D | Z1g | 0.512487 | ± 32 | -1.5 | 0.6 | | 0.282480 | ± 4 | -3.1 | 0.1 | 27.408 | 0.020 | 16.082 | 0.011 | 40.254 | 0.026 | [III] |
| Du | Z1gu | 0.512713 | ± 28 | 0.7 | 0.5 | | 0.282721 | ± 4 | -0.6 | 0.2 | 19.800 | 0.001 | 15.715 | 0.001 | 39.302 | 0.002 | [III] |
| PD | Z1p | 0.512361 | ± 67 | -2.8 | 1.3 | | 0.282356 | ± 3 | -4.3 | 0.1 | 29.183 | 0.003 | 16.195 | 0.002 | 40.888 | 0.005 | [III] |
| A | Z1p | 0.512500 | ± 8 | -1.4 | 0.2 | | 0.282493 | ± 3 | -2.9 | 0.1 | 26.596 | 0.001 | 16.061 | 0.001 | 41.279 | 0.002 | [III] |
| B | Z1p | 0.512497 | ± 5 | -1.4 | 0.1 | | 0.282940 | ± 4 | 1.5 | 0.2 | 22.335 | 0.001 | 15.843 | 0.001 | 40.231 | 0.002 | [III] |
| C | Z1p | 0.512445 | ± 7 | -1.9 | 0.1 | | 0.282405 | ± 3 | -3.8 | 0.1 | 26.108 | 0.004 | 16.042 | 0.002 | 40.830 | 0.006 | [III] |
| D | Z1p | 0.512409 | ± 19 | -2.3 | 0.4 | | 0.282360 | ± 2 | -4.3 | 0.1 | 71.334 | 0.062 | 18.373 | 0.018 | 48.073 | 0.044 | [III] |
| Du | Z1pu | 0.512615 | ± 17 | -0.2 | 0.3 | | 0.282351 | ± 2 | -4.3 | 0.1 | 22.989 | 0.005 | 15.874 | 0.004 | 40.282 | 0.009 | [III] |
| R | Z1p | 0.515126 | ± 9 | 24.9 | 0.2 | [a] | 0.282337 | ± 5 | -4.5 | 0.2 | 1385.016 | 1.036 | 87.071 | 0.065 | 214.105 | 0.156 | [III] |
| TD | Z1pu | 0.512727 | ± 8 | 0.9 | 0.2 | [a] | 0.282362 | ± 7 | -4.2 | 0.2 | 265.252 | 0.028 | 28.547 | 0.003 | 71.499 | 0.007 | [III] |
| PD | Z2g | 0.512859 | ± 57 | 2.2 | 1.1 | | 0.283166 | ± 6 | 3.8 | 0.2 | 20.196 | 0.001 | 15.730 | 0.001 | 39.247 | 0.002 | [III] |
| A | Z2g | 0.512646 | ± 3 | 0.1 | 0.1 | | 0.299939 | ± 31 | 171.5 | 1.1 | 20.844 | 0.001 | 15.761 | 0.000 | 40.746 | 0.001 | [II] |
| B | Z2g | 0.512649 | ± 6 | 0.1 | 0.1 | | 0.309927 | ± 32 | 271.4 | 1.1 | 20.632 | 0.001 | 15.757 | 0.001 | 39.903 | 0.002 | [II] |
| C | Z2g | 0.512359 | ± 7 | -2.8 | 0.1 | | | | | | 33.341 | 0.003 | 16.420 | 0.001 | 44.148 | 0.004 | [III] |
| D | Z2g | 0.512712 | ± 13 | 0.7 | 0.2 | | 0.282676 | ± 4 | -1.1 | 0.1 | 39.300 | 0.007 | 16.720 | 0.003 | 44.083 | 0.009 | [III] |
| PD | Z2p | 0.512096 | ± 131 | -5.4 | 2.5 | | 0.282211 | ± 2 | -5.7 | 0.1 | 22.815 | 0.000 | 15.872 | 0.000 | 39.779 | 0.001 | [III] |
| A | Z2p | 0.512636 | ± 9 | 0.0 | 0.2 | | 0.284397 | ± 6 | 16.1 | 0.2 | 22.570 | 0.001 | 15.854 | 0.001 | 41.131 | 0.001 | [II] |
| B | Z2p | 0.512626 | ± 5 | -0.1 | 0.1 | | 0.283125 | ± 5 | 3.4 | 0.2 | 19.679 | 0.001 | 15.707 | 0.001 | 39.314 | 0.001 | [II] |
| C | Z2p | 0.512288 | ± 6 | -3.5 | 0.1 | | 0.282368 | ± 2 | -4.2 | 0.1 | 32.135 | 0.002 | 16.352 | 0.001 | 42.391 | 0.003 | [III] |
| D | Z2p | 0.512691 | ± 29 | 0.5 | 0.6 | | 0.282246 | ± 3 | -5.4 | 0.1 | 269.642 | 0.185 | 28.797 | 0.015 | 77.459 | 0.042 | [III] |
| PD | Z3g | 0.513127 | ± 188 | 4.9 | 3.7 | | 0.282845 | ± 5 | 0.6 | 0.2 | 20.016 | 0.001 | 15.724 | 0.000 | 39.391 | 0.001 | [II] |
| A | Z3g | 0.512961 | ± 6 | 3.2 | 0.1 | | 0.282711 | ± 3 | -0.7 | 0.1 | 20.127 | 0.000 | 15.732 | 0.000 | 39.584 | 0.001 | [II] |
| B | Z3g | 0.512737 | ± 6 | 1.0 | 0.1 | | 0.312287 | ± 114 | 295.0 | 4.0 | 18.768 | 0.001 | 15.678 | 0.001 | 38.963 | 0.001 | [II] |
| C | Z3g | 0.512453 | ± 9 | -1.9 | 0.2 | | 0.283520 | ± 5 | 7.3 | 0.2 | 18.846 | 0.001 | 15.680 | 0.000 | 38.965 | 0.001 | [II] |
| D | Z3g | 0.512371 | ± 46 | -2.7 | 0.9 | | 0.282767 | ± 3 | -0.2 | 0.1 | 25.762 | 0.002 | 16.023 | 0.001 | 40.150 | 0.004 | [III] |
| PD | Z3p | 0.512651 | ± 37 | 0.1 | 0.7 | | 0.282252 | ± 3 | -5.3 | 0.1 | 21.051 | 0.001 | 15.776 | 0.000 | 39.309 | 0.001 | [II] |
| A | Z3p | 0.512766 | ± 6 | 1.3 | 0.1 | | 0.282910 | ± 3 | 1.3 | 0.1 | 19.887 | 0.001 | 15.709 | 0.000 | 39.072 | 0.001 | [II] |
| B | Z3p | 0.512770 | ± 5 | 1.3 | 0.1 | | 0.283288 | ± 4 | 5.0 | 0.1 | 20.099 | 0.001 | 15.721 | 0.000 | 39.175 | 0.001 | [II] |
| C | Z3p | 0.512424 | ± 3 | -2.1 | 0.1 | | 0.282430 | ± 3 | -3.6 | 0.1 | 23.550 | 0.002 | 15.896 | 0.001 | 39.363 | 0.003 | [III] |
| D | Z3p | 0.512589 | ± 72 | -0.5 | 1.4 | | 0.282248 | ± 2 | -5.4 | 0.1 | 62.907 | 0.016 | 17.972 | 0.004 | 44.721 | 0.011 | [III] |
| Du | Z4g | 0.512630 | ± 40 | -0.1 | 0.8 | | 0.283044 | ± 4 | 2.6 | 0.1 | 24.656 | 0.005 | 15.959 | 0.003 | 41.697 | 0.009 | [III] |
| Du | Z4p | 0.512676 | ± 171 | 0.4 | 3.3 | | 0.282304 | ± 2 | -4.8 | 0.1 | 23.760 | 0.001 | 15.924 | 0.001 | 41.038 | 0.003 | [III] |

**Table A 4: (Chapter 3) Differences of subgroup P relative to subgroup N**

| | | Hf yield | Nd yield | εNd diff | εHf diff | Pb206/Pb204 diff | Pb207/Pb204 diff | Pb208/Pb204 diff |
|---|---|---|---|---|---|---|---|---|
| **Group G** | | | | | | | | |
| grains: G 3&4 | A | 1.76 | 0.83 | -1.1 | -630.4 | 0.093 | 0.0067 | 0.108 |
| powder:G 1&2 | B | 1.20 | 1.17 | -0.1 | -1321.6 | -0.052 | -0.0002 | 0.079 |
| | C | 1.60 | 3.05 | -1.5 | -735.9 | 0.303 | 0.0167 | 0.269 |
| | R | 0.48 | 1.68 | -0.4 | 2.8 | -0.018 | 0.0030 | 0.305 |
| **Group S** | | | | | | | | |
| grains: S1-5 | A | | | -1.2 | -758.0 | -0.125 | -0.0060 | -0.146 |
| powder: S6 | B | | | -0.5 | 401.0 | 0.479 | 0.0250 | -0.004 |
| | C | | | 0.5 | 332.7 | -0.641 | -0.0360 | -0.349 |
| | R | | | -0.6 | 0.2 | 0.373 | 0.0240 | 0.401 |
| **Group Z** | | | | | | | | |
| Average | PD | 113.29 | | -3.3 | -6.4 | 4.362 | 0.2283 | 0.762 |
| | A | 11.70 | | -0.8 | -66.7 | 2.632 | 0.1344 | 0.562 |
| | B | 11.13 | | 0.3 | -218.1 | 0.698 | 0.0273 | -0.111 |
| | C | 11.61 | | -0.4 | -7.6 | 2.891 | 0.1402 | 0.025 |
| | D | 18.21 | | 0.4 | -3.6 | 103.804 | 5.4391 | 15.255 |
| | Du | 21.14 | | -0.3 | -5.5 | 1.147 | 0.0622 | 0.160 |
| Z1 | PD | 123.90 | | 2.5 | -3.7 | 9.431 | 0.4910 | 1.835 |
| | A | 26.31 | | -0.3 | -46.6 | 6.410 | 0.3328 | 1.812 |
| | B | 22.01 | | 0.5 | -96.4 | 1.715 | 0.0893 | 0.045 |
| | C | 16.92 | | -0.4 | -8.3 | 5.175 | 0.2737 | 1.434 |
| | D | 22.48 | | -0.8 | -1.2 | 43.925 | 2.2911 | 7.819 |
| | Du | 18.45 | | -1.0 | -3.7 | 3.189 | 0.1592 | 0.980 |
| Z2 | PD | 104.61 | | -7.6 | -9.6 | 2.619 | 0.1421 | 0.532 |
| | A | 4.84 | | -0.4 | -155.4 | 1.727 | 0.0929 | 0.385 |
| | B | 4.35 | | -0.1 | -268.0 | -0.953 | -0.0501 | -0.589 |
| | C | 11.40 | | -0.7 | -3.6 | -1.207 | -0.0684 | -1.756 |
| | D | 14.79 | | -0.2 | -4.3 | 230.342 | 12.0770 | 33.376 |
| Z3 | PD | 111.35 | | -4.8 | -5.9 | 1.035 | 0.0519 | -0.082 |
| | A | 3.96 | | -1.8 | 2.0 | -0.240 | -0.0226 | -0.511 |
| | B | 7.03 | | 0.5 | -290.0 | 1.331 | 0.0426 | 0.212 |
| | C | 6.51 | | -0.3 | -10.9 | 4.704 | 0.2152 | 0.398 |
| | D | 17.35 | | 2.2 | -5.2 | 37.145 | 1.9491 | 4.571 |
| Z4 | Du | 23.83 | | 0.5 | -7.4 | -0.896 | -0.0348 | -0.660 |

**Table A 5: (Chapter 3) Distributions of Nd, Hf and Pb in leaching steps normalized to the sum of the respective element released during the whole leaching sequence.**

| | | G1 | G2 | G3 | G4 | S1 | S2 | S3 | S4 | S5 | S6 | Z1g | Z1p | Z2g | Z2p | Z3g | Z3p |
|---|---|---|---|---|---|---|---|---|---|---|---|---|---|---|---|---|---|
| | PD | | | | | | | | | | | 32.93% | 73.91% | 17.07% | 62.30% | 17.47% | 64.54% |
| **Hf dist** | A | 0.5% | 0.7% | 0.1% | 0.3% | 0.3% | 0.3% | 0.3% | 0.2% | 0.1% | 0.1% | 5.4% | 2.6% | 3.8% | 0.6% | 4.1% | 0.5% |
| | B | 0.4% | 0.7% | 0.1% | 0.4% | 0.4% | 0.2% | 0.2% | 0.2% | 0.1% | 0.1% | 2.0% | 0.8% | 4.4% | 0.7% | 2.9% | 0.7% |
| | C | 0.3% | 0.5% | 0.1% | 0.2% | 0.3% | 0.2% | 0.2% | 0.1% | 0.1% | 0.1% | 15.8% | 4.8% | 18.2% | 7.2% | 25.7% | 5.6% |
| | R/D | 98.8% | 98.1% | 99.7% | 99.1% | 99.0% | 99.4% | 99.3% | 99.5% | 99.8% | 99.6% | 43.9% | 17.9% | 56.5% | 29.1% | 49.9% | 28.7% |
| | PD | | | | | | | | | | | 0.0% | 0.1% | 0.0% | 0.0% | 0.0% | 0.1% |
| **Nd dist** | A | 3.4% | 3.9% | 2.4% | 16.9% | 26.2% | 7.6% | 7.5% | 5.0% | 3.5% | 3.7% | 83.2% | 26.3% | 18.0% | 33.4% | 45.6% | 45.6% |
| | B | 10.1% | 16.7% | 6.7% | 42.8% | 40.2% | 7.0% | 4.7% | 4.9% | 3.5% | 5.7% | 8.0% | 61.9% | 62.2% | 45.3% | 40.2% | 41.4% |
| | C | 2.5% | 3.3% | 1.4% | 1.6% | 4.5% | 0.7% | 0.8% | 1.2% | 3.4% | 3.7% | 8.7% | 11.7% | 19.6% | 21.3% | 14.1% | 12.9% |
| | R/D | 84.0% | 76.2% | 89.6% | 38.7% | 29.1% | 84.8% | 87.0% | 88.9% | 89.6% | 86.9% | 0.1% | 0.0% | 0.1% | 0.0% | 0.1% | 0.0% |
| | PD | | | | | | | | | | | 15.2% | 3.7% | 5.8% | 6.8% | 5.6% | 16.2% |
| **Pb dist** | A | 17.5% | 19.7% | 28.6% | 16.4% | 14.0% | 21.6% | 21.6% | 20.7% | 18.2% | 22.1% | 38.8% | 39.9% | 35.6% | 28.9% | 11.4% | 63.6% |
| | B | 35.1% | 37.8% | 18.4% | 22.0% | 15.4% | 14.0% | 12.0% | 14.9% | 17.8% | 26.4% | 18.3% | 51.6% | 56.6% | 63.1% | 65.9% | 19.0% |
| | C | 3.2% | 4.0% | 10.0% | 2.3% | 2.4% | 1.3% | 1.1% | 1.2% | 17.2% | 21.2% | 26.4% | 3.3% | 1.6% | 1.0% | 16.9% | 1.1% |
| | R/D | 44.2% | 38.5% | 43.0% | 59.3% | 68.3% | 63.2% | 65.3% | 63.3% | 46.9% | 30.4% | 1.4% | 1.4% | 0.3% | 0.1% | 0.2% | 0.1% |

**Table A6: (Chapter 4) REE concentrations obtained by OP ICP-MS (pmol/kg). La/Yb ratio and Ce anomaly are also shown.**

| Region | Depth | La | Ce | Pr | Nd | Sm | Eu | Gd | Tb | Dy | Ho | Er | Tm | Yb | Lu | La/Yb | Ce/Ce* |
|---|---|---|---|---|---|---|---|---|---|---|---|---|---|---|---|---|---|
| I | 3 | 24.96 | 21.91 | 4.26 | 19.88 | 3.23 | 0.88 | 6.26 | 1.02 | 6.70 | 1.48 | 5.00 | 0.62 | 3.82 | 0.86 | 0.33 | 0.49 |
| I | 250 | 25.82 | 12.75 | 4.54 | 18.37 | 3.15 | 0.82 | 4.28 | 0.96 | 6.18 | 1.54 | 5.10 | 0.61 | 4.82 | 0.69 | 0.27 | 0.27 |
| I | 480 | 22.38 | 8.68 | 3.49 | 13.45 | 2.25 | 0.78 | 3.58 | 0.81 | 5.52 | 1.57 | 4.78 | 0.65 | 3.86 | 0.73 | 0.29 | 0.23 |
| I | 800 | 21.52 | 7.61 | 3.76 | 14.26 | 2.33 | 0.92 | 5.13 | 0.92 | 4.72 | 1.74 | 5.58 | 0.65 | 4.32 | 0.70 | 0.25 | 0.20 |
| I | 1100 | 21.52 | 7.81 | 3.54 | 16.67 | 2.93 | 0.78 | 5.64 | 0.96 | 5.47 | 1.59 | 5.16 | 0.83 | 4.86 | 0.76 | 0.22 | 0.21 |
| I | 1300 | 28.40 | 14.74 | 4.67 | 18.78 | 2.93 | 1.24 | 5.79 | 1.02 | 5.80 | 1.70 | 5.62 | 0.87 | 4.28 | 0.97 | 0.34 | 0.30 |
| I | 1500 | 26.25 | 8.41 | 4.20 | 18.78 | 2.48 | 0.82 | 4.55 | 1.01 | 6.08 | 1.97 | 5.68 | 0.92 | 5.28 | 0.94 | 0.25 | 0.18 |
| I | 1700 | 24.10 | 7.21 | 3.72 | 17.67 | 2.55 | 0.98 | 5.13 | 0.87 | 6.13 | 1.84 | 4.65 | 0.80 | 4.20 | 0.76 | 0.29 | 0.17 |
| I | 1869 | 24.53 | 5.18 | 4.11 | 15.96 | 2.63 | 0.73 | 5.05 | 0.83 | 5.52 | 1.79 | 4.87 | 0.79 | 4.61 | 0.87 | 0.27 | 0.12 |
| I | 2300 | 33.13 | 14.34 | 4.17 | 15.66 | 3.00 | 0.96 | 5.21 | 1.00 | 5.85 | 1.41 | 5.00 | 0.77 | 4.44 | 0.97 | 0.38 | 0.27 |
| II | 3 | 21.08 | 23.11 | 4.08 | 21.29 | 3.00 | 1.09 | 5.52 | 1.06 | 6.46 | 1.67 | 5.04 | 0.69 | 3.99 | 0.69 | 0.27 | 0.58 |
| III | 3 | 21.52 | 15.14 | 3.58 | 16.06 | 2.63 | 0.88 | 4.39 | 0.76 | 4.86 | 1.43 | 3.74 | 0.51 | 3.66 | 0.44 | 0.30 | 0.40 |
| III | 200 | 21.08 | 7.57 | 3.15 | 13.45 | 2.85 | 0.86 | 4.47 | 0.77 | 5.19 | 1.61 | 4.71 | 0.80 | 4.11 | 0.81 | 0.26 | 0.21 |
| III | 450 | 25.82 | 8.60 | 3.86 | 16.27 | 3.30 | 0.80 | 4.47 | 0.72 | 6.23 | 1.68 | 5.33 | 0.71 | 4.28 | 0.85 | 0.31 | 0.20 |
| III | 511 | 20.65 | 7.37 | 4.15 | 14.26 | 2.33 | 0.52 | 4.24 | 0.74 | 5.66 | 1.52 | 4.33 | 0.68 | 3.90 | 0.78 | 0.27 | 0.19 |
| III | 700 | 35.71 | 23.90 | 4.40 | 17.47 | 2.70 | 0.86 | 4.74 | 0.81 | 6.27 | 1.71 | 4.78 | 0.78 | 4.65 | 0.82 | 0.39 | 0.43 |
| III | 760 | 26.25 | 9.96 | 3.88 | 16.67 | 3.00 | 0.84 | 4.63 | 0.82 | 5.19 | 1.81 | 5.04 | 0.87 | 3.95 | 0.94 | 0.34 | 0.23 |
| III | 1000 | 26.25 | 9.16 | 4.15 | 15.46 | 2.25 | 0.88 | 4.66 | 1.04 | 6.13 | 1.67 | 5.71 | 0.77 | 4.86 | 0.93 | 0.27 | 0.20 |
| III | 1148 | 32.27 | 4.78 | 4.99 | 20.48 | 2.78 | 0.80 | 5.05 | 1.03 | 6.89 | 2.13 | 5.91 | 0.83 | 5.11 | 1.06 | 0.32 | 0.09 |
| III | 1248 | 24.96 | 4.86 | 3.38 | 16.57 | 3.08 | 0.73 | 5.01 | 0.82 | 5.00 | 1.59 | 5.52 | 0.83 | 4.82 | 0.81 | 0.26 | 0.12 |
| III | 1400 | 24.96 | 7.29 | 4.04 | 18.67 | 2.63 | 0.67 | 3.93 | 0.93 | 5.90 | 1.90 | 4.49 | 0.83 | 4.90 | 0.81 | 0.26 | 0.17 |
| III | 1800 | 21.08 | 4.58 | 3.27 | 14.26 | 3.15 | 0.92 | 4.82 | 0.86 | 5.05 | 1.52 | 4.52 | 0.77 | 4.15 | 0.76 | 0.26 | 0.13 |
| III | 1893 | 24.53 | 5.22 | 4.04 | 20.88 | 2.93 | 0.80 | 5.01 | 0.80 | 6.27 | 1.71 | 5.00 | 0.73 | 5.07 | 0.90 | 0.25 | 0.12 |
| III | 1993 | 23.24 | 7.13 | 3.33 | 16.97 | 2.55 | 0.73 | 4.70 | 0.84 | 4.72 | 1.36 | 4.62 | 0.90 | 4.28 | 0.85 | 0.27 | 0.18 |
| III | 2500 | 36.15 | 8.33 | 4.67 | 17.87 | 2.18 | 0.98 | 5.01 | 0.96 | 5.90 | 1.75 | 5.33 | 0.99 | 5.69 | 0.98 | 0.32 | 0.14 |
| III | 3250 | 33.13 | 8.05 | 4.51 | 18.57 | 2.85 | 1.03 | 4.82 | 1.01 | 6.46 | 1.57 | 4.58 | 0.86 | 4.86 | 1.06 | 0.35 | 0.15 |
| IV | 3 | 18.50 | 14.74 | 3.13 | 14.26 | 2.63 | 0.80 | 5.36 | 0.87 | 6.27 | 1.58 | 4.84 | 0.55 | 4.11 | 0.78 | 0.23 | 0.45 |
| IV | 3 | 19.79 | 15.14 | 3.40 | 14.06 | 2.10 | 0.69 | 4.55 | 0.74 | 5.00 | 1.59 | 4.33 | 0.66 | 2.78 | 0.69 | 0.36 | 0.43 |
| IV | 124 | 20.65 | 10.36 | 3.72 | 17.17 | 3.53 | 1.07 | 3.85 | 1.01 | 5.85 | 1.71 | 5.16 | 0.71 | 4.44 | 0.85 | 0.24 | 0.27 |
| IV | 200 | 19.79 | 8.88 | 3.36 | 13.96 | 2.33 | 0.84 | 4.59 | 0.95 | 4.67 | 1.57 | 3.81 | 0.68 | 4.07 | 0.67 | 0.25 | 0.25 |
| IV | 223 | 25.39 | 12.35 | 4.40 | 17.47 | 3.90 | 0.88 | 5.52 | 0.99 | 6.41 | 1.65 | 5.23 | 0.71 | 5.11 | 0.82 | 0.25 | 0.27 |
| IV | 450 | 26.25 | 13.94 | 4.01 | 17.57 | 2.93 | 0.98 | 6.10 | 1.17 | 6.93 | 2.03 | 5.13 | 0.82 | 4.90 | 0.93 | 0.27 | 0.31 |
| IV | 700 | 30.12 | 23.11 | 4.67 | 24.10 | 3.60 | 0.92 | 6.22 | 1.08 | 7.12 | 1.93 | 6.42 | 0.94 | 5.69 | 1.04 | 0.27 | 0.45 |
| IV | 900 | 24.10 | 4.34 | 3.79 | 20.78 | 3.38 | 1.01 | 5.75 | 1.09 | 7.03 | 1.88 | 6.10 | 0.94 | 5.32 | 0.97 | 0.23 | 0.10 |
| IV | 1500 | 38.30 | 15.94 | 3.97 | 19.18 | 3.08 | 0.88 | 5.67 | 1.04 | 7.03 | 2.16 | 6.07 | 0.96 | 5.28 | 0.94 | 0.37 | 0.28 |
| IV | 1800 | 31.41 | 13.94 | 4.74 | 18.78 | 2.48 | 1.26 | 5.91 | 1.20 | 7.40 | 2.01 | 5.33 | 0.83 | 5.44 | 1.02 | 0.29 | 0.26 |
| IV | 2300 | 37.44 | 23.50 | 6.12 | 25.10 | 3.75 | 1.26 | 6.88 | 1.13 | 7.07 | 2.04 | 6.17 | 1.00 | 5.82 | 1.08 | 0.33 | 0.36 |
| V | 3 | 15.06 | 9.16 | 2.22 | 10.24 | 1.59 | 0.61 | 3.65 | 0.61 | 3.87 | 1.13 | 3.62 | 0.56 | 2.66 | 0.42 | 0.29 | 0.36 |
| V | 200 | 18.50 | 9.16 | 3.88 | 15.06 | 2.48 | 0.73 | 4.24 | 0.86 | 5.00 | 1.62 | 4.71 | 0.63 | 3.45 | 0.85 | 0.27 | 0.25 |
| V | 550 | 24.53 | 5.70 | 4.31 | 18.57 | 2.63 | 0.94 | 5.13 | 0.84 | 5.38 | 1.95 | 4.94 | 0.84 | 4.94 | 0.78 | 0.25 | 0.13 |
| V | 750 | 23.67 | 5.74 | 4.01 | 16.37 | 2.40 | 0.98 | 4.90 | 0.85 | 5.66 | 2.11 | 4.87 | 0.77 | 4.86 | 0.81 | 0.25 | 0.14 |
| V | 798 | 28.40 | 5.70 | 3.67 | 15.86 | 2.93 | 0.88 | 5.25 | 0.88 | 6.04 | 1.61 | 5.04 | 0.77 | 4.65 | 0.89 | 0.31 | 0.13 |
| V | 900 | 21.95 | 4.54 | 3.74 | 14.26 | 2.93 | 1.03 | 5.32 | 0.92 | 4.90 | 1.92 | 5.13 | 0.80 | 4.40 | 0.93 | 0.25 | 0.12 |
| V | 1300 | 30.55 | 6.02 | 4.85 | 18.07 | 2.78 | 0.90 | 4.74 | 1.06 | 6.79 | 1.89 | 5.62 | 0.84 | 4.94 | 0.86 | 0.31 | 0.11 |
| V | 1650 | 34.42 | 7.61 | 4.69 | 19.98 | 3.15 | 0.82 | 5.40 | 0.92 | 6.27 | 1.94 | 4.75 | 0.85 | 5.48 | 0.94 | 0.32 | 0.14 |
| V | 2013 | 30.12 | 7.57 | 4.49 | 20.78 | 2.85 | 0.98 | 4.31 | 0.94 | 6.41 | 1.65 | 5.46 | 0.90 | 5.23 | 0.97 | 0.29 | 0.15 |
| GEOTRACES BATS intercalibration (van de Flierdt et al. 2012) | | | | | | | | | | | | | | | | | |
| AVG | 15 | 1.61 | 12.68 | 2.52 | 0.73 | 4.91 | 0.73 | 6.01 | 1.56 | 5.38 | 0.60 | 3.54 | 3.85 | 0.66 | | | |
| stdev*2 | | 0.07 | 2.80 | 0.71 | 0.22 | 0.49 | 0.13 | 1.83 | 0.35 | 0.38 | 0.15 | 0.53 | 0.34 | 0.13 | | | |
| %2stdev | | 4.56 | 22.08 | 28.37 | 30.24 | 10.00 | 17.50 | 30.51 | 22.57 | 7.10 | 24.61 | 15.06 | 8.90 | 19.10 | | | |

**Table A7: (Chapter 4) Hafnium and Nd isotope compositions and concentration data of all samples measured in this study together with hydrographic properties (salinity and potential temperature).**

| Meteor-Station No. | Region | Depth | Date | Latitude | Longitude | $^{176}Hf/^{177}Hf$ | ±2σ | $\varepsilon_{Hf}$ | ±2σ | $^{143}Nd/^{144}Nd$ | ±2σ | $\varepsilon_{Nd}$ | ±2σ | [Hf] [pmol/kg] | [Nd] [pmol/kg] | θ (°C) | Salinity (psu) |
|---|---|---|---|---|---|---|---|---|---|---|---|---|---|---|---|---|---|
| SW01 | I | 3 | 02/06/11 | 42°59.493´N | 9°40.101´W | 0.282831 | 0.000006 | 1.6 | 0.20 | 0.512100 | 0.000006 | -10.5 | 0.11 | | | | |
| 560 | I | 250 | 02/06/11 | 43°0.30´N | 9°43.10´W | | | | | 0.512031 | 0.000010 | -11.8 | 0.20 | 0.56 | 16.9 | 12.57 | 35.79 |
| 560 | I | 480 | 02/06/11 | 43°0.30´N | 9°43.10´W | | | | | 0.512015 | 0.000004 | -12.1 | 0.07 | 0.54 | 15.6 | 11.39 | 35.62 |
| 560 | I | 800 | 02/06/11 | 43°0.30´N | 9°43.10´W | 0.282779 | 0.000014 | -0.2 | 0.50 | 0.512092 | 0.000004 | -10.7 | 0.08 | 0.85 | 19.3 | 11.47 | 36.07 |
| 560 | I | 1100 | 02/06/11 | 43°0.30´N | 9°43.10´W | 0.282795 | 0.000007 | 0.4 | 0.24 | 0.512118 | 0.000004 | -10.1 | 0.08 | 0.82 | 18.2 | 10.98 | 36.17 |
| 559 | I | 1300 | 02/06/11 | 43°0.25´N | 9°43.11´W | 0.282768 | 0.000016 | -0.6 | 0.55 | 0.512083 | 0.000005 | -10.8 | 0.10 | 0.87 | 19.4 | 9.98 | 36.06 |
| 559 | I | 1500 | 02/06/11 | 43°0.25´N | 9°43.11´W | 0.282824 | 0.000007 | 1.4 | 0.25 | 0.512060 | 0.000005 | -11.3 | 0.09 | 0.82 | 16.3 | 7.42 | 35.61 |
| 559 | I | 1700 | 02/06/11 | 43°0.25´N | 9°43.11´W | | | | | 0.512012 | 0.000016 | -12.2 | 0.30 | 0.87 | 17.3 | 5.03 | 35.22 |
| 568 | I | 1869 | 03/06/11 | 42°59.37´N | 9°40.52´W | | | | | 0.512054 | 0.000005 | -11.4 | 0.09 | 0.81 | 17.3 | 4.25 | 35.11 |
| 559 | I | 2300 | 02/06/11 | 43°0.25´N | 9°43.11´W | | | | | 0.512025 | 0.000005 | -12.0 | 0.10 | 0.90 | 17.9 | 3.09 | 34.98 |
| SW02 | II | 3 | 04/06/11 | 43°50.776´N | 7°53.824´W | | | | | 0.512157 | 0.000006 | -9.4 | 0.12 | | | | |
| SW03 | III | 3 | 05/06/11 | 44°4.474´N | 5°59.439´W | | | | | 0.512086 | 0.000005 | -10.8 | 0.09 | | | | |
| 577 | III | 200 | 05/06/11 | 44°7.92´N | 6°0.08´W | 0.282767 | 0.000015 | -0.6 | 0.54 | 0.512051 | 0.000005 | -11.4 | 0.10 | 0.45 | 15.4 | 11.63 | 35.66 |
| 577 | III | 450 | 05/06/11 | 44°7.92´N | 6°0.08´W | 0.282942 | 0.000005 | | | 0.512051 | 0.000006 | -11.4 | 0.13 | 0.44 | 15.0 | 11.41 | 35.64 |
| 615 | III | 511 | 09/06/11 | 43°59.317´N | 5°43.575´W | 0.282853 | 0.000006 | 2.4 | 0.21 | 0.512061 | 0.000005 | -11.3 | 0.10 | 0.51 | 15.4 | 11.29 | 35.63 |
| 615 | III | 609 | 09/06/11 | 43°59.317´N | 5°43.575´W | | | | | 0.512038 | 0.000005 | -11.7 | 0.11 | 0.58 | 15.9 | 10.93 | 35.62 |
| 577 | III | 700 | 05/06/11 | 44°7.92´N | 6°0.08´W | | | | | 0.512045 | 0.000007 | -11.6 | 0.14 | 0.90 | 16.2 | 10.66 | 35.65 |
| 589 | III | 760 | 06/06/11 | 44°1.40´N | 5°42.16´W | | | | | 0.512042 | 0.000005 | -11.6 | 0.09 | 0.76 | 16.5 | 10.65 | 35.72 |
| 577 | III | 1000 | 05/06/11 | 44°7.92´N | 6°0.08´W | 0.282844 | 0.000007 | 2.1 | 0.23 | 0.512056 | 0.000004 | -11.3 | 0.08 | 0.64 | 17.3 | 9.99 | 35.83 |
| 612 | III | 1148 | 08/06/11 | 44°1.285´N | 5°50.225´W | | | | | 0.512054 | 0.000004 | -11.4 | 0.08 | | 17.5 | 9.32 | 35.78 |
| 612 | III | 1248 | 08/06/11 | 44°1.285´N | 5°50.225´W | 0.282861 | 0.000007 | 2.7 | 0.24 | 0.512037 | 0.000005 | -11.7 | 0.10 | 0.79 | 17.5 | 8.35 | 35.64 |
| 576 | III | 1400 | 05/06/11 | 44°7.92´N | 6°0.08´W | | | | | 0.512017 | 0.000006 | -12.1 | 0.12 | | 17.9 | 7.02 | 35.45 |
| 576 | III | 1800 | 05/06/11 | 44°7.92´N | 6°0.08´W | | | | | 0.511989 | 0.000005 | -12.7 | 0.09 | 0.87 | 17.4 | 4.24 | 35.04 |
| 611 | III | 1893 | 08/06/11 | 43°59.890 | 5°54.106´W | 0.282841 | 0.000006 | 2.0 | 0.22 | 0.511977 | 0.000007 | -12.9 | 0.13 | | 17.2 | 4.21 | 35.07 |
| 611 | III | 1993 | 08/06/11 | 43°59.890 | 5°54.106´W | | | | | 0.512015 | 0.000005 | -12.1 | 0.10 | 0.81 | 17.6 | 3.79 | 35.02 |
| 576 | III | 2500 | 05/06/11 | 44°7.92´N | 6°0.08´W | | | | | 0.512035 | 0.000014 | -11.8 | 0.27 | | 18.2 | 2.99 | 34.97 |
| 576 | III | 3250 | 05/06/11 | 44°7.92´N | 6°0.08´W | 0.282798 | 0.000005 | 0.4 | 0.18 | 0.512048 | 0.000006 | -11.5 | 0.11 | 0.88 | 21.3 | 2.40 | 34.93 |
| SW04 | IV | 3 | 10/06/11 | 43°42.421´N | 2°45.761´W | | | | | 0.512102 | 0.000005 | -10.5 | 0.10 | | | | |
| SW06 | IV | 3 | 17/06/11 | 43°58.409´N | 3°0.728´W | | | | | 0.512108 | 0.000005 | -10.3 | 0.11 | | | | |
| 635 | IV | 124 | 12/06/11 | 43°31.695´N | 2°45.377´W | 0.282773 | 0.000006 | -0.4 | 0.20 | 0.512072 | 0.000005 | -11.0 | 0.10 | 0.45 | 16.2 | 12.10 | 35.71 |
| 625 | IV | 200 | 10/06/11 | 43°43.995´N | 2°36.988´W | 0.282802 | 0.000018 | 0.6 | 0.64 | 0.512055 | 0.000006 | -11.4 | 0.12 | 0.46 | 16.2 | 11.86 | 35.68 |
| 635 | IV | 223 | 12/06/11 | 43°31.695´N | 2°45.377´W | 0.282785 | 0.000008 | 0.0 | 0.30 | 0.512067 | 0.000006 | -11.1 | 0.12 | 0.41 | 16.3 | 11.79 | 35.67 |
| 625 | IV | 450 | 10/06/11 | 43°43.995´N | 2°36.988´W | 0.282864 | 0.000007 | 2.8 | 0.23 | 0.512053 | 0.000007 | -11.4 | 0.13 | 0.53 | 16.8 | 11.26 | 35.62 |
| 625 | IV | 700 | 10/06/11 | 43°43.995´N | 2°36.988´W | 0.282795 | 0.000016 | 0.3 | 0.57 | 0.512045 | 0.000008 | -11.6 | 0.15 | 0.76 | 16.9 | 10.50 | 35.68 |
| 625 | IV | 900 | 10/06/11 | 43°43.995´N | 2°36.988´W | 0.282810 | 0.000006 | 0.9 | 0.21 | 0.512082 | 0.000005 | -10.8 | 0.09 | 0.75 | 16.9 | 10.00 | 35.79 |
| 624 | IV | 1200 | 10/06/11 | 43°43.995´N | 2°36.988´W | 0.282797 | 0.000013 | 0.4 | 0.46 | 0.512039 | 0.000006 | -11.7 | 0.11 | 0.80 | 23.6 | 8.56 | 35.68 |
| 624 | IV | 1500 | 10/06/11 | 43°43.995´N | 2°36.988´W | 0.282809 | 0.000006 | 0.8 | 0.20 | 0.512046 | 0.000003 | -11.5 | 0.06 | | 22.9 | 6.41 | 35.38 |
| 624 | IV | 1800 | 10/06/11 | 43°43.995´N | 2°36.988´W | 0.282812 | 0.000010 | 1.0 | 0.36 | 0.512062 | 0.000006 | -11.2 | 0.12 | 0.88 | 18.9 | 4.66 | 35.15 |
| 624 | IV | 2300 | 10/06/11 | 43°43.995´N | 2°36.988´W | | | | | | | | | 1.05 | 22.1 | 3.35 | 35.01 |
| SW05 | V | 3 | 13/06/11 | 46°11.629´N | 4°24.252´W | | | | | 0.512079 | 0.000008 | -10.9 | 0.15 | | | | |
| 639 | V | 200 | 13/06/11 | 46°9.993´N | 4°28.006´W | 0.282779 | 0.000008 | -0.2 | 0.29 | 0.512092 | 0.000003 | -10.7 | 0.05 | 0.44 | 15.7 | 11.73 | 35.67 |
| 639 | V | 550 | 13/06/11 | 46°9.993´N | 4°28.006´W | 0.282779 | 0.000006 | -0.2 | 0.22 | 0.512076 | 0.000011 | -11.0 | 0.22 | 0.58 | 16.2 | 11.00 | 35.62 |
| 639 | V | 750 | 13/06/11 | 46°9.993´N | 4°28.006´W | | | | | 0.512041 | 0.000006 | -11.7 | 0.11 | | 16.9 | 10.36 | 35.73 |
| 666 | V | 798 | 16/06/11 | 46°13.950´N | 4°19.492´W | | | | | 0.512083 | 0.000060 | -11.8 | 0.08 | 0.67 | 16.8 | 10.27 | 35.74 |
| 638 | V | 900 | 13/06/11 | 46°10.005´N | 4°28.006´W | | | | | 0.512064 | 0.000006 | -11.2 | 0.12 | 0.74 | 17.3 | 9.97 | 35.80 |
| 638 | V | 1300 | 13/06/11 | 46°10.005´N | 4°28.006´W | | | | | 0.512028 | 0.000005 | -11.9 | 0.09 | 0.80 | 17.4 | 7.72 | 35.56 |
| 638 | V | 1650 | 13/06/11 | 46°10.005´N | 4°28.006´W | | | | | 0.512003 | 0.000005 | -12.4 | 0.10 | 0.79 | 17.2 | 5.10 | 35.20 |
| 638 | V | 2013 | 13/06/11 | 46°10.005´N | 4°28.006´W | 0.282848 | 0.000006 | 2.2 | 0.20 | 0.512019 | 0.000005 | -12.1 | 0.10 | 0.83 | 18.4 | 3.69 | 35.04 |

**Table A 8: (Chapter 5) Results of Nd measurements on uncleaned, mixed-planktonic foraminiera, bulk sediment leachates and detrital material.**

| # Sample (Site/Hole/Core/Core-type/Section/Interval) | Type | Depth [mcd] | Age [Ma] | 143Nd/144Nd | 2σ | εNd | 2σ | 176Hf/177Hf | 2σ | εHf | 2σ | %NASW |
|---|---|---|---|---|---|---|---|---|---|---|---|---|
| 1088 B 1 H 1 13 - 20 | foram | 0.165 | 0.01 | 0.512160 | 0.000015 | -9.3 | 0.30 | | | | | 72% |
| 1088 B 1 H 1 43 - 44 | foram | 0.435 | 0.03 | 0.512241 | 0.000017 | -7.8 | 0.32 | | | | | 55% |
| 1088 B 1 H 1 92 - 94 | foram | 0.93 | 0.09 | 0.512212 | 0.000016 | -8.3 | 0.31 | | | | | 61% |
| 1088 B 1 H 1 125 - 127 | foram | 1.26 | 0.11 | 0.512179 | 0.000017 | -9.0 | 0.34 | | | | | 69% |
| 1088 B 1 H 1 129 - 131 | foram | 1.3 | 0.12 | 0.512175 | 0.000016 | -9.0 | 0.32 | | | | | 69% |
| 1088 B 1 H 2 73 - 74 | foram | 2.235 | 0.21 | 0.512136 | 0.000013 | -9.8 | 0.26 | | | | | 77% |
| 1088 B 1 H 2 117 - 119 | foram | 2.68 | 0.27 | 0.512197 | 0.000016 | -8.6 | 0.31 | | | | | 66% |
| 1088 B 1 H 3 5 - 7 | foram | 3.06 | 0.31 | 0.512167 | 0.000017 | -9.2 | 0.32 | | | | | 72% |
| 1088 B 1 H 3 37 - 39 | foram | 3.38 | 0.34 | 0.512186 | 0.000018 | -8.8 | 0.36 | | | | | 68% |
| 1088 B 1 H 3 62 - 64 | foram | 3.63 | 0.36 | 0.512208 | 0.000015 | -8.4 | 0.29 | | | | | 64% |
| 1088 B 1 H 3 107 - 109 | foram | 4.08 | 0.40 | 0.512170 | 0.000017 | -9.1 | 0.33 | | | | | 72% |
| 1088 B 1 H 3 137 - 139 | foram | 4.38 | 0.42 | 0.512167 | 0.000029 | -9.2 | 0.56 | | | | | 73% |
| 1088 B 1 H 4 12 - 14 | foram | 4.63 | 0.43 | 0.512266 | 0.000016 | -7.3 | 0.32 | | | | | 51% |
| 1088 B 1 H 4 40 - 42 | foram | 4.91 | 0.48 | 0.512161 | 0.000019 | -9.3 | 0.37 | | | | | 74% |
| 1088 B 2 H 1 9 - 12 | foram | 5.605 | 0.52 | 0.512215 | 0.000019 | -8.3 | 0.37 | | | | | 63% |
| 1088 B 2 H 1 22 - 24 | foram | 5.73 | 0.52 | 0.512161 | 0.000020 | -9.3 | 0.39 | | | | | 74% |
| 1088 B 2 H 1 26 - 28 | foram | 5.77 | 0.52 | 0.512197 | 0.000019 | -8.6 | 0.37 | | | | | 67% |
| 1088 B 2 H 1 102 - 104 | foram | 6.53 | 0.58 | 0.512208 | 0.000013 | -8.4 | 0.25 | | | | | 64% |
| 1088 B 2 H 1 137 - 139 | foram | 6.88 | 0.60 | 0.512137 | 0.000018 | -9.8 | 0.35 | | | | | 78% |
| 1088 B 2 H 2 27 - 29 | foram | 7.28 | 0.63 | 0.512197 | 0.000017 | -8.6 | 0.32 | | | | | 67% |
| 1088 B 2 H 2 50 - 52 | foram | 7.51 | 0.64 | 0.512254 | 0.000013 | -7.5 | 0.25 | | | | | 54% |
| 1088 B 2 H 2 127 - 129 | foram | 8.28 | 0.69 | 0.512160 | 0.000020 | -9.3 | 0.39 | | | | | 74% |
| 1088 B 2 H 3 67 - 69 | foram | 9.18 | 0.76 | 0.512206 | 0.000016 | -8.4 | 0.32 | | | | | 65% |
| 1088 B 2 H 3 140 - 142 | foram | 9.91 | 0.80 | 0.512278 | 0.000016 | -7.0 | 0.32 | | | | | 48% |
| 1088 B 2 H 4 25 - 27 | foram | 10.26 | 0.83 | 0.512188 | 0.000017 | -8.8 | 0.33 | | | | | 69% |
| 1088 B 2 H 4 97 - 99 | foram | 10.98 | 0.88 | 0.512263 | 0.000013 | -7.3 | 0.26 | | | | | 52% |
| 1088 B 2 H 5 10 - 12 | foram | 11.61 | 0.93 | 0.512264 | 0.000011 | -7.3 | 0.22 | | | | | 52% |
| 1088 B 2 H 5 67 - 69 | foram | 12.18 | 0.97 | 0.512179 | 0.000016 | -9.0 | 0.31 | | | | | 71% |
| 1088 B 2 H 5 139 - 141 | foram | 12.9 | 1.02 | 0.512134 | 0.000019 | -9.8 | 0.37 | | | | | 80% |
| 1088 B 2 H 5 141 - 143 | foram | 12.92 | 1.02 | 0.512176 | 0.000018 | -9.0 | 0.35 | | | | | 72% |
| 1088 B 2 H 6 45 - 47 | foram | 13.46 | 1.04 | 0.512193 | 0.000015 | -8.7 | 0.29 | | | | | 69% |
| 1088 B 2 H 6 77 - 79 | foram | 13.77 | 1.06 | 0.512134 | 0.000016 | -9.8 | 0.31 | | | | | 80% |
| 1088 B 2 H 6 121 - 123 | foram | 14.22 | 1.09 | 0.512158 | 0.000019 | -9.4 | 0.37 | | | | | 75% |
| 1088 B 3 H 1 43 - 45 | foram | 15.44 | 1.21 | 0.512161 | 0.000017 | -9.3 | 0.32 | | | | | 75% |
| 1088 B 3 H 1 128 - 130 | foram | 16.29 | 1.32 | 0.512183 | 0.000019 | -8.9 | 0.37 | | | | | 71% |
| 1088 B 3 H 2 37 - 39 | foram | 16.88 | 1.40 | 0.512158 | 0.000018 | -9.4 | 0.34 | | | | | 76% |
| 1088 B 3 H 2 53 - 55 | foram | 17.04 | 1.42 | 0.512223 | 0.000011 | -8.1 | 0.21 | | | | | 63% |
| 1088 B 3 H 2 111 - 113 | foram | 17.62 | 1.50 | 0.512184 | 0.000015 | -8.9 | 0.30 | | | | | 71% |
| 1088 B 3 H 4 28 - 31 | foram | 19.795 | 1.80 | 0.512228 | 0.000014 | -8.0 | 0.26 | | | | | 61% |
| 1088 B 3 H 4 62 - 64 | foram | 20.13 | 1.85 | 0.512179 | 0.000014 | -9.0 | 0.28 | | | | | 72% |
| 1088 B 3 H 4 78 - 80 | foram | 20.29 | 1.87 | 0.512216 | 0.000017 | -8.2 | 0.34 | | | | | 65% |
| 1088 B 3 H 4 127 - 129 | foram | 20.78 | 1.94 | 0.512208 | 0.000016 | -8.4 | 0.32 | | | | | 67% |
| 1088 B 4 H 1 13 - 15 | foram | 24.64 | 2.47 | 0.512204 | 0.000022 | -8.5 | 0.43 | | | | | 69% |
| 1088 B 4 H 1 137 - 139 | foram | 25.88 | 2.66 | 0.512259 | 0.000019 | -7.4 | 0.37 | | | | | 58% |
| 1088 B 4 H 2 24 - 26 | foram | 26.25 | 2.70 | 0.512209 | 0.000018 | -8.4 | 0.35 | | | | | 71% |
| 1088 B 4 H 2 73 - 75 | foram | 26.74 | 2.75 | 0.512202 | 0.000019 | -8.5 | 0.38 | | | | | 72% |
| 1088 B 4 H 2 129 - 131 | foram | 27.3 | 2.82 | 0.512300 | 0.000018 | -6.6 | 0.35 | | | | | 46% |
| 1088 B 4 H 5 134 - 136 | foram | 31.85 | 3.40 | 0.512216 | 0.000029 | -8.2 | 0.57 | | | | | 69% |
| 1088 B 5 H 3 138 - 140 | foram | 38.39 | 4.27 | 0.512178 | 0.000016 | -9.0 | 0.32 | | | | | 77% |
| 1088 B 6 H 6 78 - 80 | foram | 51.79 | 5.76 | 0.512159 | 0.000016 | -9.3 | 0.31 | | | | | 81% |
| 1088 B 7 H 7 20 - 22 | foram | 62.21 | 6.38 | 0.512220 | 0.000019 | -8.2 | 0.36 | | | | | 70% |
| 1088 B 8 H 6 134 - 136 | foram | 71.35 | 7.01 | 0.512278 | 0.000019 | -7.0 | 0.38 | | | | | 55% |
| 1088 B 10 H 3 84 - 86 | foram | 85.35 | 7.76 | 0.512250 | 0.000018 | -7.6 | 0.35 | | | | | 63% |
| 1088 B 11 H 4 139 - 141 | foram | 96.9 | 8.57 | 0.512191 | 0.000017 | -8.7 | 0.33 | | | | | 78% |
| 1088 C 4 H 3 105 - 107 | foram | 145.5 | 10.58 | 0.512244 | 0.000016 | -7.7 | 0.32 | | | | | 66% |
| 1088 C 5 H 5 30 - 32 | foram | 157.25 | 10.69 | 0.512228 | 0.000015 | -8.0 | 0.29 | | | | | 70% |
| 1088 C 8 X 1 30 - 32 | foram | 174.05 | 10.91 | 0.512269 | 0.000013 | -7.2 | 0.25 | | | | | 60% |
| 1088 C 9 X 2 81 - 83 | foram | 185.06 | 11.24 | 0.512279 | 0.000014 | -7.0 | 0.28 | | | | | 56% |
| 1088 C 11 X 3 34 - 36 | foram | 205.36 | 12.07 | 0.512204 | 0.000016 | -8.5 | 0.32 | | | | | 76% |
| 1088 C 13 X 1 20 - 22 | foram | 222.05 | 14.04 | 0.512223 | 0.000011 | -8.1 | 0.22 | | | | | 72% |
| 1088 B 1 H 1 14 - 15 | leachate | 0.145 | 0.01 | 0.512126 | 0.000006 | -10.0 | 0.12 | 0.282850 | 0.000006 | 2.9 | 0.21 | 78% |
| 1088 B 1 H 1 45 - 49 | leachate | 0.47 | 0.04 | 0.512228 | 0.000009 | -8.0 | 0.18 | 0.282875 | 0.000024 | 3.7 | 0.85 | 58% |
| duplicate | leachate | 0.47 | 0.04 | 0.512230 | 0.000011 | -8.0 | 0.22 | | | | | 58% |
| 1088 B 1 H 1 97 - 99 | leachate | 0.98 | 0.09 | 0.512180 | 0.000017 | -8.9 | 0.34 | 0.282880 | 0.000009 | 3.9 | 0.33 | 68% |
| 1088 B 1 H 2 28 - 30 | leachate | 1.79 | 0.16 | 0.512214 | 0.000015 | -8.3 | 0.29 | 0.282864 | 0.000007 | 3.3 | 0.26 | 62% |
| 1088 B 1 H 2 62 - 64 | leachate | 2.13 | 0.19 | 0.512148 | 0.000011 | -9.6 | 0.22 | 0.282863 | 0.000006 | 3.3 | 0.21 | 75% |
| 1088 B 1 H 2 77 - 79 | leachate | 2.28 | 0.21 | 0.512145 | 0.000015 | -9.6 | 0.29 | 0.282877 | 0.000005 | 3.8 | 0.19 | 76% |
| 1088 B 1 H 3 5 - 7 | leachate | 3.06 | 0.31 | | | | | 0.282824 | 0.000041 | 1.9 | 1.46 | |
| 1088 B 1 H 3 17 - 19 | leachate | 3.18 | 0.32 | 0.512139 | 0.000015 | -9.7 | 0.28 | 0.282849 | 0.000007 | 2.8 | 0.24 | 77% |
| 1088 B 1 H 3 37 - 39 | leachate | 3.38 | 0.34 | | | | | 0.282826 | 0.000027 | 2.0 | 0.94 | |
| 1088 B 1 H 3 42 - 44 | leachate | 3.43 | 0.35 | 0.512238 | 0.000016 | -7.8 | 0.32 | 0.282881 | 0.000008 | 4.0 | 0.27 | 56% |
| 1088 B 1 H 3 62 - 64 | leachate | 3.63 | 0.36 | | | | | 0.282842 | 0.000045 | 2.6 | 1.59 | |
| 1088 B 1 H 3 81 - 83 | leachate | 3.82 | 0.38 | 0.512150 | 0.000015 | -9.5 | 0.29 | 0.282893 | 0.000006 | 4.4 | 0.23 | 75% |
| 1088 B 1 H 3 116 - 119 | leachate | 4.175 | 0.41 | 0.512125 | 0.000010 | -10.0 | 0.19 | 0.282873 | 0.000007 | 3.7 | 0.24 | 80% |
| 1088 B 1 H 4 10 - 12 | leachate | 4.61 | 0.43 | 0.512255 | 0.000011 | -7.5 | 0.21 | 0.282899 | 0.000013 | 4.6 | 0.45 | 53% |
| 1088 B 1 H 4 40 - 42 | leachate | 4.91 | 0.48 | | | | | 0.282855 | 0.000027 | 3.1 | 0.96 | |

**Table A 8 (continued).**

| # Sample | (Site/Hole/Core/Core-type/Section/Interval) | Type | Depth [mcd] | Age [Ma] | 143Nd/144Nd | 2σ | εNd | 2σ | 176Hf/177Hf | 2σ | εHf | 2σ | %NASW |
|---|---|---|---|---|---|---|---|---|---|---|---|---|---|
| 1088 | B 1 H 4 44 - 46 | leachate | 4.95 | 0.49 | 0.512143 | 0.000011 | -9.7 | 0.21 | | | | | 77% |
| duplicate | | leachate | 4.95 | 0.49 | 0.512133 | 0.000010 | -9.9 | 0.19 | 0.282884 | 0.000024 | 4.1 | 0.86 | 79% |
| 1088 | B 2 H 1 22 - 24 | leachate | 5.73 | 0.52 | | | | | 0.282853 | 0.000026 | 3.0 | 0.92 | |
| 1088 | B 2 H 2 22 - 24 | leachate | 7.23 | 0.62 | 0.512153 | 0.000012 | -9.5 | 0.24 | 0.282874 | 0.000008 | 3.7 | 0.27 | 75% |
| duplicate | | leachate | 7.23 | 0.62 | 0.512155 | 0.000017 | -9.4 | 0.32 | | | | | 75% |
| duplicate | | leachate | 7.23 | 0.62 | 0.512165 | 0.000012 | -9.2 | 0.23 | | | | | 73% |
| 1088 | B 2 H 2 27 - 29 | leachate | 7.28 | 0.63 | | | | | 0.282830 | 0.000013 | 2.2 | 0.47 | |
| 1088 | B 2 H 2 70 - 72 | leachate | 7.71 | 0.65 | 0.512237 | 0.000015 | -7.8 | 0.29 | 0.282886 | 0.000009 | 4.1 | 0.32 | 58% |
| 1088 | B 2 H 3 27 - 29 | leachate | 8.78 | 0.73 | 0.512214 | 0.000017 | -8.3 | 0.33 | 0.282875 | 0.000008 | 3.7 | 0.27 | 63% |
| 1088 | B 2 H 3 64 - 66 | leachate | 9.15 | 0.76 | 0.512208 | 0.000014 | -8.4 | 0.26 | 0.282872 | 0.000008 | 3.6 | 0.27 | 64% |
| 1088 | B 2 H 3 90 - 92 | leachate | 9.41 | 0.77 | 0.512125 | 0.000011 | -10.0 | 0.22 | 0.282892 | 0.000008 | 4.3 | 0.29 | 80% |
| 1088 | B 2 H 3 105 - 107 | leachate | 9.56 | 0.78 | | | | | 0.282843 | 0.000010 | 2.6 | 0.35 | |
| 1088 | B 2 H 3 137 - 139 | leachate | 9.88 | 0.80 | 0.512272 | 0.000012 | -7.1 | 0.23 | 0.282855 | 0.000006 | 3.0 | 0.22 | 50% |
| 1088 | B 2 H 4 102 - 104 | leachate | 11.03 | 0.89 | 0.512245 | 0.000012 | -7.7 | 0.22 | 0.282878 | 0.000012 | 3.9 | 0.42 | 57% |
| 1088 | B 2 H 5 67 - 69 | leachate | 12.18 | 0.97 | | | | | 0.282863 | 0.000013 | 3.3 | 0.46 | |
| 1088 | B 2 H 5 98 - 100 | leachate | 12.49 | 1.00 | 0.512139 | 0.000011 | -9.7 | 0.21 | 0.282876 | 0.000015 | 3.8 | 0.53 | 79% |
| 1088 | B 2 H 5 117 - 119 | leachate | 12.68 | 1.01 | 0.512195 | 0.000011 | -8.7 | 0.21 | 0.282851 | 0.000035 | 2.9 | 1.25 | 68% |
| 1088 | B 2 H 5 141 - 143 | leachate | 12.92 | 1.02 | | | | | 0.282870 | 0.000013 | 3.6 | 0.45 | |
| 1088 | B 2 H 6 83 - 85 | leachate | 13.84 | 1.06 | 0.512137 | 0.000015 | -9.8 | 0.28 | 0.282901 | 0.000010 | 4.7 | 0.36 | 79% |
| 1088 | B 3 H 1 118 - 122 | leachate | 16.2 | 1.31 | 0.512262 | 0.000009 | -7.3 | 0.18 | 0.282876 | 0.000007 | 3.8 | 0.25 | 53% |
| 1088 | B 3 H 2 37 - 39 | leachate | 16.88 | 1.40 | 0.512154 | 0.000011 | -9.4 | 0.21 | 0.282910 | 0.000057 | 5 | 2.00 | 77% |
| 1088 | B 3 H 2 53 - 55 | leachate | 17.04 | 1.42 | 0.512242 | 0.000014 | -7.7 | 0.28 | 0.282834 | 0.000042 | 2.3 | 1.50 | 59% |
| 1088 | B 3 H 2 111 - 113 | leachate | 17.62 | 1.50 | 0.512170 | 0.000013 | -9.1 | 0.25 | | | | | 74% |
| 1088 | B 3 H 4 28 - 31 | leachate | 19.795 | 1.80 | 0.512225 | 0.000013 | -8.1 | 0.26 | 0.282868 | 0.000042 | 3.5 | 1.50 | 63% |
| 1088 | B 3 H 4 62 - 64 | leachate | 20.13 | 1.85 | 0.512184 | 0.000011 | -8.9 | 0.22 | | | | | 72% |
| 1088 | B 3 H 4 127 - 129 | leachate | 20.78 | 1.94 | 0.512223 | 0.000012 | -8.1 | 0.24 | | | | | 65% |
| 1088 | B 3 H 5 47 - 49 | leachate | 21.46 | 2.03 | 0.512214 | 0.000027 | -8.3 | 0.52 | | | | | 68% |
| 1088 | B 3 H 5 83 - 85 | leachate | 21.82 | 2.08 | 0.512180 | 0.000015 | -8.9 | 0.30 | | | | | 75% |
| 1088 | B 3 H 5 136 - 138 | leachate | 22.35 | 2.15 | 0.512188 | 0.000018 | -8.8 | 0.35 | | | | | 73% |
| 1088 | B 3 H 6 2 - 4 | leachate | 22.51 | 2.17 | 0.512190 | 0.000015 | -8.7 | 0.29 | | | | | 73% |
| 1088 | B 3 H 6 23 - 25 | leachate | 22.72 | 2.20 | 0.512213 | 0.000017 | -8.3 | 0.32 | | | | | 68% |
| 1088 | B 3 H 6 52 - 54 | leachate | 23.01 | 2.24 | 0.512207 | 0.000014 | -8.4 | 0.28 | | | | | 70% |
| 1088 | B 3 H 7 2 - 4 | leachate | 23.84 | 2.35 | 0.512189 | 0.000013 | -8.8 | 0.26 | | | | | 74% |
| 1088 | B 3 H 7 12 - 14 | leachate | 23.94 | 2.37 | 0.512227 | 0.000014 | -8.0 | 0.27 | | | | | 67% |
| 1088 | B 4 H 1 17 - 19 | leachate | 24.68 | 2.47 | 0.512229 | 0.000012 | -8.0 | 0.23 | 0.282945 | 0.000013 | 6.2 | 0.47 | 67% |
| 1088 | B 4 H 1 92 - 94 | leachate | 25.41 | 2.57 | 0.512200 | 0.000016 | -8.6 | 0.32 | | | | | 73% |
| 1088 | B 4 H 2 18 - 20 | leachate | 26.19 | 2.69 | 0.512203 | 0.000008 | -8.5 | 0.15 | 0.283013 | 0.000024 | 8.6 | 0.84 | 73% |
| 1088 | B 4 H 2 73 - 75 | leachate | 26.74 | 2.75 | 0.512218 | 0.000014 | -8.2 | 0.27 | 0.282899 | 0.000045 | 4.6 | 1.60 | 69% |
| 1088 | B 4 H 2 92 - 94 | leachate | 26.91 | 2.77 | 0.512191 | 0.000016 | -8.7 | 0.32 | | | | | 75% |
| 1088 | B 4 H 2 113 - 114 | leachate | 27.125 | 2.79 | 0.512231 | 0.000017 | -7.9 | 0.33 | | | | | 66% |
| 1088 | B 4 H 2 138 - 140 | leachate | 27.39 | 2.83 | 0.512296 | 0.000011 | -6.7 | 0.22 | 0.282972 | 0.000013 | 7.2 | 0.45 | 49% |
| duplicate | | leachate | 27.39 | 2.83 | 0.512285 | 0.000010 | -6.9 | 0.19 | | | | | 52% |
| 1088 | B 4 H 3 4.5 - 6 | leachate | 27.5375 | 2.84 | 0.512216 | 0.000018 | -8.2 | 0.34 | | | | | 70% |
| 1088 | B 4 H 3 123 - 124.5 | leachate | 28.715 | 3.00 | 0.512239 | 0.000025 | -7.8 | 0.49 | | | | | 65% |
| 1088 | B 4 H 5 119 - 121 | leachate | 31.7 | 3.38 | 0.512163 | 0.000011 | -9.3 | 0.21 | 0.282945 | 0.000007 | 6.2 | 0.26 | 82% |
| 1088 | B 4 H 5 134 - 136 | leachate | 31.85 | 3.40 | 0.512248 | 0.000012 | -7.6 | 0.24 | 0.282929 | 0.000010 | 5.7 | 0.35 | 63% |
| 1088 | B 5 H 1 2 - 4 | leachate | 34.03 | 3.63 | 0.512201 | 0.000010 | -8.5 | 0.19 | 0.282933 | 0.000021 | 5.8 | 0.74 | 74% |
| 1088 | B 5 H 2 67 - 69 | leachate | 36.18 | 3.96 | 0.512182 | 0.000011 | -8.9 | 0.22 | 0.282959 | 0.000033 | 6.7 | 1.18 | 79% |
| 1088 | B 6 H 2 36 - 38 | leachate | 45.37 | 5.25 | 0.512201 | 0.000010 | -8.5 | 0.20 | 0.282999 | 0.000032 | 8.1 | 1.14 | 75% |
| 1088 | B 6 H 4 56 - 58 | leachate | 48.57 | 5.53 | 0.512160 | 0.000013 | -9.3 | 0.25 | 0.282946 | 0.000023 | 6.2 | 0.83 | 84% |
| 1088 | B 6 H 6 78 - 80 | leachate | 51.79 | 5.76 | | | | | 0.282937 | 0.000009 | 5.9 | 0.32 | |
| 1088 | B 7 H 3 100 - 102 | leachate | 57.01 | 6.07 | 0.512220 | 0.000009 | -8.2 | 0.18 | | | | | 70% |
| duplicate | | leachate | 57.01 | 6.07 | 0.512207 | 0.000010 | -8.4 | 0.19 | | | | | 73% |
| 1088 | B 7 H 7 20 - 22 | leachate | 62.21 | 6.38 | | | | | 0.282939 | 0.000005 | 6.0 | 0.17 | |
| 1088 | B 8 H 3 128 - 130 | leachate | 66.79 | 6.65 | 0.512186 | 0.000011 | -8.8 | 0.22 | 0.282925 | 0.000020 | 5.5 | 0.70 | 78% |
| 1088 | B 8 H 6 134 - 136 | leachate | 71.35 | 7.01 | | | | | 0.282944 | 0.000008 | 6.2 | 0.29 | |
| 1088 | B 9 H 5 2 - 4 | leachate | 78.03 | 7.37 | 0.512226 | 0.000011 | -8.0 | 0.22 | 0.283027 | 0.000026 | 9.1 | 0.91 | 69% |
| 1088 | B 10 H 3 84 - 86 | leachate | 85.35 | 7.76 | 0.512234 | 0.000010 | -7.9 | 0.20 | | | | | 67% |
| duplicate | | leachate | 85.35 | 7.76 | 0.512262 | 0.000014 | -7.3 | 0.26 | 0.282981 | 0.000012 | 7.5 | 0.43 | 59% |
| 1088 | B 11 H 4 139 - 141 | leachate | 96.9 | 8.57 | 0.512200 | 0.000013 | -8.6 | 0.24 | 0.282953 | 0.000006 | 6.5 | 0.20 | 76% |
| duplicate | | leachate | 96.9 | 8.57 | 0.512196 | 0.000011 | -8.6 | 0.20 | | | | | 77% |
| 1088 | B 12 H 7 2 - 4 | leachate | 109.53 | 9.45 | 0.512225 | 0.000011 | -8.1 | 0.22 | | | | | 70% |
| 1088 | B 14 H 2 113 - 115 | leachate | 122.14 | 9.94 | 0.512221 | 0.000009 | -8.1 | 0.17 | 0.283031 | 0.000035 | 9.3 | 1.24 | 71% |
| 1088 | C 3 H 1 92 - 94 | leachate | 132.87 | 10.26 | 0.512225 | 0.000012 | -8.1 | 0.24 | 0.283001 | 0.000011 | 8.2 | 0.39 | 70% |
| duplicate | | leachate | 132.87 | 10.26 | 0.512236 | 0.000010 | -7.9 | 0.19 | | | | | 68% |
| 1088 | C 4 H 3 105 - 107 | leachate | 145.5 | 10.58 | 0.512238 | 0.000012 | -7.8 | 0.23 | 0.282982 | 0.000006 | 7.5 | 0.22 | 66% |
| duplicate | | leachate | 145.5 | 10.58 | 0.512221 | 0.000009 | -8.1 | 0.18 | | | | | 71% |
| 1088 | C 4 H 3 106 - 108 | leachate | 145.51 | 10.58 | 0.512221 | 0.000016 | -8.1 | 0.32 | 0.283050 | 0.000013 | 9.9 | 0.45 | 71% |
| 1088 | C 5 H 5 30 - 32 | leachate | 157.25 | 10.69 | 0.512229 | 0.000012 | -8.0 | 0.23 | 0.282983 | 0.000024 | 7.6 | 0.84 | 69% |
| duplicate | | leachate | 157.25 | 10.69 | 0.512210 | 0.000009 | -8.4 | 0.18 | | | | | 74% |
| 1088 | C 8 X 1 30 - 32 | leachate | 174.05 | 10.91 | 0.512249 | 0.000011 | -7.6 | 0.21 | 0.282981 | 0.000009 | 7.5 | 0.31 | 64% |
| duplicate | | leachate | 174.05 | 10.91 | 0.512254 | 0.000010 | -7.5 | 0.19 | | | | | 63% |
| 1088 | C 9 X 2 81 - 83 | leachate | 185.06 | 11.24 | 0.512222 | 0.000011 | -8.1 | 0.22 | 0.283079 | 0.000015 | 11.0 | 0.52 | 71% |
| duplicate | | leachate | 185.06 | 11.24 | 0.512221 | 0.000008 | -8.1 | 0.16 | | | | | 72% |
| 1088 | C 10 X 2 77 - 79 | leachate | 195.22 | 11.66 | 0.512229 | 0.000014 | -8.0 | 0.28 | 0.283081 | 0.000011 | 11.0 | 0.37 | 70% |
| 1088 | C 11 X 3 34 - 36 | leachate | 205.36 | 12.07 | 0.512217 | 0.000013 | -8.2 | 0.25 | 0.283030 | 0.000010 | 9.2 | 0.35 | 73% |
| duplicate | | leachate | 205.36 | 12.07 | 0.512220 | 0.000009 | -8.2 | 0.17 | | | | | 72% |
| 1088 | C 12 X 1 7 - 9 | leachate | 212.32 | 12.91 | 0.512199 | 0.000013 | -8.6 | 0.24 | 0.283015 | 0.000010 | 8.7 | 0.37 | 78% |
| 1088 | C 13 X 1 20 - 22 | leachate | 222.05 | 14.04 | 0.512184 | 0.000016 | -8.9 | 0.31 | 0.282999 | 0.000014 | 8.1 | 0.51 | 82% |
| duplicate | | leachate | 222.05 | 14.04 | 0.512196 | 0.000008 | -8.6 | 0.16 | | | | | 79% |
| 1088 | B 1 H 1 14 - 15 | detrital | 0.15 | 0.01 | 0.512069 | 0.000013 | -11.1 | 0.25 | 0.282565 | 0.000005 | -7.2 | 0.18 | |
| 1088 | B 1 H 1 43 - 44 | detrital | 0.44 | 0.03 | 0.512227 | 0.000012 | -8.0 | 0.22 | 0.282556 | 0.000004 | -7.5 | 0.14 | |
| 1088 | B 1 H 2 73 - 74 | detrital | 2.24 | 0.21 | 0.511992 | 0.000010 | -12.6 | 0.20 | 0.282475 | 0.000006 | -10.4 | 0.22 | |
| 1088 | B 1 H 3 37 - 39 | detrital | 3.38 | 0.34 | 0.512110 | 0.000020 | -10.3 | 0.38 | 0.282598 | 0.000008 | -6.0 | 0.28 | |
| 1088 | B 1 H 3 137 - 139 | detrital | 4.38 | 0.42 | 0.512125 | 0.000010 | -10.0 | 0.20 | 0.282578 | 0.000004 | -6.8 | 0.15 | |
| 1088 | B 2 H 2 27 - 29 | detrital | 7.28 | 0.63 | 0.512127 | 0.000009 | -10.0 | 0.18 | 0.282722 | 0.000006 | -1.7 | 0.22 | |
| duplicate | | detrital | 7.28 | 0.63 | 0.512124 | 0.000012 | -10.0 | 0.24 | | | | | |
| 1088 | B 2 H 2 50 - 52 | detrital | 7.51 | 0.64 | 0.512208 | 0.000012 | -8.4 | 0.23 | 0.282666 | 0.000007 | -3.6 | 0.24 | |
| 1088 | B 2 H 3 105 - 107 | detrital | 9.56 | 0.78 | 0.512115 | 0.000011 | -10.2 | 0.21 | 0.282628 | 0.000007 | -5.0 | 0.26 | |
| 1088 | B 2 H 4 97 - 99 | detrital | 10.98 | 0.88 | 0.512227 | 0.000029 | -8.0 | 0.57 | 0.282584 | 0.000004 | -6.6 | 0.15 | |
| 1088 | B 2 H 5 67 - 69 | detrital | 12.18 | 0.97 | 0.512059 | 0.000011 | -11.3 | 0.21 | 0.282533 | 0.000005 | -8.3 | 0.18 | |
| 1088 | B 2 H 6 77 - 79 | detrital | 13.77 | 1.06 | 0.512043 | 0.000011 | -11.6 | 0.21 | 0.282531 | 0.000007 | -8.4 | 0.24 | |
| 1088 | B 3 H 4 78 - 80 | detrital | 20.29 | 1.87 | 0.512163 | 0.000032 | -9.3 | 0.62 | 0.282605 | 0.000007 | -5.8 | 0.25 | |
| 1088 | B 4 H 5 134 - 136 | detrital | 31.85 | 3.40 | 0.511982 | 0.000012 | -12.8 | 0.23 | 0.282573 | 0.000007 | -6.9 | 0.24 | |
| 1088 | B 6 H 6 78 - 80 | detrital | 51.79 | 5.76 | 0.512125 | 0.000014 | -10.0 | 0.28 | 0.282670 | 0.000007 | -3.5 | 0.24 | |
| 1088 | B 11 H 4 139 - 141 | detrital | 96.90 | 8.57 | 0.512079 | 0.000017 | -10.9 | 0.33 | 0.282658 | 0.000006 | -3.9 | 0.23 | |
| 1088 | C 11 X 3 34 - 36 | detrital | 205.36 | 12.07 | 0.512238 | 0.000025 | -7.8 | 0.49 | 0.282761 | 0.000007 | -0.3 | 0.26 | |
| duplicate | | detrital | 205.36 | 12.07 | 0.512226 | 0.000012 | -8.0 | 0.24 | | | | | |

**Table A9: Total dissolution procedure.**

| ***Step*** | ***Remark*** | ***Time*** |
|---|---|---|
| **Preparation:** Grind samples finely with agate grinder and transfer **100 mg** into TD vials. | disintigrate grains | |
| 2 ml $H_2O_2$ (30%), 10 ml MQ, room temperature loose lids, over weekend | oxidize organics | 60 hours |
| dry down at 100°C | | 12 hours |
| 3 ml conc. HCl, 1ml conc. $HNO_3$ (aqua regia) close vials, at 140°C overnight | oxidize organics | 12+ hours |
| dry down at 140°C | | 4 hours |
| 1ml conc. $HNO_3$, 2ml conc. HF close vials, at 140° overnight | dissolve silicate | 12+ hours |
| dry down at 140° | remove Si | 3 hours |
| 2 ml conc. $HNO_3$, 1 ml conc. HF, 0.5 ml $HClO_4$ | dissolve refractory minerals and organics | |
| dry down at 180-190°C overnight | | 3.5 hours |
| 2 ml conc. $HNO_3$, 4ml conc. HF to high pressure digestion at 190-200°C for 4 days | dissolve refractory minerals (zircons) | 4 days |
| dry down at 140°C | | 5 hours |
| 1 ml perchloric acid +2 ml $HNO_3$ conc | destroy fluorides | |
| dry down at 180-190°C | remove perchloric acid | 3 hours |
| 2 ml conc. $HNO_3$ | | |
| dry down at 180-190°C | remove perchloric acid | 1 hour |
| 0.5 ml conc. $HNO_3$ | | |
| dry down at 180-190°C | remove perchloric acid | 0.25 hours |
| 1 ml conc. HCl | change to $Cl^-$ form | |
| dry down at 100°C | | 1.5 hours |
| reflux overnight with loading solution | | 12+ hours |